

**LOAD AND RESISTANCE FACTOR DESIGN (LRFD) RESISTANCE
FACTORS FOR TIP GROUTED DRILLED SHAFTS**

BDV25-977-37

FINAL REPORT

BY

Principal Investigators:

Gray Mullins, Ph.D., P.E.

Manjriker Gunaratne, Ph.D., P.E.

with

Anhar Sarsour- Doctoral Student

and

Sarah Mobley, Ph.D., P.E.



September 2019

Disclaimer

The opinions, findings, and conclusions expressed in this publication are those of the authors and not necessarily those of the State of Florida Department of Transportation.

APPROXIMATE CONVERSIONS TO SI UNITS

SYMBOL	WHEN YOU KNOW	MULTIPLY BY	TO FIND	SYMBOL
LENGTH				
in	inches	25.4	millimeters	mm
ft	feet	0.305	meters	m
yd	yards	0.914	meters	m
mi	miles	1.61	kilometers	km

SYMBOL	WHEN YOU KNOW	MULTIPLY BY	TO FIND	SYMBOL
AREA				
in²	square inches	645.2	square millimeters	mm ²
ft²	square feet	0.093	square meters	m ²
yd²	square yard	0.836	square meters	m ²
ac	acres	0.405	hectares	ha
mi²	square miles	2.59	square kilometers	km ²

SYMBOL	WHEN YOU KNOW	MULTIPLY BY	TO FIND	SYMBOL
VOLUME				
fl oz	fluid ounces	29.57	milliliters	mL
gal	gallons	3.785	liters	L
ft³	cubic feet	0.028	cubic meters	m ³
yd³	cubic yards	0.765	cubic meters	m ³
NOTE: volumes greater than 1000 L shall be shown in m ³				

SYMBOL	WHEN YOU KNOW	MULTIPLY BY	TO FIND	SYMBOL
MASS				
oz	ounces	28.35	grams	g
lb	pounds	0.454	kilograms	kg
T	short tons (2000 lb)	0.907	megagrams (or "metric ton")	Mg (or "t")

SYMBOL	WHEN YOU KNOW	MULTIPLY BY	TO FIND	SYMBOL
TEMPERATURE (exact degrees)				
°F	Fahrenheit	5 (F-32)/9 or (F-32)/1.8	Celsius	°C

SYMBOL	WHEN YOU KNOW	MULTIPLY BY	TO FIND	SYMBOL
ILLUMINATION				
fc	foot-candles	10.76	lux	lx
fL	foot-Lamberts	3.426	candela/m ²	cd/m ²

SYMBOL	WHEN YOU KNOW	MULTIPLY BY	TO FIND	SYMBOL
FORCE and PRESSURE or STRESS				
lbf	poundforce	4.45	newtons	N
lbf/in ²	poundforce per square inch	6.89	kilopascals	kPa
kip	kilopound	4.45	kilonewtons	kN

1.1.1 APPROXIMATE CONVERSIONS TO SI UNITS

SYMBOL	WHEN YOU KNOW	MULTIPLY BY	TO FIND	SYMBOL
LENGTH				
mm	millimeters	0.039	inches	in
m	meters	3.28	feet	ft
m	meters	1.09	yards	yd
km	kilometers	0.621	miles	mi

SYMBOL	WHEN YOU KNOW	MULTIPLY BY	TO FIND	SYMBOL
AREA				
mm ²	square millimeters	0.0016	square inches	in ²
m ²	square meters	10.764	square feet	ft ²
m ²	square meters	1.195	square yards	yd ²
ha	hectares	2.47	acres	ac
km ²	square kilometers	0.386	square miles	mi ²

SYMBOL	WHEN YOU KNOW	MULTIPLY BY	TO FIND	SYMBOL
VOLUME				
mL	milliliters	0.034	fluid ounces	fl oz
L	liters	0.264	gallons	gal
m³	cubic meters	35.314	cubic feet	ft ³
m³	cubic meters	1.307	cubic yards	yd ³

SYMBOL	WHEN YOU KNOW	MULTIPLY BY	TO FIND	SYMBOL
MASS				
g	grams	0.035	ounces	oz
kg	kilograms	2.202	pounds	lb
Mg (or "t")	megagrams (or "metric ton")	1.103	short tons (2000 lb)	T

SYMBOL	WHEN YOU KNOW	MULTIPLY BY	TO FIND	SYMBOL
TEMPERATURE (exact degrees)				
°C	Celsius	1.8C+32	Fahrenheit	°F

SYMBOL	WHEN YOU KNOW	MULTIPLY BY	TO FIND	SYMBOL
ILLUMINATION				
lx	lux	0.0929	foot-candles	fc
cd/m²	candela/m ²	0.2919	foot-Lamberts	fl

SYMBOL	WHEN YOU KNOW	MULTIPLY BY	TO FIND	SYMBOL
FORCE and PRESSURE or STRESS				
N	newtons	0.225	poundforce	lbf
kPa	kilopascals	0.145	poundforce per square inch	lbf/in ²
kN	kilonewtons	0.225	kilopound	kip

*SI is the symbol for the International System of Units. Appropriate rounding should be made to comply with Section 4 of ASTM E380.

Technical Report Documentation Page

1. Report No.	2. Government Accession No.	3. Recipient's Catalog No.	
4. Title and Subtitle LOAD AND RESISTANCE FACTOR DESIGN (LRFD) RESISTANCE FACTORS FOR TIP GROUTED DRILLED SHAFTS		5. Report Date September 2019	
		6. Performing Organization Code	
7. Author(s) G. Mullins, M. Gunaratne, A. Sarsour, S. Mobley		8. Performing Organization Report No.	
9. Performing Organization Name and Address University of South Florida Department of Civil and Environmental Engineering 4202 E. Fowler Avenue, ENB 118s Tampa, FL 33620		10. Work Unit No. (TRAIS)	
		11. Contract or Grant No. BDV25-977-37	
12. Sponsoring Agency Name and Address Florida Department of Transportation 605 Suwannee Street, MS 30 Tallahassee, FL 32399		13. Type of Report and Period Covered Final Report 01/17-08/19	
		14. Sponsoring Agency Code	
15. Supplementary Notes FDOT Project Manager: Juan Castellanos			
<p>Pressure grouting beneath the tip of drilled shafts, also known as postgrouting, has been used for more than fifty years throughout the world and has been shown to be an effective means to enhance both the usable and ultimate end bearing resistance. In short, postgrouting is a form of compaction grouting beneath the shaft tip (performed after concrete has cured) that can improve the soil strength and increase the axial shaft stiffness.</p> <p>Until 2006, there was no published design methodology, and hence, the anticipated performance was speculated to be a function of injected grout volume, shaft uplift, and/or the achieved grout pressure. Research leading up to a 2006 design method, funded by the Florida Department of Transportation (FDOT), found the grout pressure applied to the soils beneath the shaft tip to be the key factor most closely linked to the resulting end bearing. However, the research did not recommend safety factors or LRFD resistance factors for use in design. In fact, 13 years after the new design method and after hundreds of projects employing its use domestically and worldwide, there were no published resistance factors for postgrouted end bearing resistance of drilled shafts. The objective of this study was to establish LRFD resistance factors for postgrouted end bearing scenarios.</p> <p>As with all resistance factor calibration studies, the measured load test response was compared to the predicted capacity. The predicted capacity method was restricted to the 2006 design method and the FDOT method, adapted from the 2006 method. The pressure applied at the time of grouting was scrutinized for all 31 shafts and three values of grout pressure were identified: the highest field recorded pressure, which could have been the by-product of a blocked grout line; the office-calculated design pressure based on boring log information; and the truly applied pressure (termed <i>effective pressure</i>), which was verified by reviewing the simultaneous performance/trends of increasing grout volume, pressure, and shaft uplift. Bias values (the measured to predicted capacity ratios) were determined for each pressure level of each shaft and at all displacements under which the shaft was load tested.</p> <p>Resistance factors were found to be higher for effective pressure bias values and lowest for office-calculated design pressure. Further, both the 2006 and FDOT design methods resulted in the same resistance factor (0.65) for toe displacements up to 1% of the shaft diameter, D. The findings further recommend adoption of strict field quality control measures to support the use of the computed resistance factor.</p>			
17. Key Words Drilled shaft, postgrouting, resistance factor, end bearing		18. Distribution Statement No restrictions.	
19. Security Classif. (of this report) Unclassified.	20. Security Classif. (of this page) Unclassified.	21. No. of Pages 248	22. Price

Acknowledgments

The authors would like to acknowledge the Florida Department of Transportation for funding this project, with specific thanks to Juan Castellanos, Dr. David Horhota, Larry Jones, Rodrigo Herrera, and the entire FDOT review team for their insightful contributions.

Executive Summary

Pressure grouting beneath the tip of drilled shafts, also known as postgrouting, has been used for more than fifty years throughout the world and has been shown to be an effective means to enhance both the usable and ultimate end bearing resistance. In short, postgrouting is a form of compaction grouting beneath the shaft tip (performed after concrete has cured) that can improve the soil strength and increase the axial shaft stiffness. Until 2006, there was no published design methodology, and hence, the anticipated performance was speculated to be a function of injected grout volume, shaft uplift, and/or the achieved grout pressure. Research leading up to a 2006 design method, funded by the Florida Department of Transportation (FDOT), found the grout pressure applied to the soils beneath the shaft tip to be the key parameter most closely linked to the resulting end bearing. However, the research did not recommend safety factors or LRFD resistance factors for use in design. In fact, 13 years after the new design method and after hundreds of projects employing its use domestically and worldwide, there were no published resistance factors for postgrouted end bearing resistance of drilled shafts.

Today, FDOT restricts the use of shaft end bearing in sands, and as such, no resistance factors are provided in FDOT design manuals. However, end bearing is permitted if postgrouting is employed, and an adaptation of 2006 design method is provided. Even then, when postgrouting is used, there is no resistance factor for design computations, and a load test is usually required, from which the load test specific resistance factor is used. The objective of this study was to establish LRFD resistance factors for postgrouted end bearing scenarios. To this end, a database of 31 test shafts was established in which the shaft diameter, length, boring logs, grouting logs, and load test reports were compiled.

As with all resistance factor calibration/determination studies, the measured load test response was compared to the predicted capacity. The predicted capacity methods were restricted to the FDOT method and the 2006 design method on which the FDOT method is founded. These design methods are dependent on two factors: (1) the amount of end bearing displacement and (2) the grout pressure imparted to the end bearing strata. Where no grout pressure is applied, the end bearing responds as a conventional ungrouted shaft. Therefore, the pressure applied at the time of grouting was scrutinized for all 31 shafts, and three values of grout pressure were identified: the highest field recorded pressure, which could have been the by-product of a blocked grout line; the office-calculated design pressure based on boring log information; and the truly applied pressure (termed effective pressure), which was verified by reviewing the simultaneous performance/trends of increasing grout volume, pressure, and shaft uplift. Bias values (the measured to predicted capacity ratio) were determined for each pressure level of each shaft and at all displacements under which the shaft was load tested.

Resistance factors were found to be higher for *effective* pressure bias values and lowest for office-calculated design pressure. Further, both the 2006 and FDOT design methods resulted in the same resistance factor (0.65) for toe displacements up to 1% of the shaft diameter, D . The findings further recommend adoption of strict field quality control measures to support the use of the computed resistance factor.

TABLE OF CONTENTS

LIST OF TABLES	xi
LIST OF FIGURES	xii
Chapter One: Introduction	1
1.1 Overview	1
1.2 Organization of Report.....	3
Chapter Two: Literature Review	4
2.1 Grout Delivery Systems	4
2.2 Design Considerations	6
2.3 Grouting Effectiveness	9
2.3.1 Pressure.....	9
2.3.2 Net Volume	9
2.3.3 Uplift.....	10
2.3.4 Toe Strain.....	10
2.4 Quality Assurance and Control.....	11
2.5 Derivation of Resistance Factors	13
2.6 Statistics of Resistance Bias Factors	14
2.7 Statistics of Load Factors	15
2.8 Determination of the Design Reliability	16
2.9 Determination of ϕ_R	16
2.10 Frequency of Tests	17
2.11 Studies Focused on Determining Foundation Resistance Factors	18
2.11.1 Development of LRFD Procedures for Bridge Pile Foundations in Iowa... 18	
2.11.2 Evaluation of Pile Load Tests for Use in Missouri LRFD Guidelines	19
2.11.3 FDOT Calibration of Pile Resistance Factors.....	19
2.12 Further Considerations	20
2.1 Chapter Summary	22
Chapter Three: Geotechnical Design Data Collection	23
3.1 Royal Park Bridge, West Palm Beach, Florida	24
3.2 PGA Boulevard, West Palm Beach, Florida	24
3.3 Broadway Bridge Viaduct Improvements, Council Bluffs, Iowa.....	25
3.4 Gerald Desmond Bridge, Long Beach, California.....	26
3.5 Huey P. Long Bridge, Mississippi River, New Orleans, Louisiana	26
3.6 University of Houston, Houston, Texas.	27
3.7 Natchez Trace Parkway Bridge, Natchez, Mississippi.	27
3.8 Clearwater Sites I and II, Clearwater, Florida.	28
3.9 Flagler Memorial Bridge, West Palm Beach, Florida.....	29
3.10 Security Checkpoint building concourse “C” West Palm Beach Airport, West Palm Beach, Florida. 29	
3.11 Plant Daniel, Escatawpa, Mississippi.	30
3.12 SR-80 Southern Blvd Bridge, West Palm Beach, Florida.....	30
3.13 Overland Bridge Widening, Jacksonville, Florida.....	31
3.14 Carolina Bays Parkway, Myrtle Beach, South Carolina.	31
3.15 Gilmerton Bridge Replacement, Chesapeake, Virginia.	32
3.16 Peninsula Condominium, Jacksonville, Florida.	33
3.17 West Rail Bypass, Brownsville, Texas.	33

Chapter Four: Data Processing and Analysis	35
4.1 Data Plots	35
4.1.1 Tri-axis Plots	35
4.1.2 Design and Bias Curves.....	36
4.2 Analysis.....	36
4.2.1 Data Set 1, Royal Park Bridge (RPB) LT-2.....	38
4.2.2 Data Set 2, Royal Park Bridge (RPB) LT-3.....	40
4.2.3 Data Set 3, PGA Boulevard- LT-2	42
4.2.4 Data Set 4, Iowa Broadway Bridge Viaduct Improvements – TS-4.....	44
4.2.5 Data Set 5, Gerald Desmond Bridge, TP-2.....	46
4.2.6 Data Set 6, Gerald Desmond Bridge, TS-3C	48
4.2.7 Data Set 7, Huey P. Long Bridge	50
4.2.8 Data Set 8, The University of Houston (UH), S-2	52
4.2.9 Data Set 9, Natchez Trace Parkway Bridge, S-1	54
4.2.10 Data Set 10, Clearwater Site I, FJ-1	56
4.2.11 Data Set 11, Clearwater Site I, FJ-2	58
4.2.12 Data Set 12, Clearwater Site I, SP-1	60
4.2.13 Data Set 13, Clearwater Site I, SP-2	62
4.2.14 Data Set 14, Clearwater Site II, FJ-1.....	64
4.2.15 Data set 15, Clearwater Site II, SP-1.....	66
4.2.16 Data Set 16, Flagler Memorial Bridge, S-1	68
4.2.17 Data Set 17, Security Checkpoint building concourse “C”, S-1.....	70
4.2.18 Data Set 18, Plant Daniel - 501	72
4.2.19 Data Set 19, Plant Daniel - 528.....	74
4.2.20 Data Set 20, Plant Daniel – 530	76
4.2.21 Data Set 21, SR-80 Southern Blvd Bridge, S-1	78
4.2.22 Data Set 22, SR-80 Southern Blvd Bridge, S-2	80
4.2.23 Data Set 23, SR-80 Southern Blvd Bridge, S-3	82
4.2.24 Data Set 24, Overland Bridge Widening, S-1	84
4.2.25 Data Set 25, Overland Bridge Widening, S-2.....	86
4.2.26 Data Set 26, Overland Bridge Widening, S-3.....	88
4.2.27 Data Set 27, Carolina Bays Parkway, S-1	90
4.2.28 Data Set 28, Gilmerton Bridge Replacement, S-1	92
4.2.29 Data Set 29, Peninsula Condominium.....	94
4.2.30 Data Set 30, West Rail Bypass, 41E	96
4.2.31 Data Set 31, West Rail Bypass, 41W	98
4.3 Bias Factors	100
4.4 Bias Factors FDOT Method	104
4.5 Chapter Summary	109
Chapter Five: Discussion and Conclusions.....	110
5.1 Overview	110
5.2 Reliability Index Selection	111
5.3 Design Equation Refinement.....	115
5.4 Recommendations.....	119
5.4.1 Limit the Design End Bearing Displacement	119
5.4.2 New FDOT Design Equation.....	120

5.4.3	Field Inspection Requirements.....	120
5.5	Limitations.....	124
	References	125
	APPENDIX A - SOIL INFORMATION.....	131
	APPENDIX B - LOAD TEST RESULTS.....	169
	APPENDIX C - FDOT METHOD BIAS FACTOR PLOTS	200
	APPENDIX D - DESIGN EXAMPLE USING NEW FDOT DESIGN EQUATION ...	231

LIST OF TABLES

Table 2.1 Resistance factor expressed as function of site variability and number of load tests (reproduced from AASHTO, 2015).17

Table 2.2 AASHTO resistance factors for drilled shafts (reproduced from AASHTO, 2015).....20

Table 2.3 FDOT resistance factors (reproduced from FDOT, 2017).22

Table 4.1 Data set shaft ID summary37

Table 4.2 Shaft bias versus percent displacement for effective pressure.100

Table 4.3 Shaft bias versus percent displacement for maximum field pressure.101

Table 4.4 Shaft bias versus percent displacement for maximum calculated design pressure.102

Table 4.5 Shaft bias versus percent displacement for effective pressure using an end bearing cap.105

Table 4.6 Shaft bias versus percent displacement for maximum field pressure using end bearing cap.....106

Table 4.7 Shaft bias versus percent displacement for maximum calculated pressure using end bearing cap.107

Table 5.1 Bias criteria vs resistance factor summary for 1%D and all displacements.113

Table 5.2 Bias criteria vs resistance factor summary using a grout pressure end bearing cap (FDOT method).113

Table 5.3 Summary of grout pressures and grout pressure ratios.115

Table 5.4 Coefficient and intercept values used to define design equation.116

Table 5.5 Resistance factors using updated equation.118

Table 5.6 Comparison of resistance factors by design method.119

Table 5.7 FDOT resistance factor values including postgrouted end bearing.120

LIST OF FIGURES

Figure 2.1 Sleeve-port (<i>tube-a-manchette</i>) grout delivery systems as used in China (left), Taipei (middle), and south Florida (right).	5
Figure 2.2 Flat jacks used in West Palm, FL (top left), Houston, TX (top right), Taipei, Taiwan (bot left), and Tampa, FL (bot right).	5
Figure 2.3 Grout pressure vs. L/D ratio for published grouting studies (Mullins and Winters, 2004).	7
Figure 2.4 Quality assurance plots for postgrouting drilled shafts (Winters, 2014).	11
Figure 2.5 Proper grout performance shown from effectiveness plots.....	12
Figure 2.6 End bearing control followed by grout system blockage which masked ineffective grouting; true grout pressure 60% the design pressure; effectiveness plots detected the problem. 13	
Figure 2.7 Grout distribution system blockage caused design pressure criterion to be artificially achieved; true grout pressure was half the design pressure; effectiveness plots detected the problem.	13
Figure 3.1 Project location map.	23
Figure 4.1 Concept tri-axis grouting effectiveness plots.	35
Figure 4.2 Data set 1 design curves.....	38
Figure 4.3 Data set 1 tri-axis plots.....	38
Figure 4.4 Data set 1 predicted/design and load test response (top); bias vs disp. (bottom).	39
Figure 4.5 Data set 2 design curves.....	40
Figure 4.6 Data set 2 tri-axis plots.....	40
Figure 4.7 Data set 2 predicted/design and load test response (top); bias vs disp. (bottom).	41
Figure 4.8 Data set 3 design curves.....	42
Figure 4.9 Data set 3 augmented tri-axis plots.....	42
Figure 4.10 Data set 3 predicted/design and load test response (top); bias vs disp. (bottom).	43
Figure 4.11 Data set 4 design curves.....	44
Figure 4.12 Data set 4 tri-axis plots.....	44
Figure 4.13 Data set 4 predicted/design and load test response (top); bias vs disp. (bottom).	45
Figure 4.14 Data set 5 design curves.....	46
Figure 4.15 Data set 5 tri-axis plots.....	46
Figure 4.16 Data set 5 predicted/design and load test response (top); bias vs disp. (bottom).	47
Figure 4.17 Data set 6 design curves.....	48
Figure 4.18 Data set 6 tri-axis plots.....	48
Figure 4.19 Data set 6 predicted/design and load test response (top); bias vs disp. (bottom).	49
Figure 4.20 Data set 7 design curves.....	50
Figure 4.21 Data set 7 tri-axis plots.....	50
Figure 4.22 Data set 7 predicted/design and load test response (top); bias vs disp. (bottom).	51
Figure 4.23 Data set 8 design curve based on 1in displacement.....	52
Figure 4.24 Data set 8 tri-axis plots.....	52
Figure 4.25 Data set 8 predicted/design and load test response (top); bias vs disp. (bottom).	53

Figure 4.26 Data set 9 design curves.....	54
Figure 4.27 Data set 9 tri-axis plots.....	54
Figure 4.28 Data set 9 predicted/design and load test response (top); bias vs disp. (bottom).	55
Figure 4.29 Data set 10 design curves.....	56
Figure 4.30 Data set 10 modified tri-axis plots.....	56
Figure 4.31 Data set 10 predicted/design and load test response (top); bias vs disp. (bottom).	57
Figure 4.32 Data set 11 design curves.....	58
Figure 4.33 Data set 11 modified tri-axis plots.....	58
Figure 4.34 Data set 11 predicted/design and load test response (top); bias vs disp. (bottom).	59
Figure 4.35 Data set 12 design curves.....	60
Figure 4.36 Data set 12 modified tri-axis plots.....	60
Figure 4.37 Data set 12 predicted/design and load test response (top); bias vs disp. (bottom).	61
Figure 4.38 Data set 13 design curves.....	62
Figure 4.39 Data set 13 tri-axis plots.....	62
Figure 4.40 Data set 13 predicted/design and load test response (top); bias vs disp. (bottom).	63
Figure 4.41 Data set 14 design curves.....	64
Figure 4.42 Data set 14 tri-axis plots.....	64
Figure 4.43 Data set 14 predicted/design and load test response (top); bias vs disp. (bottom).	65
Figure 4.44 Data set 15 design curves.....	66
Figure 4.45 Tri-axis plots for data set 15.....	66
Figure 4.46 Data set 15 predicted/design and load test response (top); bias vs disp. (bottom).	67
Figure 4.47 Data set 16 design curves.....	68
Figure 4.48 Data set 16 tri-axis plots.....	68
Figure 4.49 Data set 16 predicted/design and load test response (top); bias vs disp. (bottom).	69
Figure 4.50 Data set 17 design curves.....	70
Figure 4.51 Data set 17 tri-axis plots.....	70
Figure 4.52 Data set 17 predicted/design and load test response (top); bias vs disp. (bottom).	71
Figure 4.53 Data set 18 design curves.....	72
Figure 4.54 Data set 18 tri-axis plots.....	72
Figure 4.55 Data set 18 predicted/design and load test response (top); bias vs disp. (bottom).	73
Figure 4.56 Data set 19 design curves.....	74
Figure 4.57 Data set 19 tri-axis plots.....	74
Figure 4.58 Data set 19 predicted/design and load test response (top); bias vs disp. (bottom).	75
Figure 4.59 Data set 20 design curves.....	76
Figure 4.60 Data set 20 tri-axis plots.....	76
Figure 4.61 Data set 20 predicted/design and load test response (top); bias vs disp. (bottom).	77
Figure 4.62 Data set 21 design curves.....	78
Figure 4.63 Data set 21 tri-axis plots.....	78
Figure 4.64 Data set 21 predicted/design and load test response (top); bias vs disp. (bottom).	79
Figure 4.65 Data set 22 design curves.....	80

Figure 4.66 Data set 22 tri-axis plots.....	80
Figure 4.67 Data set 22 predicted/design and load test response (top); bias vs disp. (bottom).	81
Figure 4.68 Data set 23 tri-axis plots.....	82
Figure 4.69 Data set 23 predicted/design and load test response (top); bias vs disp. (bottom).	83
Figure 4.70 Data set 24 design curves.	84
Figure 4.71 Data set 24 tri-axis plots.....	84
Figure 4.72 Data set 24 predicted/design and load test response (top); bias vs disp. (bottom).	85
Figure 4.73 Data set 25 design curves.	86
Figure 4.74 Data set 25 tri-axis plots.....	86
Figure 4.75 Data set 25 predicted/design and load test response (top); bias vs disp. (bottom).	87
Figure 4.76 Data set 26 design curves.	88
Figure 4.77 Data set 26 tri-axis plots.....	88
Figure 4.78 Data set 26 predicted/design and load test response (top); bias vs disp. (bottom).	89
Figure 4.79 Data set 27 design curves.	90
Figure 4.80 Data set 27 volume vs pressure plot.	90
Figure 4.81 Data set 27 predicted/design and load test response (top); bias vs disp. (bottom).	91
Figure 4.82 Data set 28 design curves.	92
Figure 4.83 Data set 28 grout tri-axis plots.....	92
Figure 4.84 Data set 28 predicted/design and load test response (top); bias vs disp. (bottom).	93
Figure 4.85 Data set 29 design curves.	94
Figure 4.86 Data set 29 pressure vs disp. plot.....	94
Figure 4.87 Data set 29 predicted/design and load test response (top); bias vs disp. (bottom).	95
Figure 4.88 Data set 30 design curves.	96
Figure 4.89 Data set 30 tri-axis plots.....	96
Figure 4.90 Data set 30 predicted/design and load test response (top); bias vs disp. (bottom).	97
Figure 4.91 Data set 31 design curves.	98
Figure 4.92 Data set 31 tri-axis plots.....	98
Figure 4.93 Data set 31 Predicted/design and load test response (top); bias vs disp. (bottom).....	99
Figure 4.94 Resistance factor vs target reliability graph for effective pressure.....	103
Figure 4.95 Resistance factor vs target reliability graph for maximum field pressure.	103
Figure 4.96 Resistance factor vs target reliability graph for maximum calculated pressure.	104
Figure 4.97 Resistance factor vs reliability graph for effective pressure using end bearing cap..	108
Figure 4.98 Resistance factor vs reliability graph for maximum field pressure using end bearing cap.....	108
Figure 4.99 Resistance factor vs target reliability graph for maximum calculated pressure using an end bearing cap.....	109
Figure 5.1 Reliability index vs probability of failure (Allen, 2005).	111
Figure 5.2 End bearing movement from grouting.	112
Figure 5.3 Effect of pressure limit on bias and resistance factors.....	114

Figure 5.4 TCM defined by linear and non-linear relationships between GPI and %D, respectively (Mullins et al. 2006).	116
Figure 5.5 Original and refined GPI coefficient determination approaches.	117
Figure 5.6 TCM intercepts (Table 5.1) match O'Neill design graph (adapted from AASHTO 2016 and O'Neill 1988).	117
Figure 5.7 Updated equation using additional data sets.	118
Figure 5.8 Tri-axis plots using strain gauge instead of uplift measurements.	122
Figure 5.9 Eccentric grout bulb formation noted by strain gauges.	123
Figure 5.10 Eccentricity as a function of grouting time.	123
Figure 5.11 Thermal integrity profile near toe of shaft showing more cement on one side.	124

Chapter One: Introduction

A drilled shaft is a cast-in-place deep foundation element often chosen over other foundation options due to its ability to withstand large axial and lateral loading. The axial capacity of a drilled shaft is the result of a combination of side shear and end bearing, but design guidelines vary throughout the industry and can often be conflicting. Some agencies exclude the use of side shear depending completely on the end bearing; others design based solely on side shear and disregard end bearing. Both rationales are defensible, especially given the regional variability of the existing soil strata. In reality, both end bearing and side shear always contribute to the overall shaft capacity where the contributing load-carrying components depend on shear strain for side shear resistance and toe displacement for end bearing. The issue then becomes one of developing both the side shear and the end bearing simultaneously.

The controlling mechanisms for the development of side shear and end bearing capacity require significantly different displacements. Shafts tipped in competent (hard) material require only small displacements to mobilize the socket side shear or end bearing. In such cases, soft or loose overburden soil layers never experience the magnitude of displacement (shear strain) needed to produce meaningful capacity. When tipped in less competent materials or constructed in uniform soils over the entire length, the side shear contributes to the overall capacity, but end bearing movement may not be sufficient to mobilize a significant portion of the ultimate end bearing. Further, the ultimate end bearing value is often small in loose materials. So strain incompatibility between side shear and end bearing has the most effect on the ability for a given component (side shear or end bearing) to participate in the load-carrying resistance.

The Florida Department of Transportation (FDOT) restricts the use of shaft end bearing when tipped in sands such that no end bearing can be used unless verified by load testing. However, if the soils beneath the tip of the shaft are injected with high pressure grout, known as postgrouting, then the FDOT-prescribed end bearing design equations can be used. To date, postgrouted shafts used for FDOT structures have been accompanied by some form of load testing, and the resistance factor associated with the load test method was then applied. In the event that postgrouted shafts are used without a load test, the present design specifications have no prescriptive resistance factor for those conditions. In fact, there are no published resistance factors for postgrouted shafts anywhere in the U.S. or abroad. Setting resistance factors for postgrouted end bearing capacity forms the basis for this study.

1.1 Overview

Pressure grouting beneath the tip of drilled shafts, also known as postgrouting, has been used for more than fifty years throughout the world and has shown to be an effective means to enhance both the usable and ultimate end bearing resistance. In short, postgrouting is a form of compaction grouting beneath the shaft tip (performed after concrete has cured) that can improve the soil strength and increase the axial shaft stiffness. Until 2006, there was no published design methodology, and hence, the anticipated performance was speculated to be a function of injected grout volume, shaft uplift, and/or the achieved grout pressure. Research leading up to the new design methods (Mullins

et al., 2000, 2001, 2004, 2006, 2008; Mullins and O'Neill, 2003; Mullins and Dapp, 2002; Mullins, 2015) found the grout pressure applied to the soils beneath the shaft tip to be the key parameter.

Prediction of the achievable grout pressure (and the grouted end bearing) hinges on the available side shear to resist the fluid grout pressing upward on the shaft tip area. Three assumptions accompany this approach: (1) the fluid grout distributes across the entire tip area, (2) side shear can be estimated with reasonable confidence, and (3) the end bearing strata can withstand the “design” grout pressure. To this end, field quality control measures were adopted in an effort to: ensure grout distribution in the form of a minimum grout volume criterion; show side shear was not exceeded via a maximum uplift threshold; and verify the design pressure is sustained for a minimum amount of time. To date, however, designers have not been required to impose any form of safety factor on the predicted grout pressure which are dependent on side shear values; rather, upper limits on grout pressure have only been based on equipment capabilities (i.e. 1,000-1,600 psi) or contractor suggested upper limits based on experience (less than 800 psi). This oversight has led to numerous cases where the design pressure could not be achieved due to excessive shaft uplift (side shear failure) or excessive grout volume (end bearing soil failure). Application of reliability-based resistance factors applied to side shear and/or end bearing can mitigate these problems which are usually only unveiled during production shaft construction and grouting.

In cases where the design grout pressure is not achieved, the current state of practice has accepted the use of stage grouting as a catch-all fix or reset of any grouting criterion that has not been satisfied. This second attempt to achieve the grout pressure in effect produces a drastically smaller, fluid grout bulb beneath the shaft and therefore cannot produce the same force or soil modification effectiveness. This can also violate the assumption that the entire tip of the shaft is in contact with grout. However, some postgrouting design approaches are based on multi-stage grouting practices which result in lower end bearing predictions. Conversely, single stage grouting methods produce higher end bearing capacity for a given grout pressure. This suggests that the construction practice must adhere to the design method used, and that a unique resistance factor should be applied to the various design methods based the bias factor associated with each approach. This speaks to one primary goal of this study.

Postgrouting inherently increases the confidence in the as-built shaft performance. If grout is truly distributed over the entire shaft tip, then the associated bi-directional forces test both the side shear and mobilized end bearing. Current FDOT design guidelines for postgrouted shafts in sand incorporate a displacement dependent end bearing strength which also cannot exceed the applied grout pressure. So, at the time of grouting the design capacity is essentially fully tested which suggests a near 1.0 resistance factor could be appropriate. However, even then, there is still reserve capacity in both side shear and end bearing where the proofed uplift side shear is less than downward loading capacity and the true ultimate end bearing continues to increase with additional displacement. In clay or rock, grouted capacity design approaches are not explicitly stated but generally exhibit the same limits. Assessing how soil type affects grouting performance and confidence is similarly important.

Finally, the motivation for postgrouting has primarily been to increase capacity which in turn reduces shaft size and foundation costs. Increased reliability afforded by grouting has not yet been considered in design; therefore, an increase in the resistance factors could also reduce overall

expense by reducing the required ultimate capacity. Equally important, the improved soil structure and the size of grout bulb are in essence constructed elements and therefore inspection in the form of quality assurance and control must be robust. Detailed field practices that verify or disprove the design assumptions must be employed and will be discussed herein. Use of such methods provide basis for increased reliability that if omitted would constitute rationale for lower resistance factors. Determination of resistance factors for the various aspects of postgrouted shaft design and construction is the primary objective of this study.

1.2 Organization of Report

This study entailed four tasks in the process of defining resistance factors for postgrouted end bearing capacity of drilled shafts including a literature search, collection of data sources, analysis of data, and development of recommendations. These steps are outlined in the ensuing chapters: Chapter two provides a background of postgrouting design and construction methods. Chapter three consists of a detailed summary of the collected data. Chapter four details the procedures used to process and evaluate the collected data. The conclusions drawn from the study are summarized in Chapter five, recommendations are provided based on the findings.

Chapter Two: Literature Review

In the early nineteen sixties the process of pressure grouting beneath shaft tips was first used to improve end bearing (Bolognesi and Moretto, 1973). In the ensuing 60 years, numerous grout distribution systems were developed and tested but the basic approach remained the same. Despite the almost certain presence of in-house proprietary design methods throughout the world, it took forty years for the first rational design approach to be published (Mullins et al, 2006).

Pressure grouting is a form of compaction that densifies the soil and is therefore most effective in granular, free draining soils capable of structurally reorienting in the short timeframe of the grouting process (i.e. less than 1hr). The term postgrouting comes from the fact that the pressure grouting is performed after/post construction. Pressure grouting should not be confused with permeation grouting. Permeation grouting uses highly-mobile, thin fluid grouts to flow through while filling in and around the soil particles to cement the materials together. Designing capacity from the two methods is completely different as pressure grouting relies on the applied pressure and the area over which it is applied. Permeation grouting relies on the strength of the cementing fluid and the size of the bulb that is formed. The bulb size is then used as an increased end bearing area where conventional end bearing computations can be applied. However, prediction of the bulb size from permeation grouting and the resulting end bearing area is difficult and not the subject of this study.

In general, dense sands provide relatively good end bearing without grouting and therefore improvements from postgrouting are modest. The same material at a lower relative density will achieve a higher percent improvement for a similar magnitude of grout pressure. Where dense sands may show only 40% capacity increase as a result of postgrouting, loose sands can show 800-900% increase (Mullins et al, 2004). Although it is never the intent to allow poor construction practices and needlessly leave debris or soils loosened by the drilling, these conditions can be restored to an improved higher relative density than that which originally existed through the use of postgrouting.

2.1 Grout Delivery Systems

Grout delivery systems vary in concept but all must provide a means to place grout in the locations/areas slated for improvement. These systems can be categorized as sleeve ports (*tube-a-manchette, French*), flat jacks, or stem ports. For drilled shaft end bearing applications, sleeve ports are tubing circuits that allow grout to flow into and out of the target grouting area in a continuous looped tube. Orifices are drilled in the tubing at the desired grouting locations and covered with a rubber sleeve to keep debris from clogging the orifices during concreting. Figure 2.1 shows three example sleeve ports systems used around the world (Bittner, et al. 2007 and Mullins, et al. 2001). In the United States, sleeve port systems commonly use a separation plate to isolate the shaft concrete from the grouting zone which also minimizes soil disturbance from tremie placed concrete rushing into the base of the excavation.

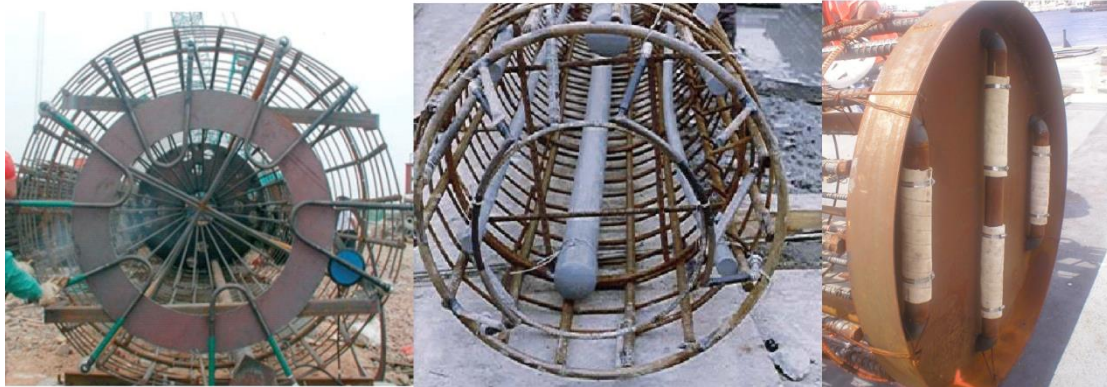


Figure 2.1 Sleeve-port (*tube-a-manchette*) grout delivery systems as used in China (left), Taipei (middle), and south Florida (right).

Flat jack assemblies also form circuits via grout delivery tubes that go to and from the grouting area; however, at the grouting site, the grout is free to distribute across the base of a flat plate establishing a predefined initial pressurized area much like a hydraulic jack (hence the name flat jack). Generally, flat jacks have the ability to introduce grout beneath the plate via a plurality of tubes around the circumference of the plate. Grout flow out of all tubes demonstrates proper grout distribution. Figure 2.2 shows example flat jack assemblies (Mullins and O’Neill, 2003; Mullins et al., 2001).



Figure 2.2 Flat jacks used in West Palm, FL (top left), Houston, TX (top right), Taipei, Taiwan (bottom left), and Tampa, FL (bottom right).

Flat jacks are further classified as closed or open systems. Open systems, the most common, simply provide a separation membrane (rubber or light gauge sheet metal) or a protected cavity that keeps

concrete from bonding to the underside of the plate and maintains the predefined grouting area. At the time of grouting, the membrane expands and may burst allowing the grout to directly contact the soil. Closed systems provide a highly expansive bladder that prevents grout migration. The system shown in Figure 2.2 (bottom right) is a double plate closed system that would eventually become an open system after 4in of lower plate travel. The others shown are considered open systems. Both sleeve port and flat jack systems benefit from a gravel pack below the grout delivery system to aid in lateral grout distribution across the shaft tip.

Stem ports are usually used as a remedial response to unexpected loss in side shear or end bearing for any number of scenarios. This approach is essentially the same as compaction grouting to stabilize sink holes (or similar); but for shafts, it may involve coring the shaft to the base to provide a conduit for grout. If multiple stem ports are used, a circuit beneath the shaft can be established. However, no predefined pathway or loading area can be guaranteed. Only one stem port is often used due to the difficulty of coring accurately the full length of the shaft.

Further details of postgrouting systems can be found elsewhere (Gouvenot and Gabiax 1975; Sliwinski and Flemming 1984; Bruce 1986; Dapp 2002; Mullins, et al. 2000, 2001, 2004; Bittner, 2007).

2.2 Design Considerations

The most simplistic and conservative design approach for postgrouted shaft tips is to limit the end bearing to the applied grout pressure. This in essence is a proof load test of both the end bearing material and the side shear required to achieve that load. Like bi-directional load tests, the full proof load is twice the side shear or end bearing load (Eqn 2.1).

$$Proof\ Load = 2(grout\ pressure)(tip\ area) \quad (2.1)$$

Longer shafts with smaller end bearing areas and higher unit side shear resistance can withstand higher grout pressures. Conversely, shorter shafts with larger diameters and lower unit side shear withstand less grout pressure (Eqn 2.2).

$$maximum\ grout\ pressure = \frac{(unit\ side\ shear)(length)(circumference)}{tip\ area} \quad (2.2)$$

For sand, the upper pressure limit (aside from side shear control, Eqn 2.2) can be estimated from cavity expansion theory and can exceed 1000psi (Vesic, 1967). However, even when shafts are tipped in sand, layers of weaker clayey soils within the influence zone of the grout bulb (2-3D below tip) can cause end bearing / punching failures and thereby stop the increase in grout pressure.

More practically, grout pressure is limited to equipment capabilities (1000-1600psi), side shear capacity, and the grout working life (e.g. pressure that can be achieved while grout is still fluid). Figure 2.3 demonstrates the maximum grout pressure possible for various values of side shear as a function of length (L) and diameter (D). It also shows published grout pressures for various projects worldwide and indicates that the average mobilized side shear for these projects was less than 1tsf

at the time of grouting. Note the highest pressure recorded by these case studies was approximately 870 psi.

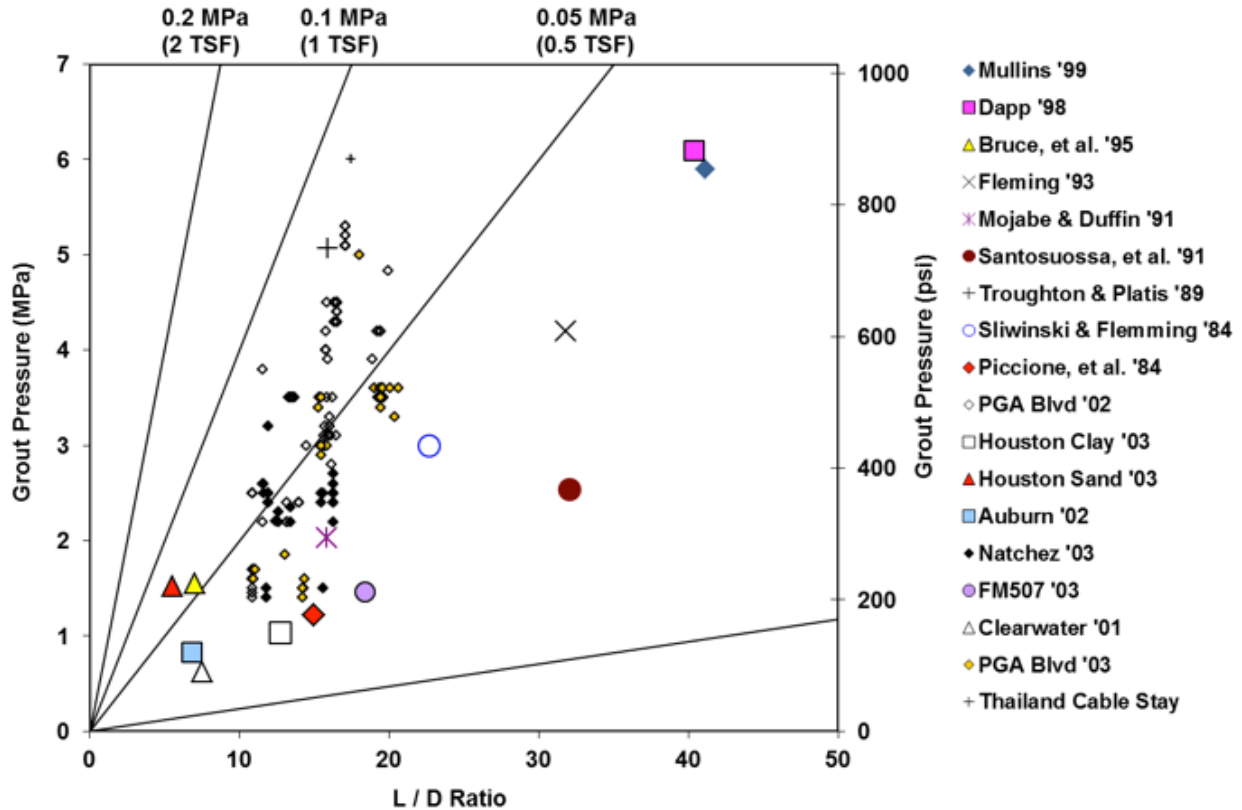


Figure 2.3 Grout pressure vs. L/D ratio for published grouting studies (Mullins and Winters, 2004).

For clayey materials, the achieved grout pressure is a good indication of usable end bearing. For sands, cemented soils and rock, far more capacity can be demonstrated. Focusing on sands, the ability to develop more capacity than just the applied grout pressure stems from the understanding that (1) while the ultimate end bearing capacity is typically taken at a displacement equivalent to 5% of the shaft diameter, smaller allowable displacements restrict the usable capacity, and (2) sands continue to gain capacity at larger displacements up to as much as 15% of the shaft diameter (Bruce, 1986). At such large displacements, however, structural deformations are excessive and the side shear resistance can degrade. While postgrouting does change the soil structure and improve ultimate capacity, it more practically precompresses the end bearing soils making higher capacities available at lower displacements. In fact, when postgrouting is employed, the grouted end bearing capacity at small/allowable displacements is often higher than the ungrouted capacity at ultimate capacity (or a larger 5%D displacement).

The postgrouted end bearing design method developed by Mullins et al. (2006) combined the achievable grout pressure with the predicted ungrouted end bearing capacity to predict the end bearing capacity at a selected displacement (Eqns 2.3 and 2.4). The usable end bearing capacity is therein defined by the tip capacity multiplier, TCM, multiplied by the ungrouted end bearing capacity. The ungrouted capacity is taken from O'Neill and Reese (1999) to be $0.6(N)$ in units of tsf where N is the standard penetration blow count. However, where O'Neill and Reese provide an

upper limit on end bearing of 40tsf (AASHTO, 2014), the Mullins et al. (2006) method did not intend to limit the ungrouted capacity when using that approach (Eqn 2.3); O’Neill and Reese had applied this limit on the basis that no data had been collected to higher levels when preparing their relationship.

$$q_{\text{grouted}} = (TCM)(q_{\text{ungrouted}}) \quad (2.3)$$

where

$$TCM = 0.713(GPI)(\%D)^{0.364} + \frac{\%D}{0.4(\%D)+3.0} \quad (2.4)$$

and

GPI = grout pressure / ungrouted end bearing capacity (dimensionless)

%D = tolerable displacement / shaft diameter, in percent (dimensionless)

The 2006 design procedure was described for a given shaft diameter and embedment length, and involved the following steps follows:

1. Calculate the ungrouted end bearing capacity at 5%D displacement, $q_p \text{ Ultimate}$.
2. Calculate the ultimate side shear resistance, F_s , for the total length of embedded shaft.
3. Divide the ultimate side shear resistance by the cross sectional area, A , of the shaft to determine the maximum anticipated grout pressure, GP_{max}

$$GP_{max} = F_s / A$$

4. Calculate the grout pressure index, GPI , as the ratio of the maximum anticipated grout pressure (Step 3) to the ungrouted unit tip resistance (Step 1)

$$GPI = GP_{max} / q_p \text{ Ultimate}$$

5. Establish the maximum design displacement as the ratio of the shaft diameter, $\%D$.
6. Determine the tip capacity multiplier, TCM , given the grout pressure index (Step 4) and the permissible displacement (Step 5) using Eqn. 2.4
7. Estimate the grouted unit tip resistance as the product of the tip capacity multiplier (Step 6) and the ultimate ungrouted end bearing capacity (Step 1)

$$q_{\text{grouted}} = (TCM)(q_p \text{ Ultimate})$$

For example, a 0.91 m (3 ft) diameter drilled shaft with an ultimate side shear resistance of 1,780 kN (200 t) will have a grouted end bearing capacity of 3.97 MPa (41.8 tsf). This is with a permissible shaft displacement of 25 mm (1 in.) and an ungrouted end bearing capacity of 1.71 MPa (18 tsf) again using Eqn. 2.4 and where $N=30$.

FDOT adapted the Mullins et al (2006) design approach by following the above steps and applying an upper limit such that the predicted postgrouted end bearing value did not exceed the applied grout pressure value expressed in terms of available side shear (FDOT Soils and Foundation Handbook, 2019). Throughout this report, this adapted method is referred to as the FDOT method.

FDOT Method Total Shaft Capacity = Side Shear Force + (q_{grouted})(tip area) \leq 2*Side Shear Force

Dapp and Brown (2010) later modified the TCM component of equation 2.3 to fit the response of load tests performed to predict the site-specific end bearing and effectiveness of the grouting methods used for that project (Eqn 2.5).

$$TCM = 0.713(GPI)(\%D^{0.2}) + \frac{\%D}{4.0(\%D)+6.0} \quad (2.5)$$

Close review of Dapp and Brown's work revealed that multi-stage grouting was used on that site as the design grout pressure could not be achieved in a single stage. Both design methods use the same basic computations for side shear determination and the associated grout pressure (side shear capacity / tip area). This supports the premise that multi-stage grouting and single stage grouting do not provide the same level of improvement. Therefore, field practices to use or not use multi-stage grouting should not be decided by the contractor, but rather established at the design phase.

The inability to achieve the target design grout pressure is a strong indication that reliability based resistance factors should be applied. In all cases, the grouting process should demonstrate that the anticipated physical phenomena are actually occurring (i.e. grout pressure is loading the entire tip area). To this end, a grout monitoring / quality control program should be carefully established.

2.3 Grouting Effectiveness

Criteria for effective grouting are site and design dependent but all must consider monitoring and recording the grout pressure, grout volume and shaft uplift as a means of quality assurance and quality control.

2.3.1 Pressure

Design approaches, such as those suggested by equations 2.4 and 2.5 set a minimum grout pressure from which an anticipated end bearing is computed. Field monitoring must verify that this pressure is achieved for a minimum sustained time (e.g. > 2min). If the grouting proceeds as expected, grout pressure should increase with additional volume in response to straining the end bearing soils. Increases in pressure without an associated increase in grout volume can be caused by grout system blockages and are an indication of ineffective grouting. Commonly, a minimum net grout volume criterion must be met by the time the design pressure is achieved as a means to demonstrate the grouted area is sufficient.

2.3.2 Net Volume

A minimum net grout volume criterion is assigned on the basis of a required quantity of grout needed to cover the tip area with an estimated amount of end bearing soil movement. Where the total grout volume includes that volume required to fill the grout system as well as that volume pumped thereafter, the net volume only considers that grout that actively improves the soil (after filling the system lines, etc.). A quick estimate of minimum net grout volume can be accomplished by multiplying the tip area by 5% of the shaft diameter (D). This makes the simplistic assumption

that a disk of grout will form below the shaft as if the soil beneath the shaft tip had displaced that distance during a load test to ultimate end bearing. This value tends to underestimate the actual volume but serves as a reasonable starting point. In reality, the minimum net grout volume threshold is best set by an initial grout test which incorporates the compressibility of the soil on site (stiffer soils require less volume and vice versa); but minimum volume criteria tend to over simplify the system and quality assurance considerations.

Increases in volume without an increase in pressure can indicate no additional side shear or end bearing resistance is available or the grout is piping/migrating to an unknown location. Shaft uplift measurements can be used to differentiate between side shear and end bearing failures. Failure to achieve grout pressure as volume increases can be catastrophic to the design whereby remediation to the design will be required and construction will be delayed.

2.3.3 Uplift

Shaft uplift measurements are perhaps the most telling indicator of grouting performance and are a direct indication of applied force. As many designs are balanced where the grout pressure and end bearing improvement are limited to available side shear, it is reasonable to expect the side shear strain and uplift to be appreciable at the point where the design grout pressure is achieved. In these cases, uplift will be proportional to the grout pressure and should be expected if grouting is performed correctly.

Maximum permissible uplift should be set such that no degradation to the side shear resistance results. Uplift values of 0.5 to 1.0%D are reasonable starting values but site specific soil response may vary and more appropriate values can be obtained from load tests or in some cases a demonstration grout test.

Uplift measurements can also be used to identify or rule out side shear control when excessive grout volume is taken. If the shaft does not continue to uplift with additional volume and also without increases in pressure, the end bearing has been exceeded or grout is piping/migrating elsewhere (no positive benefit). Conversely, persistent uplift with increasing volume and without additional grout pressure indicates side shear failure.

2.3.4 Toe Strain

Instrumenting grout tests with strain gauges provides a means to demonstrate whether or not grout is distributed across the full tip area. When grout is uniformly distributed, strain in the shaft tip should be reasonably uniform. The magnitude of observed strain is often a point of contention where the grouted area of the tip and the mobilized unit side shear have offsetting effects. Using estimated unit side shear values (f_s) for the length of the shaft segment between the toe elevation and the elevation of the strain gauges (L_{seg}), the force at the strain gauges is expected to be less than the force applied to the tip via the grouted area. During grouting, the average gauge level strain (ϵ) can be estimated using equation 2.6.

$$\epsilon_{gauge\ level} = \frac{PA_{grout} - \pi D L_{seg} f_s}{A_{shaft} E_{comp}} \quad (2.6)$$

It becomes apparent that a smaller than expected strain value can be caused by a smaller than expected grout area or a larger than expected unit side shear value. This is based on reliable values of shaft area (A_{shaft}), composite shaft modulus (E_{comp}), shaft diameter, gauge level elevation, and an accurate measurement of grout pressure (P). In any event, change in strain should be proportional to change in grout pressure to ensure lines have not become blocked. Furthermore, strains should be uniform to verify the entire tip area is experiencing grout improvements.

2.4 Quality Assurance and Control

Contradictory results of the individual performance measures can lead to inadvertent acceptance of ineffectively grouted shafts. As a result, a performance review is recommended wherein the three field measurements are plotted in tri-axis graphs to show the actual grouted outcome and to confirm proper grouting has been achieved (Figure 2.4).

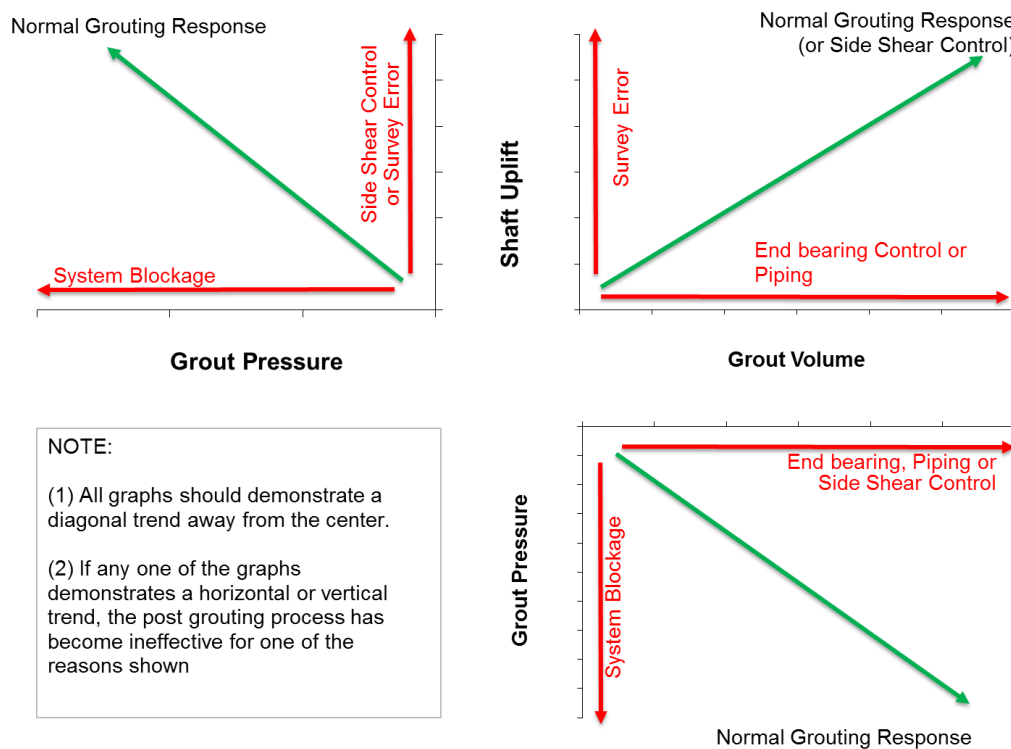


Figure 2.4 Quality assurance plots for postgrouting drilled shafts (Winters, 2014).

In short, all graphs should demonstrate a diagonal trend away from the center. If any one of the graphs demonstrates a horizontal or vertical trend and it is confirmed by a second graph, the postgrouting process has become ineffective for one of the reasons shown. Figures 2.5-2.7 show examples of effective grouting, end bearing failure, and grout system blockage, which all would have been missed without using proper quality control/assurance methods as each individual criterion was satisfied. The dashed red lines denote the individual grouting criterion required for each project. Only Figure 2.5 shows all criteria were met “effectively.”

For this study, it was imperative that all data collected be pre-processed using the tri-axis plots to identify the grout pressure at which the grouting process was still effective instead of automatically taking the highest pressure recorded in the field logs. However, statistical evaluation of the same data where no quality control method (QA/QC) was used provides rationale for developing different resistance factors for cases where QA/QC is not employed (e.g., resistance factors for QA/QC and for no QA/QC).

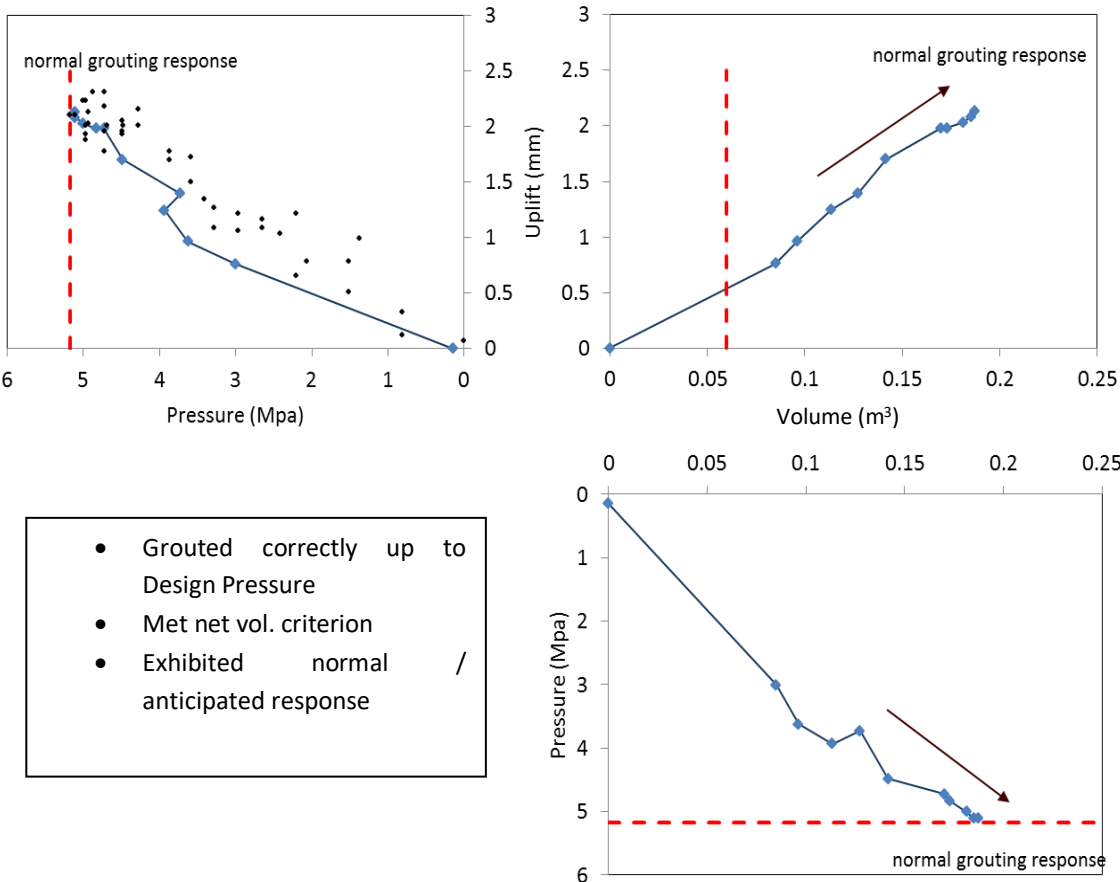


Figure 2.5 Proper grout performance shown from effectiveness plots.

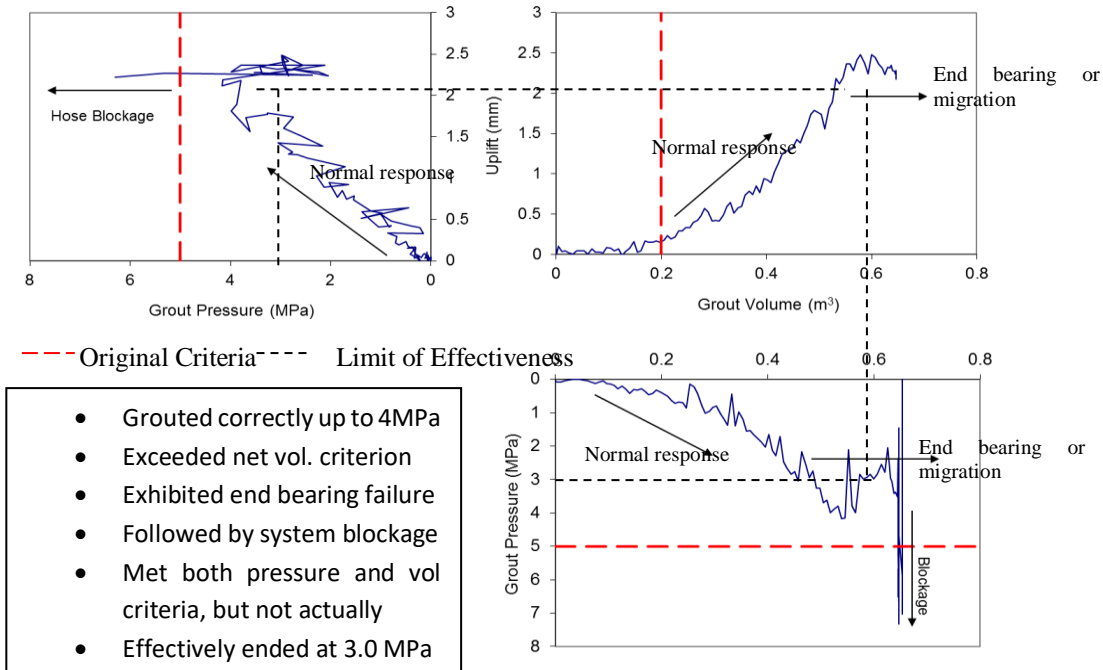


Figure 2.6 End bearing control followed by grout system blockage which masked ineffective grouting; true grout pressure 60% the design pressure; effectiveness plots detected the problem.

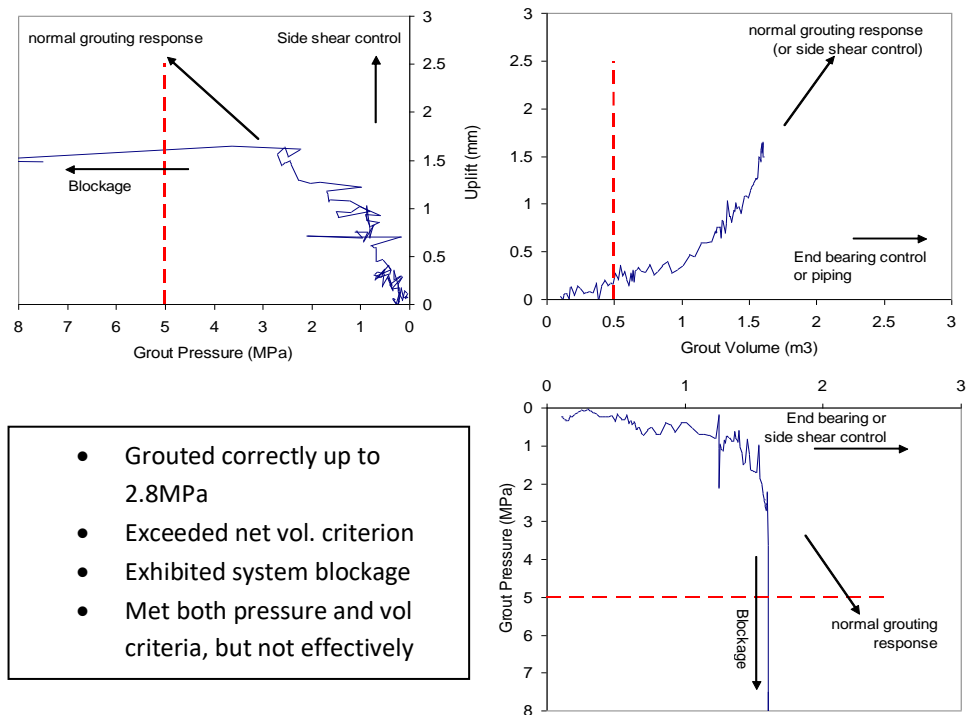


Figure 2.7 Grout distribution system blockage caused design pressure criterion to be artificially achieved; true grout pressure was half the design pressure; effectiveness plots detected the problem.

2.5 Derivation of Resistance Factors

LRFD – based evaluation of strength limit states (FHWA, 1998, AASHTO, 2010) can be summarized in Eqn. (2.7a)

$$\phi R_n \geq \eta \sum \gamma_i Q_i \quad (2.7a)$$

where

- R_n = nominal resistance
- Q_i = load effect
- ϕ = resistance factor
- γ_i = load factors
- η = load modifier

Load factors account for the uncertainties in magnitude and direction of loads, location of application of loads and combinations of loads. On the other hand, resistance factors can be made to incorporate variability of soil properties, reliability of predictive equations, quality control of construction, extent of soil exploration and even the consequences of failure.

For the combination of dead load and live load and a load modifier of 1.0, Eqn. (2.7a) can be rewritten as

$$\phi R_n > \sum \gamma_D Q_D + \gamma_L Q_L \quad (2.7b)$$

The procedure used for the selection of load and resistance factors is known as the calibration of LRFD. Two methods are popularly adopted to select the resistance and load factors (FHWA, 1998): calibration by matching the results of previously acceptable allowable stress designs (ASD) or use of reliability theory.

The measured resistance R_m can be expressed in terms of the predicted (nominal) resistance, R_n as:

$$R_m = \lambda_R R_n \quad (2.8)$$

where λ_R represents the bias factor for resistance.

2.6 Statistics of Resistance Bias Factors

The bias factors are random variables that include the net effect of various sources of error such as the tendency of a particular method (e.g. method of computing the skin friction capacity) to under-predict foundation resistance, energy losses in the equipment in obtaining SPT blow counts, and soil borings in strata not being representative of the site, etc. For n number of sources of error with individual factors affecting the strength of resistance prediction procedure, the mean (average) bias factor can be expressed in terms of the *means* of each individual bias factor as follows:

$$\lambda_R = \bar{\lambda}_1 \bar{\lambda}_2 \dots \bar{\lambda}_n \quad (2.9)$$

COV_i of any bias factor, λ_i , can be determined based on its mean and the standard deviation based on the following expressions:

$$COV(\lambda_i) = \frac{\sigma_i}{\mu_i} \quad (2.10a)$$

where

$$\mu_i = \frac{\sum_{j=1}^m \lambda_{i,j}}{m} \quad (2.10b)$$

and

$$\sigma_i = \frac{\sum_{j=1}^m (\lambda_{i,j} - \mu_i)^2}{m-1} \quad (2.10c)$$

where

m = number of observations of the λ_i factor.

Then, based on the principles of statistics, the coefficient of variation (COV) of λ_R is given by

$$COV_R^2 = COV_1^2 + COV_2^2 + \dots + COV_n^2 \quad (2.11)$$

Alternatively, COV_R^2 can also be determined directly by combined λ_R estimates obtained from an l number of individual load test data (measured resistance R_m) and the corresponding predictions (nominal resistance R_n) using equation 2.8 and the following expressions:

$$\bar{\lambda}_R = \frac{\sum_{k=1}^l \lambda_{R,k}}{l} \quad (2.12a)$$

$$s_{\lambda_R} = \frac{\sum_{k=1}^l (\lambda_{R,k} - \bar{\lambda}_R)^2}{l-1} \quad (2.12b)$$

$$COV(\lambda_R) = \frac{s_{\lambda_R}}{\bar{\lambda}_R} \quad (2.12c)$$

2.7 Statistics of Load Factors

Similarly for the measured load, one can write:

$$Q_m = \lambda_{QD}Q_D + \lambda_{QL}Q_L \quad (2.13)$$

where the load bias factor includes various uncertainties associated with dead and live loads.

2.8 Determination of the Design Reliability

Due to the above mentioned uncertainties in the soil parameters used in the resistance computation and the uncertainties in the axial load applied on a drilled shaft, the resistance and the load can be modeled by random variables Q and R respectively,

Then the reliability of the design can be expressed as

$$Reliability = Re = Probability [\phi_R R_n > (\gamma_D Q_D + \gamma_L Q_L)] \quad (2.14a)$$

or

$$Re = Pr [\phi_R R_n - (\gamma_D Q_D + \gamma_L Q_L) > 0] \quad (2.14b)$$

Typically, as an alternative to a target probability measure expressed in equation 2.14b, a corresponding target reliability index (β_T) yielding the above probability from an appropriate probability density function (F), associated with the random variation of the resistance (R) and load effect (Q) (or the quantity ($R-Q$)), is used to express the reliability (Re) of the design. Then, the reliability of the design would be

$$Re = F(\beta_T) \quad (2.14c)$$

A common probability distribution used for expressing F is the lognormal distributions of R and Q . Then, based on the probability theory and the central limit theorem, the resistance factor can be derived as

$$\phi_R = \frac{\lambda_R [\gamma_D Q_D + \gamma_L Q_L] \sqrt{\frac{(1 + COV_{QD}^2 + COV_{QL}^2)}{(1 + COV_R^2)}}}{Q_m \exp\{\beta_T \sqrt{\ln[(1 + COV_{QD}^2 + COV_{QL}^2)(1 + COV_R^2)]}\}} \quad (2.15a)$$

$$\text{where } Q_m = \lambda_{QD}Q_D + \lambda_{QL}Q_L \quad (2.15b)$$

and β_T = the target reliability index.

2.9 Determination of ϕ_R

Inspection of equations 2.15a and 2.15b shows that the resistance factor can be computed based on an assumed dead load to live load ratio (Q_D / Q_L). Such ratios of 2.0 or 3.0 are commonly used in LRFD computations. AASHTO (2010) recommended statistics for the load factors are $\lambda_{QL} = 1.15$, $COV_{QL} = 0.18$ and $\lambda_{QD} = 1.08$, $COV_{QD} = 0.13$. Furthermore, it is assumed that $\gamma_L = 1.75$ and $\gamma_D = 1.25$ also from AASHTO.

As stated in section 2.5, λ_R and COV_R^2 are needed for manipulation of equations 2.15a and 2.15b and can be obtained from a combination of either equations 2.9 and 2.11 or a combination of 2.12a and 2.12c.

2.10 Frequency of Tests

The Florida Department of Transportation establishes the threshold of load tests required for a given site that would support the use of the higher resistance factors for static load-tested shafts (later presented in Table 2.3). This factor is based on a PD&E study where regions of the project are broken into representative areas. This provides a convenient alternative to AASHTO-recommended testing frequency based on Paikowski (2004) in Table 2.1.

Table 2.1 gives the AASHTO relationships between resistance factor, site variability and the number of static load tests performed. While table 2.1 is primarily established for driven piles, when used for drilled shafts an upper limit on the resistance factor of 0.7 is imposed. This table implies that most projects qualify for a 0.7 resistance factor with one static load test and all projects qualify with two tests.

Schmertmann and Hayes (1997) cite a case study in Los Angeles, California where 27 shafts were constructed with a toe level O-cell to reduce uncertainty and the safety factor from 2 to 1.5. While static testing to such high frequency is uncommon (relative to AASHTO recorded values), building with postgrouted shafts approaches that level of confidence. However, postgrouting is still a construction process which has associated uncertainties.

Table 2.1 Resistance factor expressed as function of site variability and number of load tests (reproduced from AASHTO, 2014).

Number of Static Load Tests per Site	Resistance Factor		
	Site Variability		
	Low	Medium	High
1	0.80	0.70	0.55
2	0.90	0.75	0.65
3	0.90	0.85	0.75
≥4	0.90	0.90	0.80

The number of test records needed to obtain λ_R for each class in Table 2.1 can be estimated using equation 2.16.

$$n \geq \left(\frac{z^* \sigma}{MOE} \right) \quad (2.16)$$

where,

Z^* = Z value from the standard normal distribution corresponding to the desired confidence level (e.g. $Z^* = 1.645$ for 90% confidence)

σ = population standard deviation of λ_R which can be estimated from the corresponding sample standard deviation in Eqn. (12b), using a *preliminary* computation based on the DSTG database prepared by the investigators.

MOE = desired margin of error allowed for λ_R

2.11 Studies Focused on Determining Foundation Resistance Factors

2.11.1 Development of LRFD Procedures for Bridge Pile Foundations in Iowa

The motivation of this study was a FHWA-issued policy requiring all new bridges designed after 2007 be designed according to the LRFD approach. In response to the policy, many states (Illinois, Wisconsin, and Florida) have made an effort to collect load test data and create a regionally calibrated database for the design and construction of driven piles. The implementation of a calibrated database insures design consistency and reliability in the construction of bridge foundations.

In Iowa, the policy was implemented in four different phases labeled Volume 1 through IV. Volume I (Roling et al., 2010) focused on collecting reliable and usable static and dynamic pile load test data from different regions in Iowa and developing a user friendly, quality assured, electronic database (PILOT). Once the data was collected, it was separated into different fields (Contractor, Location, and Project No. etc.) and entered into different columns in excel. Even though PILOT included a large number of data, it did not have enough data to represent all the different soil profiles found in Iowa.

The second phase of the study concentrated on gathering information to fill all the gaps found during the previous volume. Volume II (Ng et al., 2010) included conducting ten (10) full scale driven pile field tests in different regions in Iowa. The field testing included site characterization using subsurface investigation (SPT and CPT), laboratory tests, installation of push-in pressure cells, strain gauges and use of PDA. Once testing was complete, all results were plotted, reviewed and added to the PILOT created in Volume I.

Volume III (AbdelSalam et al., 2012) focused on developing LRFD factors for static and dynamic pile analysis based on the existing PILOT database. Resistance factors were computed following the AASHTO LRFD framework and the results were compared with the old ASD method. The

outcome from this research was used in the fourth and final volume which was to be the database to be used by Iowa DOT.

The final phase of the research incorporated the results from Volume III along with specifications in the AASHTO LRFD bridge design specifications (2010). In Volume IV (Green et al., 2012), a new LRFD method for driven pile foundations in Iowa with considerations to design specifications was developed. The outcomes of the in-depth study enabled Iowa DOT to fulfill the FHWA requirement.

2.11.2 Evaluation of Pile Load Tests for Use in Missouri LRFD Guidelines

As a response to AASHTO's adoption of the LRFD method for all federally funded bridges, the Missouri Department of Transportation (MoDOT) performed three driven pile load tests in two different regions with relatively firm ground. The first selected region was in the southeastern lowlands (Sikeston and Poplar Bluff) and included two load tests. The second location was in the northern glaciated plains regions (Chillicothe) and had one load test.

The initial portion of the study (Luna, R., 2014) consisted of installing, load testing and plotting results of all the static and dynamic load tests performed. For quality assurance purposes, all driven piles were installed by the same contractor and in accordance to industry and MoDOT standards. The second phase of the research (Stuckmeyer et al., 2014) incorporated the load test results to develop LRFD factors. Once data was available, pile resistance capacity were calculated using the Davisson method as specified by AASHTO and values were used to determine LRFD resistance factors. It was concluded that the piles installed could have been smaller because the measured resistance was greater than the calculated resistance.

2.11.3 FDOT Calibration of Pile Resistance Factors

Similar to the Iowa and Missouri studies, the Florida Department of Transportation has undertaken several projects to evaluate and assign resistance factors for piles driven with various methods of computer monitoring (i.e. PDA and EDC). Both pile driving analyzers (PDA) and embedded data collectors (EDC) are methods of monitoring driving effectiveness through measurements of strain (converted to force) and acceleration (converted to velocity and displacement). Differences in the instrumentation schemes make it possible to predict pile capacity using alternate methods. Hence, the resistance factor determination was not based on soil properties from lab tests and predicted capacity but rather was based on the relative capacity of two measurement/pile capacity prediction methods compared to conventional static capacity.

Gunaratne et al. (2019) evaluated the bias from 27 test piles which extended the previous studies by McVay and Wasmann (2015) and McVay et al. (2013) which dealt with 11 test piles. The Gunaratne et al. study concluded with resistance factors from various methods of determination other than equation 2.15a (FOSM) which included the alternate FOSM (AFOSM) and Monte Carlo (MC) simulations. In general, 5 or 6 difference cases were evaluated from which different resistance factors were established. Factors considered to influence the resistance factor were: the method of measuring and predicting capacity from measurements, the time lapse between dynamic driving

measurements and the static load test, end of drive vs. restrrike measurements and predictions and the method of determining the resistance factor (FOSM, AFOSM, and MC). AFOSM and MC values were generally similar.

Each of the cited studies provided a framework for which this study could follow in the assessment of resistance factor for postgrouted end bearing prediction.

2.12 Further Considerations

Side shear determination using alpha or beta methods (FHWA, 1999; AASHTO, 2010) assumes downward loading. Studies have shown that uplift shear capacity can be between 0.66 and 0.74 times that of the downward resistance (O’Neill, 2001; Fellenius, 2002; Mayne, 2002). These variations come as a result of decreased vertical effective stress and hence horizontal soil pressures when a shaft is pulled in tension. This is reflected in code assigned resistance factors being 25 percent less in uplift (e.g. 0.6 downward, 0.45 uplift for sands, FDOT, 2017; 0.55 downward, 0.45 upward, AASHTO 2014). Postgrouted applications are equally affected by these conditions, yet no present code restrictions or recommendations are in place.

Where AASHTO permits the use of end bearing in sands and has assigned resistance factors accordingly (Table 2.2), FDOT does not provide analogous values. Rather, the Soils and Foundations Handbook (p. 91) states:

Resistance factors and associated design methods for geotechnical resistance of drilled shafts are in SDG Table 3.6.3-1 [Table 2.3]. It is implicitly shown in the table that the resistance factors for drilled shafts tipped in sand or clay are based on side shear design methods only (i.e. FHWA alpha method in clay and FHWA beta method in sand).

However, it further states for postgrouted shafts:

*In sand, drilled shafts with pressure grouted tips should be considered. Pressure grouted tips are most effective in loose to medium dense sands. Guidance for the design of drilled shafts with pressure grouted tips may be found in Appendix D and in Reference 9.**

*The design example provided in Appendix D follows from Mullins, et al. (2006), except that an upper limit is placed on the end bearing not to exceed the design grout pressure. For all practical purposes, this limit only engages in designs with higher permissible displacements.

No reference to end bearing resistance factors for grouted shafts in sand is provided and this absence, in part, was the motivation for this study.

Table 2.2 AASHTO resistance factors for drilled shafts (reproduced from AASHTO, 2014).

Method/Soil/Condition		Resistance Factor
	Side resistance in Clay	alpha method (O’Neill and Reese, 1999)
		0.45

Nominal Axial Compressive Resistance of Single-Drilled Shafts	Tip resistance in clay	Total Stress (O'Neill and Reese, 1999)	0.40
	Side resistance in sand	beta method (O'Neill and Reese, 1999)	0.55
	Tip resistance in sand	O'Neill and Reese (1999)	0.50
	Side resistance in IGMs	O'Neill and Reese (1999)	0.60
	Tip resistance in IGMs	O'Neill and Reese (1999)	0.55
	Side resistance in rock	Horvath and Kenney (1979) O'Neill and Reese (1999)	0.55
	Side resistance in rock	Carter and Kulhawy (1988)	0.50
	Tip resistance in rock	Canadian Geotechnical Society (1985) Pressuremeter Method (CGS, 1985) O'Neill and Reese (1999)	0.50
Block Failure	Clay		0.55
Uplift Resistance of Single-Drilled Shafts	Clay	alpha method (O'Neill and Reese, 1999)	0.35
	Sand	beta method (O'Neill and Reese, 1999)	0.45
	Rock	Horvath and Kenney (1979) Carter and Kulhawy (1988)	0.40
Group Uplift Resistance	Sand and clay		0.45
Horizontal Geotechnical Resistance of Single Shaft or Shaft Group	All Materials		1.0
Static Load Test (compression)	All Materials		Values in AASHTO Table 10.5.5.2.3-2 [Table 2.1] but no greater than 0.70
Static Load Test (uplift)	All Materials		0.60

Table 2.3 FDOT resistance factors (reproduced from FDOT, 2017).

Loading	Design Method	Construction QC Method	Resistance Factor	
			Redundant	Non-redundant
Compression	For soil: FHWA alpha or beta method	Specifications	0.6	0.5
	For rock socket: McVay's method neglecting end bearing	Specifications	0.6	0.5
	For rock socket: McVay's method including 1/3 end bearing	Specifications	0.55	0.45
	For rock socket: McVay's method	Statnamic Load Testing	0.7	0.6
	For rock socket: McVay's method	Static Load Testing	0.75	0.65
Uplift	For clay: FHWA alpha method	Specifications	0.35	0.25
	For sand: FHWA beta method	Specifications	0.45	0.35
	For rock socket: McVay's method	Specifications	0.5	0.4
Lateral	FBPIER	Specifications Or Lateral Load Test	1.00	0.9

2.1 Chapter Summary

While postgrouting shaft tips has great potential to improve shaft capacity and reduce costs, it can be problematic to implement effectively while ensuring the intended outcome is obtained. During the process of postgrouting, the grout is expected to cover and pressurize the entire base area, as was demonstrated in the numerous instrumented case studies used to develop the design relationships. Today, routine grouting procedures monitor grout pressure, grout volume, and survey shaft uplift, whereby each parameter must achieve or stay below a given threshold (e.g., $\text{pressure} > \text{threshold}_p$; $\text{volume} > \text{threshold}_v$; $\text{uplift} < \text{threshold}_u$). However, abiding by these thresholds does not in itself define effectiveness. It is therefore conceivable to meet all criteria and yet not grout the end bearing soils effectively or as expected.

It will be shown that in the assignment of LRFD resistance factors to postgrouted shafts, the use of quality control/assurance standards should also be introduced to ensure the statistics used to establish resistance factors are meaningful. This study scrutinized a wide range of data set types from different grout delivery systems and design methods to ensure the data incorporated into the analysis meets this standard of care. This means that grouting case studies / projects were ranked on the basis of data type, quality, and completeness; and, that resistance factors were assigned based on the level of verification testing and quality assurance provided.

Chapter Three: Geotechnical Design Data Collection

Data was obtained from 35 projects wherein postgrouting was administered. Of these 35 sites, 17 were found to contain sufficient information to warrant inclusion in this study. A summary of those 17 applicable projects is contained herein. Particular notes on the information pertaining to load testing, pressure grouting, soil classification, and strain gauges are listed below each project description. A project location map is given in Figure 3.1. The project list is as follows:

1. Royal Park Bridge in West Palm Beach, Florida.
2. PGA Boulevard in Palm Beach Gardens, Florida.
3. Broadway Bridge Viaduct Improvements in Council Bluffs, Iowa.
4. Gerald Desmond Bridge in Long Beach, California.
5. Huey P. Long Bridge, New Orleans, Louisiana.
6. University of Houston, Houston, Texas.
7. Natchez Trace Parkway Bridge, Natchez, Mississippi.
8. Clearwater Sites I and II, Clearwater, Florida.
9. Flagler Memorial Bridge, West Palm Beach, Florida.
10. West Palm Beach Airport, West Palm Beach, Florida.
11. Plant Daniel, Escatawpa, Mississippi.
12. SR 80 Southern Blvd Bridge, West Palm Beach, Florida.
13. Overland Bridge Widening, Jacksonville, Florida.
14. Carolina Bays Parkway, Myrtle Beach, South Carolina.
15. Gilmerton Bridge Replacement, Chesapeake, Virginia.
16. Peninsula Condominium, Jacksonville, Florida.
17. West Rail Bypass, Brownsville, Texas.

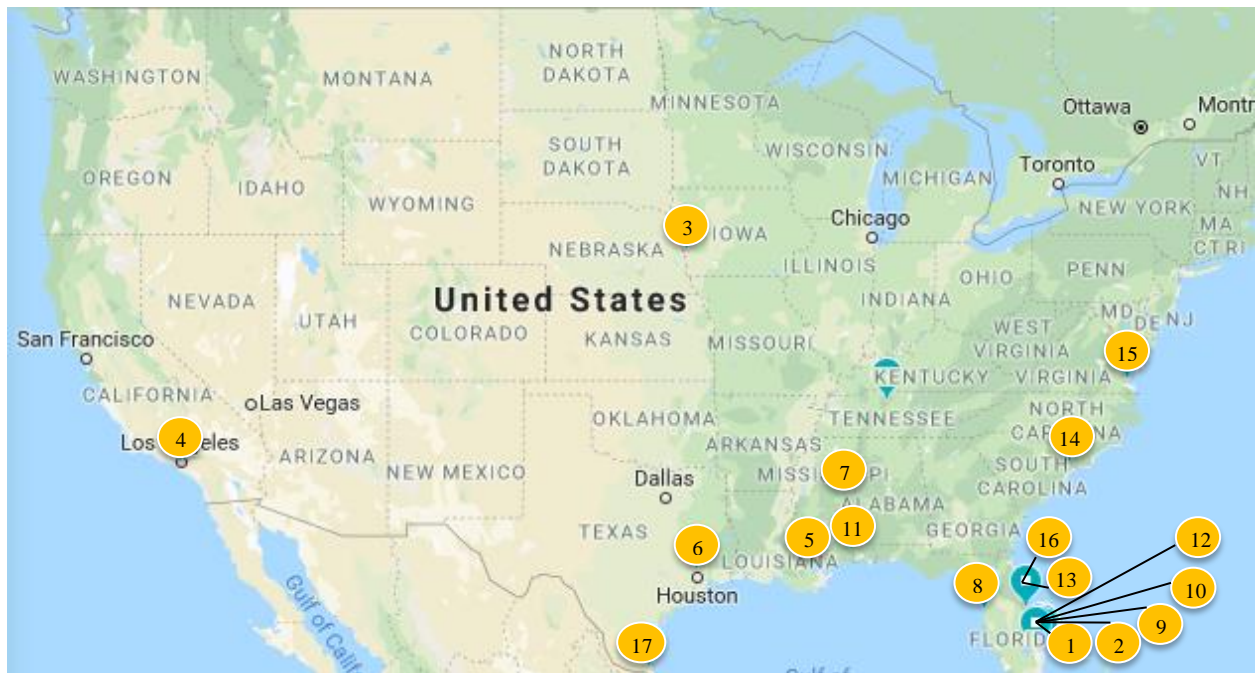


Figure 3.1 Project location map.

3.1 Royal Park Bridge, West Palm Beach, Florida

This study was conducted at Royal Park Bridge in West Palm Beach, Florida. The bridge crosses the Intracoastal Waterway, and connects Royal Palm Way to Highway 704. The project was part of a bridge construction program wherein a temporary bridge was constructed for use during the replacement of the existing bridge. Drilled shafts were constructed and load tested through large openings that were cut from the existing bridge deck and installed into a soil strata consisting of mostly sandy-cemented sands and coquina (Mullins et al, 2001). Two postgrouted shafts (LT-2 and LT-3) were installed on the Royal Bridge site in West Palm Beach, Florida. LT-2 and LT-3 were both 4-ft in diameter and planned to be 114.2-ft long; LT-2 was later shortened to 87.4 feet due to shaft LT-3 having a capacity that exceeded the load limit of the load testing device. During pressure grouting and load testing processes, strain gauges, shaft displacement and pressure were monitored using computerized data acquisition. The geotechnical consultant on the site was Professional Services Industries (PSI), drilled shafts were installed and grouted by Coastal Caisson Corp, load testing was performed by Applied Foundation Testing (AFT) and all grouting apparatus and data reporting was performed by the University of South Florida (USF).

Load Test

Load testing was performed using a 30MN Statnamic device. Load test shafts (LT-2 and LT-3) were tested before and after the postgrouting process was performed.

Pressure Grouting

Graphs and logs for grout pressure, uplift and volume were obtained from the project load test report. All data was digitized for this analysis.

Soil Classification

Boring logs for the two test shaft locations were performed to a depth of 100-ft. Shafts were tipped in sand and cemented/partially cemented coquina sand.

Strain Gauge

Five levels of strain gauges were used for verification of the design side shear values. Data from toe level strain gauges were available to assess the effectiveness/uniformity of the grout bulb beneath the toe.

3.2 PGA Boulevard, West Palm Beach, Florida

The study was conducted as part of the PGA Boulevard Grade Separation Construction Project in West Palm Beach, Florida and consisted of intersection improvements with Alt A1A. Improvements included three bridge structures, PGA Blvd Alt A1A, A1A southwest ramp to interstate I-95 and Alt A1A southwest ramp over FEC Railway. The originally submitted foundation on the site was designed per LRFD approach on 24-inch driven piles using a resistance factor of 0.65 and factored loads ranging from 135 to 220 tons. A total of one hundred and eight 36-inch in diameter drilled shafts replaced 234, 24 inch driven piles. The new design used a higher resistance factor (0.75) and factored loads (195 to 490 tons). The testing program included the

installation of two 3-ft in diameter, 60-ft long shafts (LT-1 and LT-2) tipped in shelly sand. LT-1 was an ungrouted control shaft and LT-2 was postgrouted.

Load Test

A total of two load tests were performed on the site. One load test on postgrouted shaft (LT-2) and one test on the control shaft (LT-1). Results from both tests are accessible.

Pressure Grouting

Grout pressure, uplift and volume data for LT-2 is available.

Soil Classification

Drilled shaft LT-1 corresponds to Boring B-1 and LT-2 corresponds to Boring PGAB-1. Generally, the site consisted of very loose to medium dense sand in the upper 30 feet of the boring and medium to very dense sand in the bottom 50 feet of the boring (Mullins et al, 2004). At the time of construction, the ground water table was at a depth of about 8 feet.

Strain Gauge

Three levels of strain gauges were used for verification of the design side shear values. Data from toe level strain gauges are available to assess the effectiveness/uniformity of the grout bulb beneath the toe.

3.3 Broadway Bridge Viaduct Improvements, Council Bluffs, Iowa.

The Broadway Bridge was constructed in 1955 and is located between 8th and 16th streets in Council Bluffs, Iowa. The bridge cross section consists of two 26-foot roadways, a 4-foot raised median, and a 6-foot sidewalk on the north side of the bridge. The superstructure consists of a reinforced concrete deck on continuous steel rolled I-beams. The substructure include three-column reinforced concrete bents supported by driven piles, and cellular reinforced concrete abutments. The bridge is a critical east-west arterial with a traffic volume of approximately 34,600 vehicles per day which is considered to be at its maximum capacity. A study was performed to assess the use of postgrouted shafts for pier foundation improvements. (CH2MHILL, 2007)

Load Test

One load test was performed for TS-4 and data was digitized for analysis.

Pressure Grouting

Grout pressure, uplift and volume data for shaft TS-4 is accessible.

Soil Classification

Soil geology in the area consist of loess, alluvium and glacial till underlain by shale and limestone bedrock.

Strain Gauge

Strain gauges were used for verification of the design side shear values. Data from four toe level strain gauges are available.

3.4 Gerald Desmond Bridge, Long Beach, California

The Gerald Desmond Bridge is an access point to Long Beach Port, California. The existing bridge is four lanes with no emergency / storage lanes and is being replaced to carry a six lane roadway with emergency lanes on each side, a pedestrian/bike path and observation deck along the south side of the bridge. The design also included an approximately 200 foot clearance to allow ship entry to the port. To maintain traffic flow, the new bridge was constructed alongside the existing bridge. The new bridge is founded on drilled shafts with postgrouted tips. All shaft construction is currently completed.

Load Test

Data from two static load tests were made available and digitized for further analysis.

Pressure Grouting

Graphs and logs for grout pressure and volume are available for TP-2 and TS-3C.

Soil Classification

SPT and CPT testing was performed throughout the project. On site geology consisted of silty/fine grained sand followed by dense sand to termination depth.

Strain gauge

Six segments of strain gauges were used for verification of the design side shear values. Data from toe level strain gauges are available to assess the effectiveness/uniformity of the grout bulb beneath the toe.

3.5 Huey P. Long Bridge, Mississippi River, New Orleans, Louisiana

The Huey P. Long Bridge in New Orleans is part of US Hwy 90 over the Mississippi River. The bridge has two lanes in each direction and is one of the three Mississippi river crossings in New Orleans. The project scope was to retrofit the existing piers at the crossings to widen the deck for additional traffic lanes. The foundation included the construction of a new pier on postgrouted shafts. A total of 13 drilled shafts, 9 feet in diameter and 184 feet in length, were constructed under the existing bridge.

Load Test

Only one postgrouted shaft was tested and the test was performed before grouting. The data for the load test is available.

Pressure Grouting

One shaft was grouted on this project. Pressure, uplift and volume graphs for the grouting process are available.

Soil Classification

Borings for this project consisted of clay, silty sand and sand. One soil boring is available for the locations of the postgrouted shaft.

Strain Gauge

Seven segments of strain gauges were used for verification of the design side shear values. Data from four toe level strain gauges are available for further analysis.

3.6 University of Houston, Houston, Texas.

The study was conducted in collaboration between the University of South Florida (USF) and the University of Houston (UH) along with A.H Beck Foundation Co., Inc., Applied Foundation Testing, Inc. and Fugro South, Inc. (Mullins and O'Neill, 2003). The purpose of the study was to test the effectiveness of the postgrouting method in drilled shafts and to evaluate shaft capacity using load test. Four piles were installed on the University of Houston campus. Soils in the area were mostly overconsolidated clays and fine silty and clayey sand and water was found at depths ranging from 8 to 15 feet. Two shafts were tipped in clay and two tipped in sand. One of each pair was postgrouted. The postgrouted shaft tipped in sand will be the only shaft used for this study; shaft is 48-inch in diameter and 22-feet in depth.

Load Test

Only one postgrouted shaft was tested and the test was performed after grouting. The data for the load test is available.

Pressure Grouting

One shaft was grouted on this project. Pressure, uplift and volume graphs for the grouting process are available.

Soil Classification

Soils in the area were mostly overconsolidated clays and fine silty and clayey sand and water was found at depths ranging from 8 to 15 feet. One soil boring is available for the locations of the postgrouted shaft.

Strain Gauge

Three segments of strain gauges were used for verification of the design side shear values. Data from four toe level strain gauges are available for further analysis.

3.7 Natchez Trace Parkway Bridge, Natchez, Mississippi.

The construction was performed as part of the Natchez Trace Parkway Bridge over Catherine Creek and Melvin Bayou in Natchez, Mississippi. The team of Wilbur Smith Associates and Hill Brother, Inc. were selected by the Eastern Federal Lands Highway Division of the Federal Highway

Administration (FHWA) to design and build the project. The project included the construction of the final 4.3 mile segment of the Natchez Trace Parkway in which seven new bridge structures were required to complete the highway construction; one of which was a 1,700 foot long bridge crossing Catherine Creek and Melvin Bayou. Postgrouted shafts were 6 foot in diameter and 75 feet in length.

Load Test

Only one postgrouted shaft was tested and the test was performed after grouting. The data for the load test is available.

Pressure Grouting

One shaft was grouted on this project. Pressure, displacement and volume graphs for the grouting process are available.

Soil Classification

One soil boring is available for the location of the postgrouted shaft. Boring consisted of stiff clay followed by dense sand.

Strain Gauge

Four levels of strain gauges were used for verification of the design side shear values. Data from three toe level strain gauges are available for further analysis.

3.8 Clearwater Sites I and II, Clearwater, Florida.

Clearwater Site I consisted of four postgrouted drilled shafts (FJ-1, FJ-2, SP-1 and SP-2) and Clearwater Site II consisted of two drilled shafts (FJ-1 and SP-1). Shafts for both sites were installed in the Coastal Caisson Corporations equipment yard in Clearwater, Florida. All shafts were 2-ft in diameter and 15-feet in length; soils on the site consisted of sand and clay.

Load Test

Six postgrouted shafts were tested and the tests were performed after grouting. The data for the load tests is available.

Pressure Grouting

Six shafts were grouted on this project. Pressure and displacement graphs for the grouting process are available. Volume data was not available.

Soil Classification

One soil boring is available for each one of the locations of the postgrouted shafts. Site 1 consisted of sand and clay while Site 2 was all sand. All shafts were tipped in sand.

Strain Gauge

One toe level of strain gauges was installed for side shear analysis and the data from two toe level gauges are available for further analysis.

3.9 Flagler Memorial Bridge, West Palm Beach, Florida.

The Flagler Memorial Bridge Replacement Project is located in West Palm Beach, Florida. Some of the shafts were constructed in limestone material and those shafts derived capacity from side shear. However, many areas of the bridge consist of sandy material and in those cases, resistance was derived by a combination of side shear and postgrouted end bearing. Generally, soil conditions of the postgrouted shafts consisted of 2 feet of organic soils followed by limestone fragments and sand to termination depth. The shafts were 60-inches in diameter and 100-feet in length.

Load Test

Only one postgrouted shaft was tested and data is available.

Pressure Grouting

One shaft was grouted on this project. Pressure, uplift and volume graphs for the grouting process are available.

Soil Classification

One soil boring is available for the locations of the postgrouted shaft. Generally, soil conditions consisted of 2 feet of organic soils followed by limestone fragments and sand to termination depth.

Strain Gauge

Eight levels of strain gauges were installed for side shear evaluation. Data for four toe-level strain gauges results are available to further assess the effectiveness/uniformity of the grout bulb beneath the toe.

3.10 Security Checkpoint building concourse “C” West Palm Beach Airport, West Palm Beach, Florida.

The Security Checkpoint building concourse “C” project is located at the West Palm Beach Airport in West Palm beach, Florida. One 48-inch in diameter postgrouted shaft was embedded at a length of 52 feet. The shaft was installed on August 31st, 2004 and was postgrouted 10 days after and load tested 16 days after construction. The shaft was constructed at a production location AA.7-50 using a temporary casing method and water as drilling fluid.

Load Test

Only one postgrouted shaft was tested and the test was performed after grouting. The data for the load test is available.

Pressure Grouting

One shaft was grouted on this project. Pressure, uplift and volume graphs for the grouting process are available.

Soil Classification

Subsurface conditions for the postgrouted shaft consisted of all sand.

Strain Gauge

Three levels of strain gauges were tested for side shear; data for four toe-level strain gauges are available for further analysis.

3.11 Plant Daniel, Escatawpa, Mississippi.

Plant Daniel Scrubber Foundation is located in Escatawpa, Mississippi. The project consisted of three postgrouted drilled shafts (501, 528 and 530) with similar geometry.

Load Test

All three postgrouted shafts were tested and the test was performed before grouting. The data for the load tests is available.

Pressure Grouting

One shaft was grouted on this project. Pressure and volume graphs for the grouting process are available.

Soil Classification

One soil boring is available for each drilled shaft location. Generally, soil conditions consisted of 20 feet of soft to medium stiff clays and silts underlain by medium dense to very dense sands.

Strain Gauge

Four levels of strain gauges were tested for side shear; data for four toe-level strain gauges are available for further analysis.

3.12 SR-80 Southern Blvd Bridge, West Palm Beach, Florida.

The State Road 80 Southern Blvd Bridge project included two spans over the Atlantic Intracoastal Waterway and the Lake Worth Lagoon connecting SR 80 in the city of West Palm Beach to the town of Palm Beach in Palm Beach County. The new main bridge was designed to be a movable bridge while the second bridge was a fixed-span bridge over a narrow section of open water along the eastern shore of the lagoon. Drilled shafts for the main bridge in piers 2 through 11 utilize pressure grouted tips.

Load Test

Three postgrouted shafts were tested and the tests were performed after grouting. The data for the load tests is available.

Pressure Grouting

Three shafts were grouted on this project. Pressure, displacement and volume graphs for the grouting process are available.

Soil Classification

One soil boring is available for each of the locations of the postgrouted shaft.

Strain Gauge

Six segments with strain gauges were installed for side shear testing and results are available to further assess the effectiveness/uniformity of the grout bulb beneath the toe.

3.13 Overland Bridge Widening, Jacksonville, Florida.

The I-95 Overland Bridge project included the reconstruction of I-95 in downtown Jacksonville, Florida. Project location map is shown in Figure 3.13. The construction included 14 new bridges and 3 bridge widenings. The I-95 over Palm Ave/San Marco Blvd/ St. Johns River was constructed on a foundation of 16 postgrouted shafts with three (3) of those shafts subjected to Statnamic load testing. Shafts range from 60 to 72-inches in diameter and were 72 to 96-feet in length.

Load Test

Three postgrouted shafts were tested and the tests were performed after grouting. The data for the load tests is available.

Pressure Grouting

Three shafts were grouted on this project. Pressure, displacement and volume graphs for the grouting process are available.

Soil Classification

Generally, soil conditions consist of 13 feet of loose to medium dense sand followed by weathered limestone then a layer of clayey sand with shell and limestone fragments until termination depth.

Strain Gauge

Ten levels with strain gauges were installed to evaluate shaft side shear. Results for four toe-level strain gauges are available to further assess the effectiveness/uniformity of the grout bulb beneath the toe.

3.14 Carolina Bays Parkway, Myrtle Beach, South Carolina.

This project was located at SC 544 Carolina Bays Parkway in Myrtle Beach, South Carolina. The shaft had a planned diameter of 54 inches and was constructed using 56-inch diameter permanent casing in the upper 12.4 feet. The actual constructed tip elevation was -42.15 feet with the top of shaft at elevation +24 feet which resulted in an as-built length of 66.15 feet. Postgrouting was performed four days after shaft construction and left to cure for three days before the Statnamic load test was performed.

Load Test

Only one postgrouted shaft was tested, and the test was performed after grouting. The data for the load test are available.

Pressure Grouting

One shaft was grouted on this project. Pressure, displacement, and volume graphs for the grouting process are available.

Soil Classification

One soil boring consisting of sand, clay, and silty sand is available for the location of the postgrouted shaft.

Strain Gauge

Four levels of strain gauges were used for verification of the design side shear values. Data from toe level strain gauges are available to assess the effectiveness and uniformity of the grout bulb beneath the toe.

3.15 Gilmerton Bridge Replacement, Chesapeake, Virginia.

Postgrouting was performed on Pier 9 at the Gilmerton Bridge Replacement project in Chesapeake, Virginia. The purpose of the project was to provide a new lift span bridge over the southern branch of the Elizabeth River to replace the existing double-leaf bascule bridge that was constructed in 1938. The new bridge is 1,908 feet long with a vertical clearance of 35 feet in the closed position and up to 135 feet when the lift span is opened. The project is to be constructed in stages on the existing Military Highway alignment and will provide a bridge width of 85 feet to accommodate future widening of Military Highway from four to six lanes. Postgrouted drilled shafts installed were 12 feet in diameter and approximately 112.5 feet long.

Load Test

Only one postgrouted shaft was tested and the test was performed after grouting. The data for the load test is available.

Pressure Grouting

One shaft was grouted on this project. Pressure, displacement and volume graphs for the grouting process are available.

Soil Classification

Soil profiles consisted of 40-feet of alluvial sands followed by Yorktown formation which extended to the termination depth.

Strain Gauge

Ten levels with strain gauges were installed to evaluate shaft side shear. Results for four toe-level strain gauges are available to further assess the effectiveness/uniformity of the grout bulb beneath the toe

3.16 Peninsula Condominium, Jacksonville, Florida.

The postgrouted drilled shaft was installed in the Peninsula Condominium in Jacksonville, Florida. The drilled shaft was 36-inch in diameter and 60-feet in length and was tested using the Statnamic load testing technique.

Load Test

Only one postgrouted shaft was tested and the test was performed after grouting. The data for the load test is available.

Pressure Grouting

One shaft was grouted on this project. Pressure, displacement and volume graphs for the grouting process are available.

Soil Classification

Soil strata on the site consisted of approximately 20-feet of sand followed by 10-feet of limestone and marl to termination depth. A boring is available for each postgrouted shaft location.

Strain Gauge

Three strain gauge segments were used for side shear calculations; four toe-level strain gauges are available to further analyze the shaft.

3.17 West Rail Bypass, Brownsville, Texas.

Testing was performed on the drilled shaft located on the bent 41 at West Rail Bypass project in Brownsville, Texas. Bent 41 is supported by two 8-foot diameter drilled shafts that have been base grouted; both shafts are 8-feet in diameter and 115 feet in length. The bridge designer for this project was HNTB and the general contractor was McCarthy Building Companies, Inc. and foundation construction was performed by Weber-Balke Foundation Company.

Load Test

Two postgrouted shafts were tested and the tests were performed after grouting. The data for the load tests is available.

Pressure Grouting

Two shafts were grouted on this project. Pressure, displacement and volume graphs for the grouting process are available.

Soil Classification

Borings for this project were drilled to 165 feet below ground which was around +30 feet elevation; geotechnical subsurface profiles consisted of 67 feet of clay followed by silty sand and sandy silt to a depth of approximately 107 feet and finally sand was found to extend to the boring termination depth of 165 feet.

Strain Gauge

Four strain gauge segments were used for side shear calculations; three toe-level strain gauges are available to further analyze the shaft.

Chapter Four: Data Processing and Analysis

All collected data was digitized and re-plotted to confirm conformance with reported values. The premise of the analysis revolved around proper or improper assignment of the applied grout pressure to the design method. Artificially high field values affect the predicted load and provide a false sense of field performance. Design graphs are the result of the calculated grouted and ungrouted capacity that can be obtained based on the soil profiles. Boring log data was used to compute side resistance, anticipated grout pressure and grouted capacity using the USF method and the FDOT method described in Chapter 2. Load test versus displacement graphs were obtained directly from load test reports and are used to obtain the measured shaft capacity data used in plotting bias curves.

4.1 Data Plots

In analyzing the grouting and load test data, several types of plots were employed: tri-axis grouting plots, comparative load test plots, bias vs displacement plots and typical design plots.

4.1.1 Tri-axis Plots

Tri-axis plots represent the three quality control or quality assurance (QA/QC) thresholds used for grouted shafts. In order to validate the grouting process, all field grouting data was analyzed and graphs correlating pressure vs displacement, pressure vs volume and volume vs displacements were plotted. These were used to determine the true effective grout pressure and the peak field recorded pressure which is often caused by blockage and different from the effective pressure. Data from each site was scrutinized for possible errors or conditions by which grouting became ineffective as indicated by the red arrows in Figure 4.1 (replotted for convenience from Chapter 2).

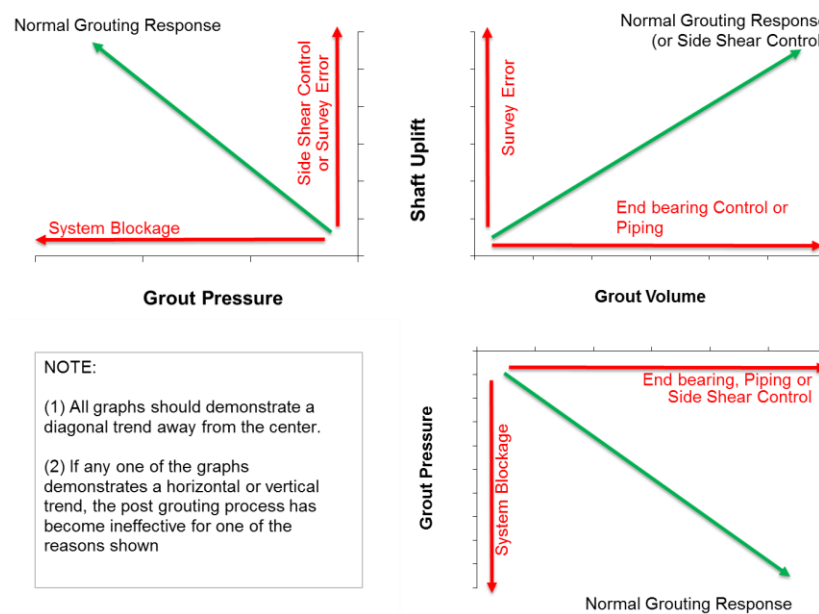


Figure 4.1 Concept tri-axis grouting effectiveness plots.

4.1.2 Design and Bias Curves

Load test (measured) data was compared to each of three prediction methods to compute the associated bias (measured/predicted) values. Prediction methods varied largely on the basis of the grout pressure which was either calculated/designer selected, or measured in the field. Field measured values were further delineated by quality of the scrutiny used (use or no use of tri-axis plots). Once all the above graphs were provided, criteria for bias design curves were established as follows:

- Effective Pressure – verified grout pressure achieved in the field (obtained from tri-axis plots). This is considered to be the most reliable.
- Maximum Field Pressure – maximum grout pressure obtained in the field. This is often not reliable but is presently used for contractual acceptance of satisfactory grouting.
- Maximum Calculated Pressure – Side shear predicted resistance is used to determine maximum grout pressure that can be withstood; determined from soil profiles (calculated from soil boring information using the highest possible / ultimate side shear predictions).

For the FDOT method, any computed end bearing capacity that exceeded the side shear predicted grout pressure was capped to equal the predicted grout pressure. Further, both the USF and FDOT end bearing capacity predictions were computed using each one of the pressure criteria above. Predicted and measured capacities were then plotted against toe displacement and the bias between the two values was found and plotted on the same graph. Finally, data was summarized and bias tables created for displacements of 0.3, 1, 2, 3, 4, and 5%D where D is the shaft diameter. Statistical analyses were performed to obtain a resistance factor versus the reliability index for each of the conditions mentioned above.

4.2 Analysis

In all, thirty-one shafts populated the database for this analysis. The data came from seventeen sites discussed in Chapter 3 and analyzed below. Each shaft was given a data set identification number. Those numbers can be found in Table 4.1. Each data set includes a summary of project circumstances, a plot of the design curves, tri-axis plots and the predicted load vs displacement response for both grouted and ungrouted scenarios. In some cases, modified or augmented tri-axis plots are provided which either use time in lieu of volume data or the displacement data is augmented with strain data, respectively. Three pressure values were identified in each case study which in turn affected the predicted design value: (1) Effective pressure, (2) Maximum field pressure, and (3) Maximum calculated pressure. Additionally, the bias (measured/predicted) is plotted vs displacement as a function of shaft diameter (in percent) for all three predicted capacity values (from each pressure).

Table 4.1 Data set shaft ID summary

Project	Data Set #	Shaft ID	Shaft Diameter (ft)	Shaft Length (ft)
Royal Park Bridge	1	LT-2	4	114.2
Royal Park Bridge	2	LT-3	4	87.4
PGA	3	LT-2	3	60
Iowa	4	TS-4	5	70
Gerald Desmond	5	TP-2	6	156
Gerald Desmond	6	TS-3C	8.2	187
Huey P Long	7	TS-1	9	184
TXDOT	8	S-2	4	22
Natchez	9	S-1	6	75
Clearwater Site I	10	FJ-1	2	15
Clearwater Site I	11	FJ-2	2	15
Clearwater Site I	12	SP-1	2	15
Clearwater Site I	13	SP-2	2	15
Clearwater Site II	14	FJ-1	2	15
Clearwater Site II	15	SP-1	2	15
Flagler	16	S-1	5	100
WPB Airport	17	S-1	4	52
Plant Daniel	18	501	5	-
Plant Daniel	19	528	5	-
Plant Daniel	20	530	5	-
Southern 80 SR	21	S-1	4	-
Southern 80 SR	22	S-2	4	-
Southern 80 SR	23	S-3	5.2	-
Overland	24	S-1	6	72
Overland	25	S-2	6	72
Overland	26	S-3	6	72
Carolina Bay	27	S-1	4.66	66.15
Gilmerton	28	S-1	12	112.5
Peninsula	29	S-1	3	60
West Rail	30	41E	8	115
West Rail	31	41W	8	115

4.2.1 Data Set 1, Royal Park Bridge (RPB) LT-2

No design pressure was noted in the grouting and load testing report but figure 4.2 gives the design curves which provides a maximum design grout pressure for the test shaft length.

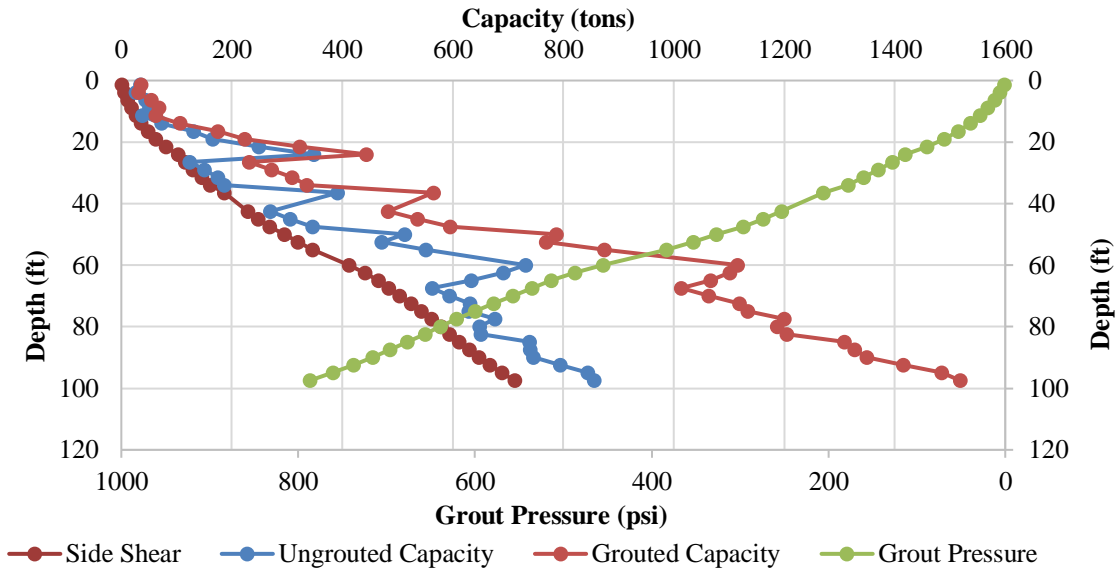


Figure 4.2 Data set 1 design curves.

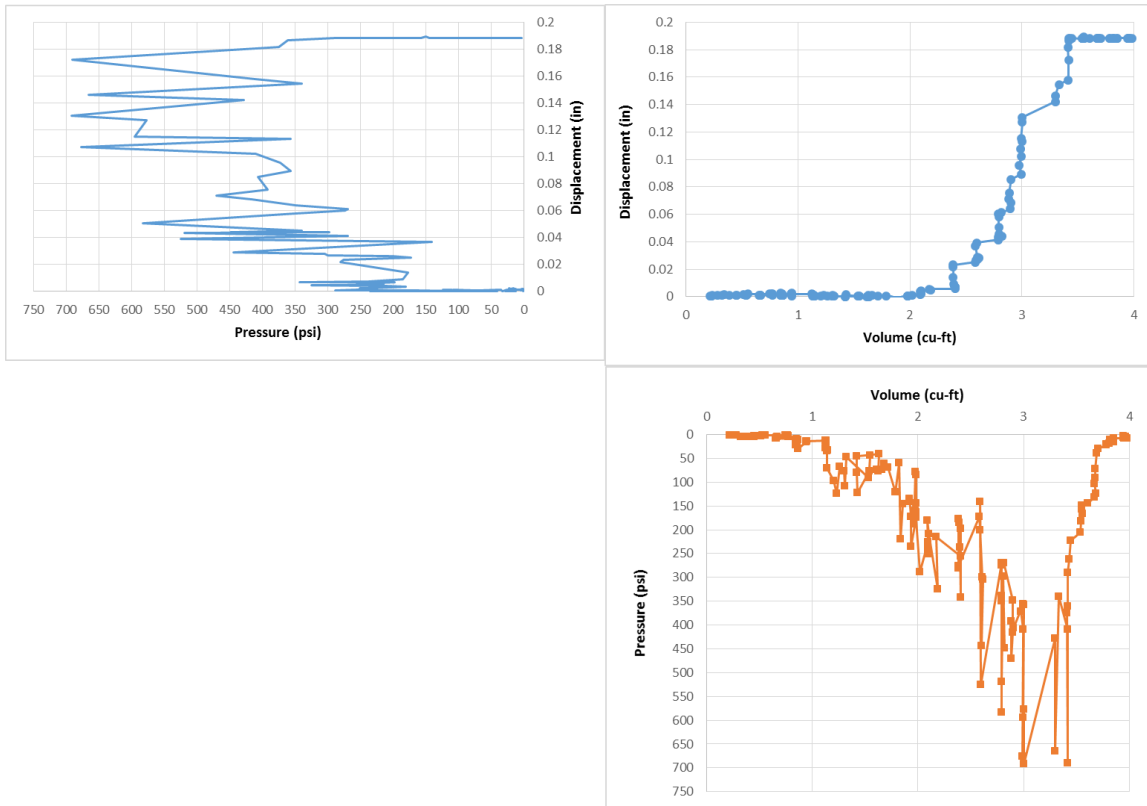


Figure 4.3 Data set 1 tri-axis plots.

As noted in Figure 4.1, horizontal data lines in volume vs. pressure graph indicate an end bearing failure or grout loss to a surrounding void or cavern. This should be supported with a similar horizontal line in the volume vs. displacement graph. In this case, the horizontal lines occur at near zero pressure making the volume data suspicious although after the grouting event. Similarly unusual, is the increase in displacement as pressure decreases noted in the pressure vs. displacement graph. No explanations for the anomalous end of grouting conditions are presented, but this would be usually attributed to survey or reference beam disturbance. The max effective pressure was taken at 400 psi; peak measured pressure was 700 psi. Design pressure was 787 psi.

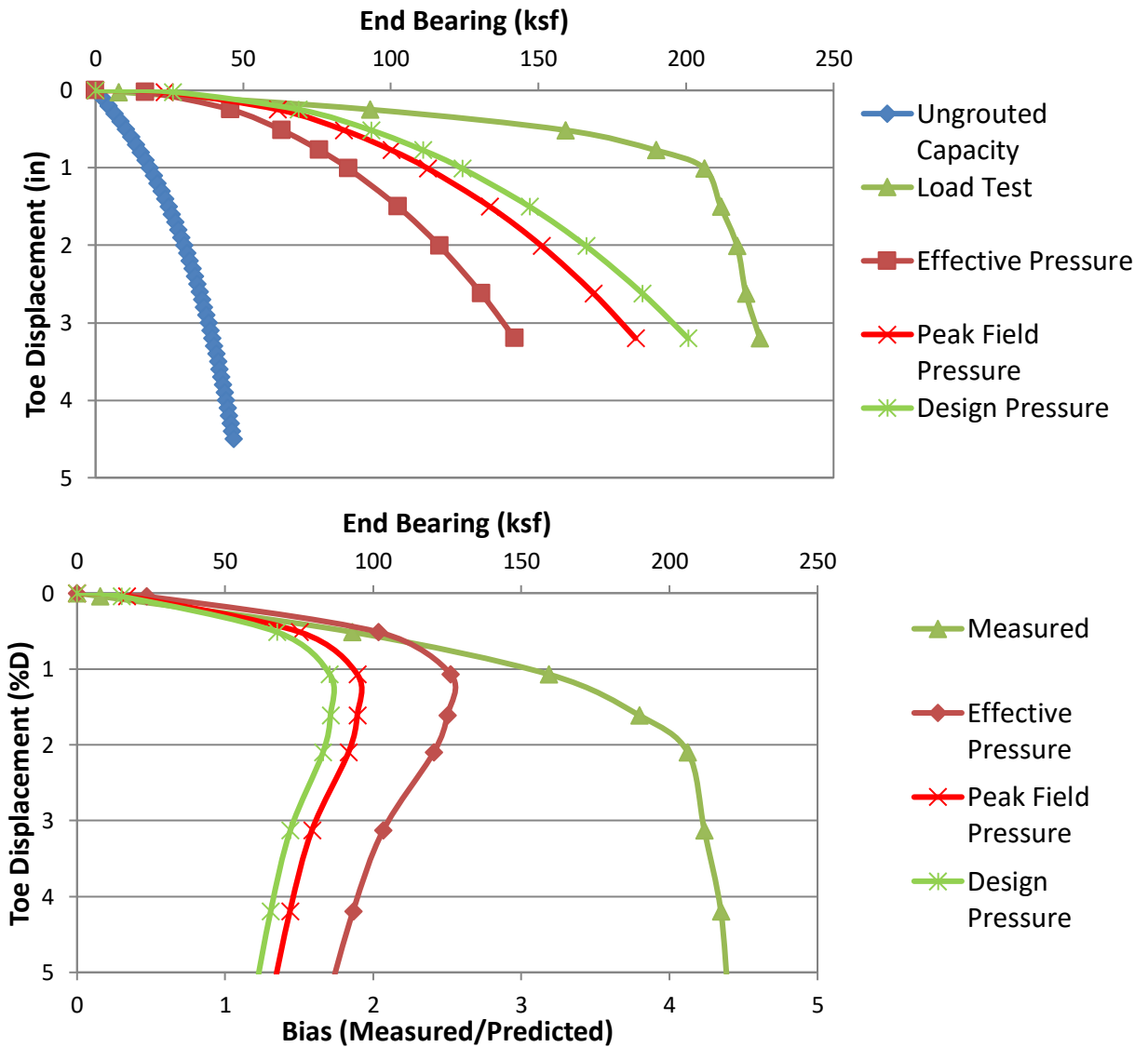


Figure 4.4 Data set 1 predicted/design and load test response (top); bias vs disp. (bottom).

4.2.2 Data Set 2, Royal Park Bridge (RPB) LT-3

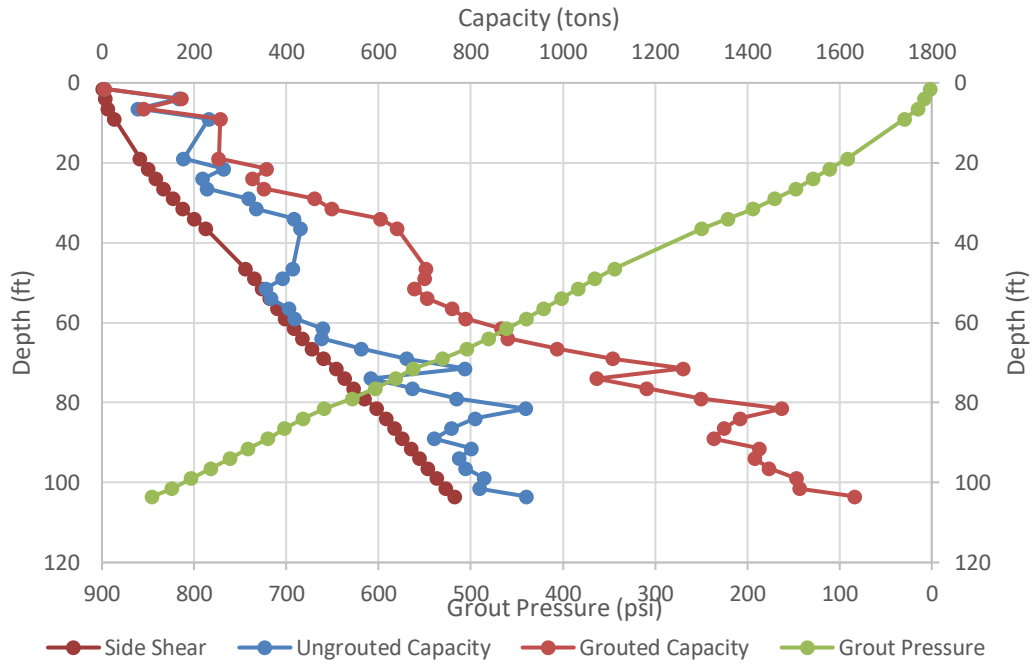


Figure 4.5 Data set 2 design curves.

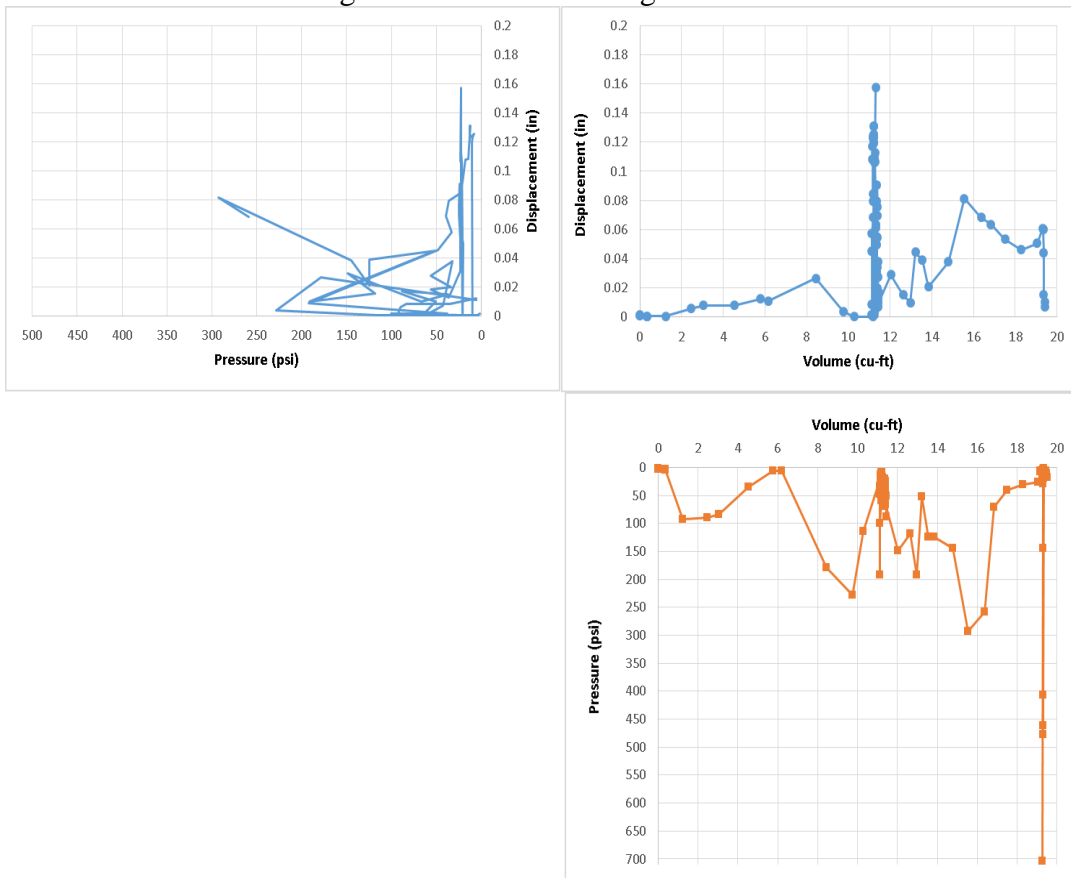


Figure 4.6 Data set 2 tri-axis plots.

As outlined in Figure 4.1, vertical data lines in displacement indicate a survey error if supported by similar features in both the volume vs. displacement and pressure vs. displacement graphs. This data set supports that type of error. At approximately 11.3 cu. ft. the displacement data original jumped 0.16-in without a commensurate increase in volume. These graphs have been replotted with an assumed displacement offset to account for this error. The maximum effective pressure was taken at 300 psi as at that point an increase in volume accompanied the increase in pressure. The peak recorded pressure was taken at 700 psi which occurred at the point where a vertical line in the data is observed in the pressure vs. volume graph. Again, as noted in Figure 4.1, this indicates an error in grouting which is common for a blocked grouting line.

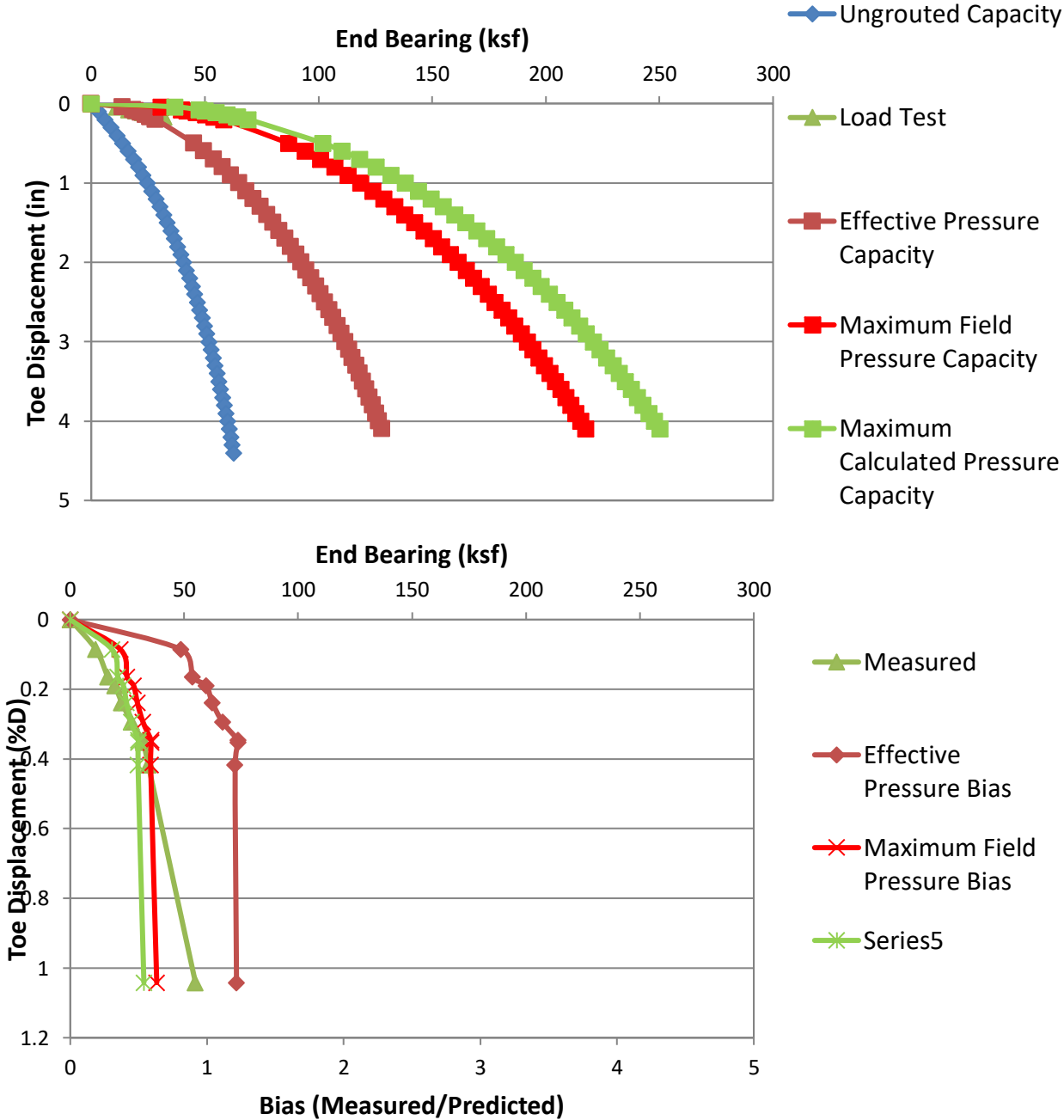


Figure 4.7 Data set 2 predicted/design and load test response (top); bias vs disp. (bottom).

4.2.3 Data Set 3, PGA Boulevard- LT-2

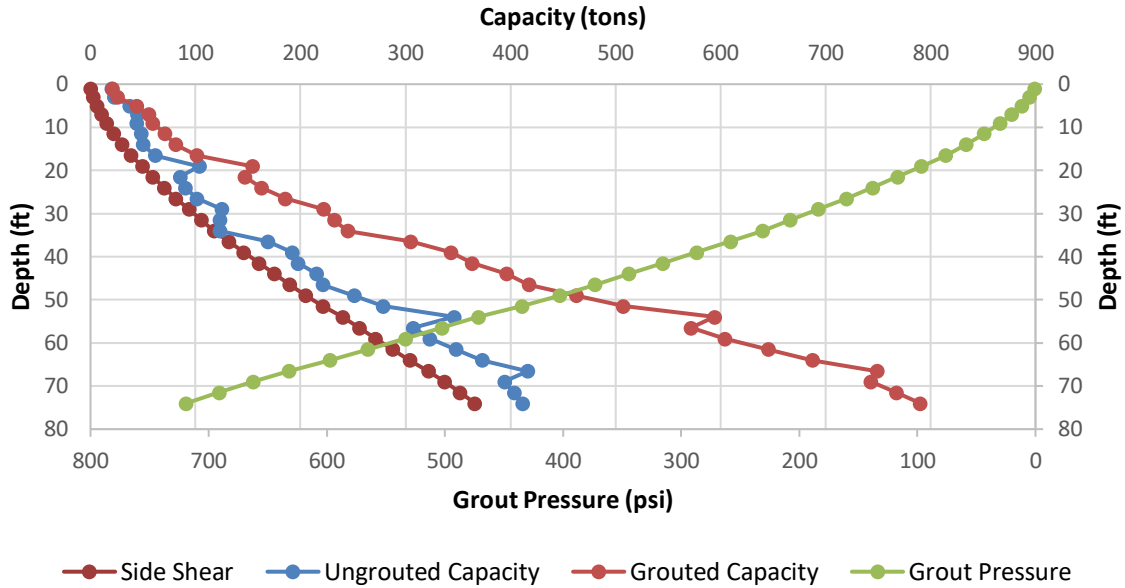


Figure 4.8 Data set 3 design curves.

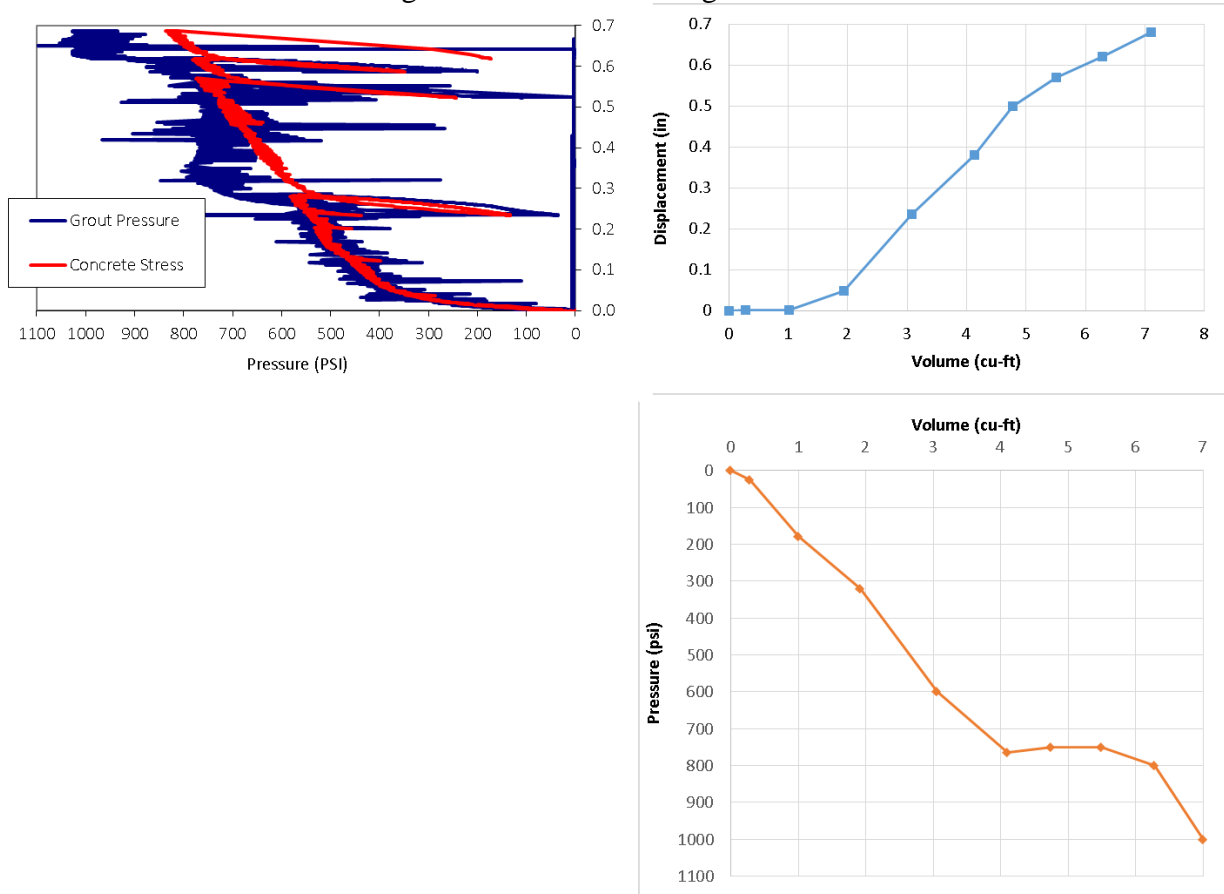


Figure 4.9 Data set 3 augmented tri-axis plots.

Figure 4.9 shows the tri-axis grouting quality assurance plots for shaft LT-2 and where no grouting / data collections errors occurred. This conclusion is based on the additional information offered by toe level strain gauges used to delineate side shear from end bearing during the load test. During grouting, however, concrete stress at the toe correlated well to grout pressure up to 600 psi. The effective pressure was taken at 750 psi where a flat pressure/volume response corresponded to a vertical press/disp. response. Peak pressure was 1,097 psi. Grouting was terminated from a ruptured grout line but well above the anticipated side shear predicted pressure of 719 psi.

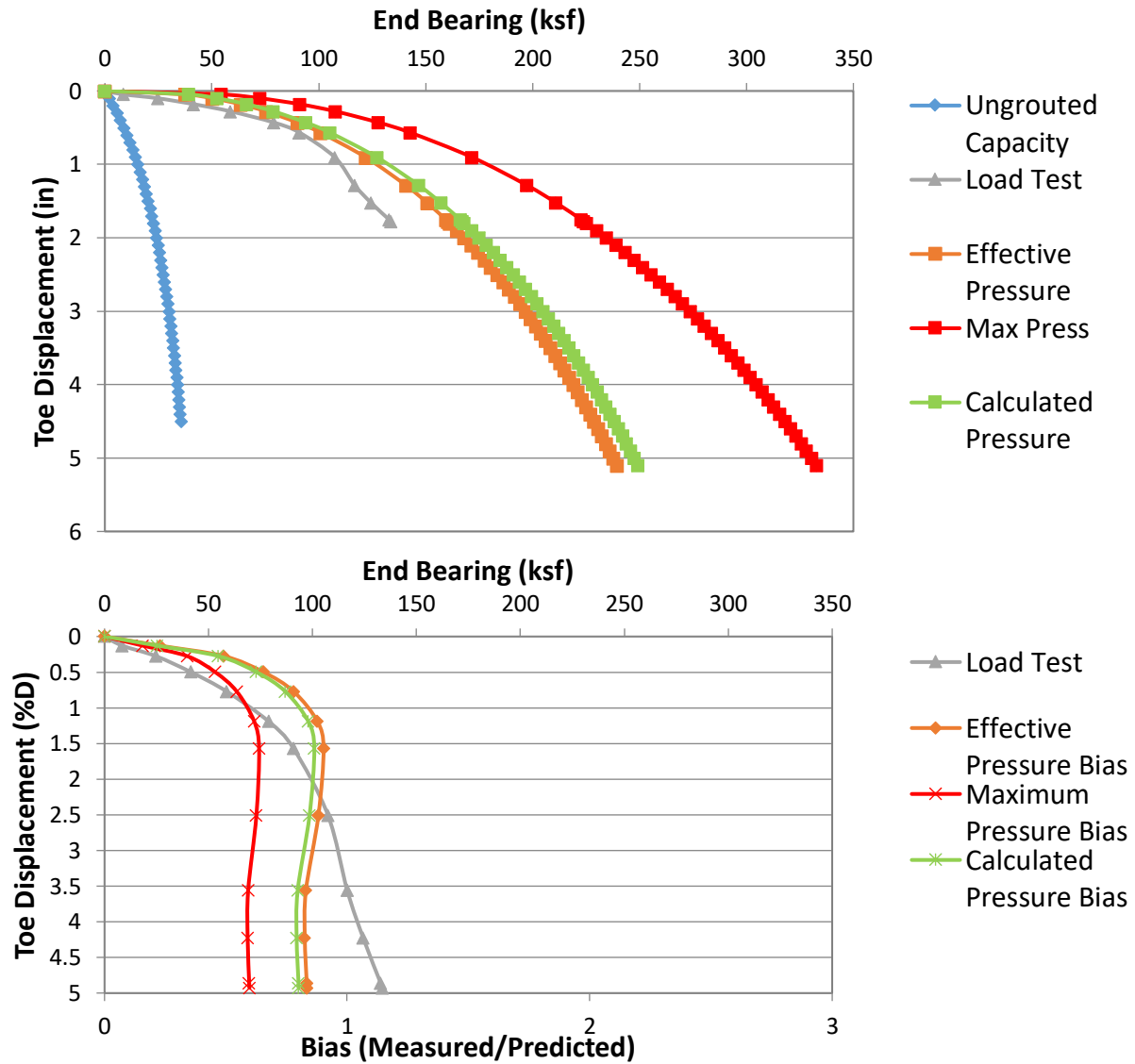


Figure 4.10 Data set 3 predicted/design and load test response (top); bias vs disp. (bottom).

4.2.4 Data Set 4, Iowa Broadway Bridge Viaduct Improvements – TS-4

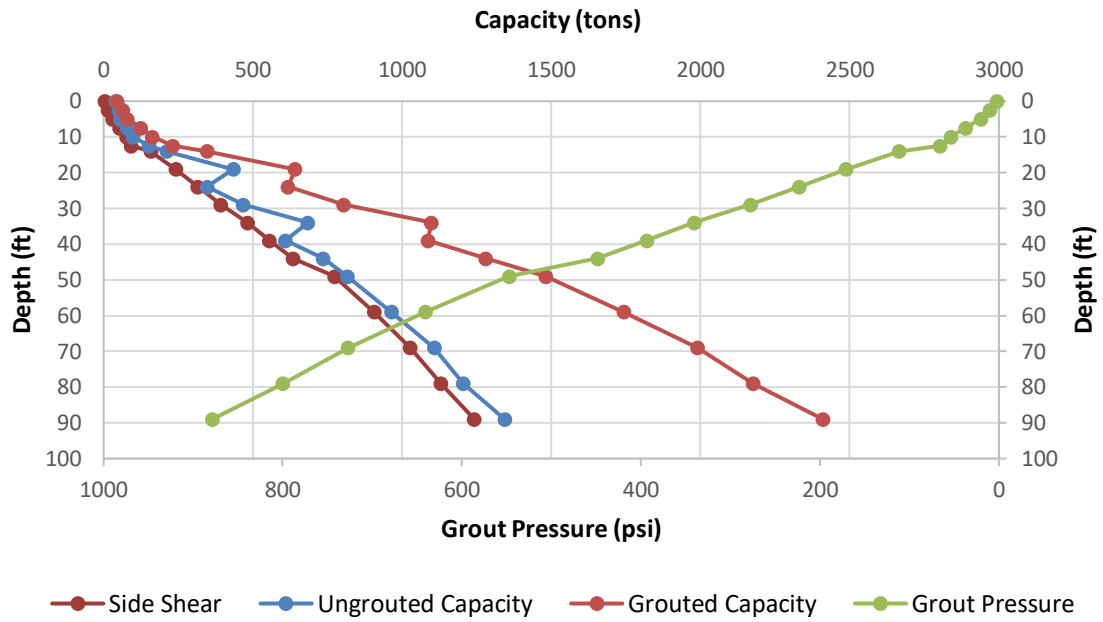


Figure 4.11 Data set 4 design curves.

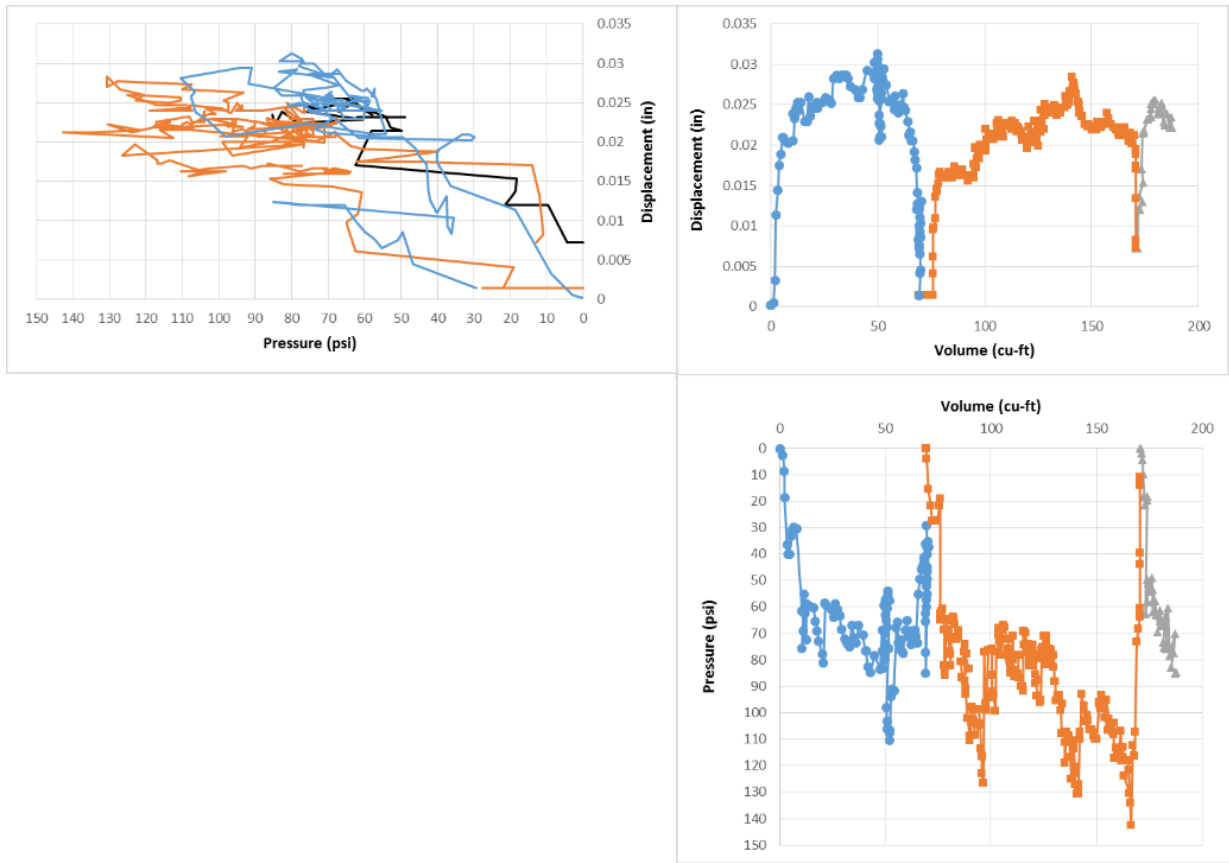


Figure 4.12 Data set 4 tri-axis plots.

Figure 4.12 shows the tri-axis effectiveness plots for data set 4. Grouting was performed in three stages. The first stage shows an end bearing / piping grouting failure where both the press/vol and press / disp. show a horizontal trend. Cycle 2 shows the same response after a slight increase in grout pressure. Cycle 3 shows no effective grouting as both the highest pressure and uplift were not achieved from the previous cycle. Recall, uplift is the best measure of global force application as the shaft is responding to toe load. For cycle 3 the same level of uplift was not achieved. The effective grout pressure was taken from the first cycle (80 psi) as the second cycle did not align with the press/vol of the previous cycle, hence the grout bulb was smaller than the original and eventually demonstrated end bearing/ piping grouting phenomenon. Max pressure of 142 psi was selected for the statistical evaluation used in this study.

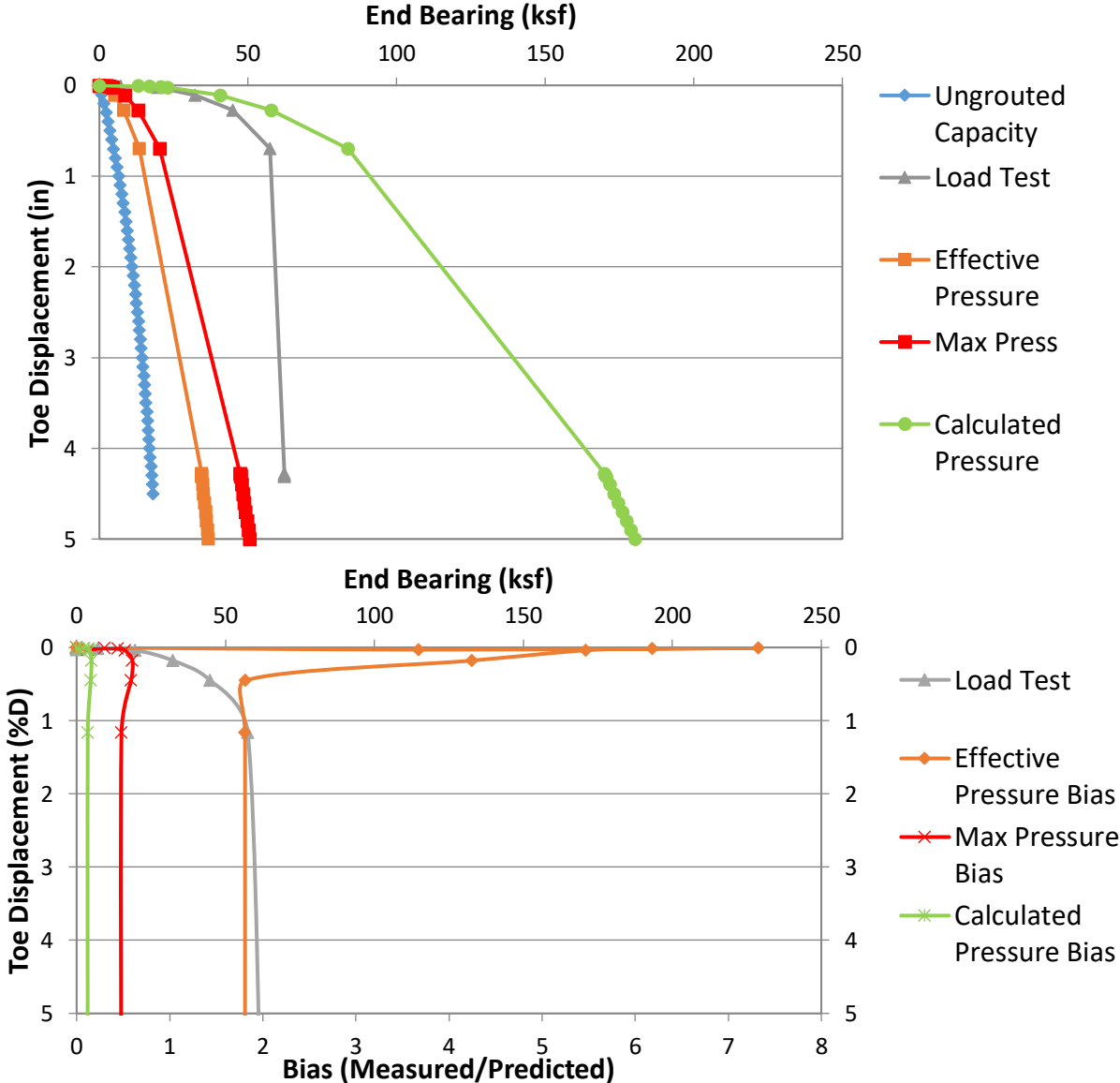


Figure 4.13 Data set 4 predicted/design and load test response (top); bias vs disp. (bottom).

4.2.5 Data Set 5, Gerald Desmond Bridge, TP-2

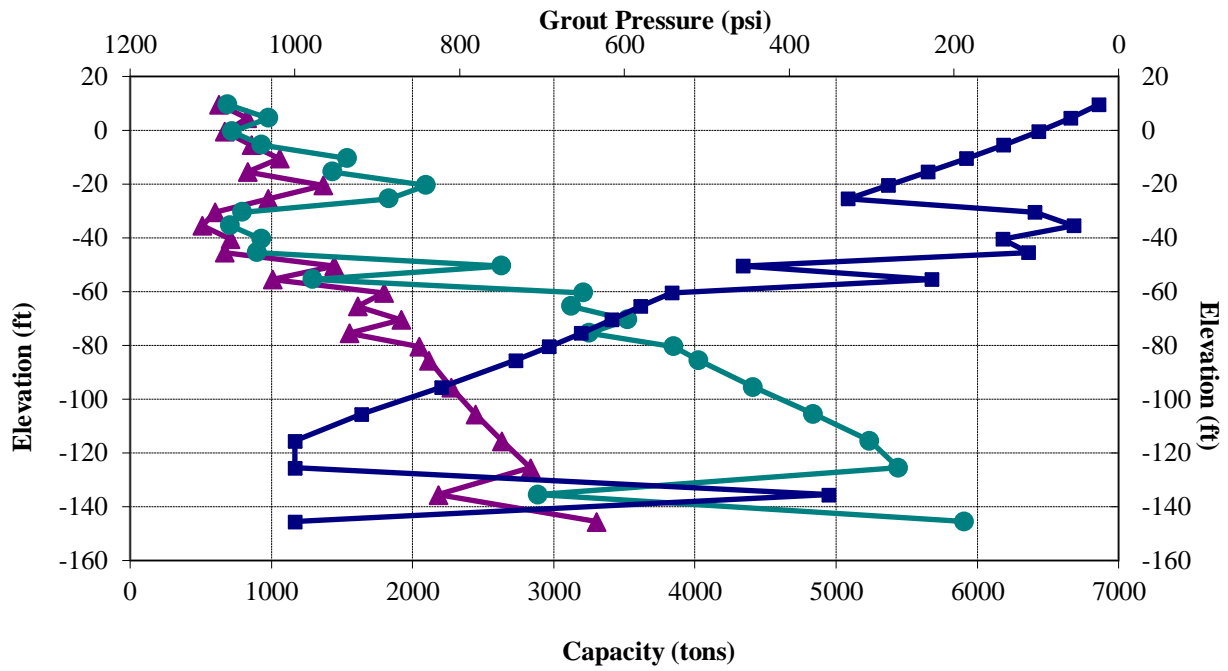


Figure 4.14 Data set 5 design curves.

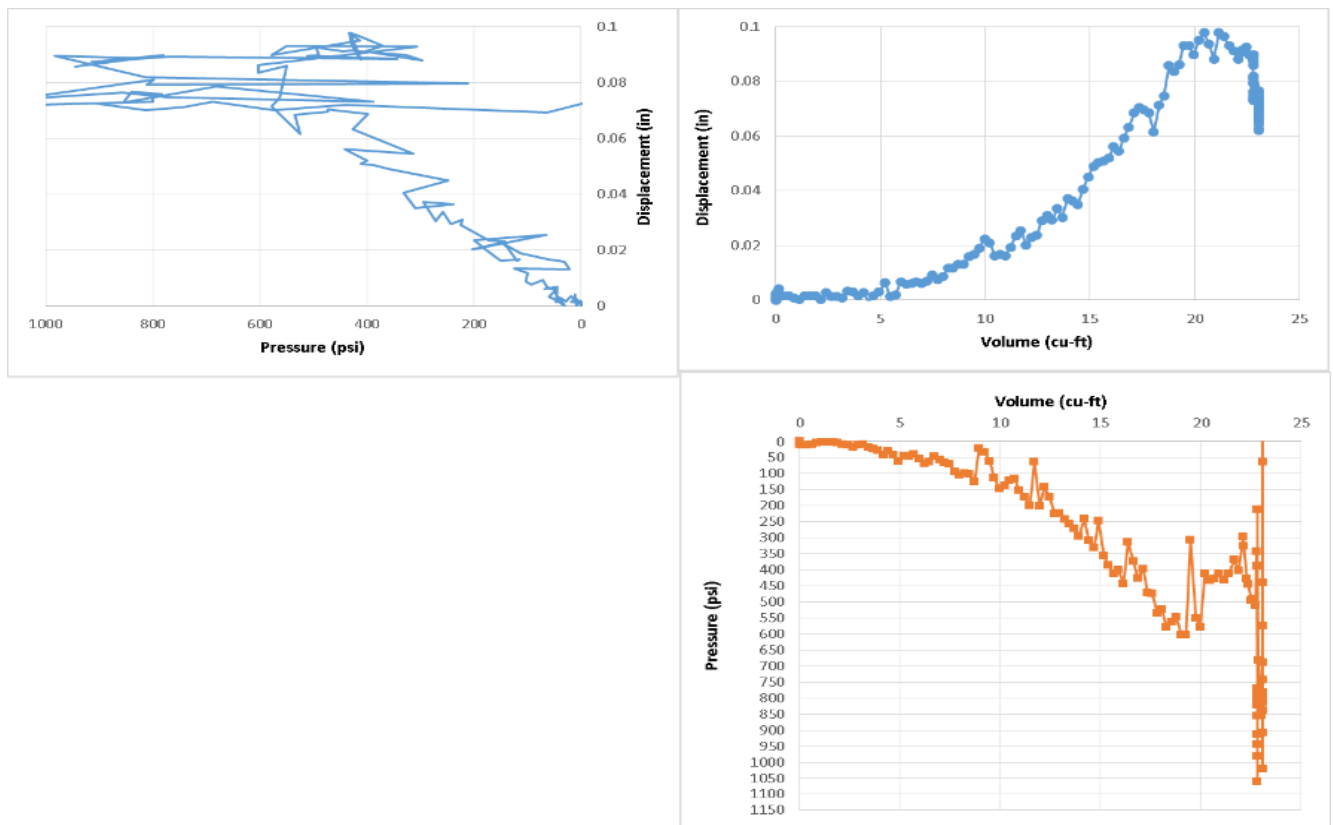


Figure 4.15 Data set 5 tri-axis plots.

Figure 4.15 shows the tri-axis plots for data set 5 and indicates two issues only visible when using the effectiveness plots. Both the pressure vs. volume and volume vs. displacement show horizontal trends supporting end bearing failure or piping at around 600 psi. Both the pressure vs. volume and pressure vs. uplift show spikes in pressure without an associated uplift or volume increase which indicates a grout line blockage at the end of grouting. Effective pressure could be argued to be either 600 or 450 psi. The 600 psi value was legitimately achieved during effective grouting, but that pressure could not be maintained with additional volume which suggests a change in soil structure beneath the shaft tip. The ensuing 400 psi value was sustainable up to the point where the grout line became blocked and spiked a maximum field recorded pressure of 1,060 psi. Effective pressure was taken at 400 psi. Based on shaft length, tip area, and soil strength, the maximum calculated grout pressure was 1,000 psi.

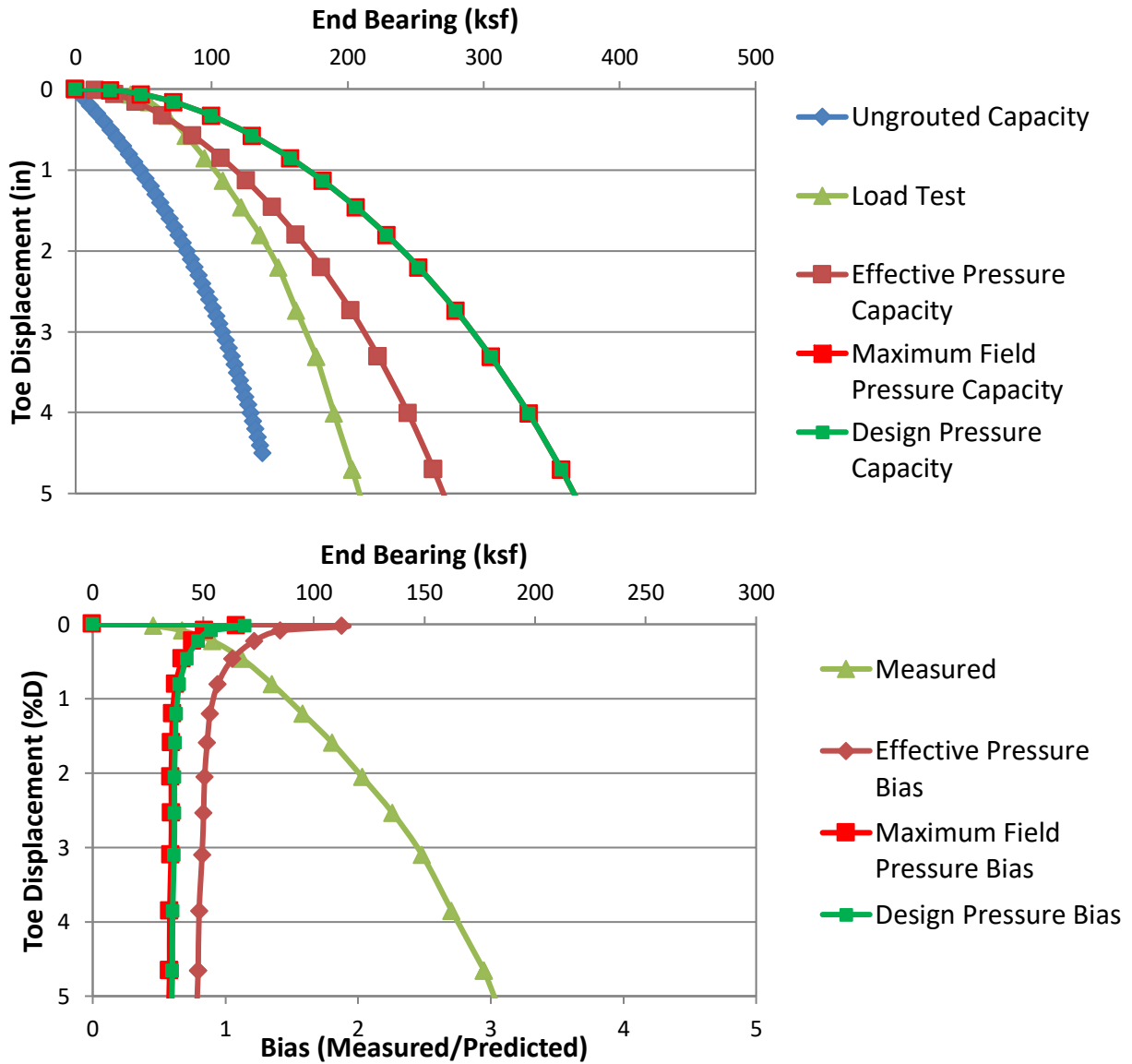


Figure 4.16 Data set 5 predicted/design and load test response (top); bias vs disp. (bottom).

4.2.6 Data Set 6, Gerald Desmond Bridge, TS-3C

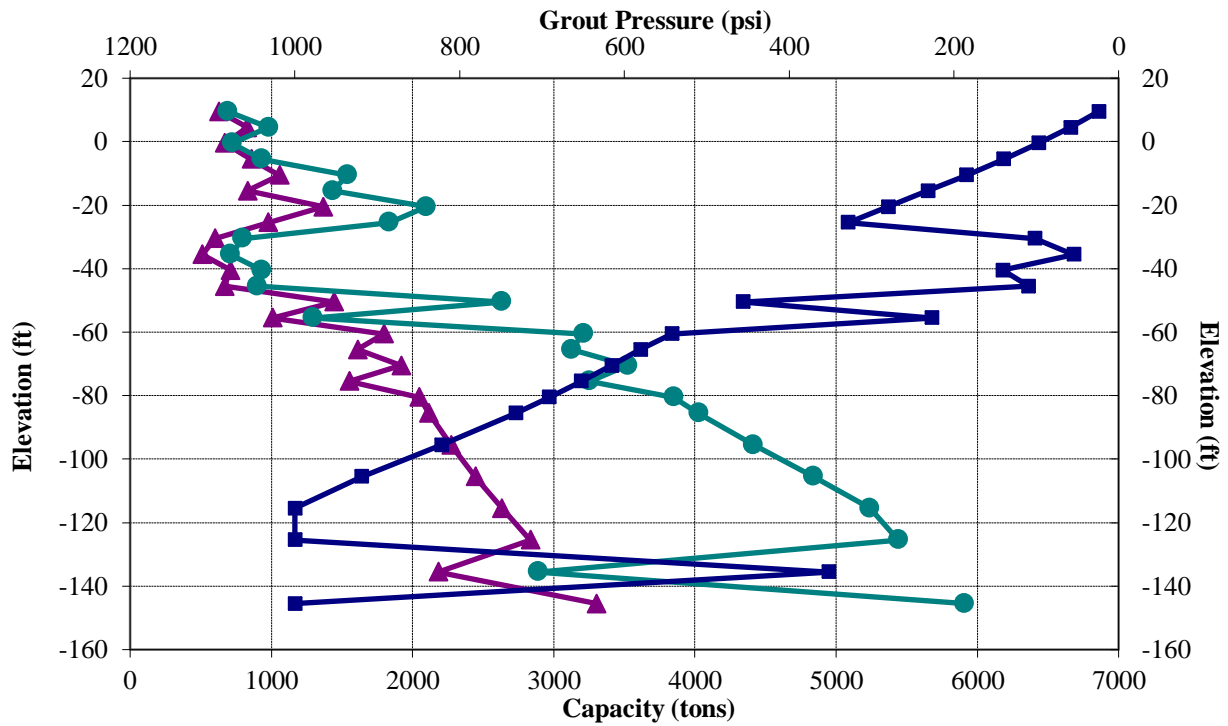


Figure 4.17 Data set 6 design curves.

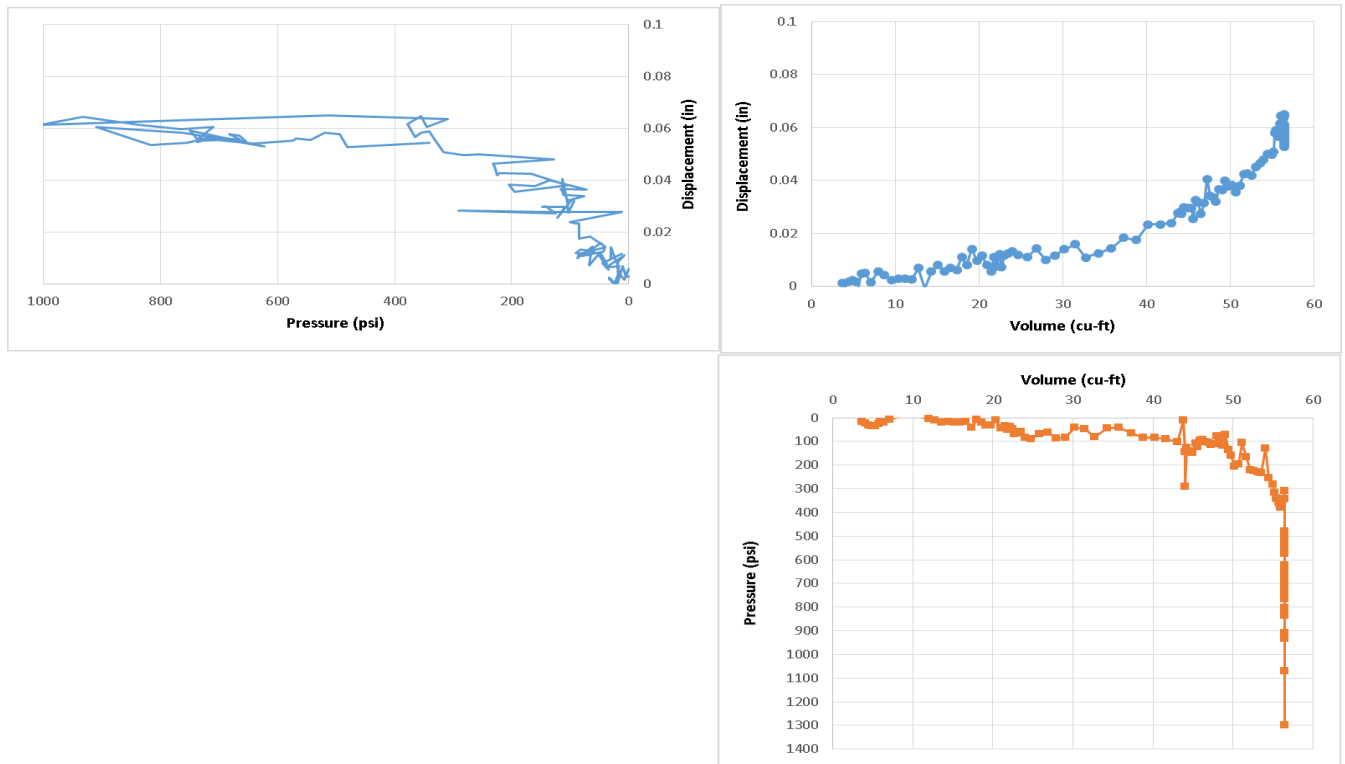


Figure 4.18 Data set 6 tri-axis plots.

Figure 4.18 shows the tri-axis plots for data set 6. Again, using the Figure 4.1 criteria for effective / ineffective grouting, the vertical pressure spike in the pressure vs. volume graph coupled with the horizontal pressure spike in the pressure vs. displacement plot confirm grouting became ineffective due to system blockage. The effective pressure was 350 psi and maximum field recorded pressure was 1,300 psi.

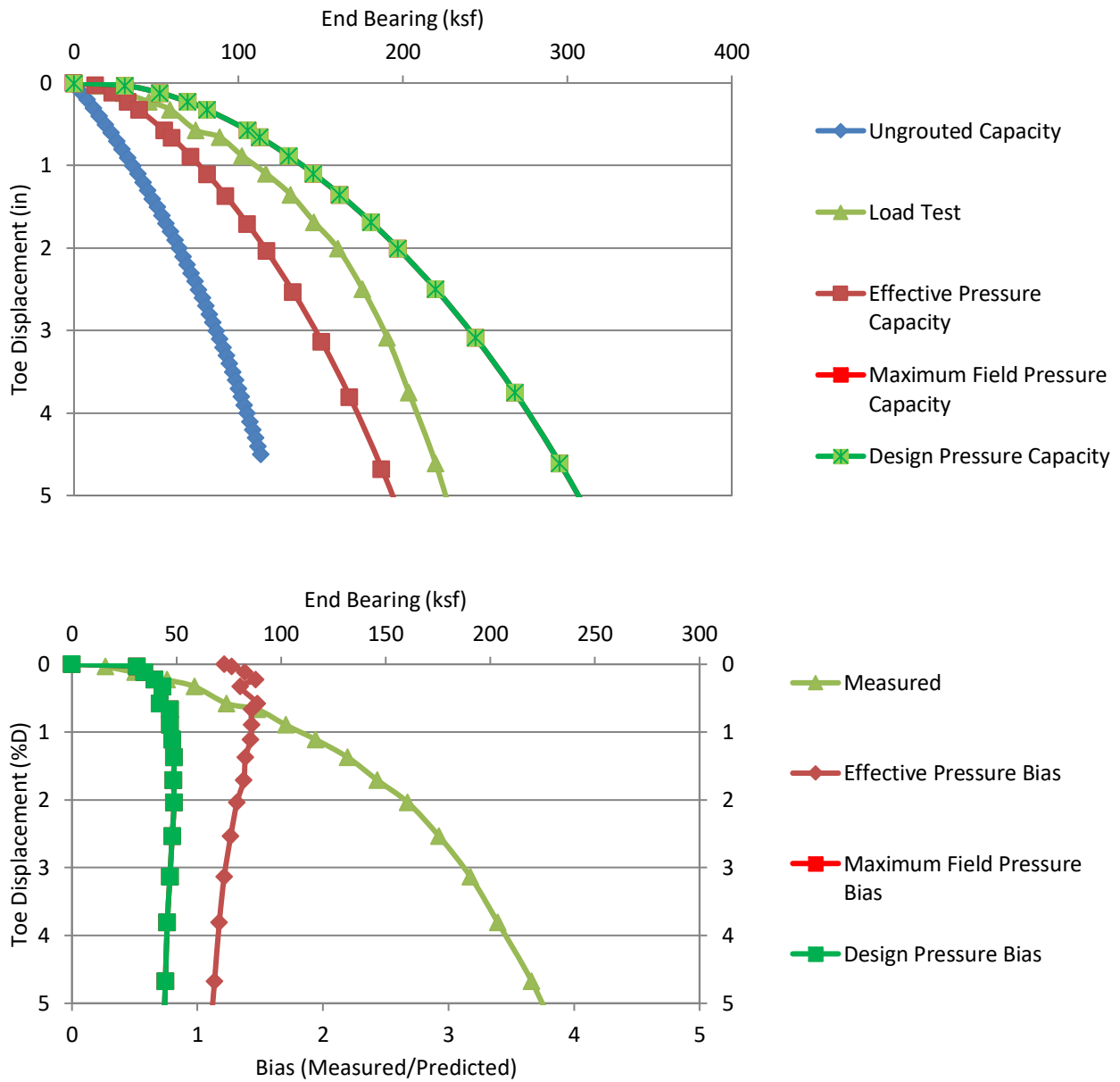


Figure 4.19 Data set 6 predicted/design and load test response (top); bias vs disp. (bottom).

4.2.7 Data Set 7, Huey P. Long Bridge

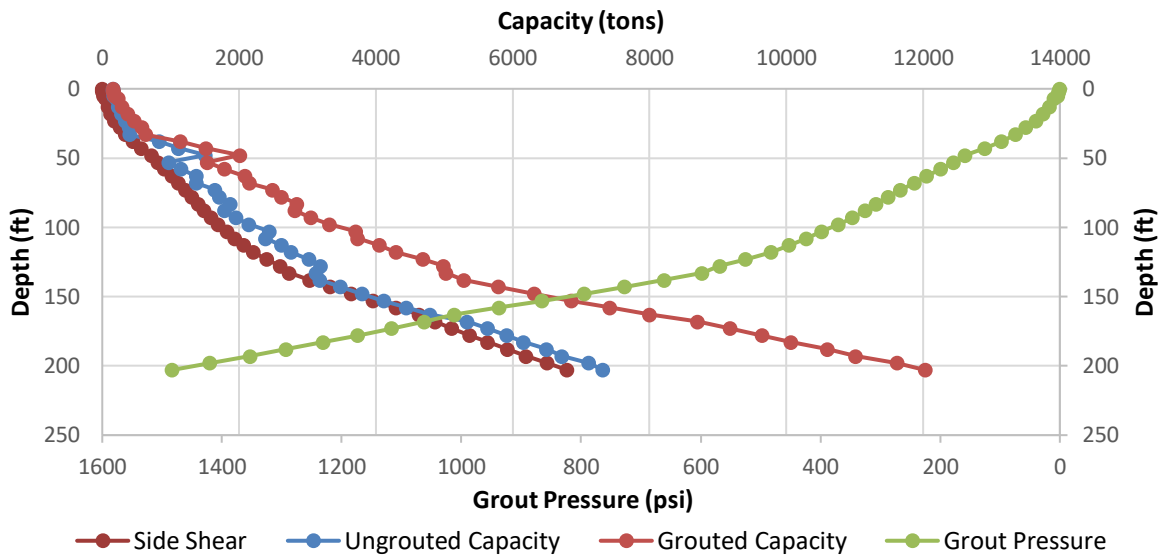


Figure 4.20 Data set 7 design curves.

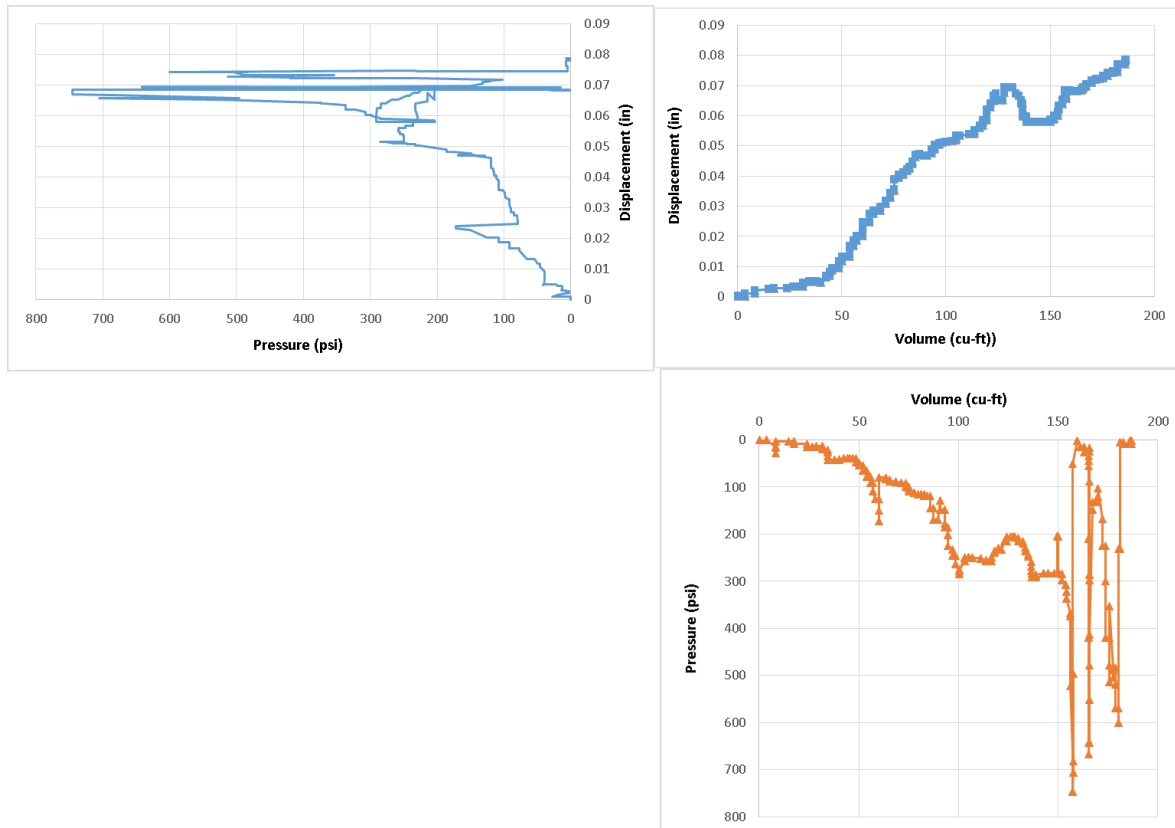


Figure 4.21 Data set 7 tri-axis plots.

Figure 4.21 shows the tri-axis plots for the data set 7 grouting program. Again, using the Figure 4.1 criteria for ineffective grouting, the vertical pressure spike in the pressure vs. volume graph coupled with the horizontal pressure spike in the pressure vs. volume plot confirm grouting became ineffective at pressure levels above 300 psi. Additionally, there is a peculiar increase in displacement and volume with near zero pressure which should not be considered to be valid; increases in volume beyond the 300 psi time frame are likely due to the volume used to clear the line or change grouting lines. Peak field recorded pressure was 750 psi. Side shear restricted design pressure was 276 psi. The 184-foot shaft length provided for up to 1,230 psi of calculated grout pressure (beyond practical limits usually imposed by equipment).

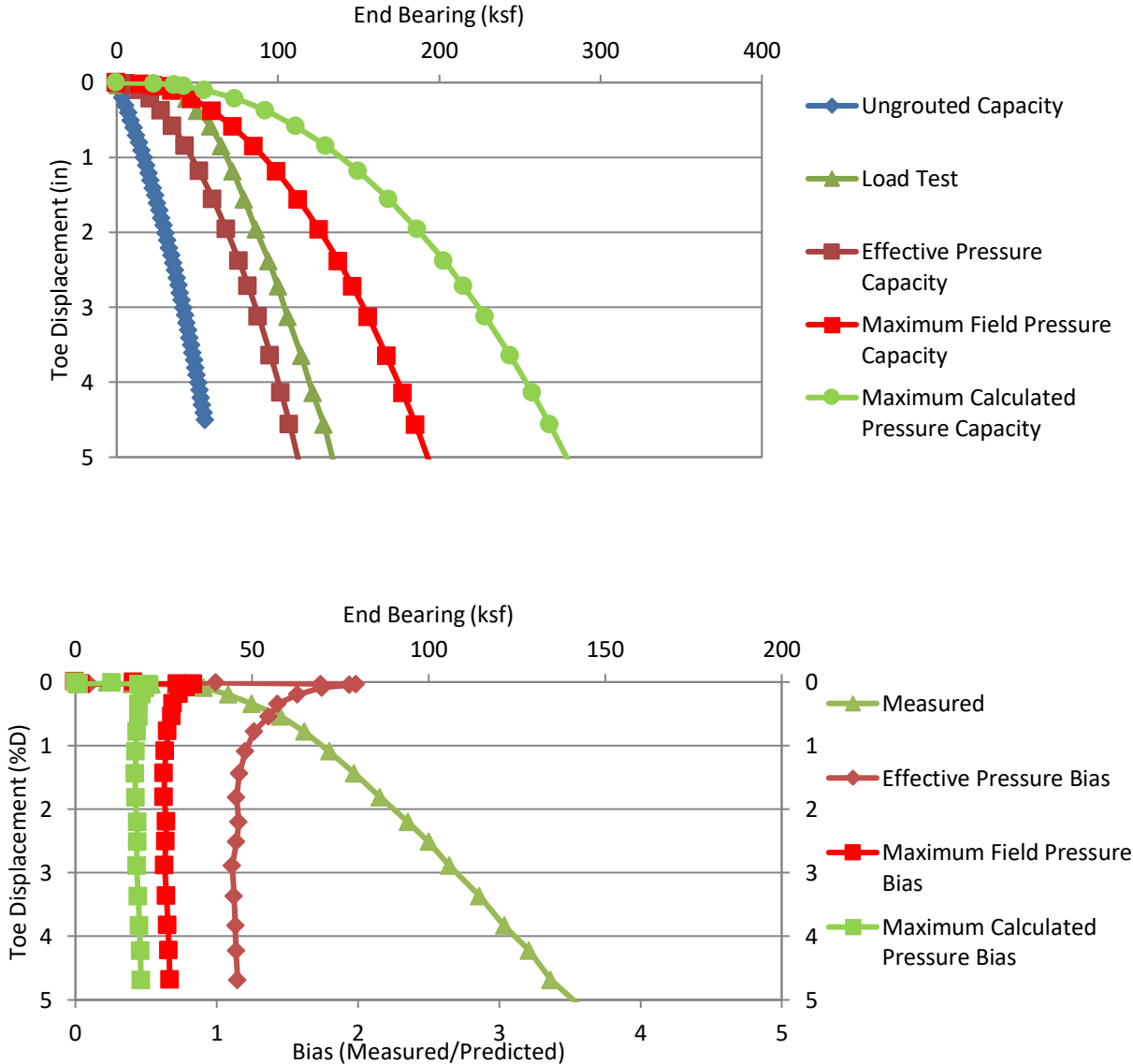


Figure 4.22 Data set 7 predicted/design and load test response (top); bias vs disp. (bottom).

4.2.8 Data Set 8, The University of Houston (UH), S-2

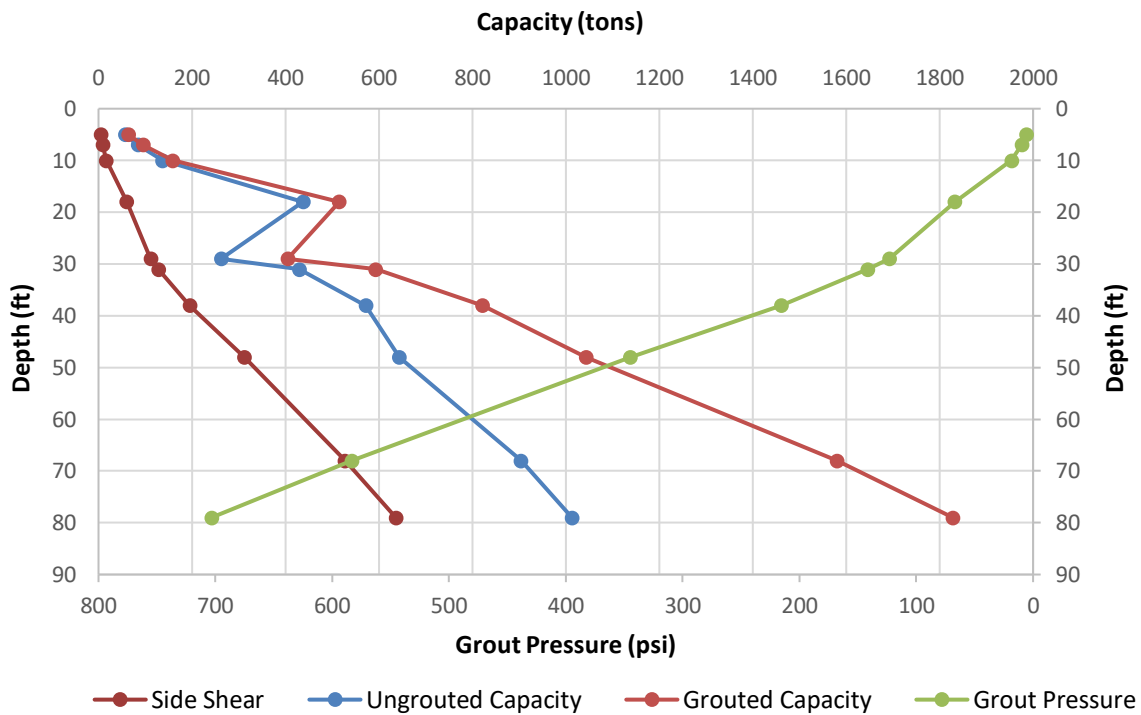


Figure 4.23 Data set 8 design curve based on 1 in displacement.

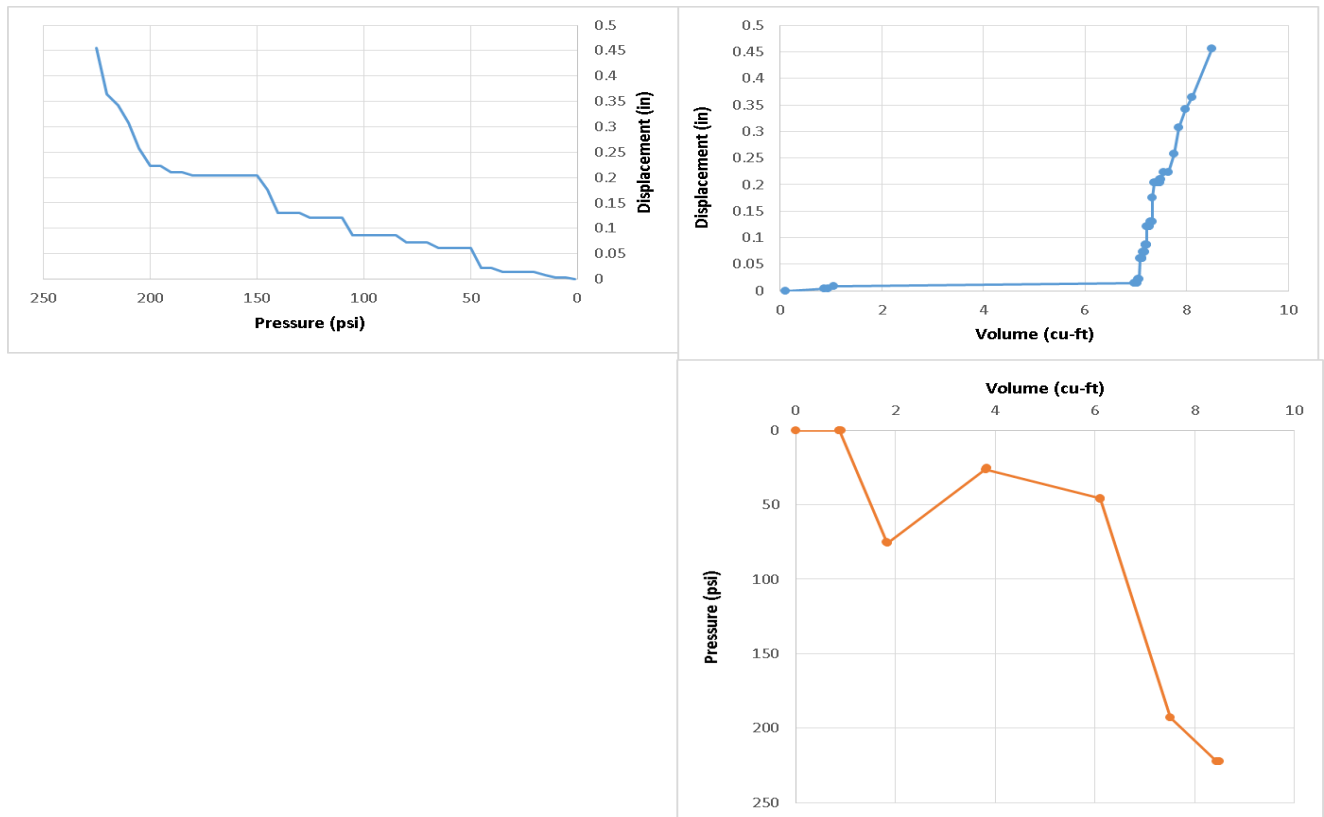


Figure 4.24 Data set 8 tri-axis plots.

Figure 4.24 shows the tri-axis grouting quality assurance plots for data set 8 and where no grouting or data collections errors can be seen. As noted in Figure 4.1, a vertical data lines in volume vs. displacement graph indicates a side shear failure which is presented in the pressure vs. displacement graph. The max effective pressure can be taken at 225 psi based solely on the negative effects on side shear. For end bearing computations, 230 psi could be legitimately selected as the effective pressure for the anticipated end bearing and for the peak pressure. Design pressure was 95 psi.

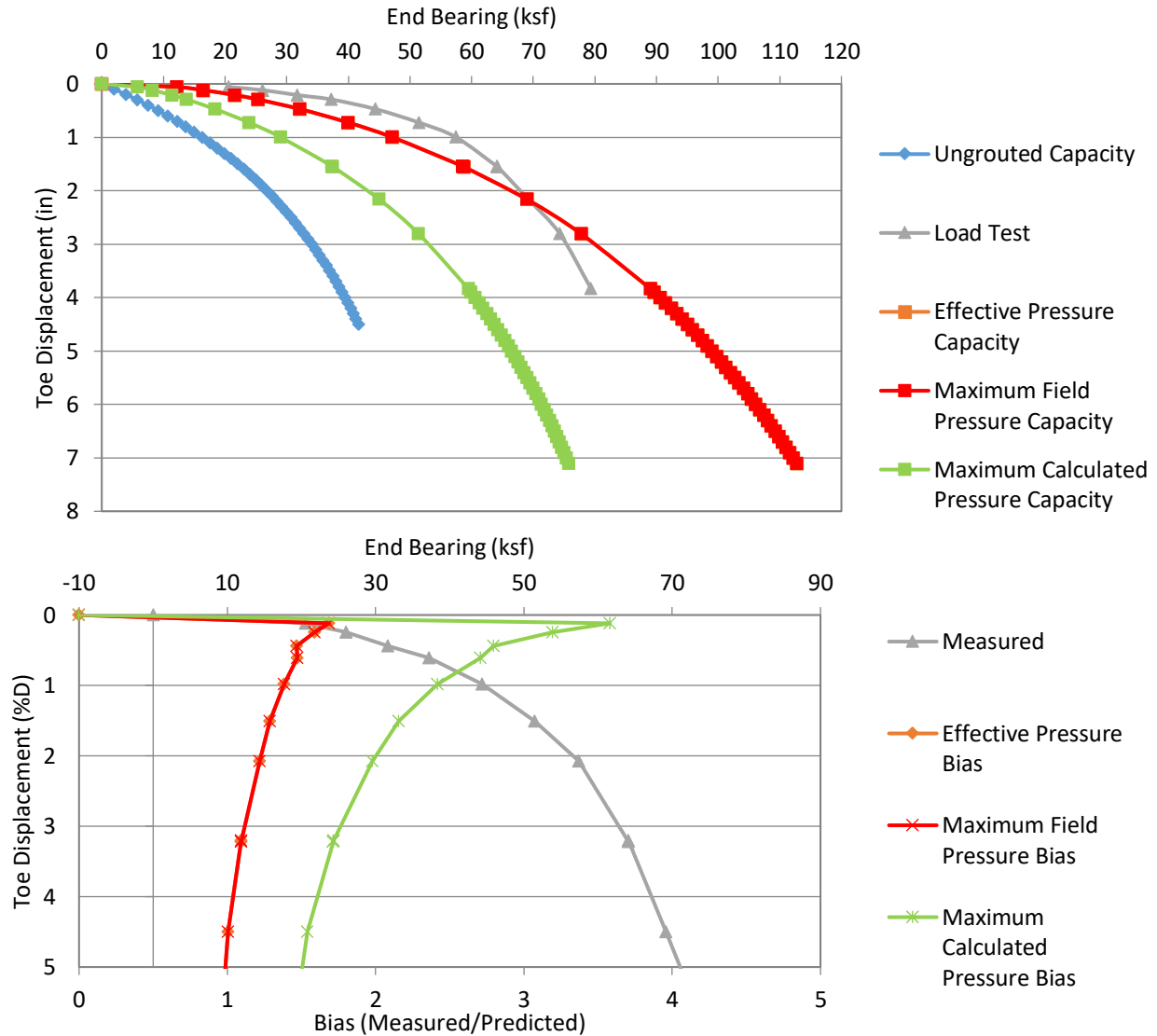


Figure 4.25 Data set 8 predicted/design and load test response (top); bias vs disp. (bottom).

4.2.9 Data Set 9, Natchez Trace Parkway Bridge, S-1

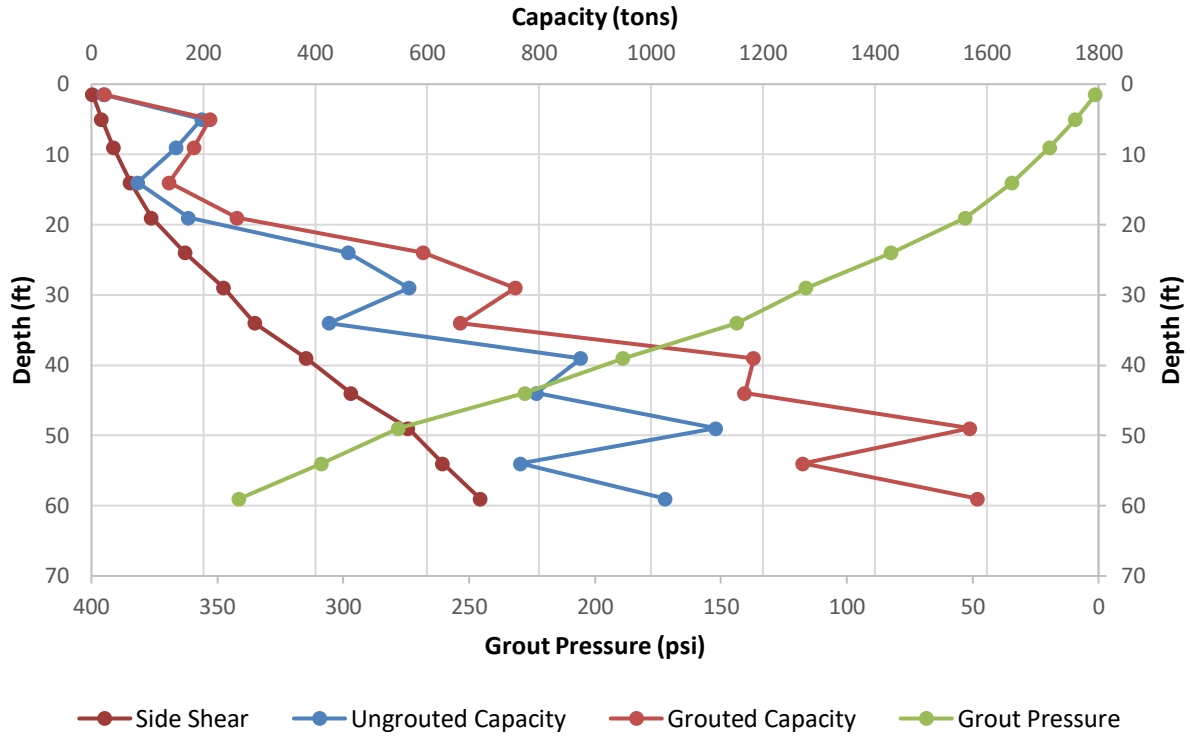


Figure 4.26 Data set 9 design curves.

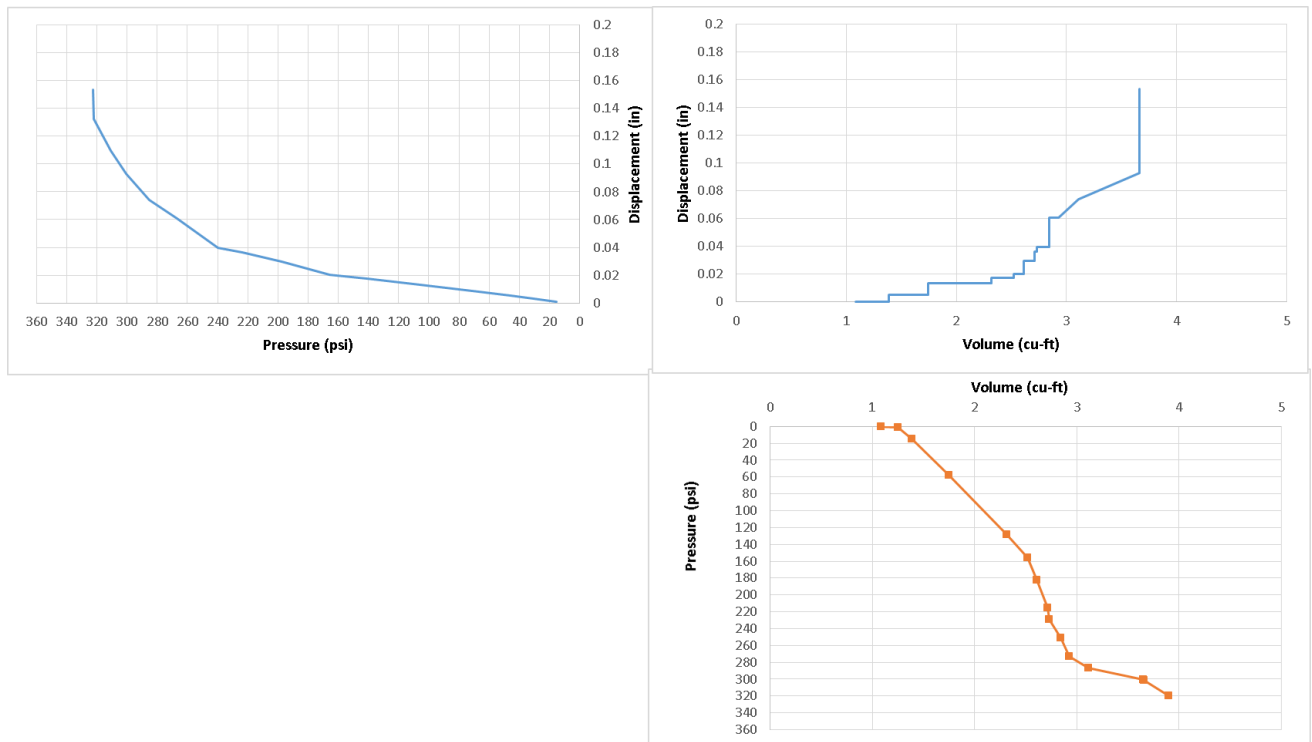


Figure 4.27 Data set 9 tri-axis plots.

Figure 4.27 shows the grouting quality assurance plots for data set 9. As noted in Figure 4.1, the vertical line in the press/disp. graph at the end of grouting indicates near or full side shear failure, however, the press/vol graph showed no additional volume increase but with increasing displacement. This physical impossibility denotes an error in survey/disp. data. The pressure/vol relationship was unaffected by the displacement error and the max effective pressure can be taken at approximately 320 psi which was also the peak measured pressure.

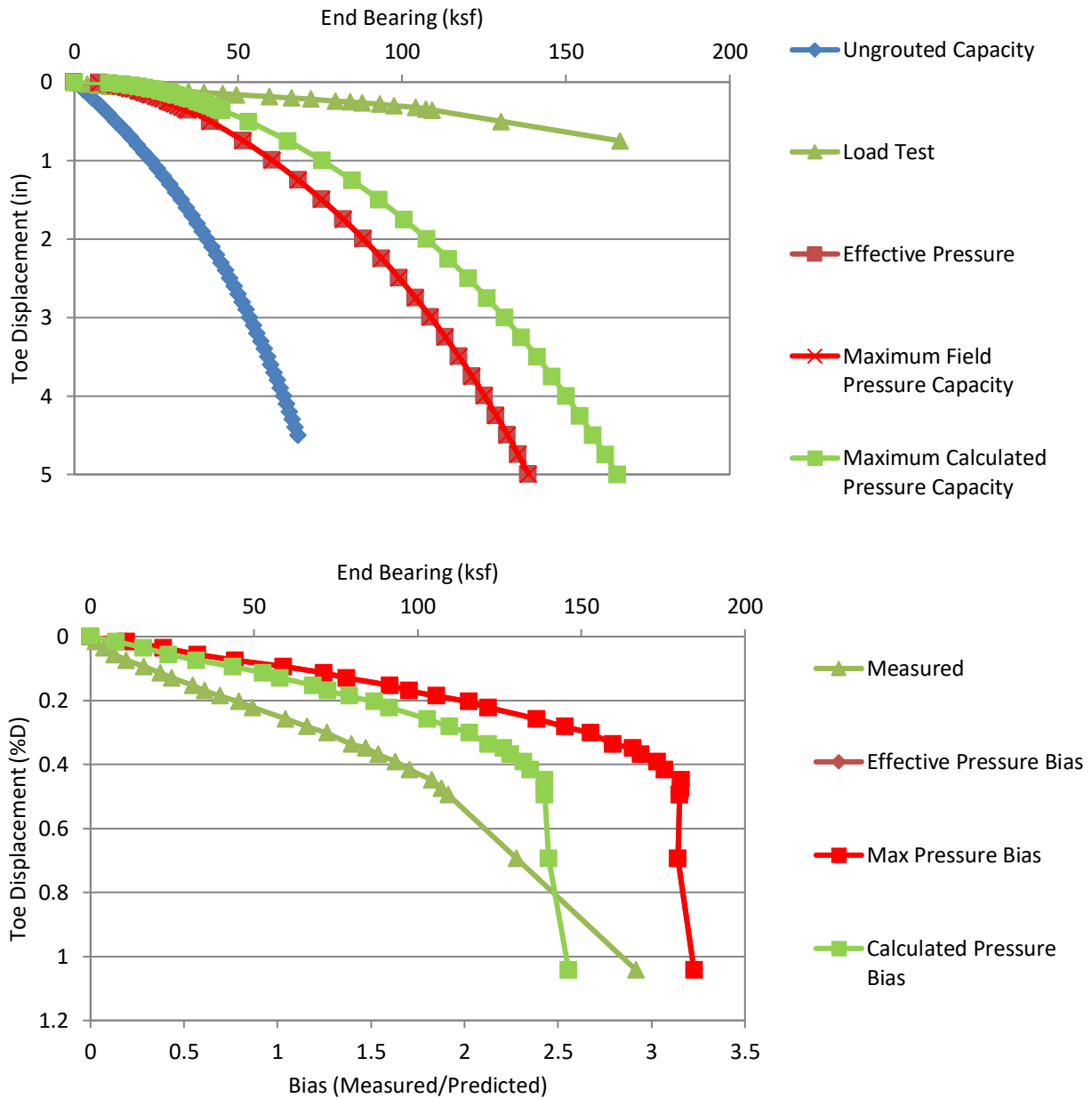


Figure 4.28 Data set 9 predicted/design and load test response (top); bias vs disp. (bottom).

4.2.10 Data Set 10, Clearwater Site I, FJ-1

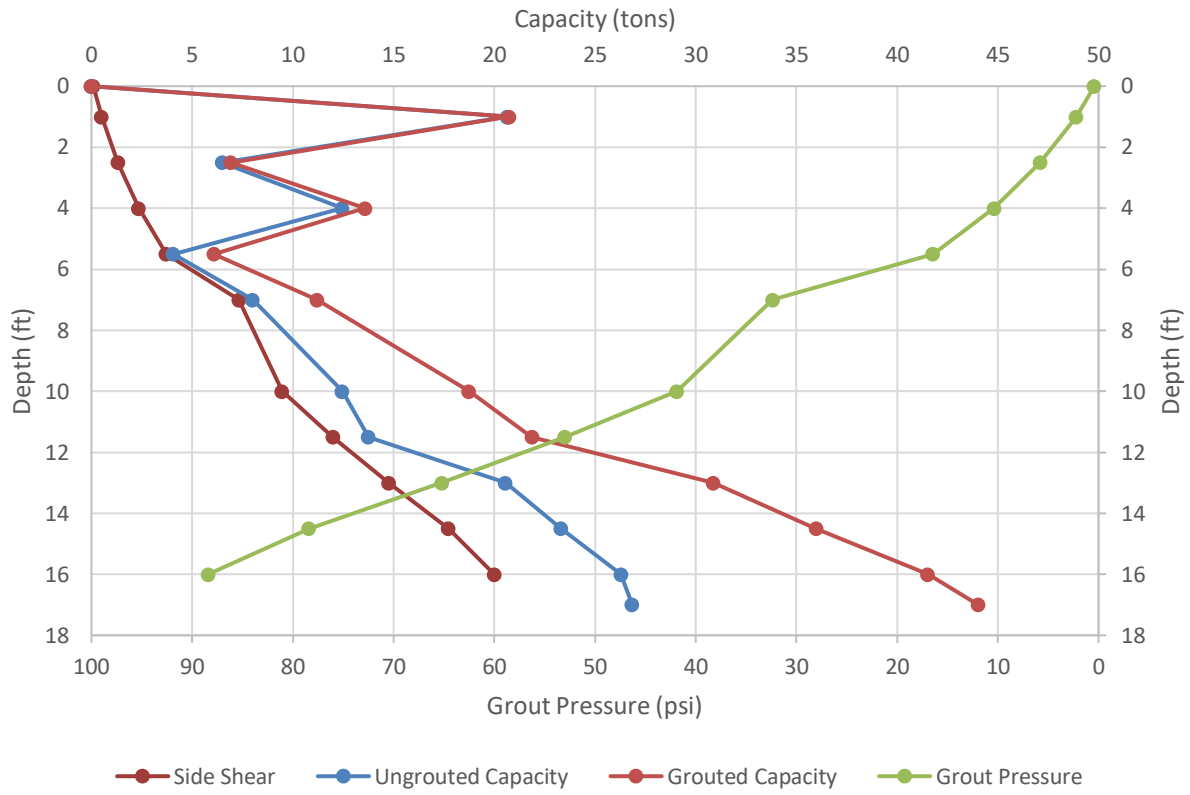


Figure 4.29 Data set 10 design curves.

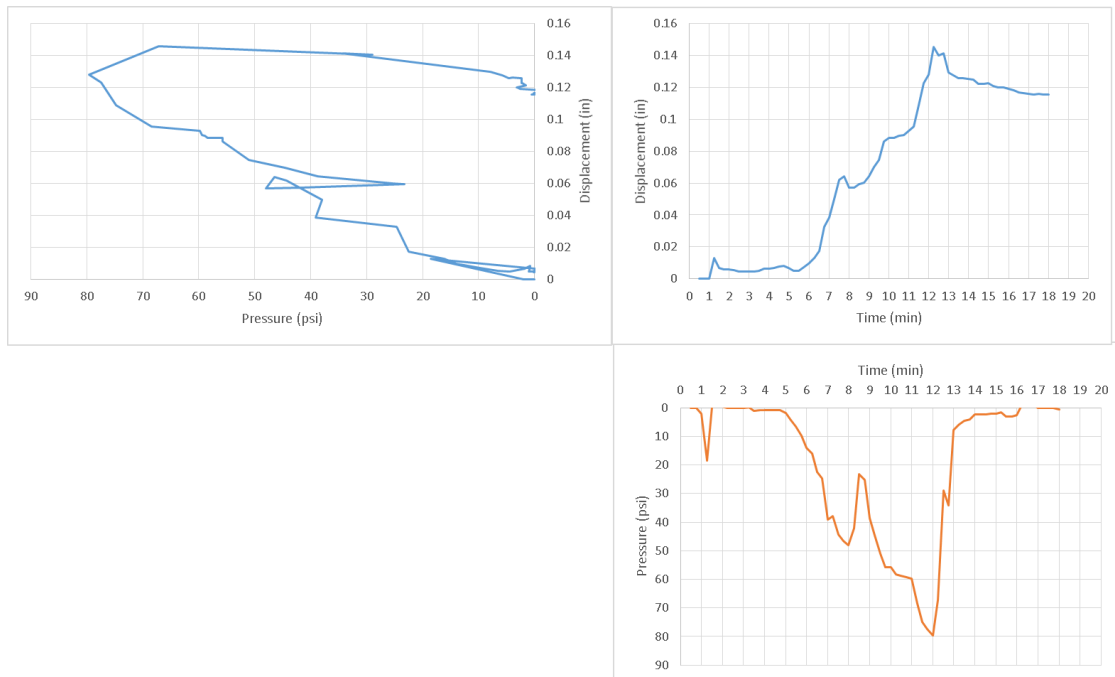


Figure 4.30 Data set 10 modified tri-axis plots.

Figure 4.30 shows the grouting quality assurance plots for data set 10. Incremental volume measurements were not taken, so time was used in lieu of volume. The progressive uplift with increasing pressure made this data usable. Effective pressure was selected from both pressure curves. The max effective pressure can be taken at 80 psi. Peak pressure was also 80 psi. Anticipated design pressure was 88.42 psi.

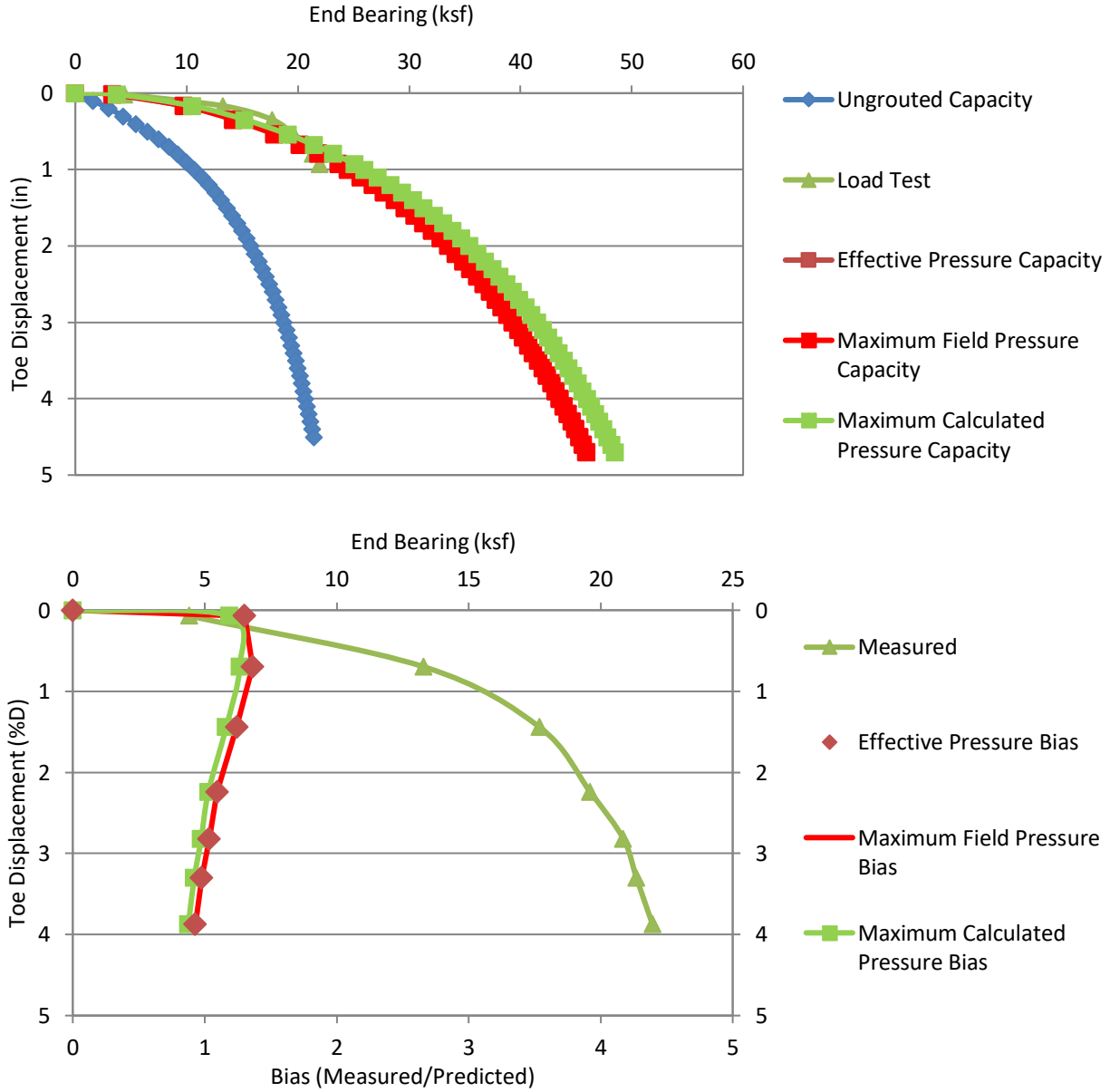


Figure 4.31 Data set 10 predicted/design and load test response (top); bias vs disp. (bottom).

4.2.11 Data Set 11, Clearwater Site I, FJ-2

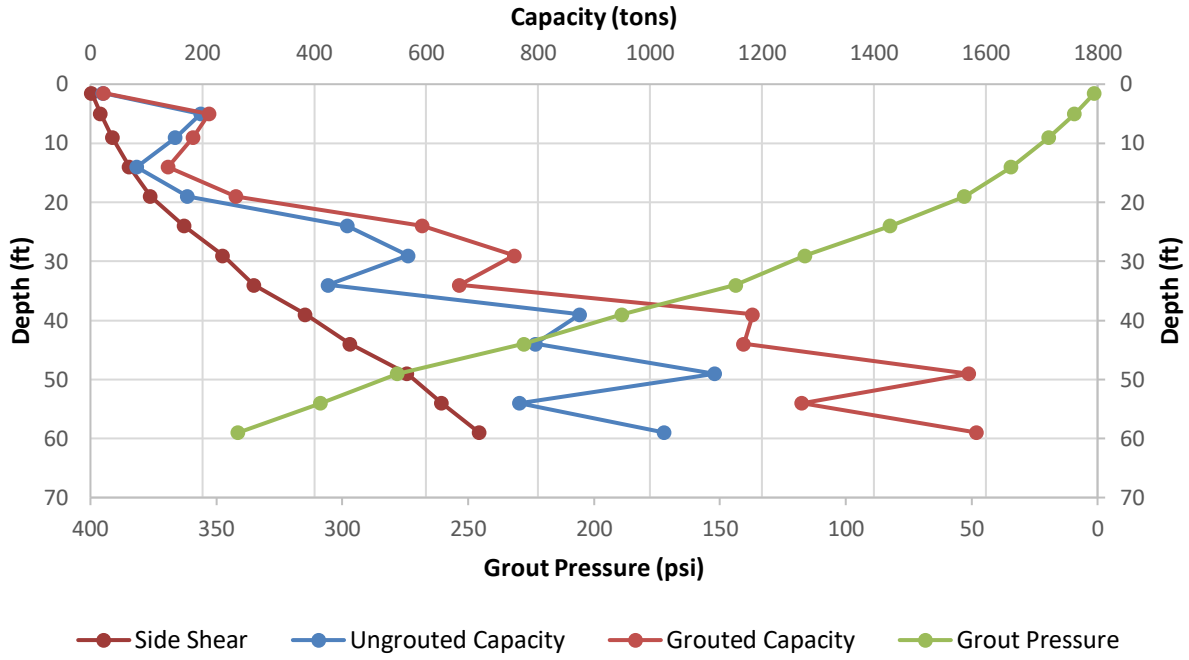


Figure 4.32 Data set 11 design curves.

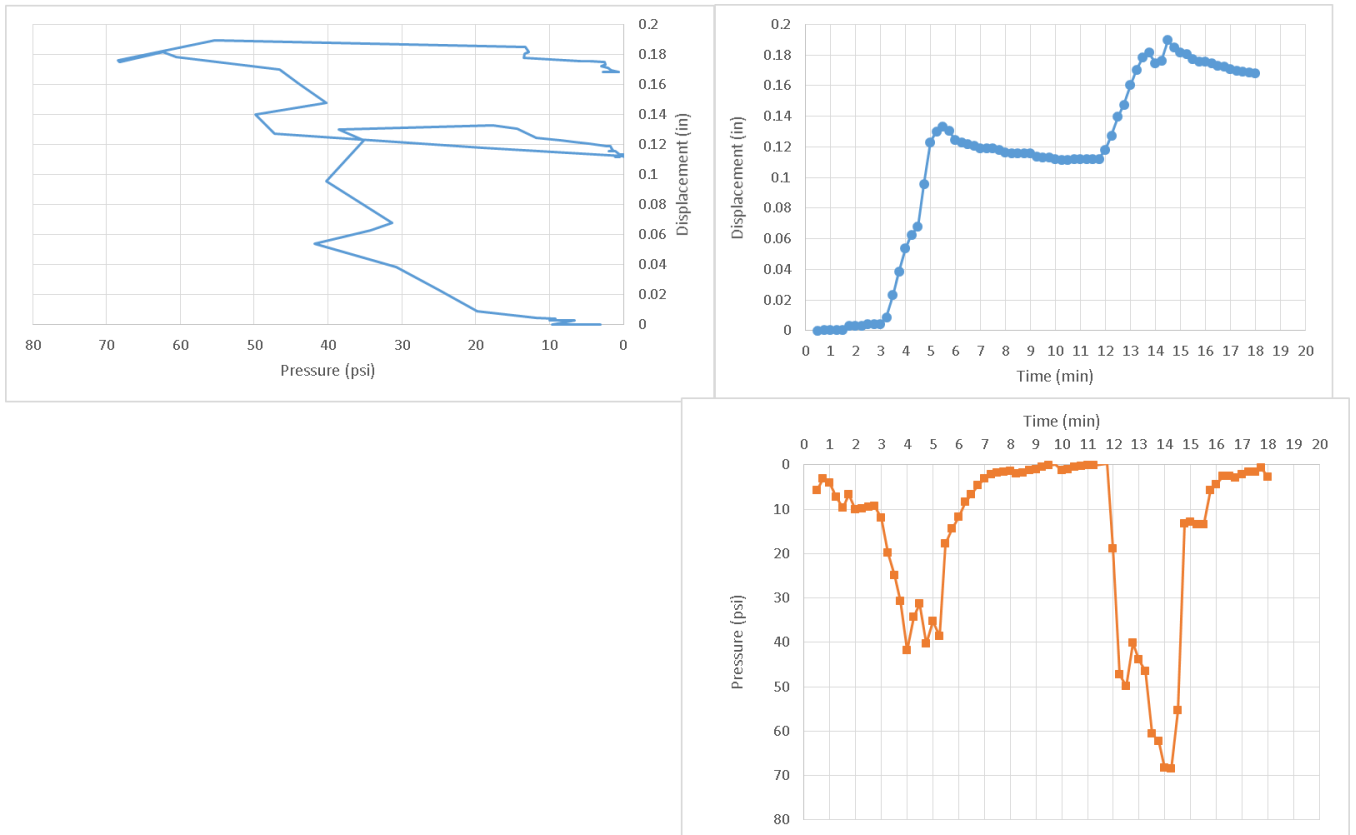


Figure 4.33 Data set 11 modified tri-axis plots.

Pressure was again confirmed by both pressure curves. The maximum effective pressure can be taken at 70 psi. Peak pressure was 70 psi. Peak anticipated design pressure was 35 psi.

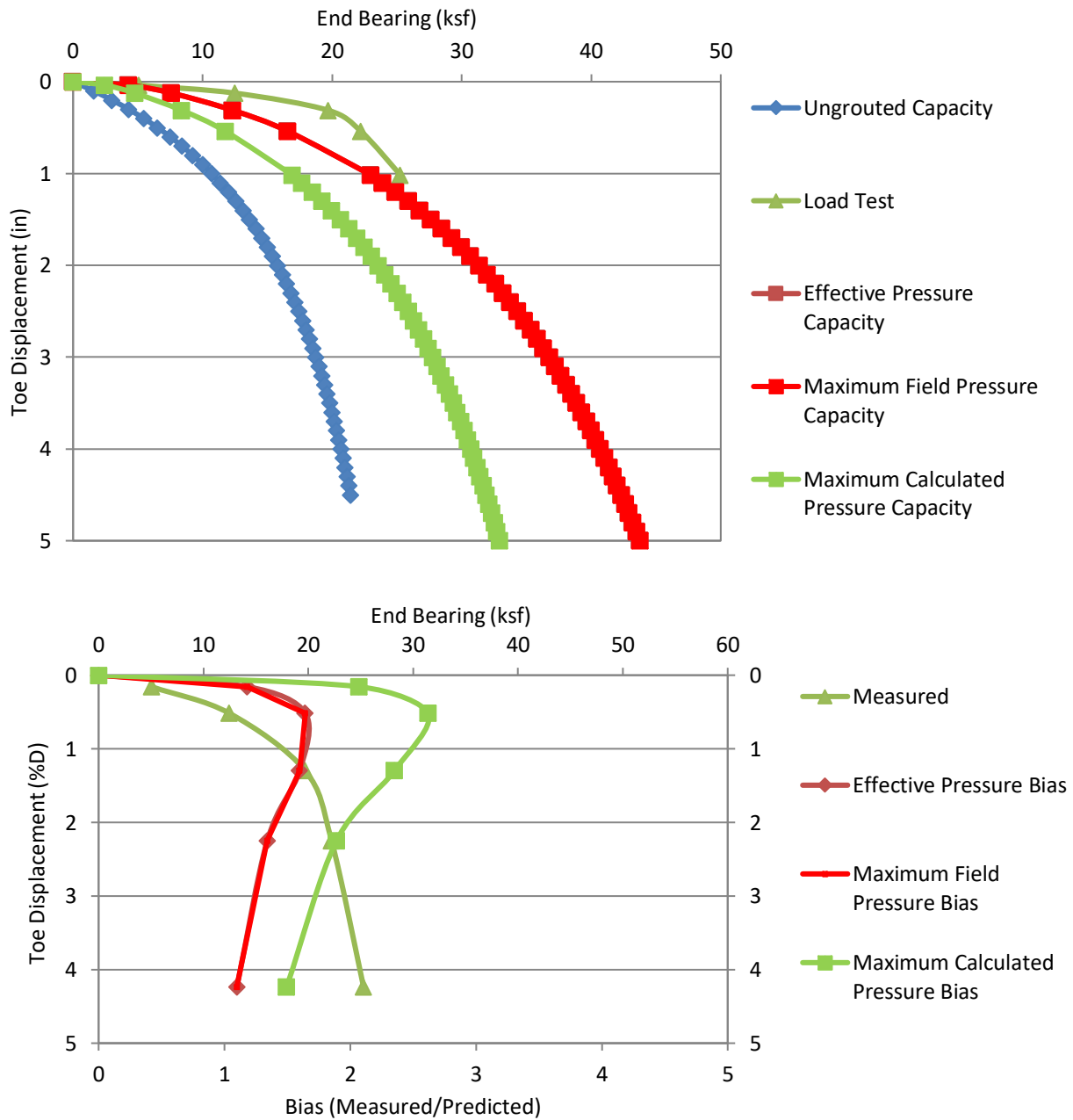


Figure 4.34 Data set 11 predicted/design and load test response (top); bias vs disp. (bottom).

4.2.12 Data Set 12, Clearwater Site I, SP-1

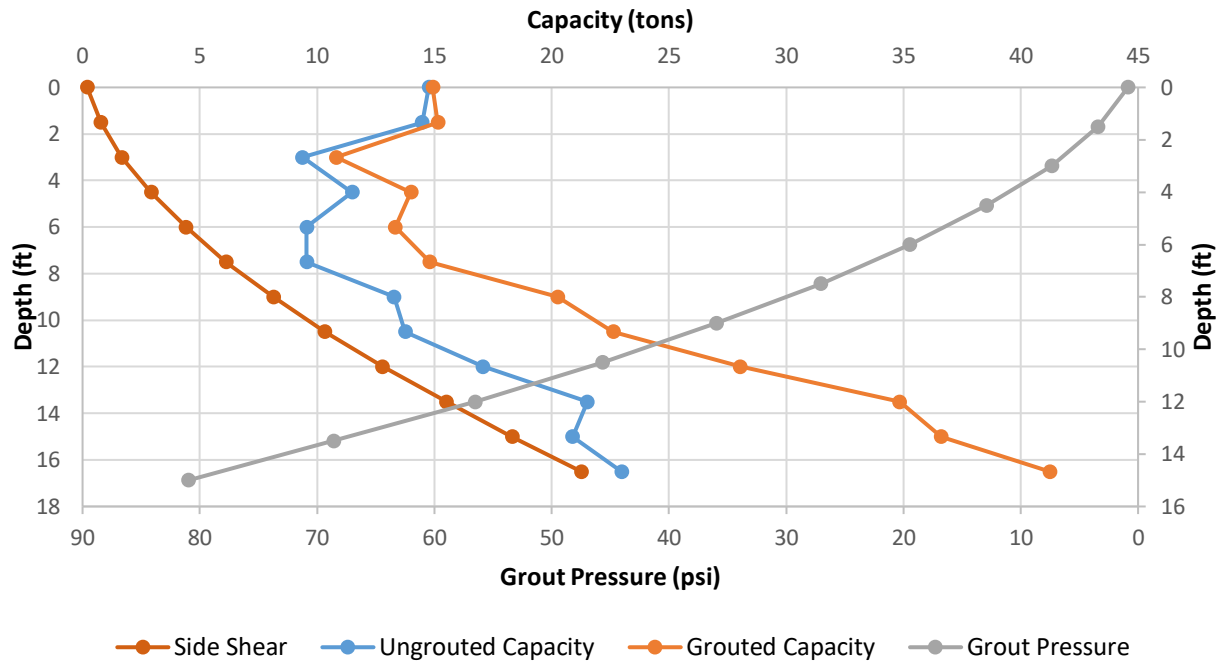


Figure 4.35 Data set 12 design curves.

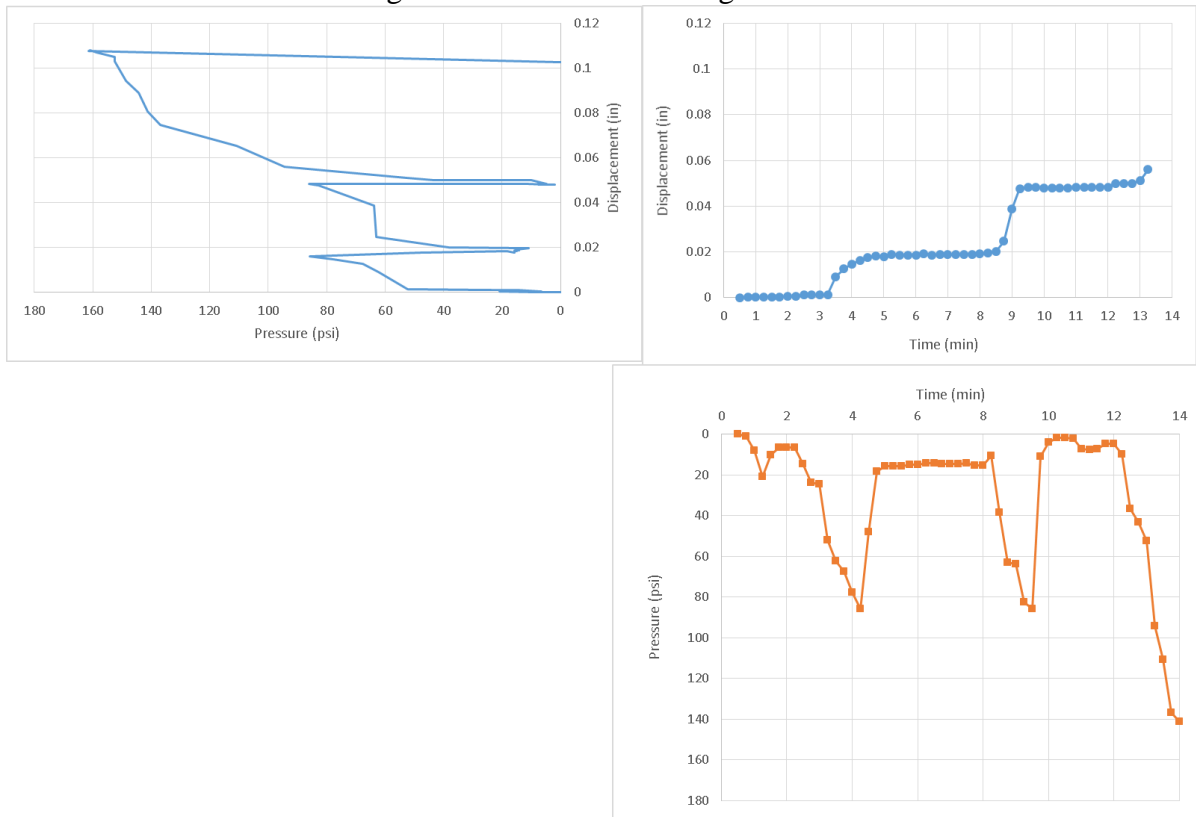


Figure 4.36 Data set 12 modified tri-axis plots.

Pressure was selected based on both pressure graphs. The maximum effective pressure was taken at 151 psi. Peak pressure was 162 psi. Peak anticipated design pressure was 68 psi.

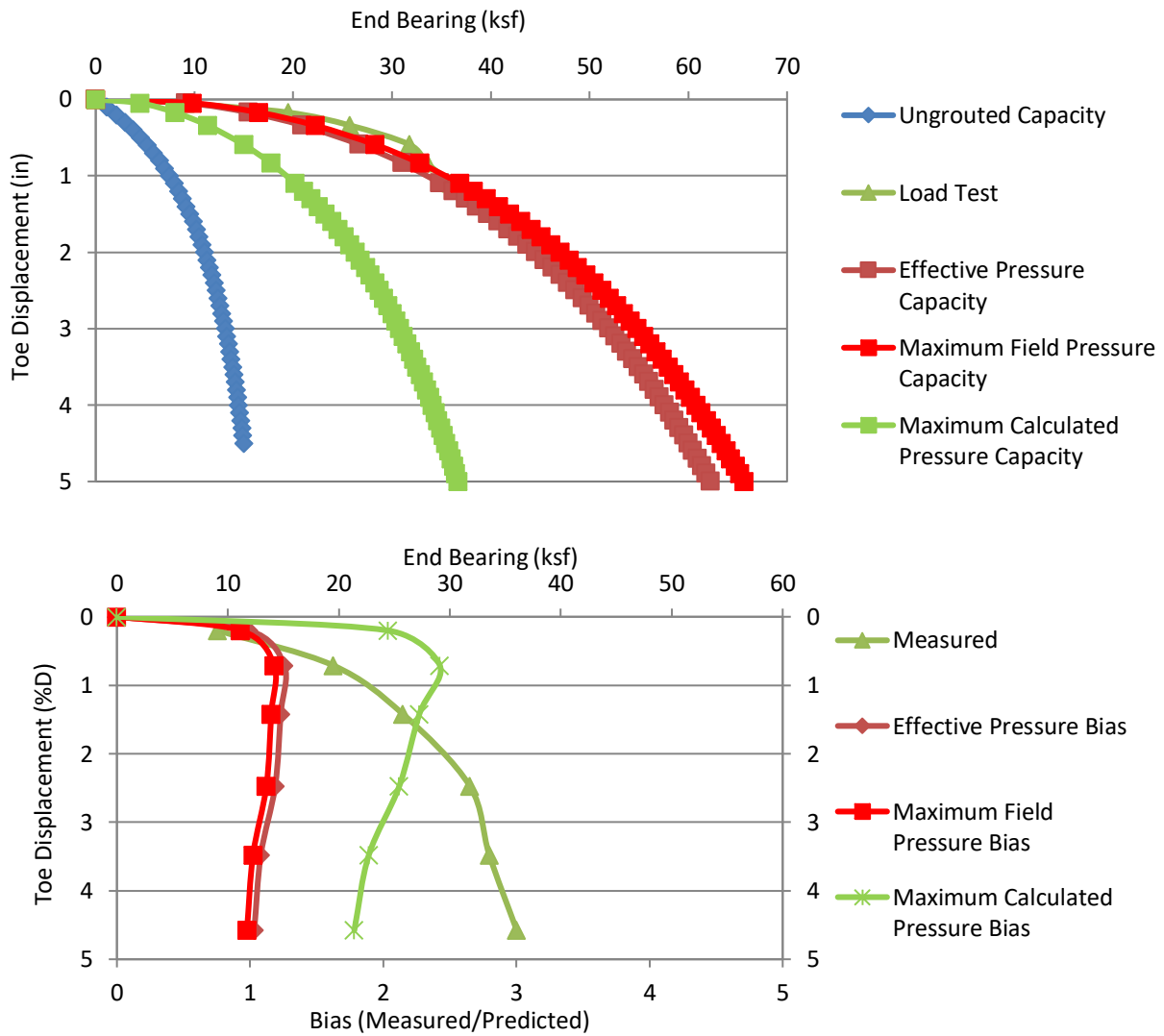


Figure 4.37 Data set 12 predicted/design and load test response (top); bias vs disp. (bottom).

4.2.13 Data Set 13, Clearwater Site I, SP-2

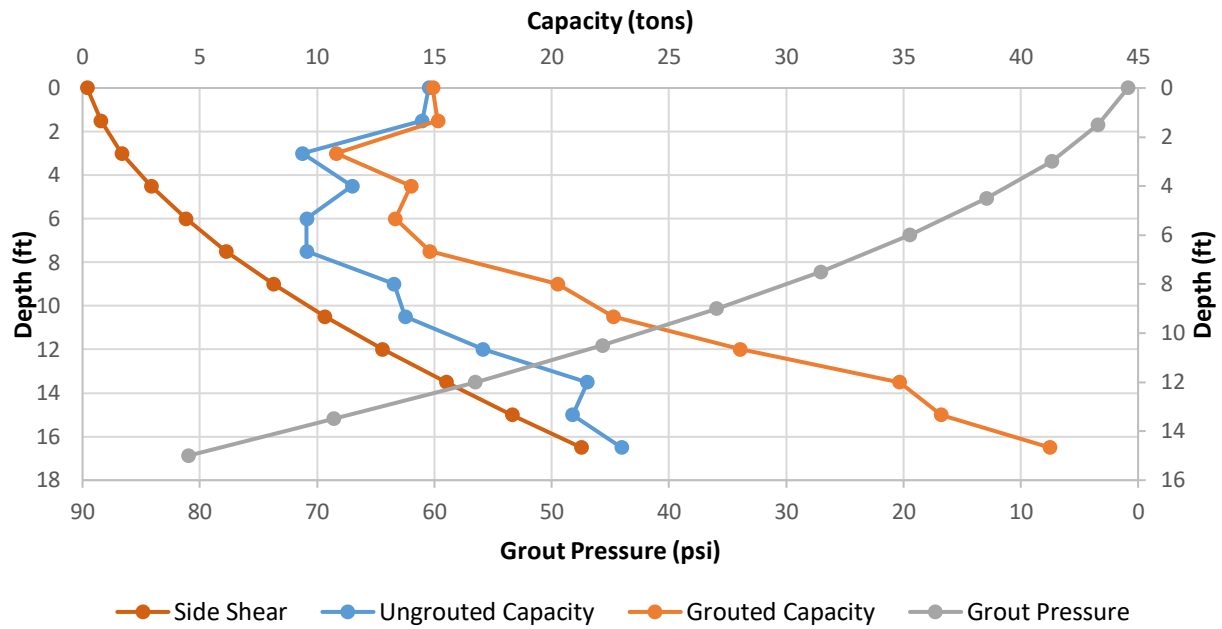


Figure 4.38 Data set 13 design curves.

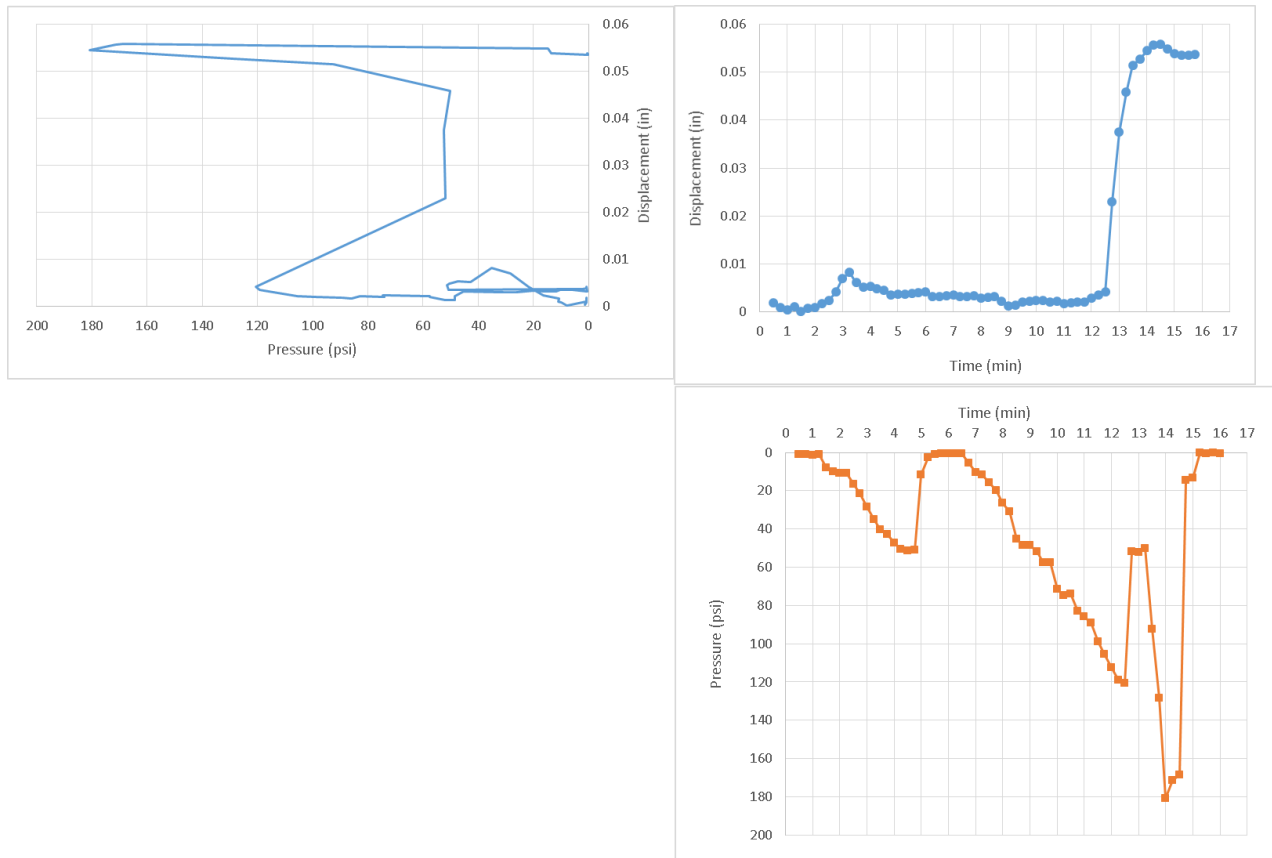


Figure 4.39 Data set 13 tri-axis plots.

Again incremental volume measurements were not available. The SP designation of this shaft indicates it was a sleeve port and which had two circuits. A vertical line in the pressure/disp. graph denotes a disturbance of the reference frame but which did not degrade the usability of the data. The max effective pressure can be taken at 170 psi. Peak pressure was 180 psi. Peak anticipated design pressure was 68 psi.

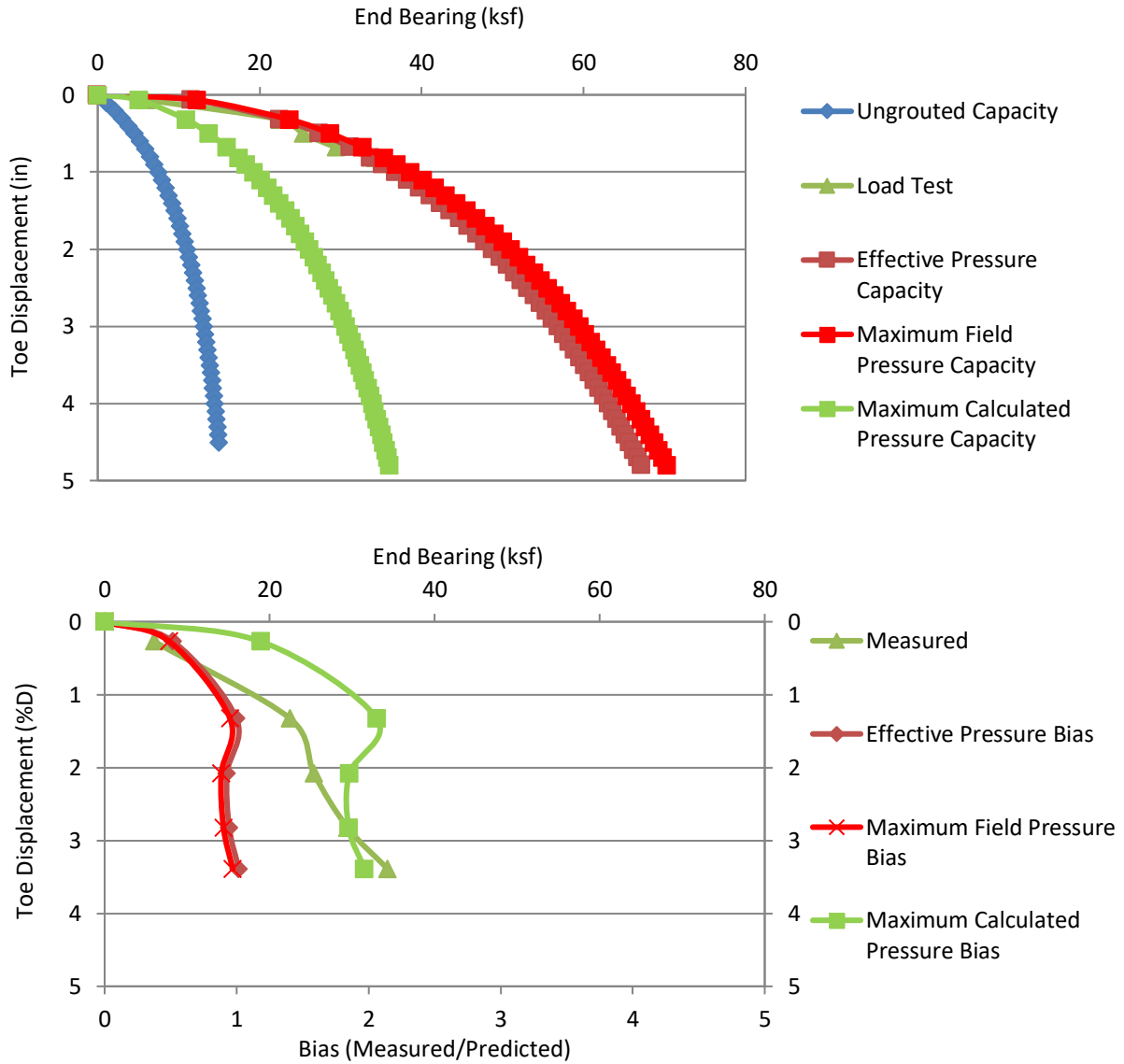


Figure 4.40 Data set 13 predicted/design and load test response (top); bias vs disp. (bottom).

4.2.14 Data Set 14, Clearwater Site II, FJ-1

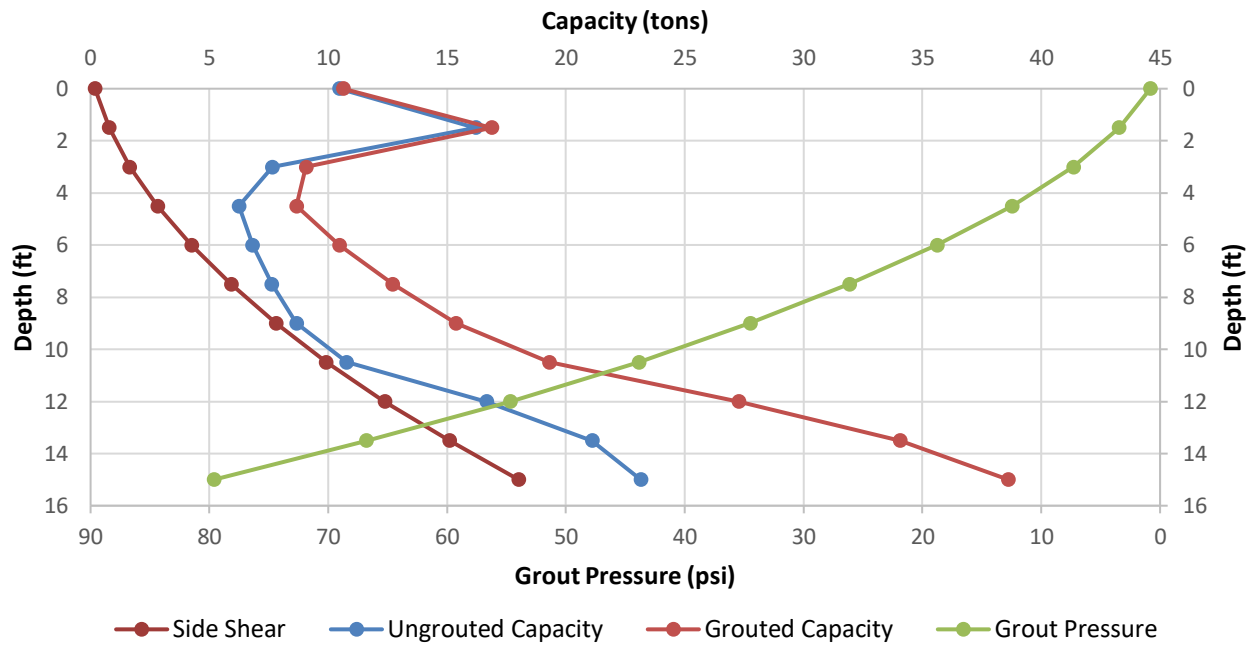


Figure 4.41 Data set 14 design curves.

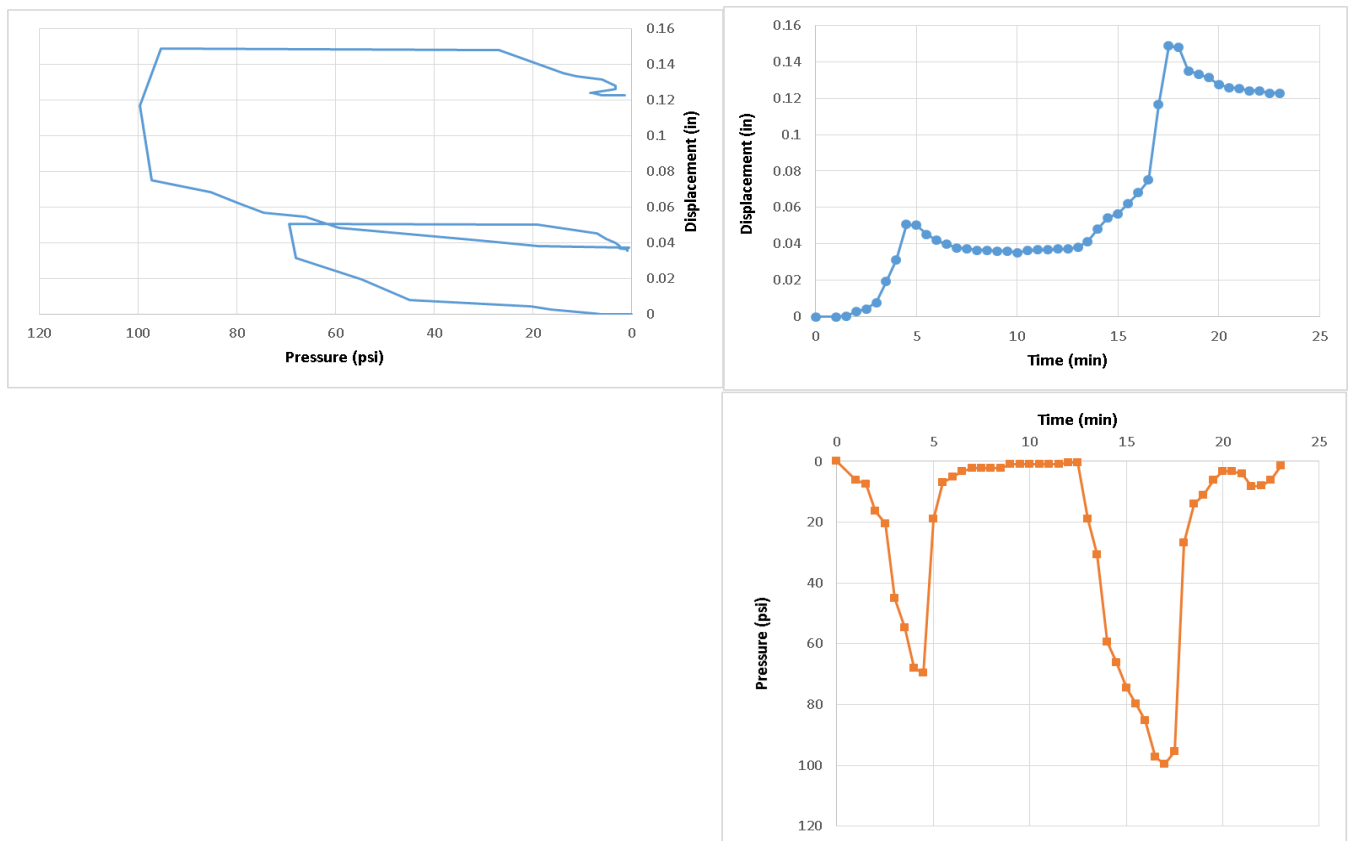


Figure 4.42 Data set 14 tri-axis plots.

Figure 4.42 shows the grouting quality assurance plots for data set 14. Pressure was selected based on both pressure graphs. The max effective and peak pressure can be taken at 100 psi. This shaft exhibited side shear control where no further grout pressure could be applied. Peak anticipated design pressure was 79.6 psi.

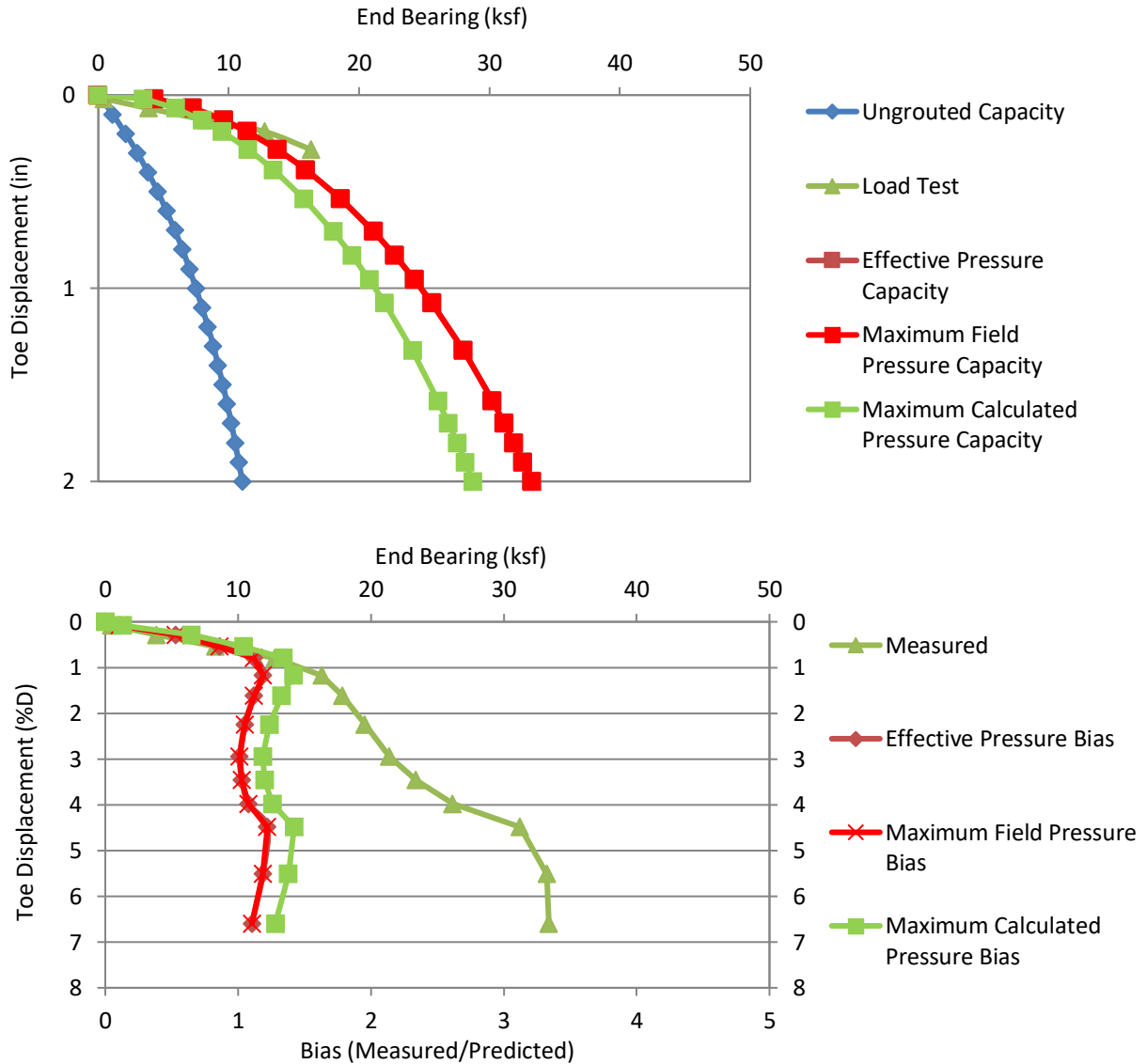


Figure 4.43 Data set 14 predicted/design and load test response (top); bias vs disp. (bottom).

4.2.15 Data set 15, Clearwater Site II, SP-1

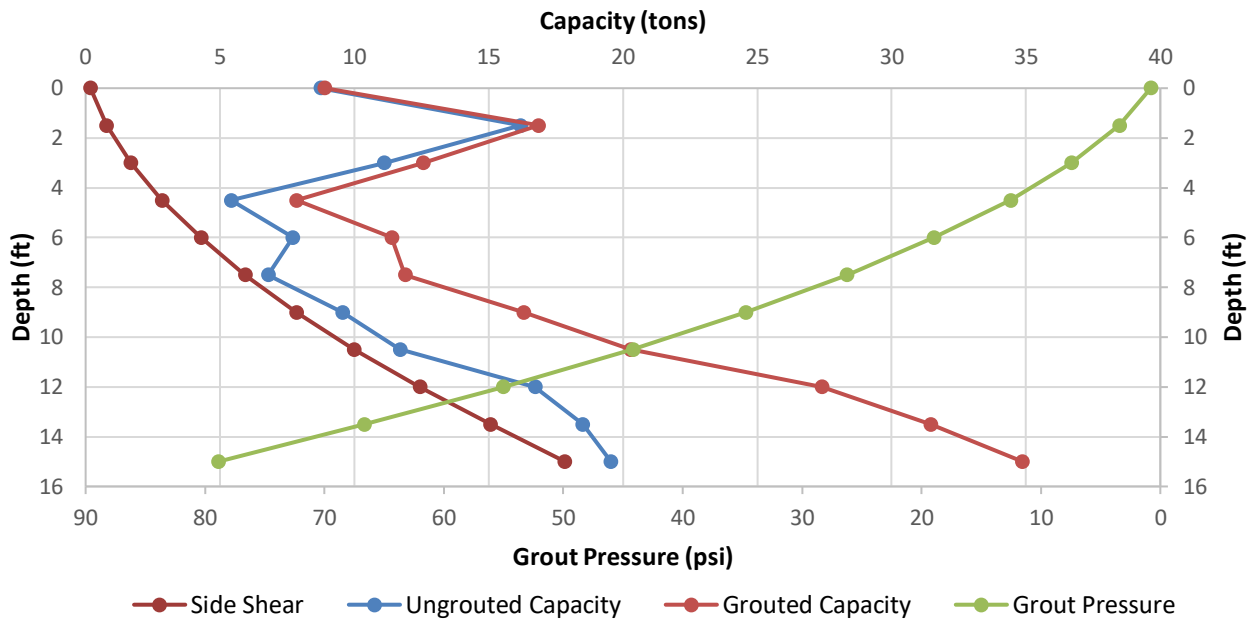


Figure 4.44 Data set 15 design curves.

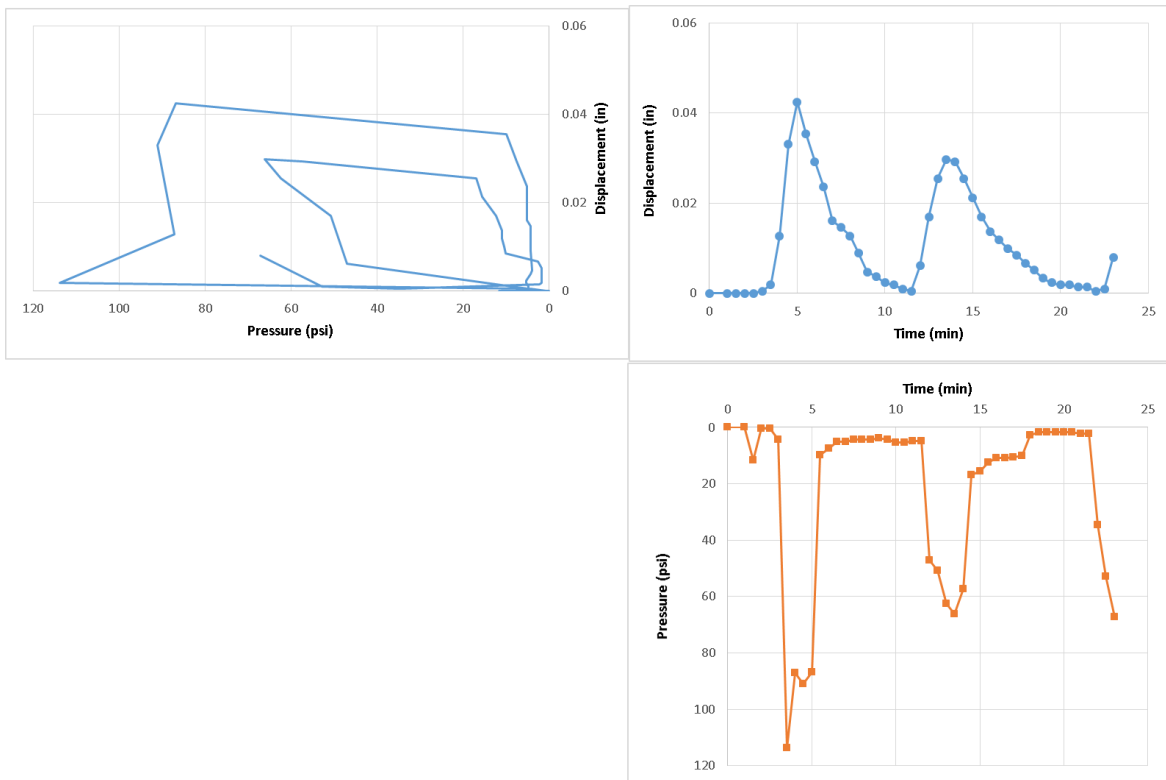


Figure 4.45 Tri-axis plots for data set 15.

Figure 4.45 shows the grouting quality assurance plots for data set 15. For this site, SP again refers to sleeve port and where two different grout delivery circuits were used. This is clearly noted by the two rises and falls in the grout pressure corresponding to the two circuits grouted sequentially. Effective pressure was selected based on the time versus pressure and displacement graphs where the displacement was maximum (not pressure) which is a global indication of applied force. The max effective pressure can be taken at 90 psi. Peak pressure was 114 psi. The second circuit did not achieve the same pressure level.

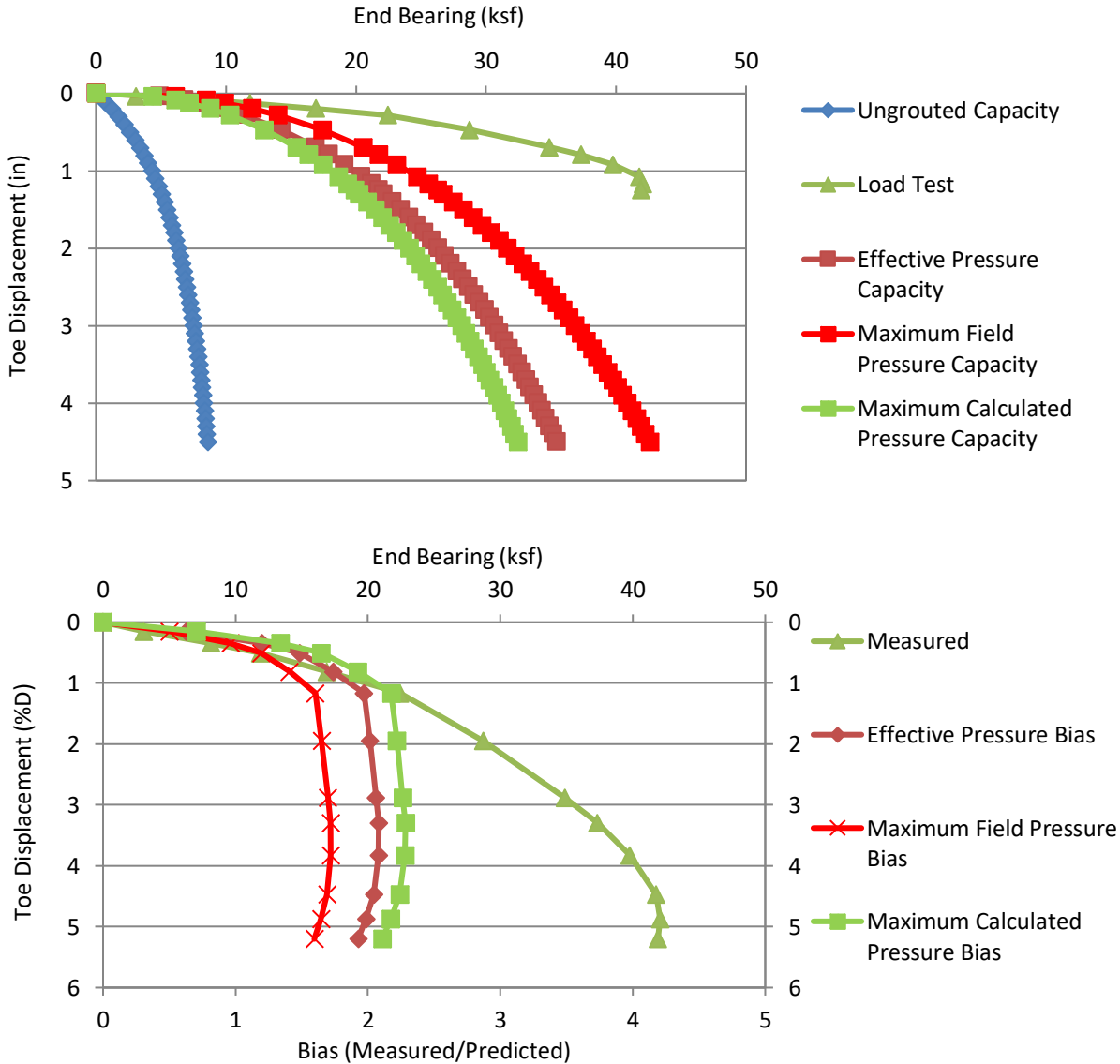


Figure 4.46 Data set 15 predicted/design and load test response (top); bias vs disp. (bottom).

4.2.16 Data Set 16, Flagler Memorial Bridge, S-1

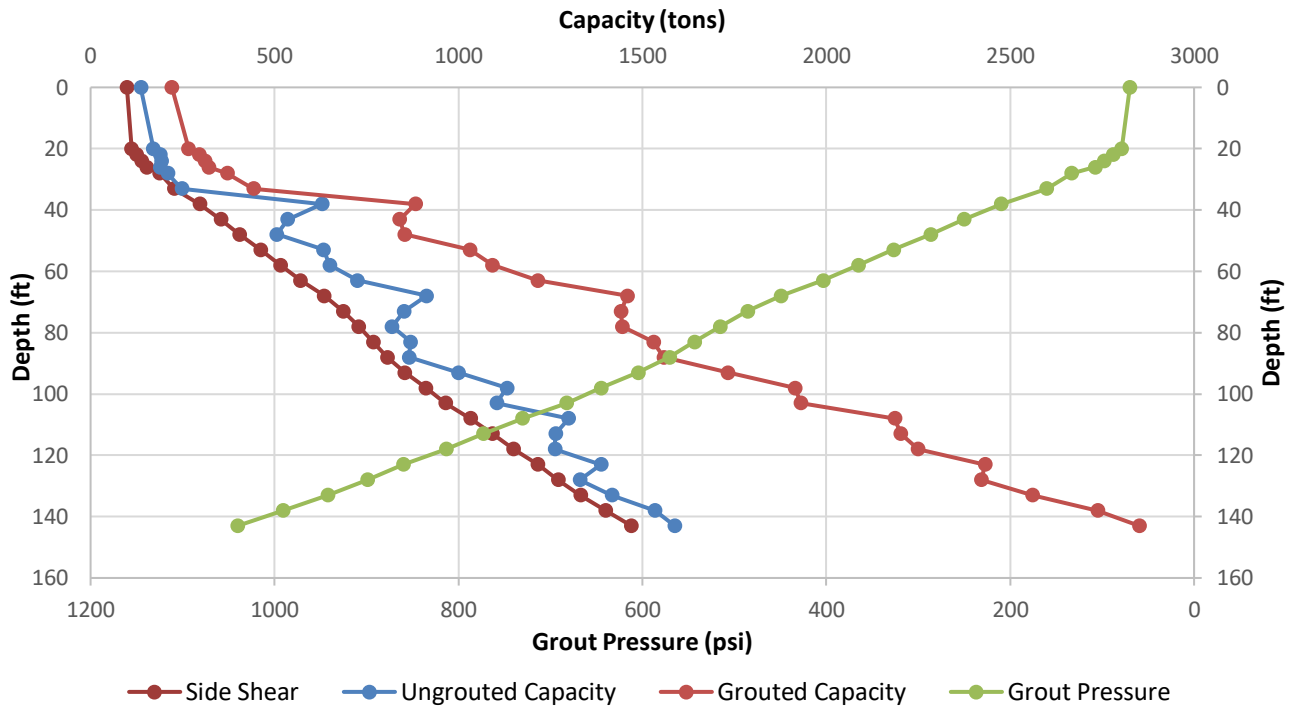


Figure 4.47 Data set 16 design curves.

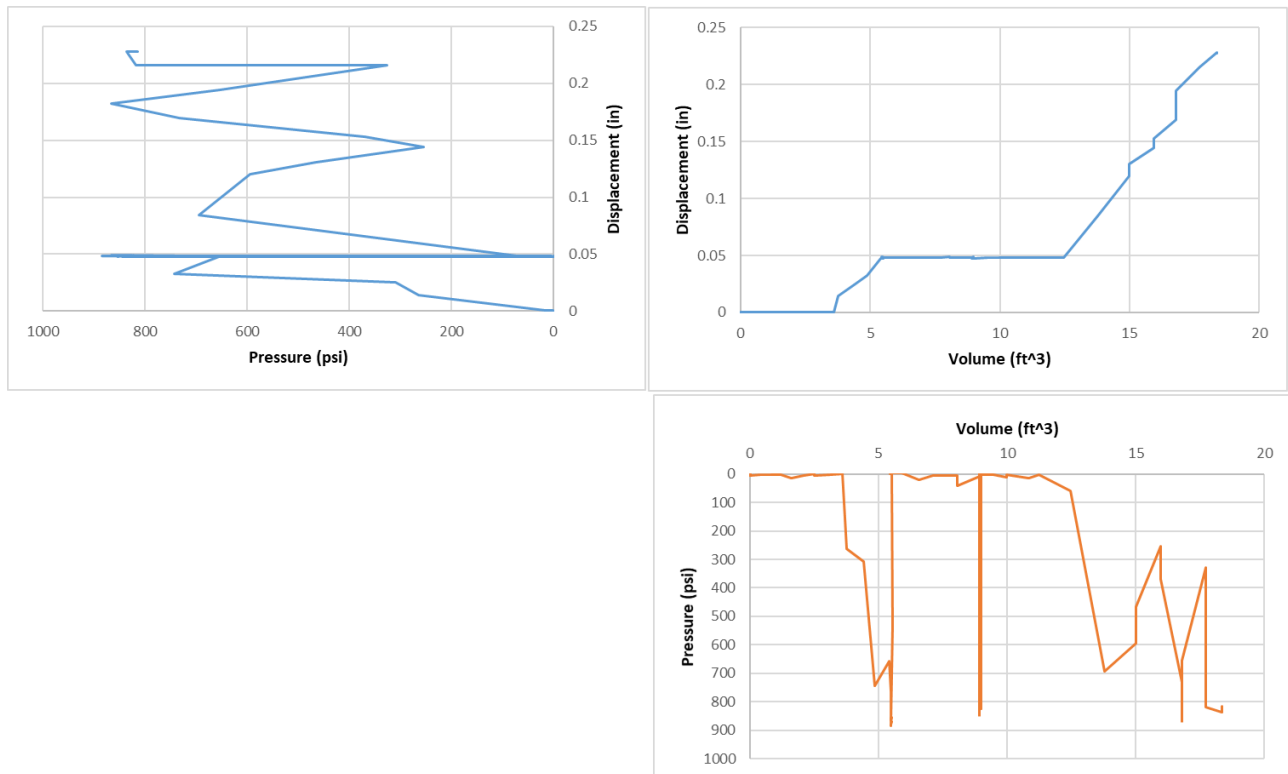


Figure 4.48 Data set 16 tri-axis plots.

Figure 4.48 shows the tri-axis plots for the Flagler Memorial Bridge shaft and indicate two issues only visible when using the effectiveness plots. Grouting was performed through 3 sleeve port circuits below a steel plate. The first circuit ended with line blockage, the second circuit took no grout and showed line blockage, the third circuit continued the work of the first circuit with the same effective pressure of 700 psi. The maximum field recorded pressure was 880 psi. Large volumes without accompanied increases in volume or uplift indicate pumping to fill lines or expel old grout. Approximate 10 cu. Ft. of the grout volume shown did not participate in active grouting. The maximum anticipated design pressure was 645 psi.

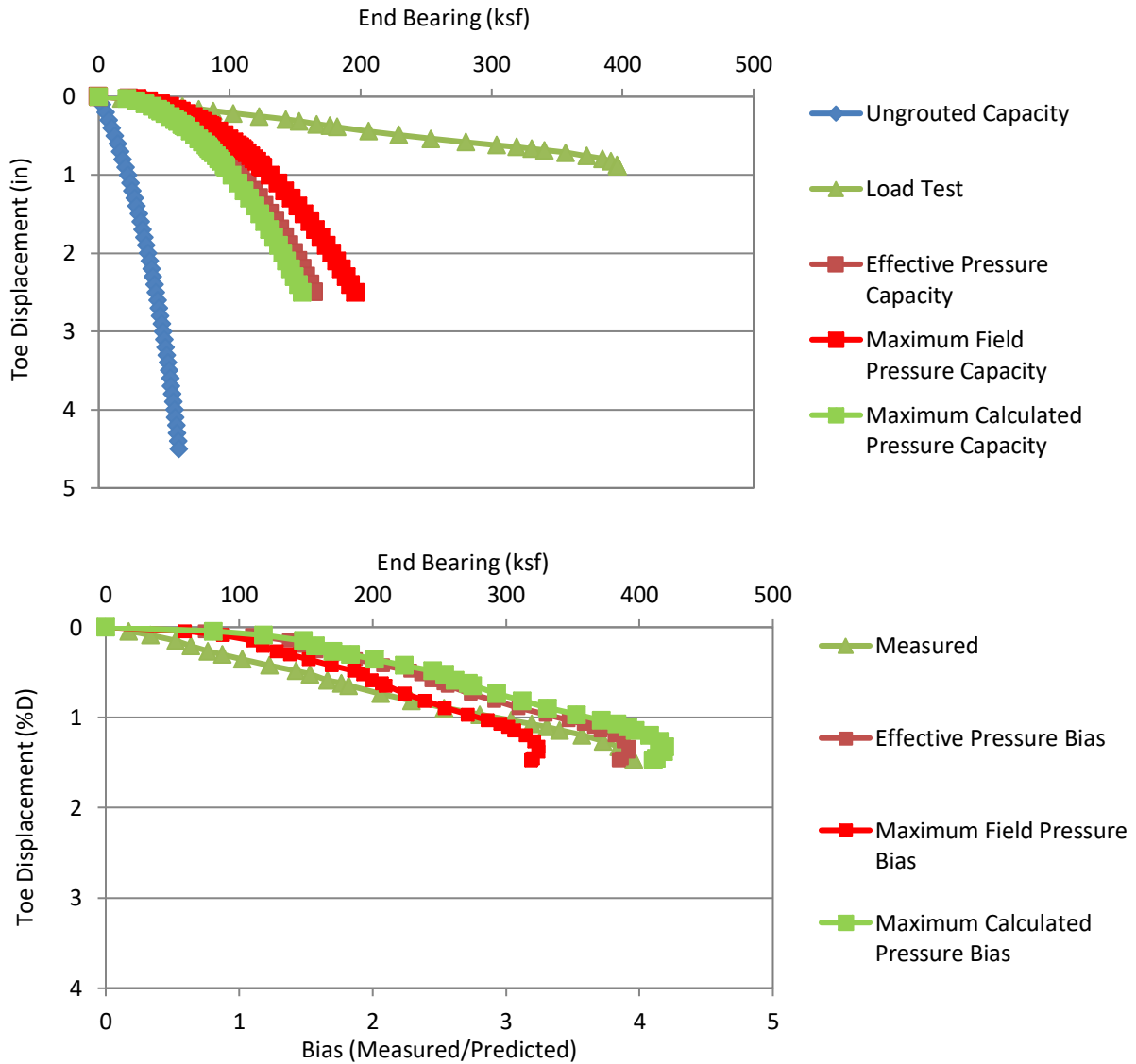


Figure 4.49 Data set 16 predicted/design and load test response (top); bias vs disp. (bottom).

4.2.17 Data Set 17, Security Checkpoint building concourse “C”, S-1

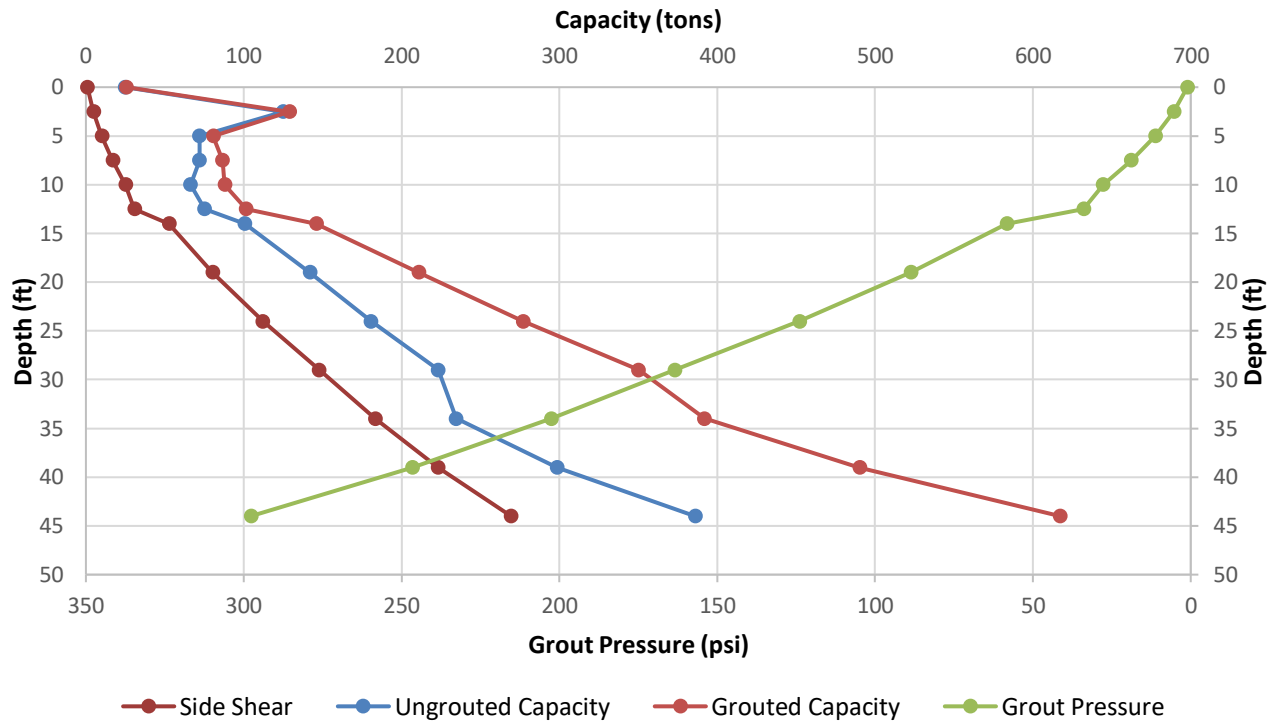


Figure 4.50 Data set 17 design curves.

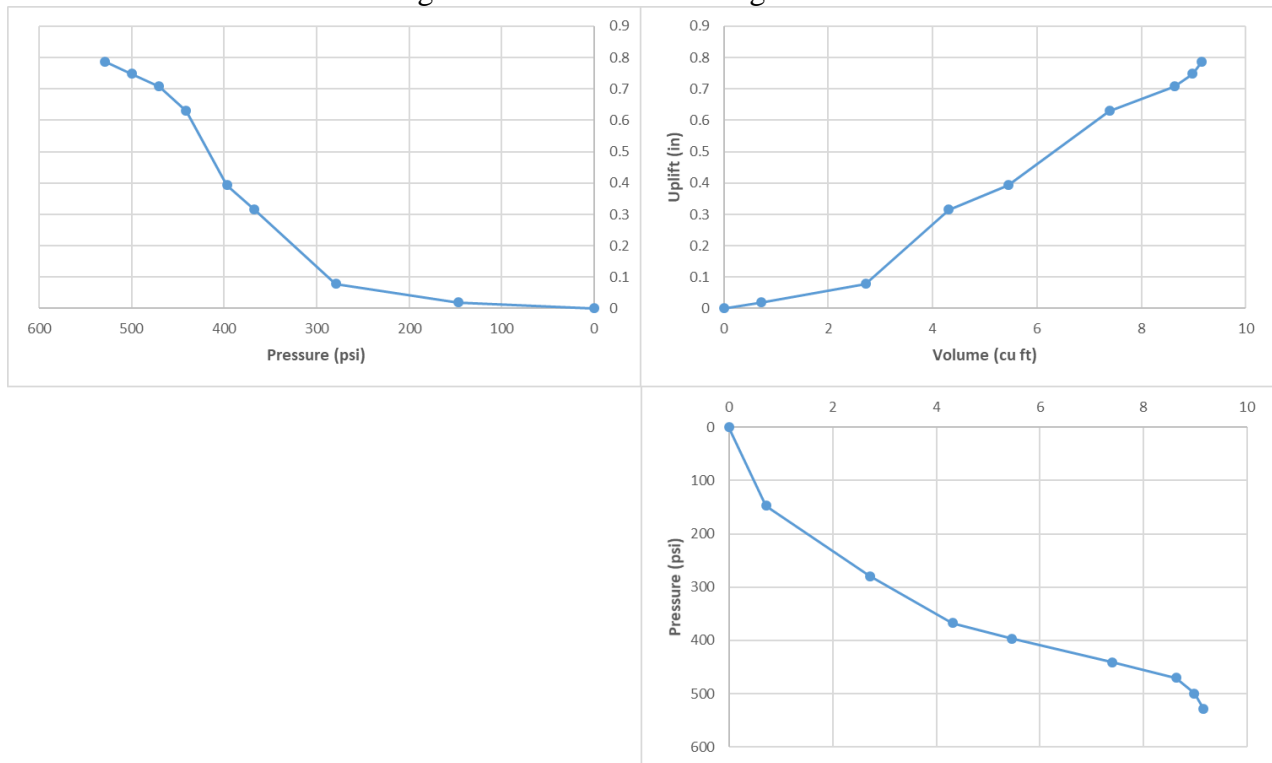


Figure 4.51 Data set 17 tri-axis plots.

Figure 4.51 shows the tri-axis plots for data set 17. Both the pressure vs. volume and volume vs. displacement showed a trend away from effective grouting in the form of a restriction but not full blockage. Effective grouting used was observed up to 470 psi; maximum field recorded pressure was 529 psi. Maximum anticipated design pressure was approximately 375 psi extrapolated from a shorter that shaft length boring.

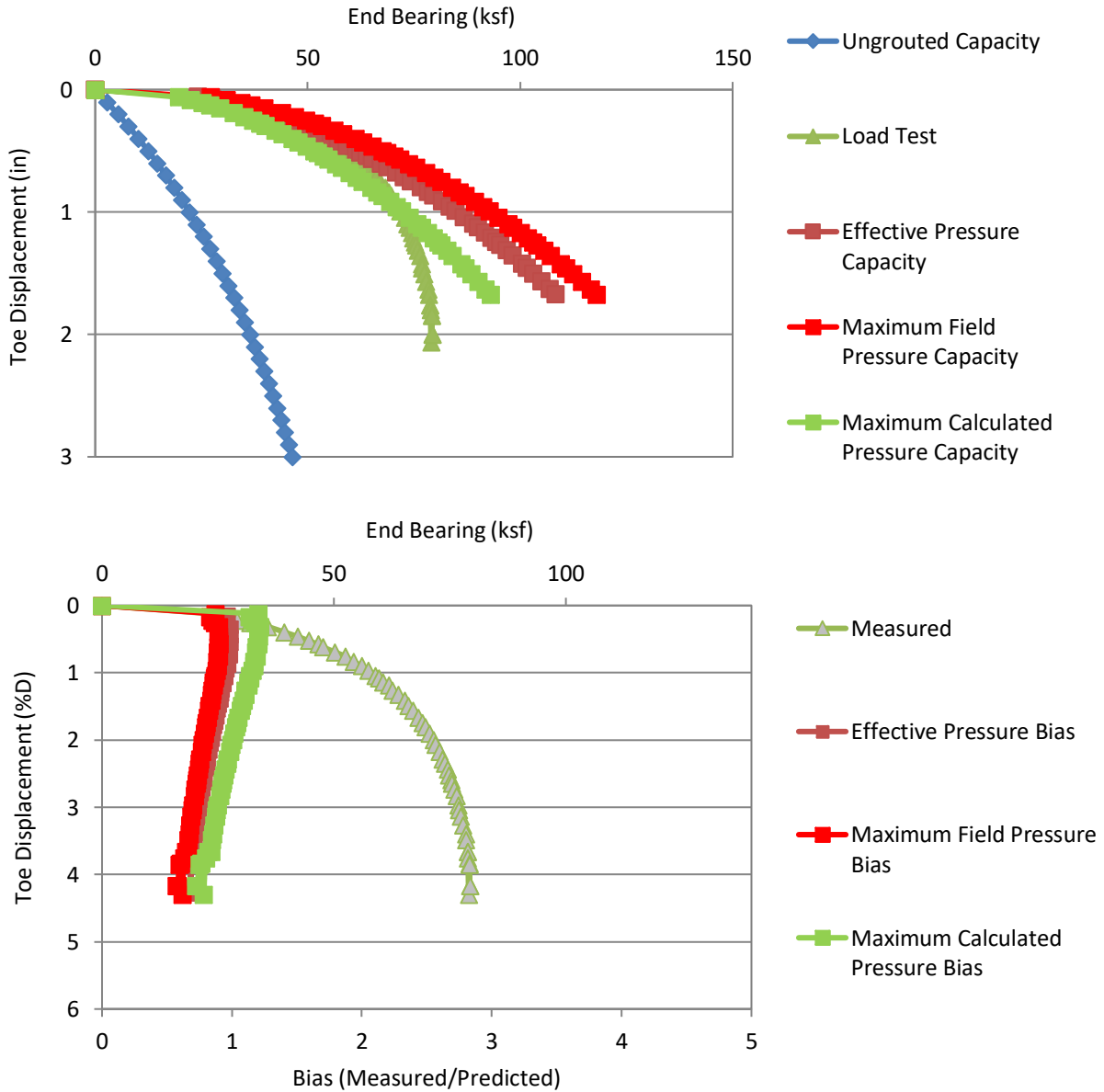


Figure 4.52 Data set 17 predicted/design and load test response (top); bias vs disp. (bottom).

4.2.18 Data Set 18, Plant Daniel - 501

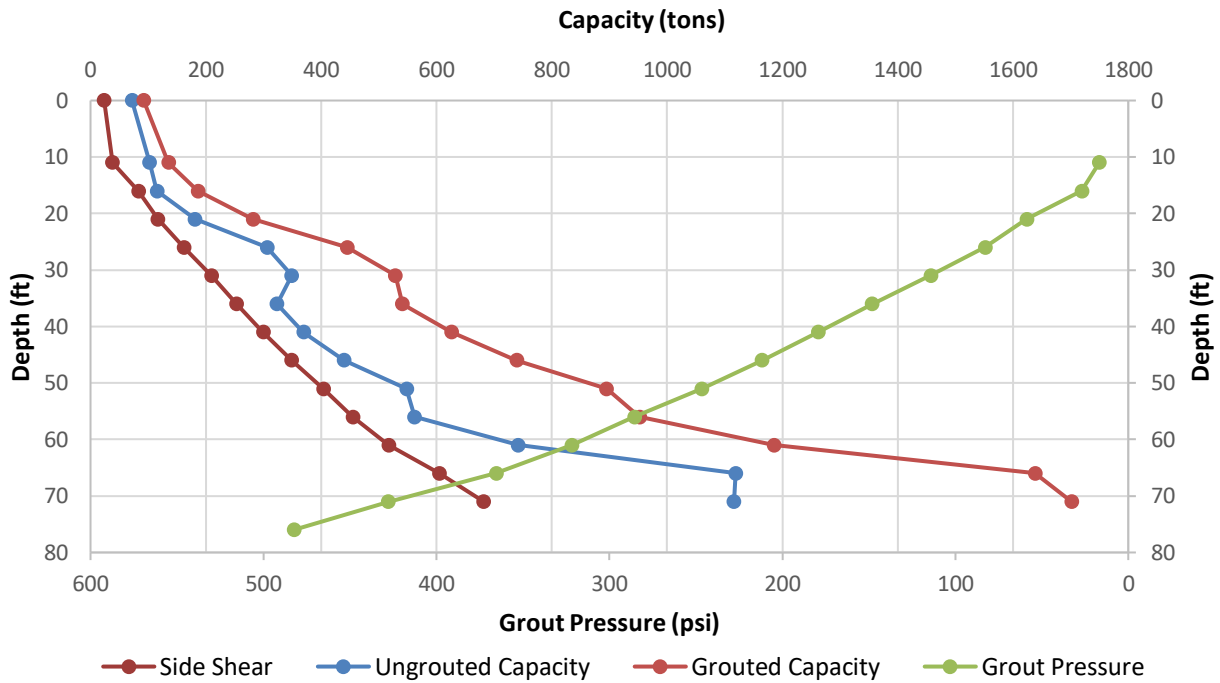


Figure 4.53 Data set 18 design curves.

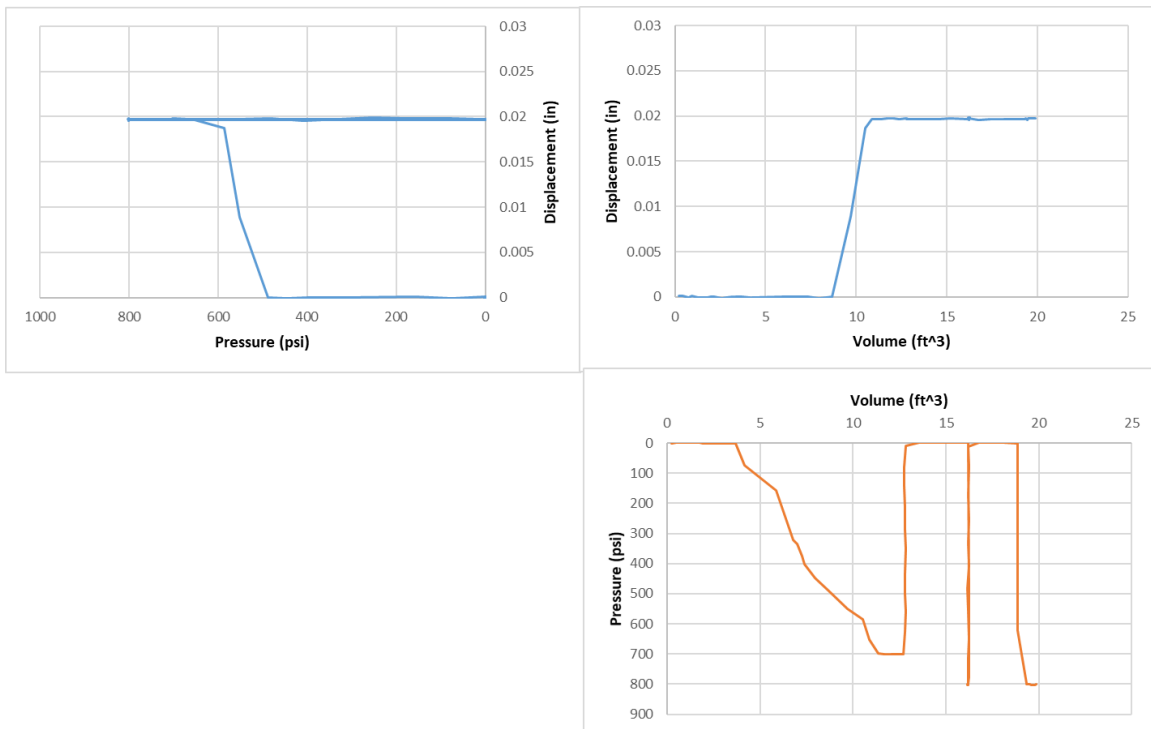


Figure 4.54 Data set 18 tri-axis plots.

Figure 4.54 shows the tri-axis plots for data set 18 and indicates two issues only visible when using the effectiveness plots. Both the pressure vs. volume and volume vs. displacement show horizontal trends supporting end bearing failure or piping. Also, both the pressure vs. volume and pressure vs. uplift show spikes in pressure without an associated uplift or increase in volume which indicates a grout line blockage. Effective pressure was determined to be 700 psi which was sustainable up to the point where the grout line became blocked and spiked a maximum field recorded pressure of 800 psi.

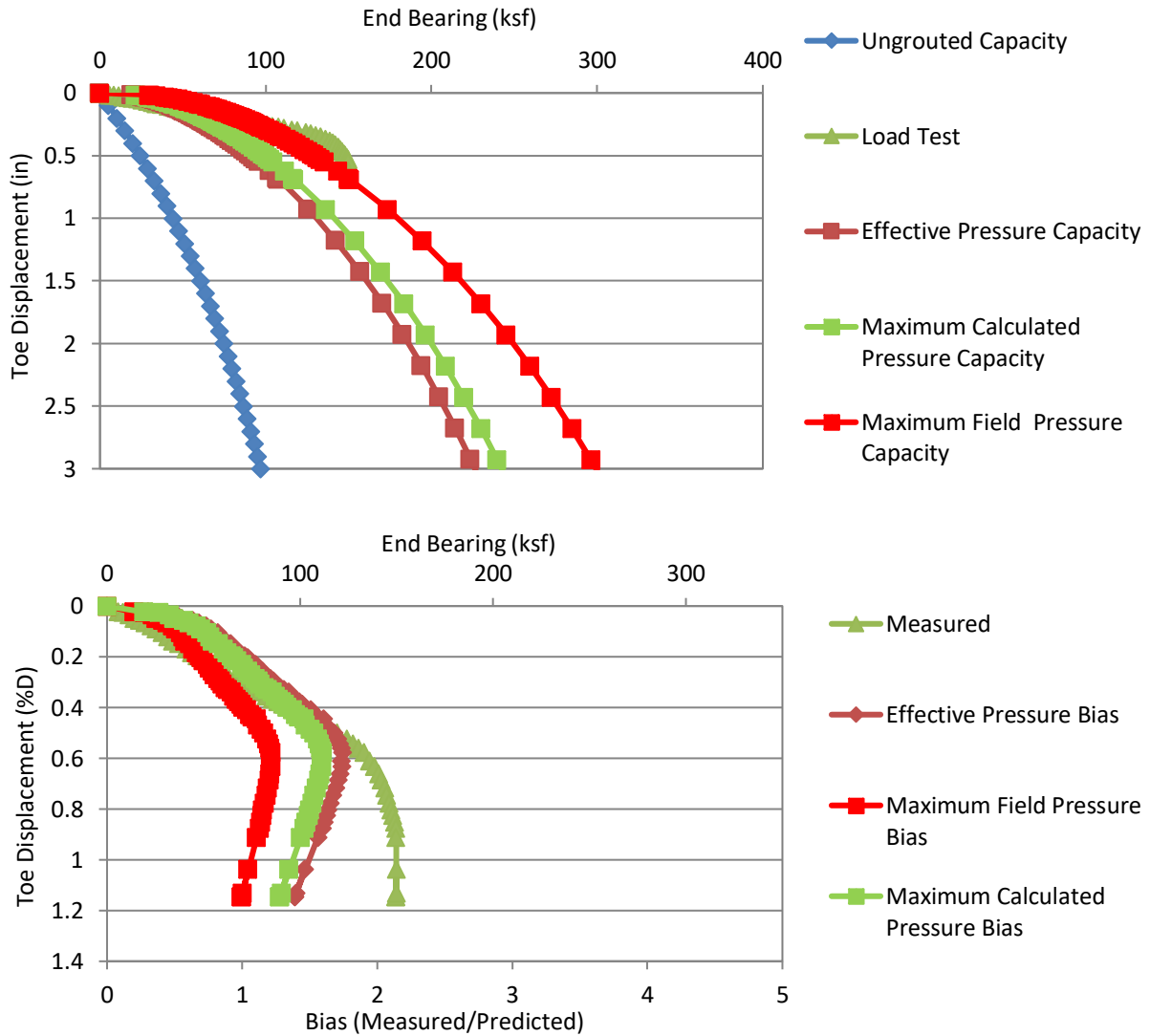


Figure 4.55 Data set 18 predicted/design and load test response (top); bias vs disp. (bottom).

4.2.19 Data Set 19, Plant Daniel - 528

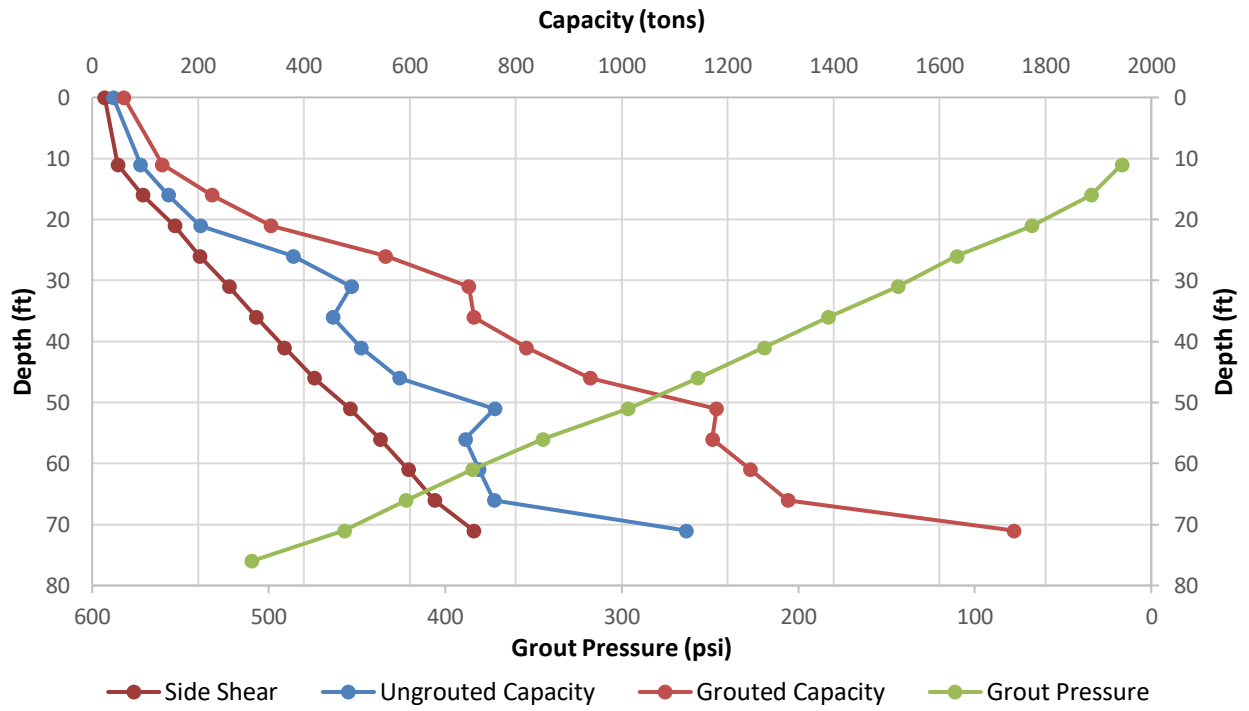


Figure 4.56 Data set 19 design curves.

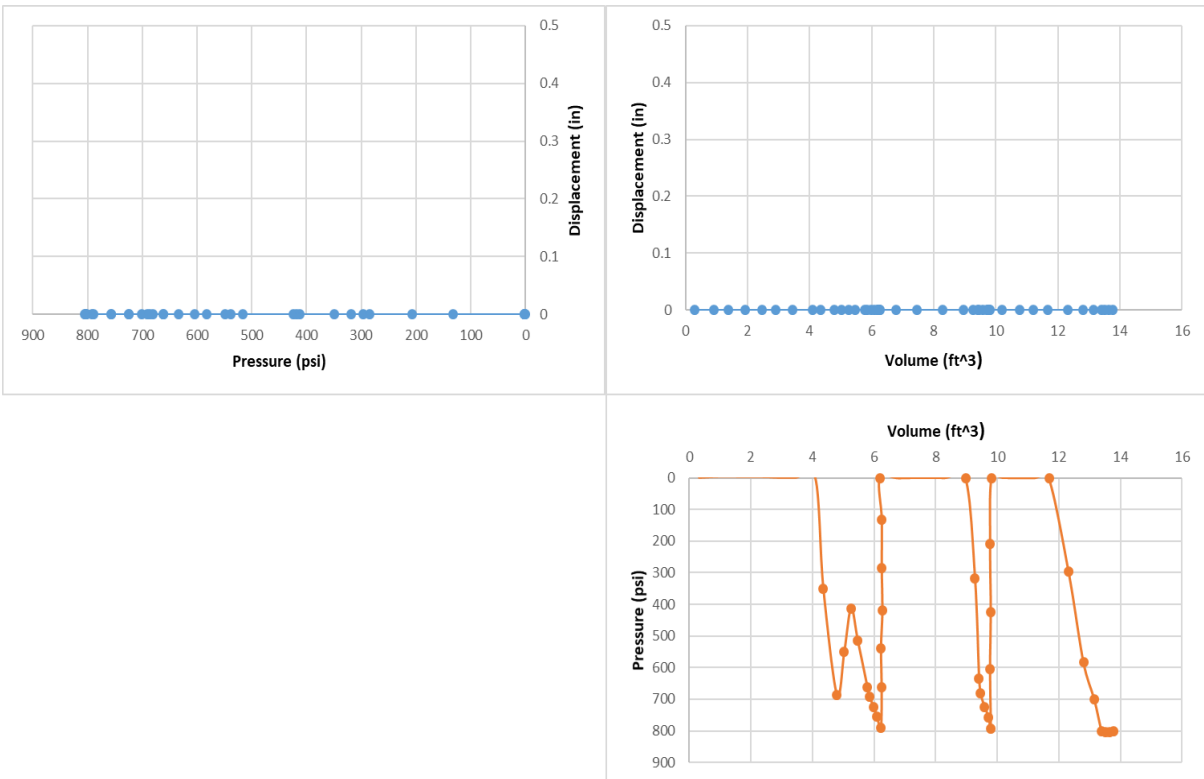


Figure 4.57 Data set 19 tri-axis plots.

Figure 4.57 shows the grouting quality assurance plots for data set 19. Effective pressure was selected based on the volume versus pressure graphs where the effective pressure was taken as 700 psi and peak pressure was 800 psi. However, with no displacement/uplift during grouting it is likely the displacement measuring system was not working. While this can be caused by an excessively unbalanced amount of side shear (long shaft), the anticipated/calculated pressure was well in line with the measured levels. An alternate explanation would indicate the small amount of grout volume did not cover the base of the shaft and therefore produced a small uplift force.

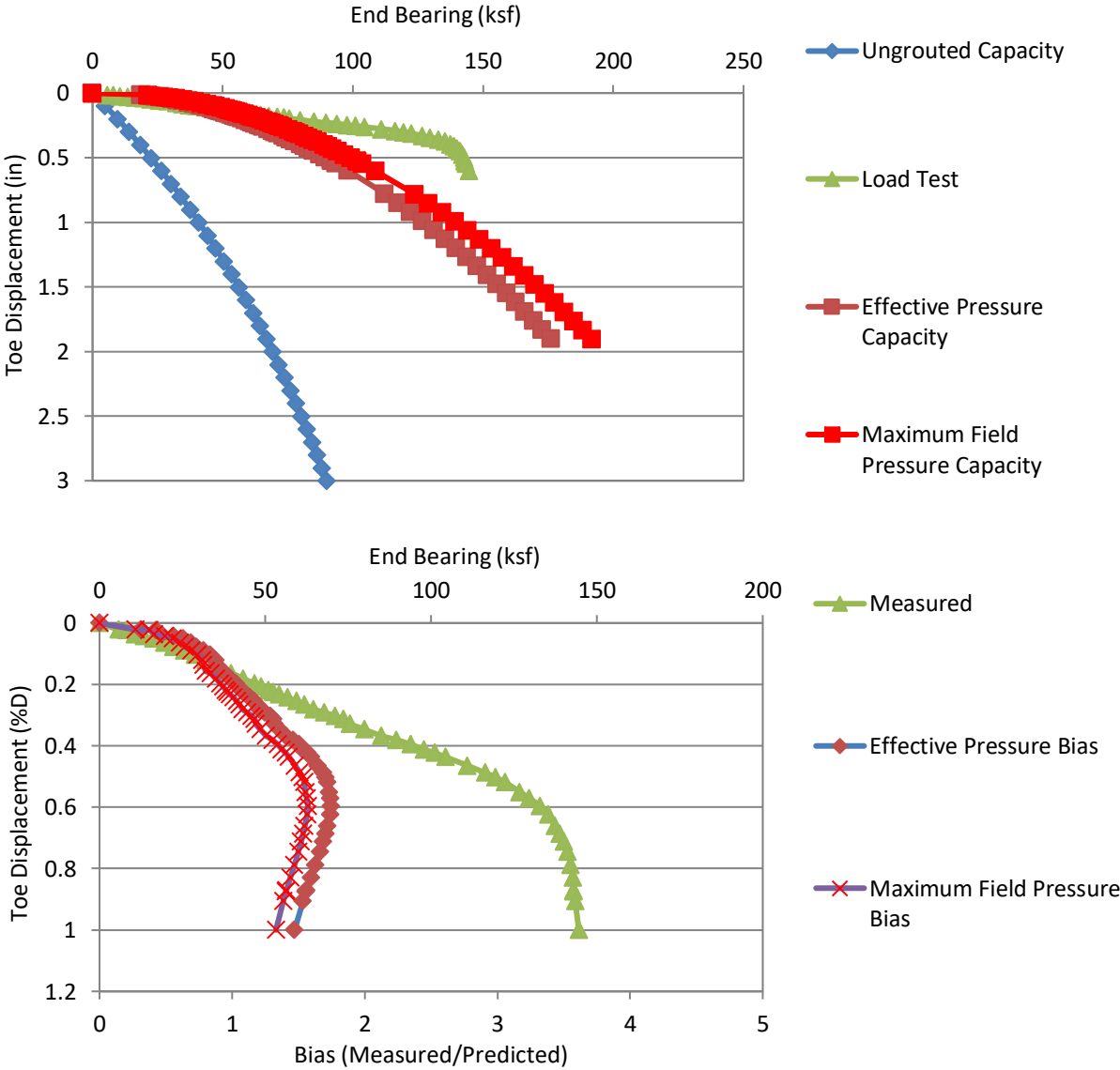


Figure 4.58 Data set 19 predicted/design and load test response (top); bias vs disp. (bottom).

4.2.20 Data Set 20, Plant Daniel – 530

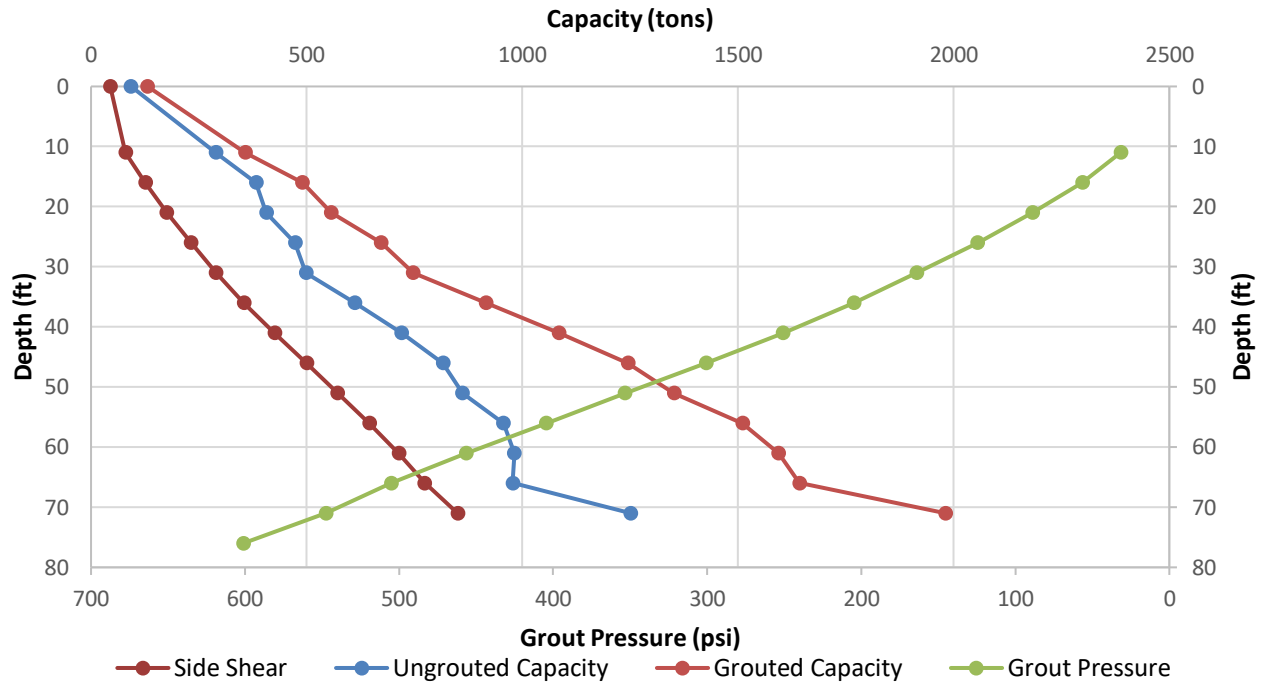


Figure 4.59 Data set 20 design curves.

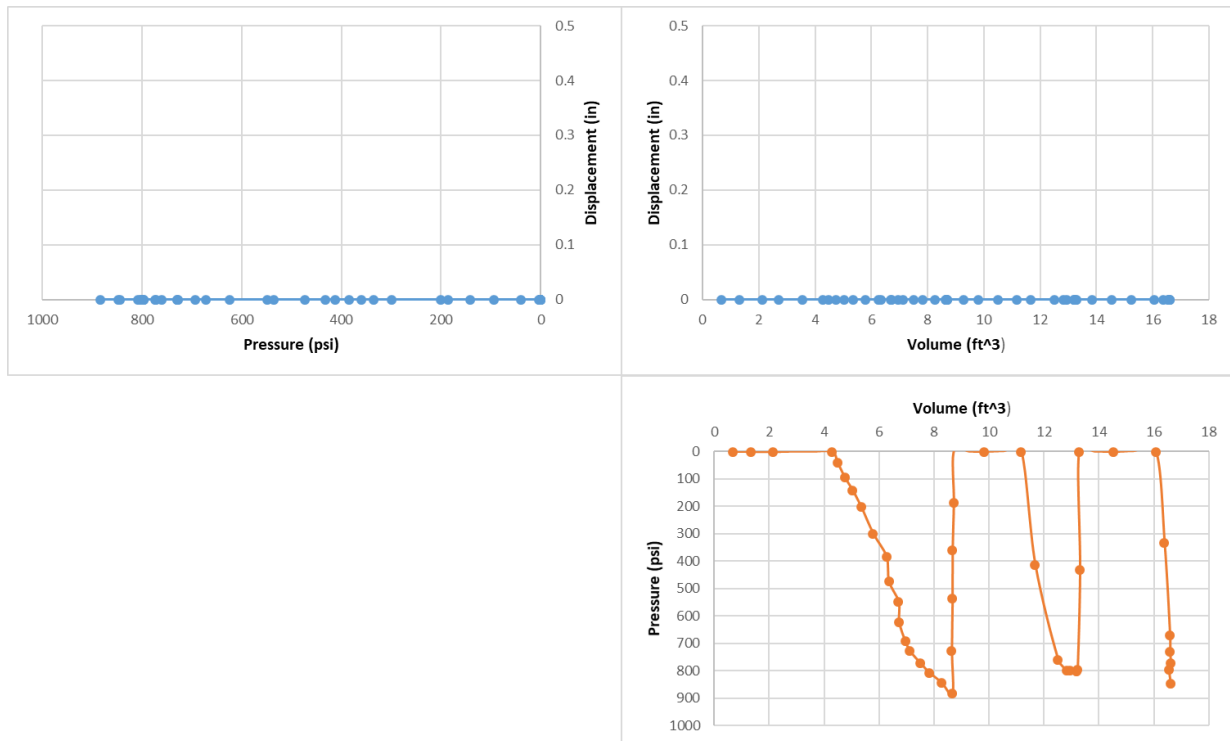


Figure 4.60 Data set 20 tri-axis plots.

Figure 4.60 shows the grouting quality assurance plots for data set 20; Effective pressure was selected based on the volume versus pressure graphs where the effective pressure was taken as 800 psi and peak pressure was 900 psi. The same discussion offered for data set 19 applies here.

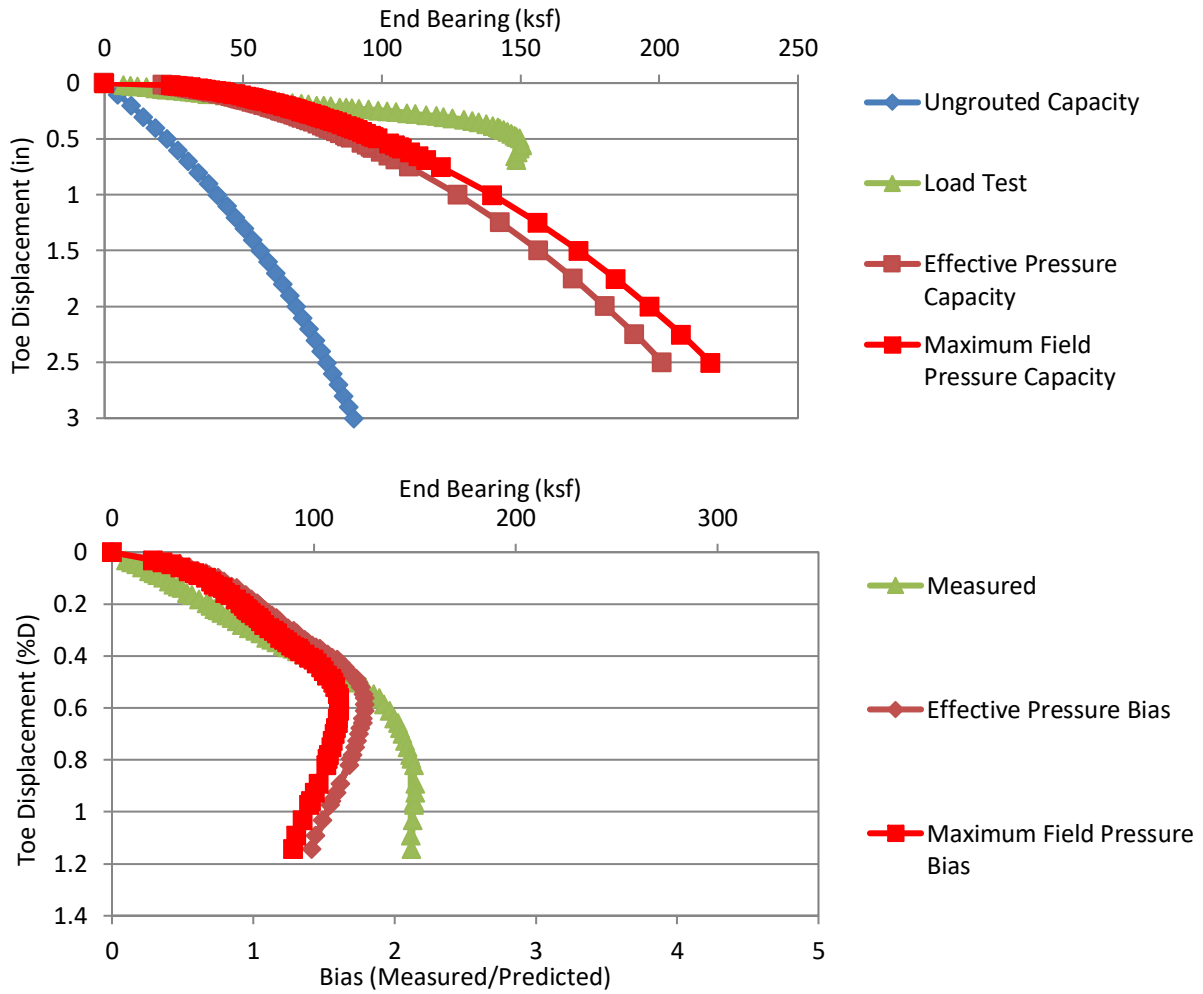


Figure 4.61 Data set 20 predicted/design and load test response (top); bias vs disp. (bottom).

4.2.21 Data Set 21, SR-80 Southern Blvd Bridge, S-1

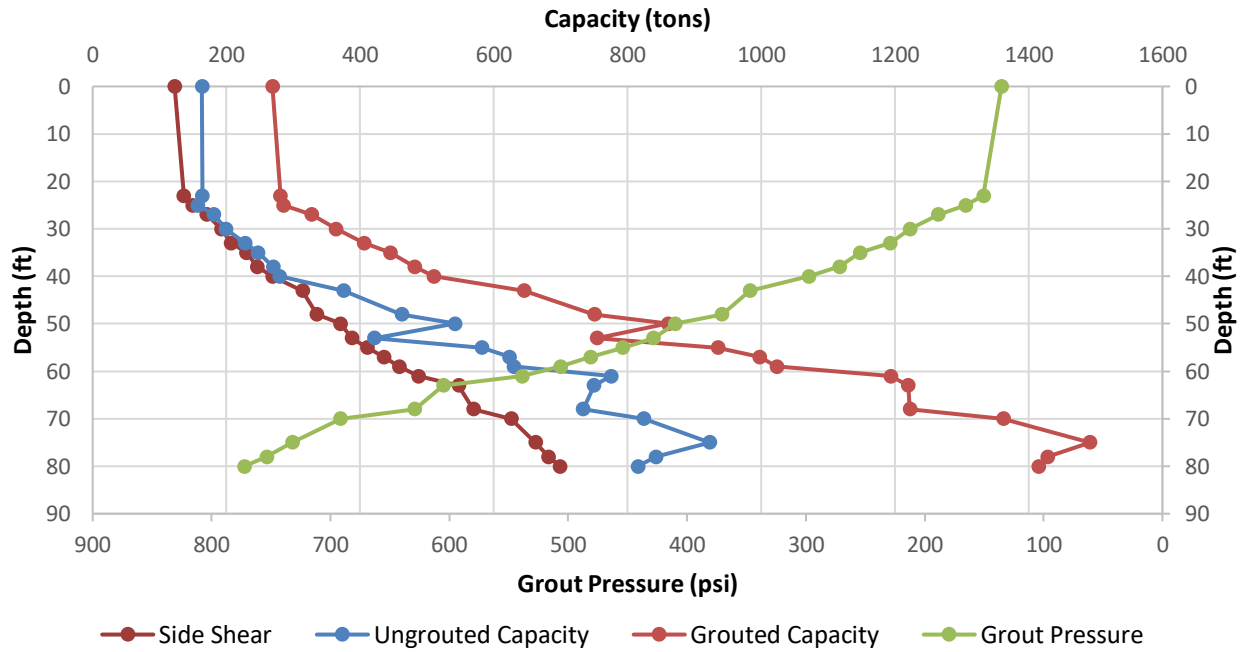


Figure 4.62 Data set 21 design curves.

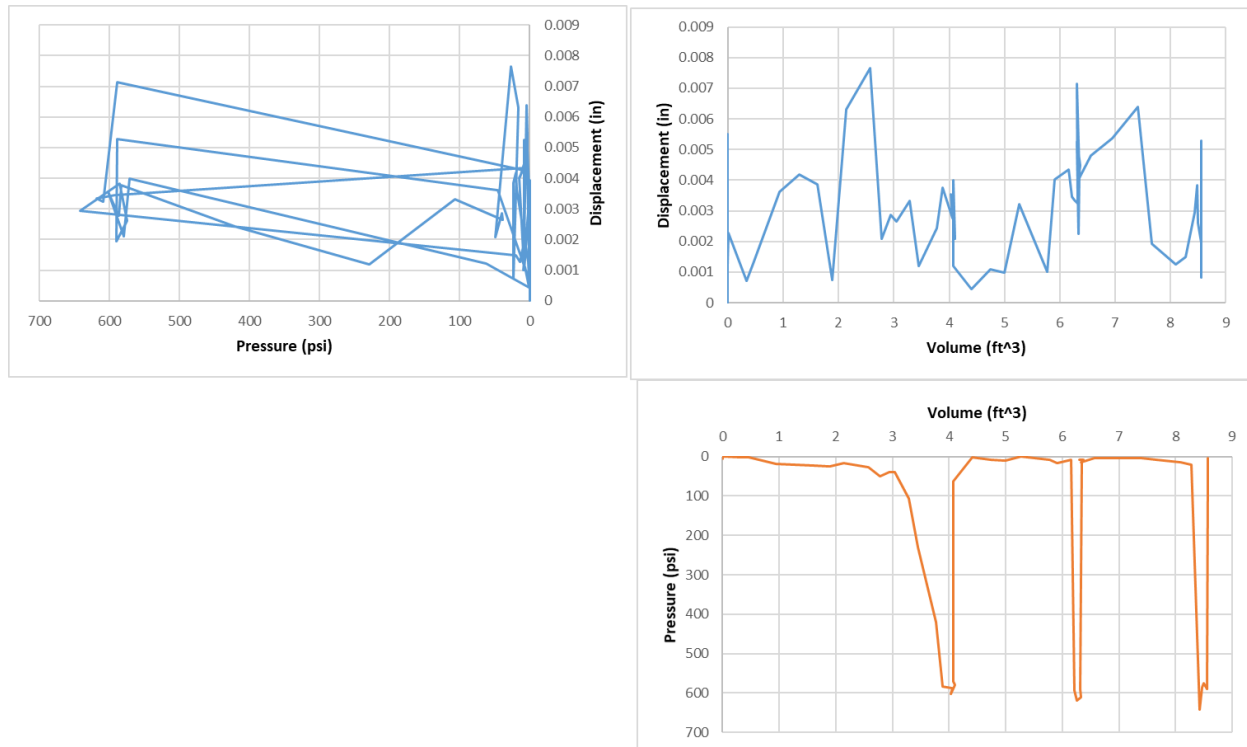


Figure 4.63 Data set 21 tri-axis plots.

Figure 4.62 shows the tri-axis plots for data set 21 and indicates two issues only visible when using the effectiveness plots. Pressure vs. displacements and volume vs. displacement show the effects of very small displacements that appear to be registering the noise in the displacement measurements caused by electrical sensitivity or reference system movement. Low volume quantities from what appear to be 3 grouting circuits indicate poor grout distribution and most likely a small uplift force (also noted by small displacements). Effective pressure was taken as 590 psi while the maximum pressure was recorded as 640 psi. The load test data supports very competent material that, with such small amounts of grout, would have performed well without grouting.

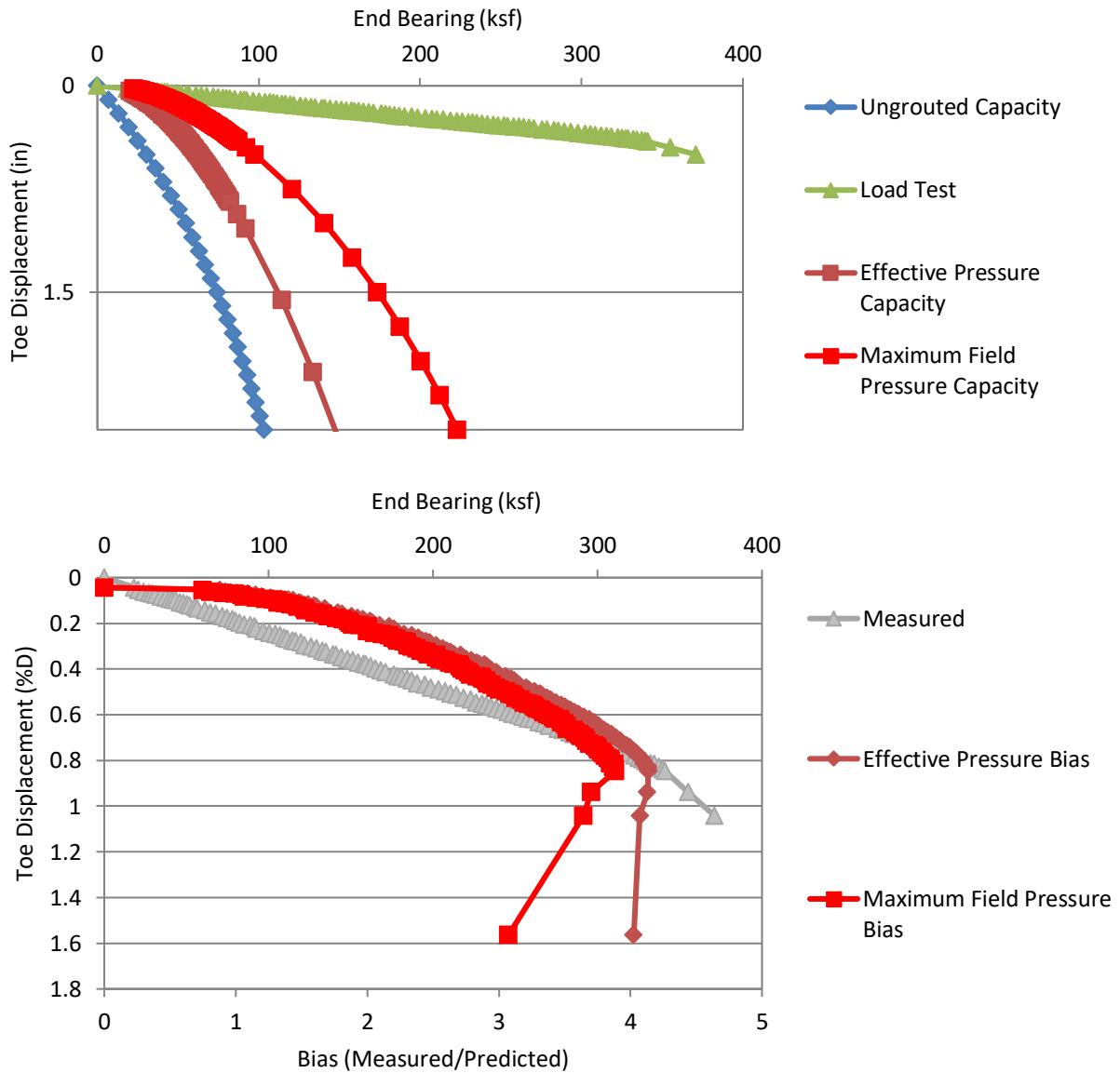


Figure 4.64 Data set 21 predicted/design and load test response (top); bias vs disp. (bottom).

4.2.22 Data Set 22, SR-80 Southern Blvd Bridge, S-2

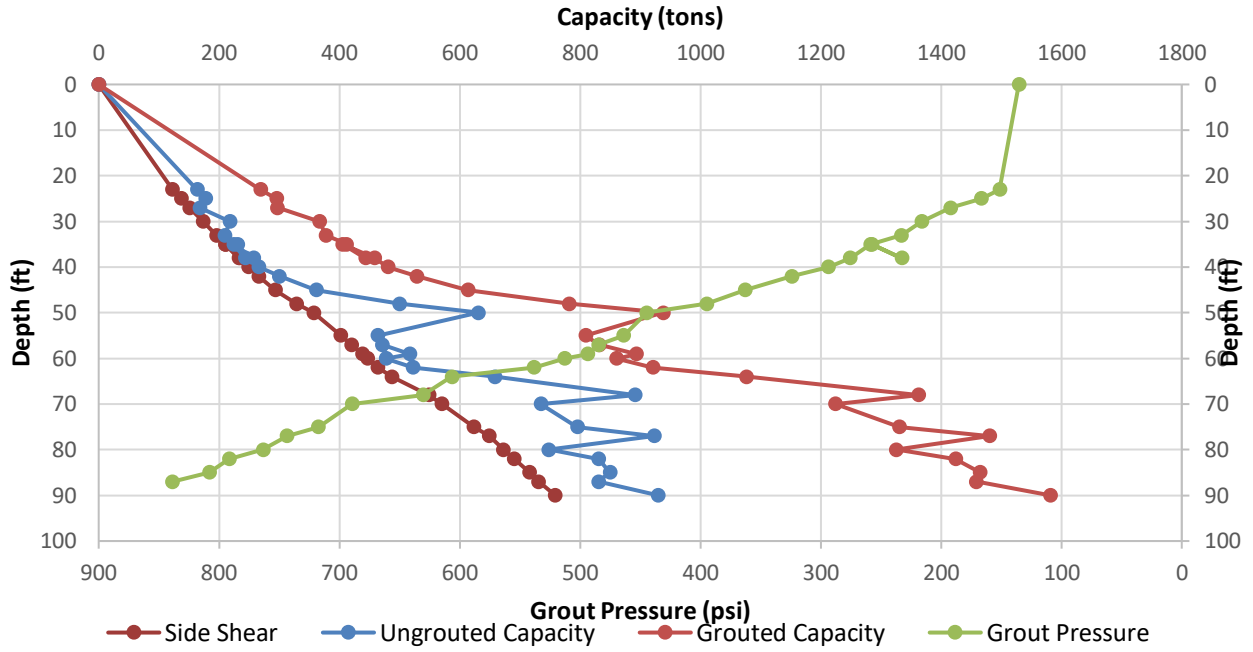


Figure 4.65 Data set 22 design curves.

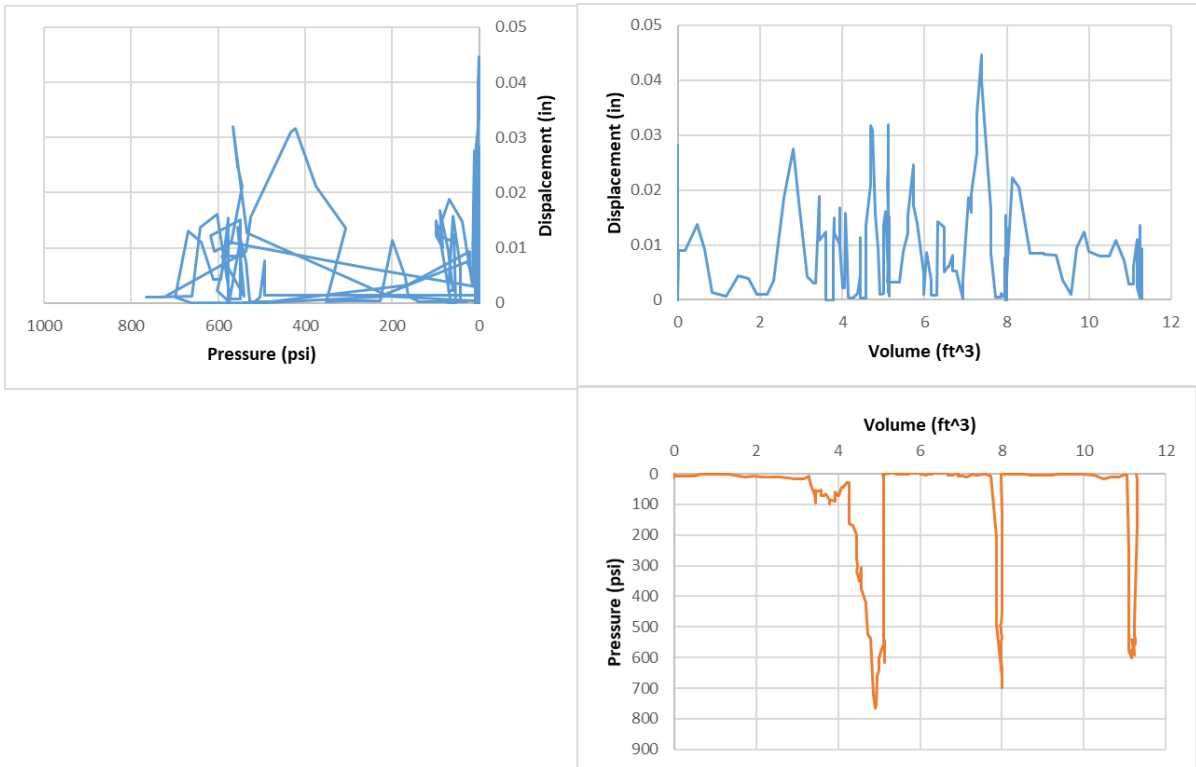


Figure 4.66 Data set 22 tri-axis plots.

Figure 4.65 shows the tri-axis plots for data set 22 and indicates the same issues as data set 21 (same comments). Effective pressure was taken as 600 psi while the maximum pressure was recorded as 765 psi. Statistically the data has been retained despite the poor grouting effectiveness.

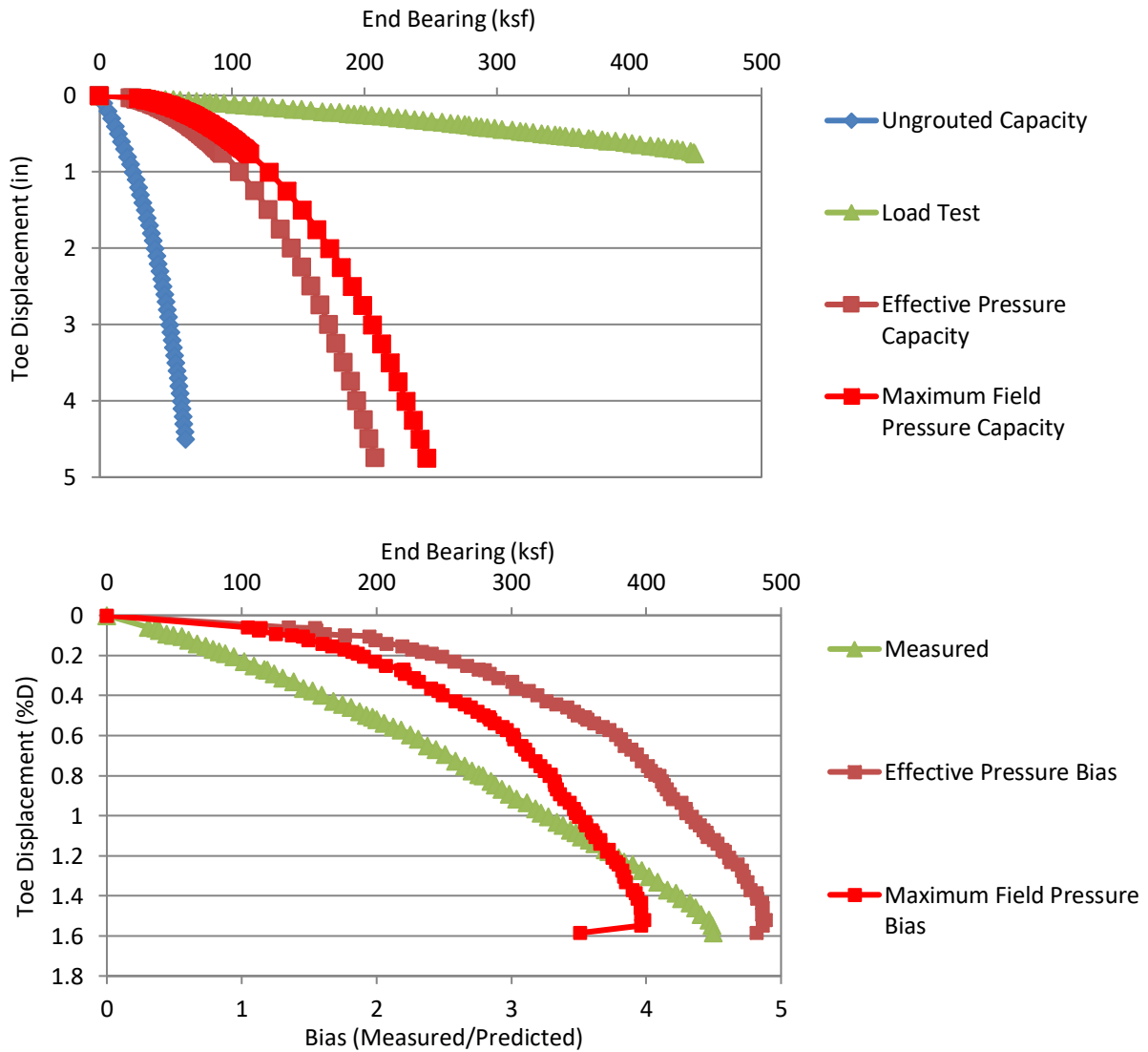


Figure 4.67 Data set 22 predicted/design and load test response (top); bias vs disp. (bottom).

4.2.23 Data Set 23, SR-80 Southern Blvd Bridge, S-3

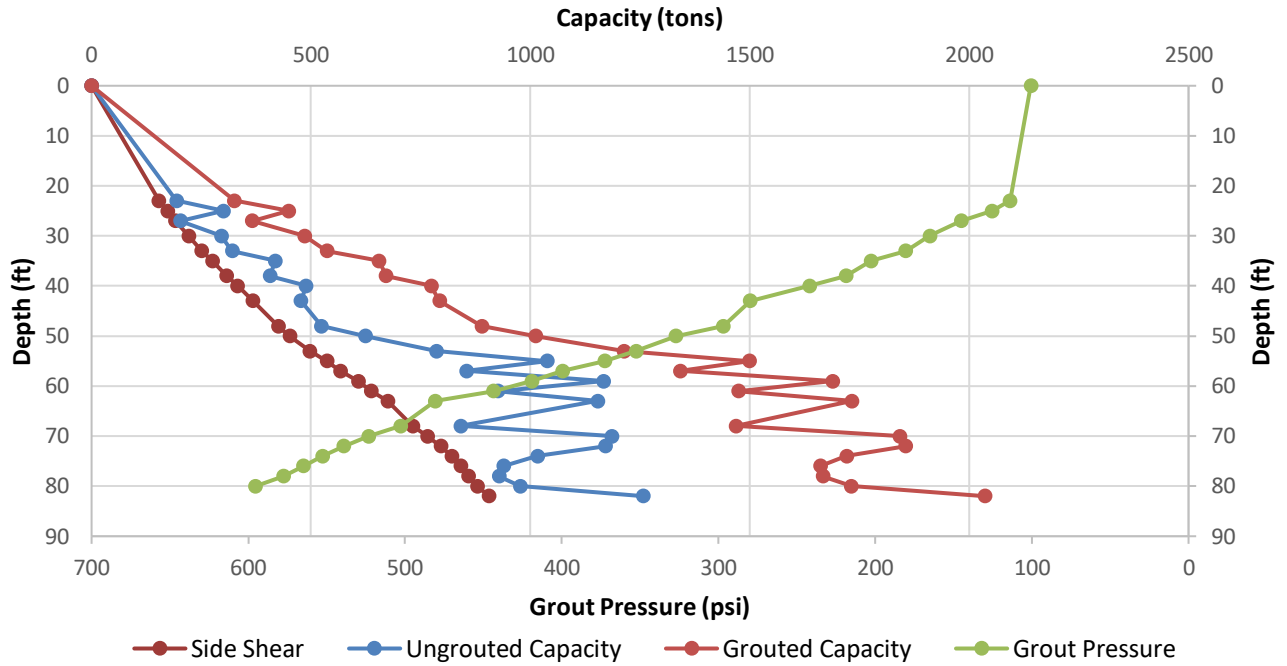


Figure 4.68 Data set 23 design curves

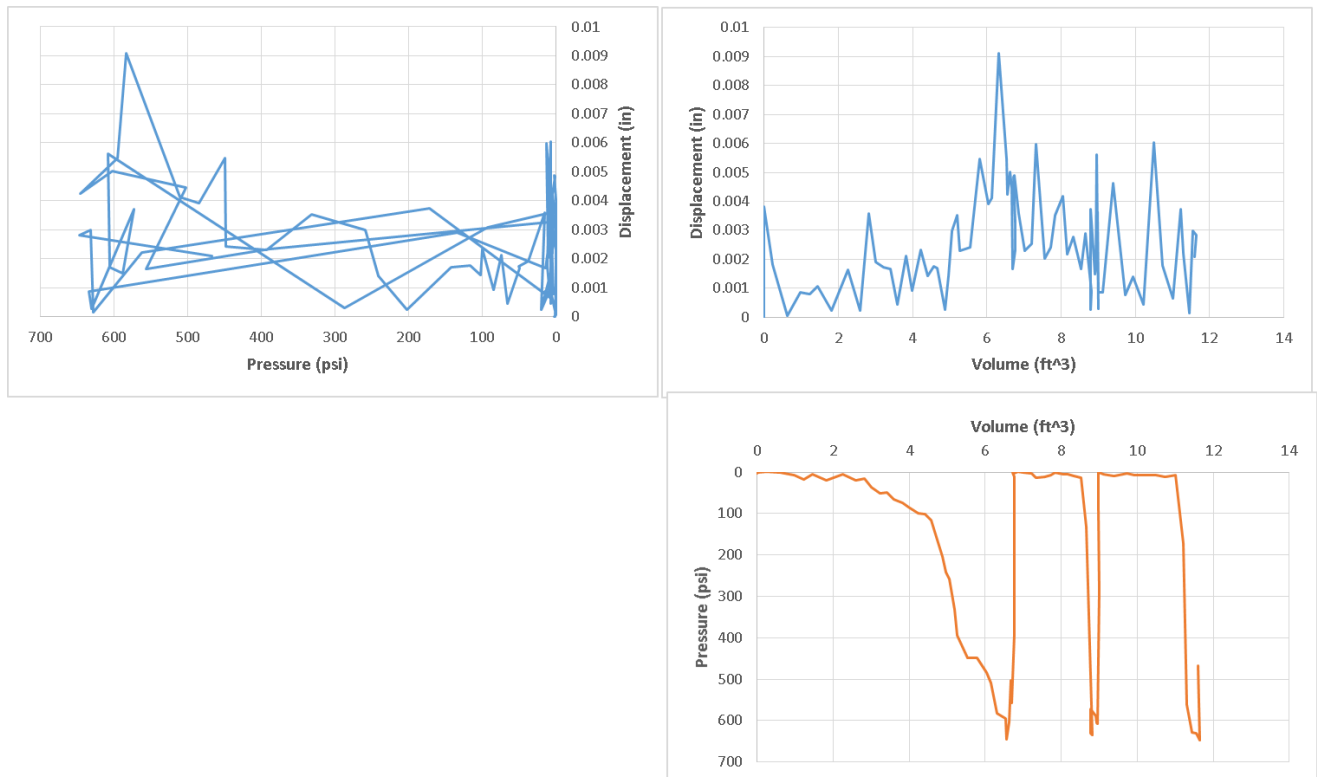


Figure 4.68 Data set 23 tri-axis plots.

Figure 4.69 shows the tri-axis plots for data set 23. Three circuits again are noted, the first of which produced a normal response up to 590 psi and approximately 6.7 cu. ft. of grout. The second two circuits had no effect. Horizontal lines in the pressure vs. volume plot show the volume used to fill the next circuit and did not contribute to the net volume. Effective pressure was taken as 590 psi while the maximum pressure was recorded as 647 psi. Like the other shafts grouted at this site, the grouting process aided only in proofing the end bearing, not improving it.

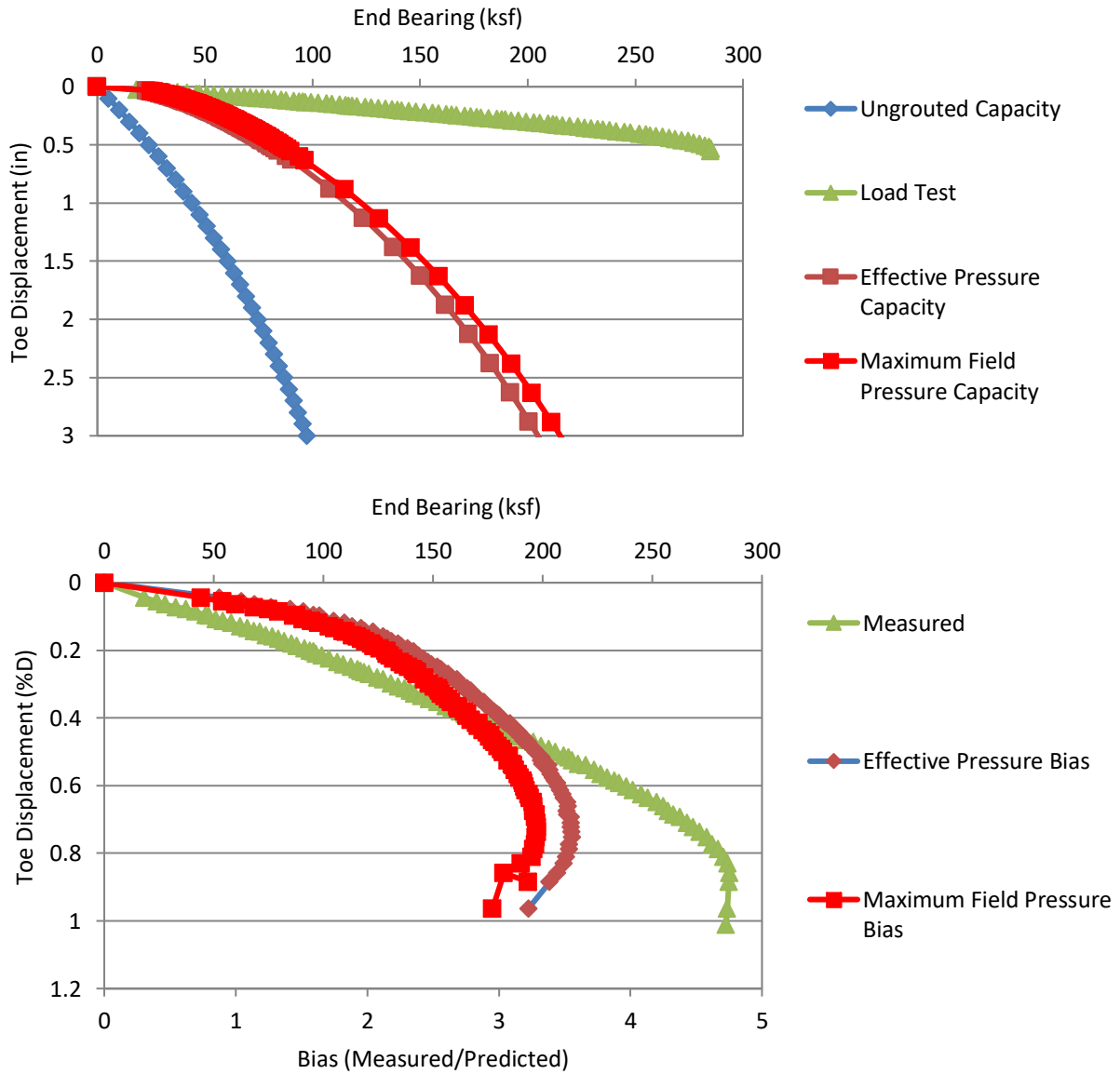


Figure 4.69 Data set 23 predicted/design and load test response (top); bias vs disp. (bottom).

4.2.24 Data Set 24, Overland Bridge Widening, S-1

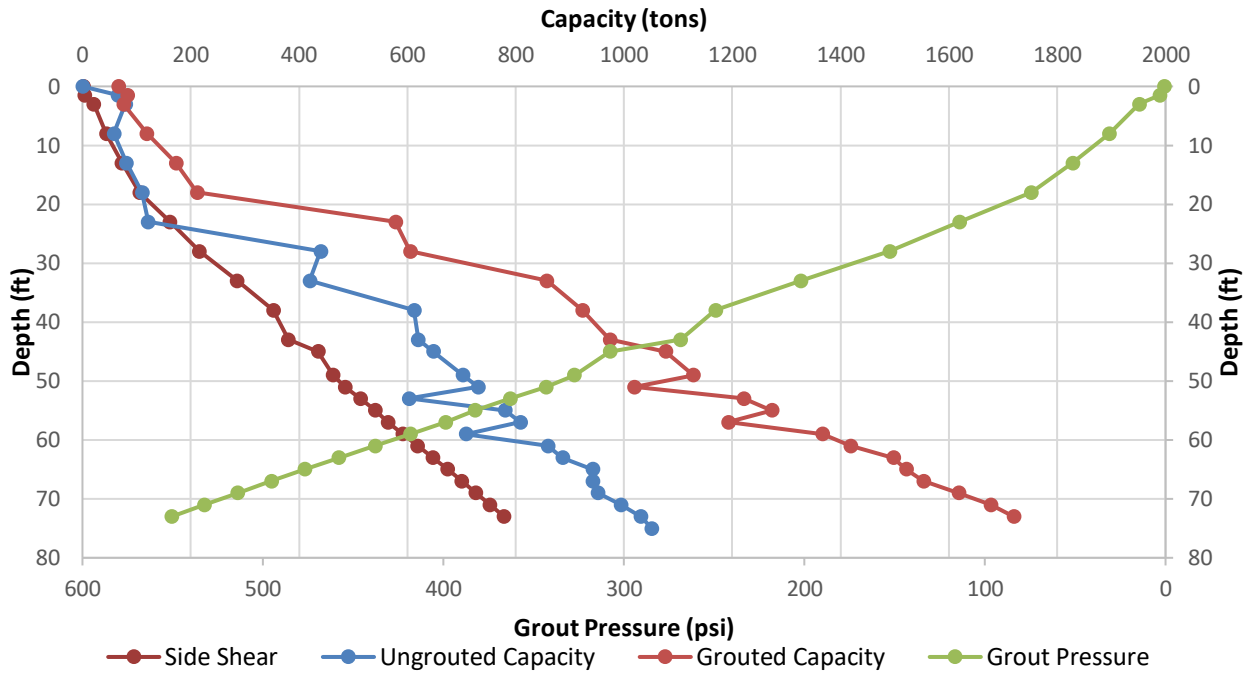


Figure 4.70 Data set 24 design curves.

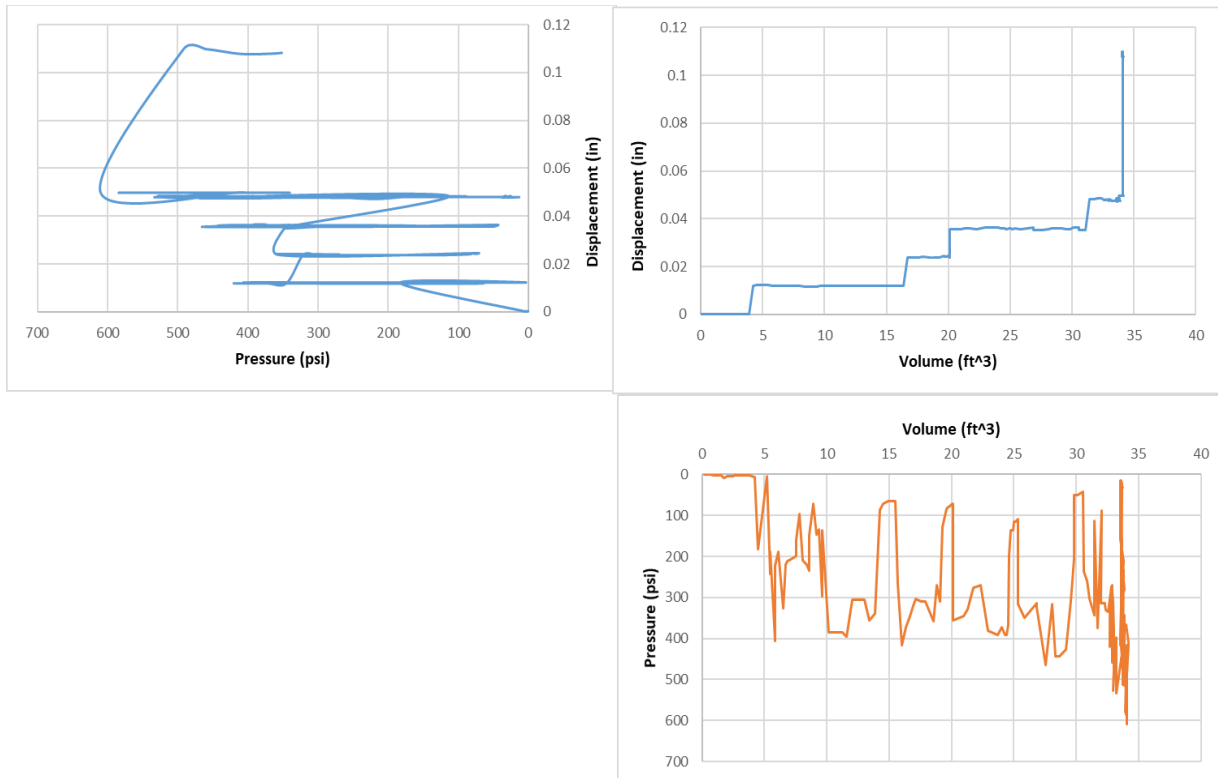


Figure 4.71 Data set 24 tri-axis plots.

Figure 4.72 shows the tri-axis plots for data set 24. Displacement measurements were coarse relative to the overall amount of displacement with a minimum sensitivity of approximately 0.012 in. This makes the effectiveness difficult to assess, but pressure vs. volume shows a generally increasing pressure with volume; pressure drops in that plot suggest reorientation of soil from the compaction grouting effects or migration into nearby voids. Grouting appears to have ended with line blockage (press/vol plot). The sudden increase in displacement at the end of grouting with a reduction in grout pressure and no increase in volume suggests a displacement error. Effective pressure was taken as 400 psi while maximum pressure was 609 psi. The anticipated maximum design pressure was 541 psi.

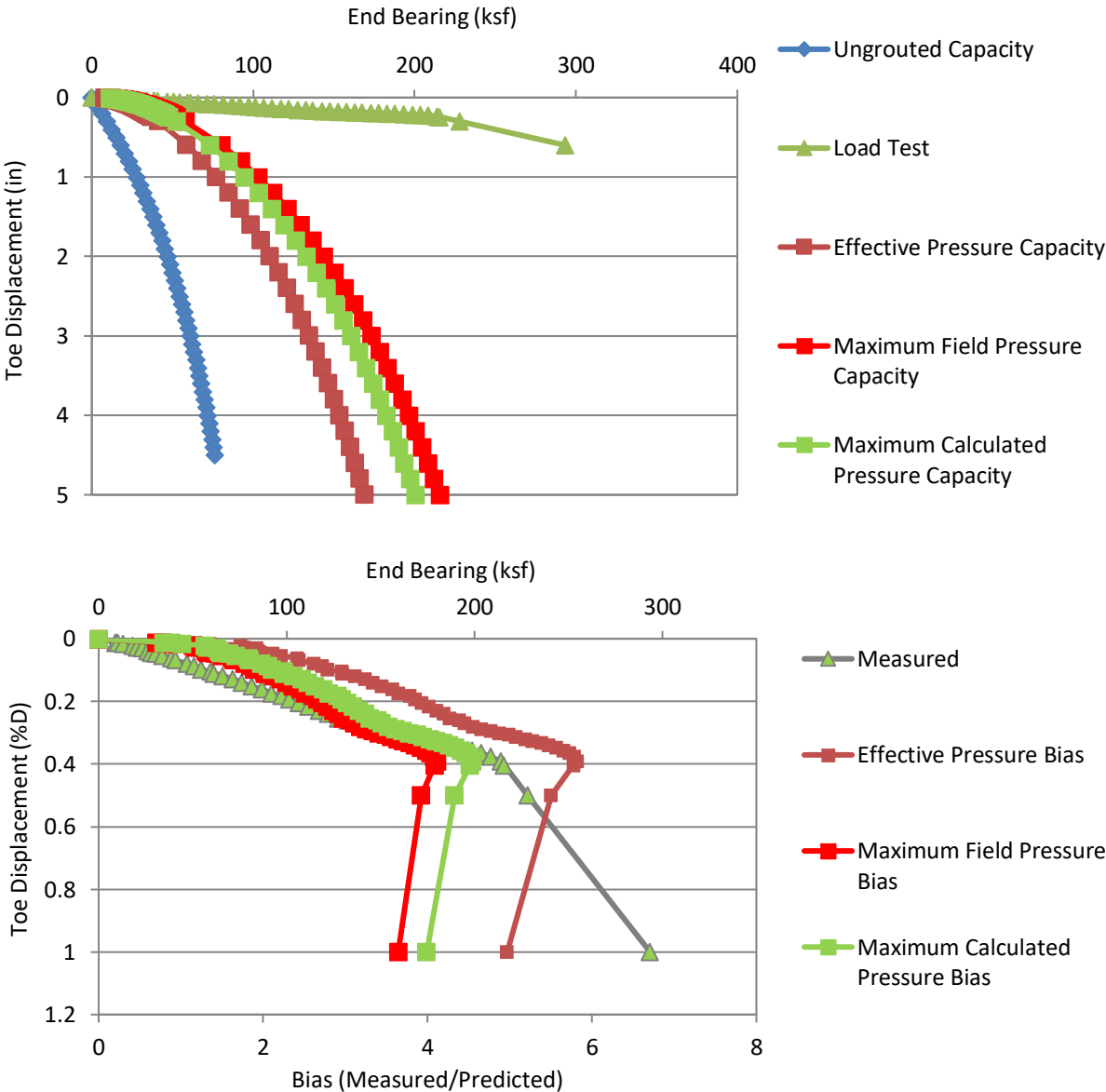


Figure 4.72 Data set 24 predicted/design and load test response (top); bias vs disp. (bottom).

4.2.25 Data Set 25, Overland Bridge Widening, S-2

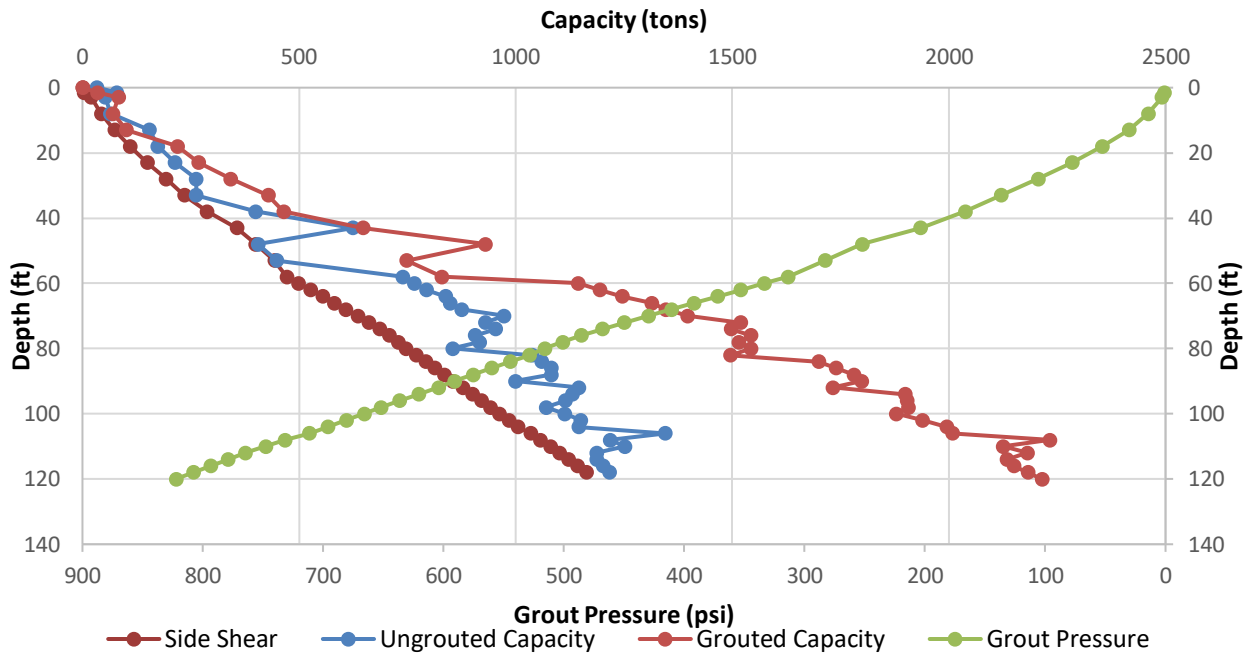


Figure 4.73 Data set 25 design curves.

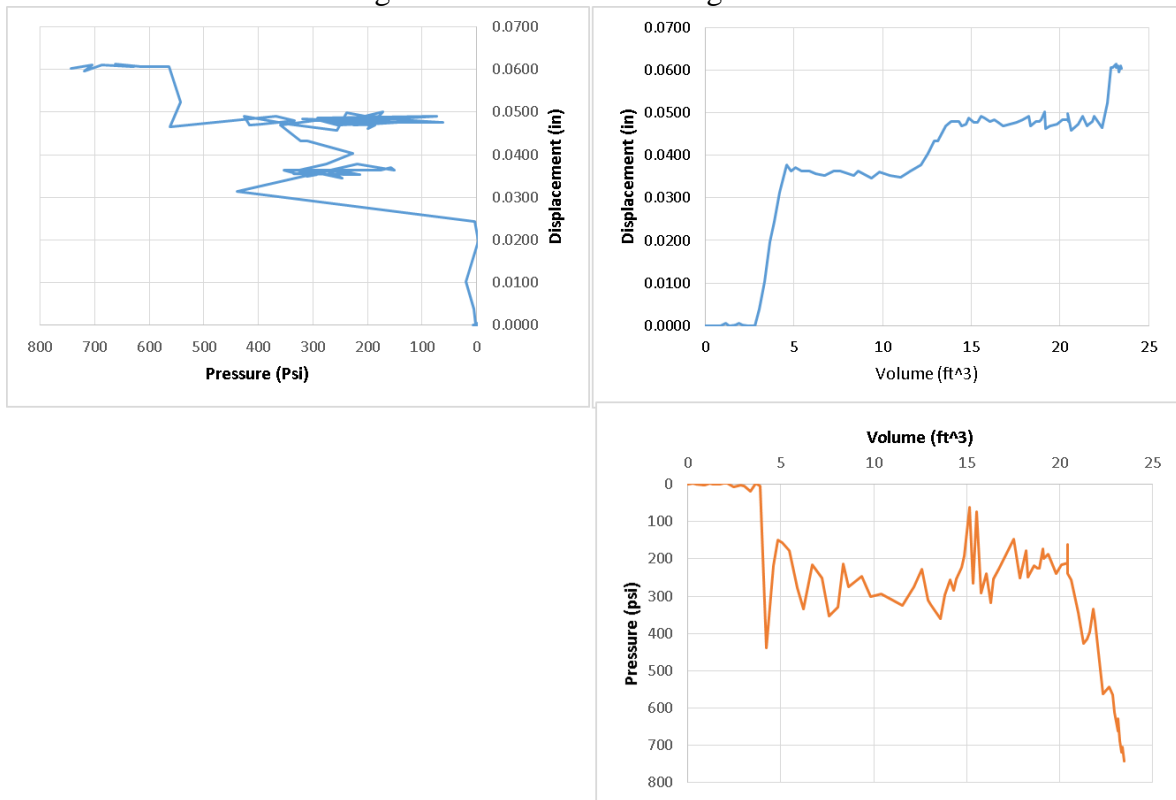


Figure 4.74 Data set 25 tri-axis plots.

Figure 4.75 shows the grouting quality assurance plots for data set 25. Several issues become clear upon reviewing the tri-axis plots: the initial jump in displacement without pressure (disp. error); the horizontal nature of the pressure vs. volume plot indicates and end bearing failure or migration but nearing the end of the grouting the increase in pressure with volume is not supported by uplift; uplift data is already questionable but the near vertical pressure vs. volume response at the end of grouting with the horizontal pressure vs. displacement suggests progressive closing of the grouting lines (eminent blockage). Effective pressure was taken as 300 psi while the maximum pressure was recorded as 743 psi.

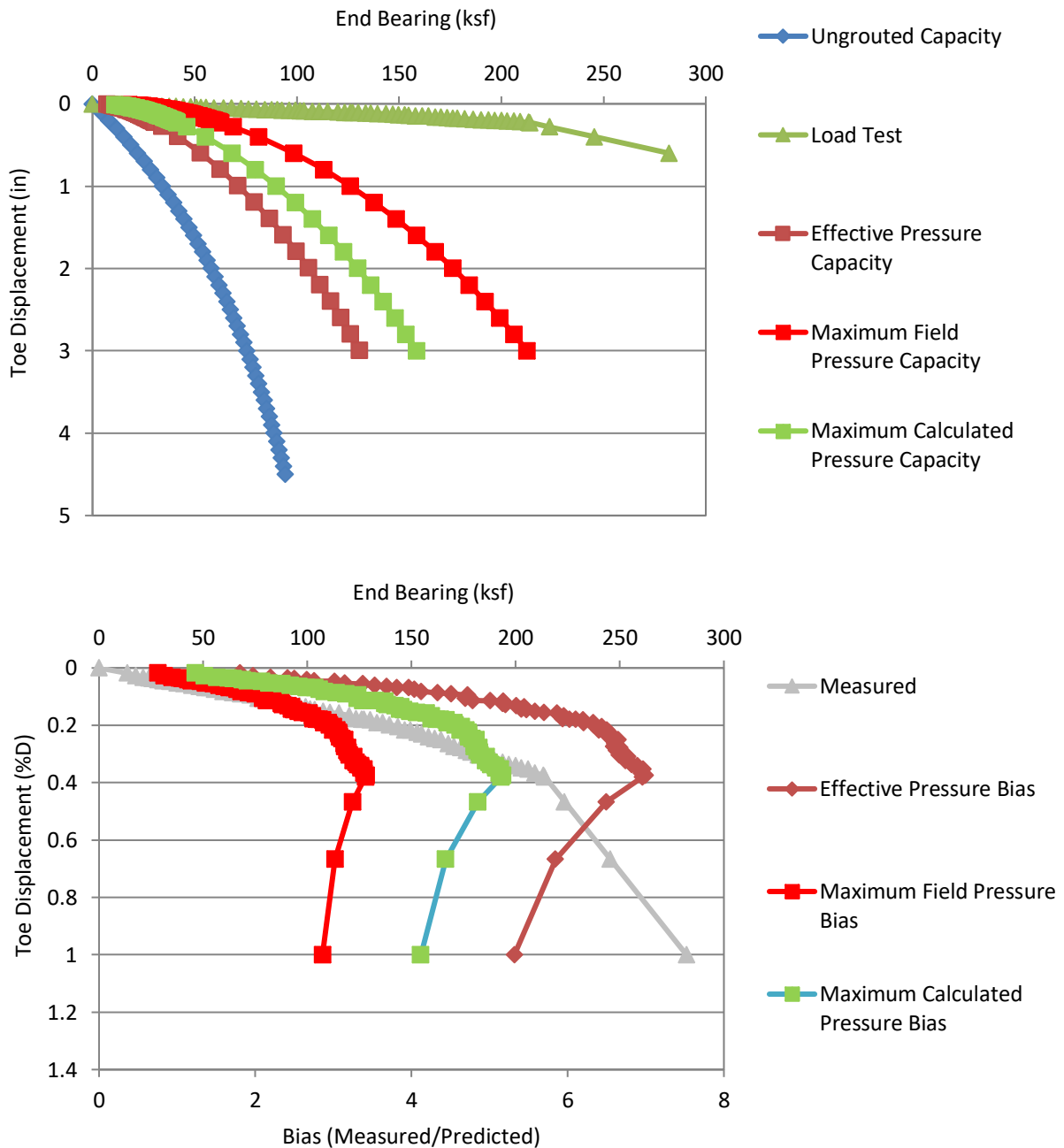


Figure 4.75 Data set 25 predicted/design and load test response (top); bias vs disp. (bottom).

4.2.26 Data Set 26, Overland Bridge Widening, S-3

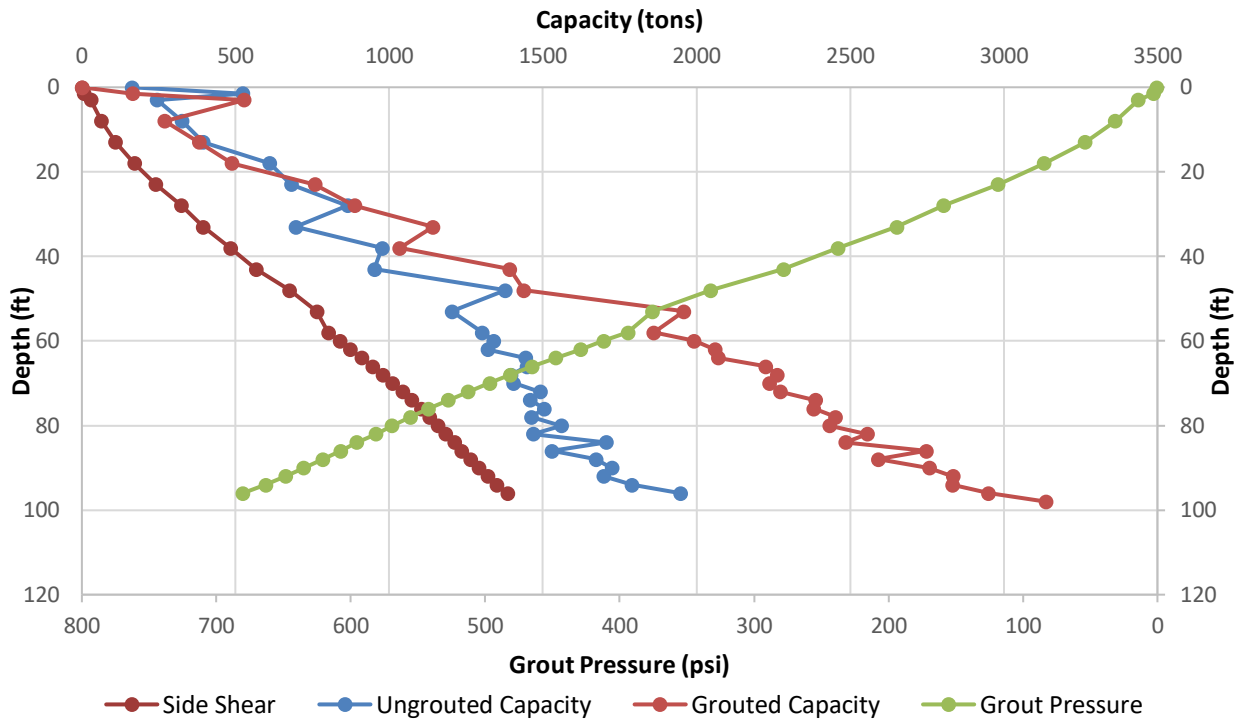


Figure 4.76 Data set 26 design curves.

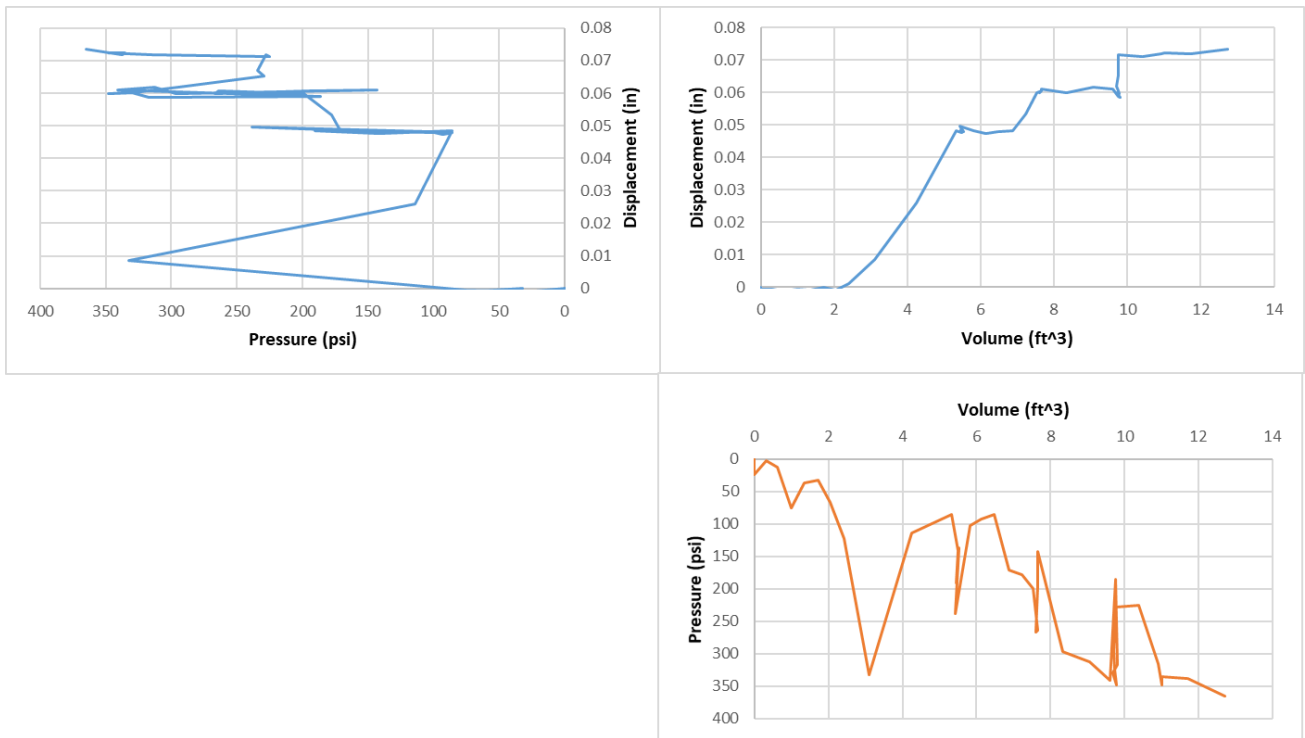


Figure 4.77 Data set 26 tri-axis plots.

Figure 4.78 shows the grouting quality assurance plots for data set 26. Uplift displacement from 0.01 to 0.05 with decreasing pressure indicates grout was not fully distributed across the base area. This is not an error in measurements but rather a transference of high pressure on a small area to lower pressure on a larger area while still increasing uplift force. The pressure spikes in both the pressure vs displacement and pressure vs volume suggest momentary line blockage which miraculously cleared. Grouting appears to have remained mostly effective throughout. Effective pressure was taken as 345 psi while the maximum pressure was recorded as 365 psi. The maximum anticipated design pressure was 513 psi.

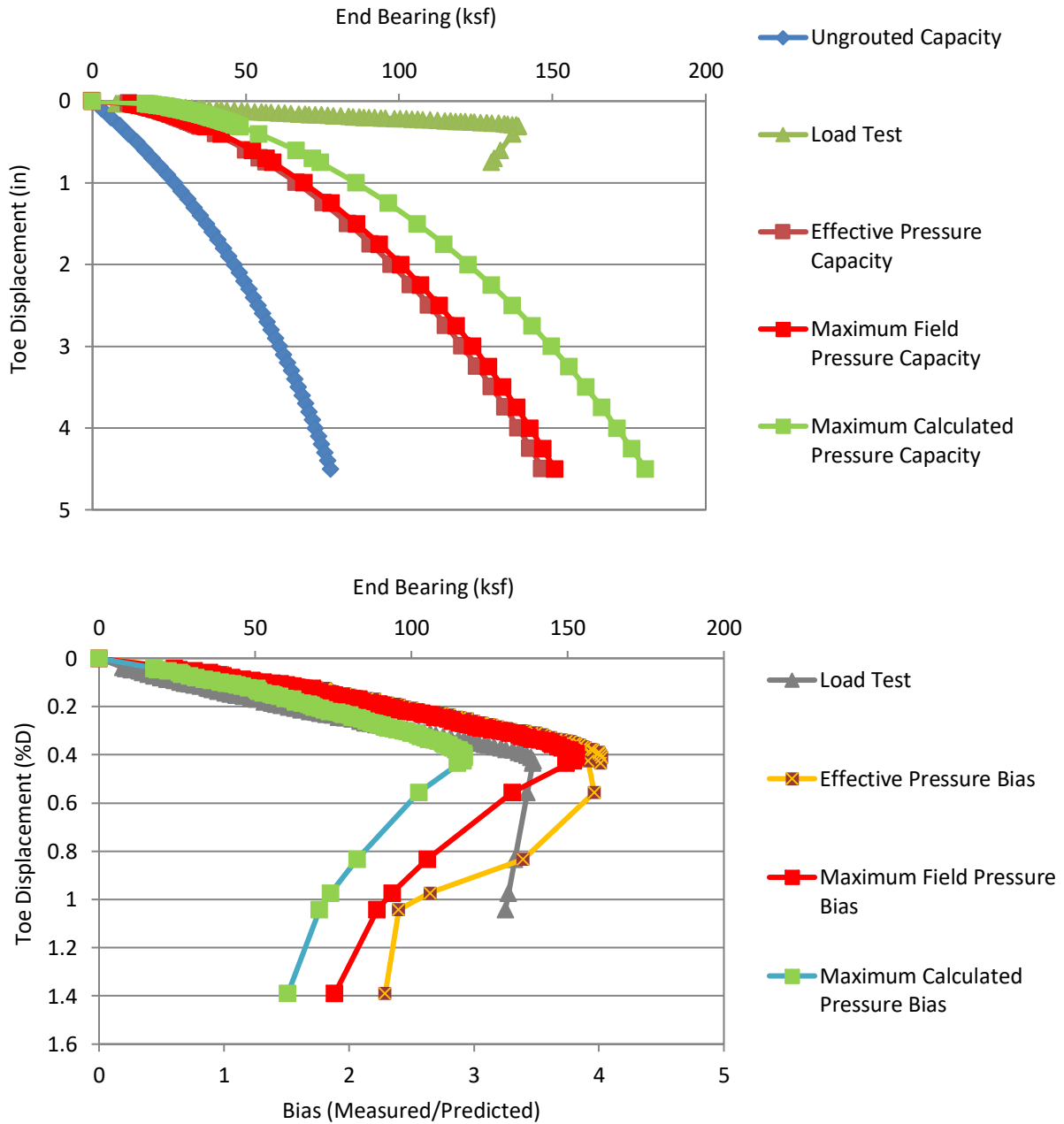


Figure 4.78 Data set 26 predicted/design and load test response (top); bias vs disp. (bottom).

4.2.27 Data Set 27, Carolina Bays Parkway, S-1

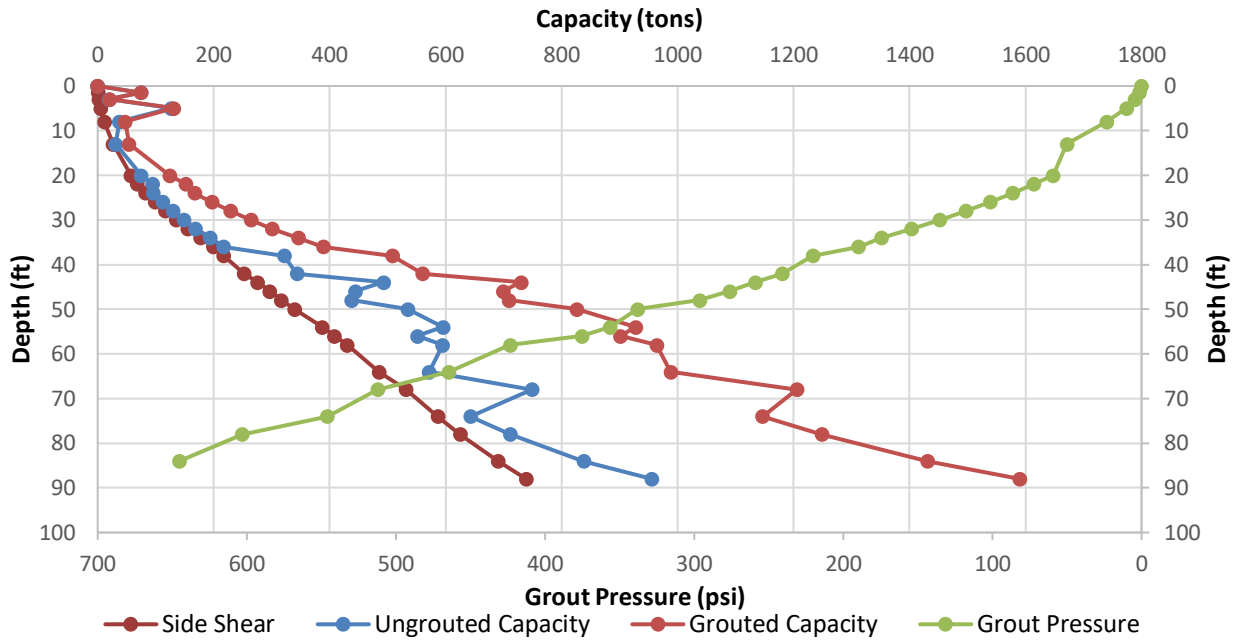


Figure 4.79 Data set 27 design curves.

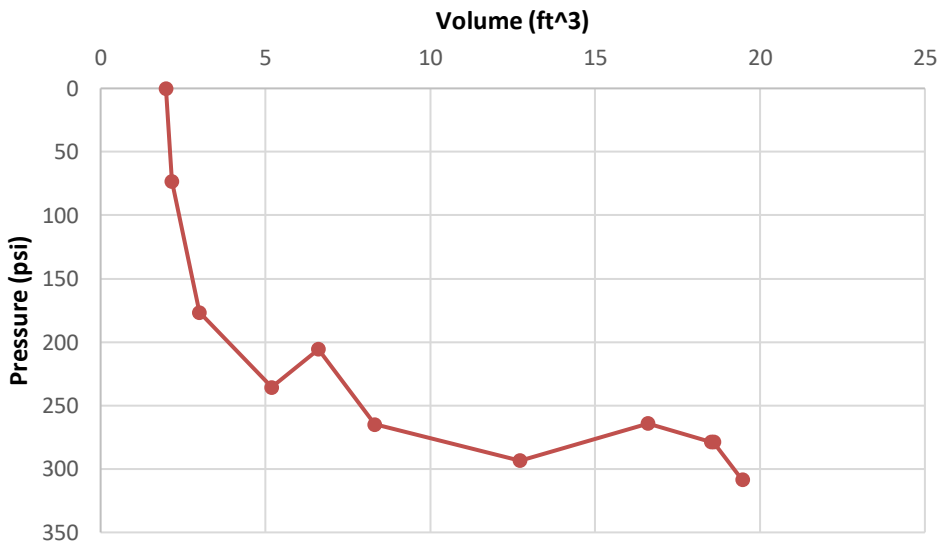


Figure 4.80 Data set 27 volume vs pressure plot.

No displacement data was available for data set 27, but the pressure vs. volume plot showed proper shape. Figure 4.81 shows the pressure versus volume graph for data set 27 where effective pressure was determined to be 293 psi and the maximum pressure was 308 psi. Without displacement data the horizontal trend at approximately 300 psi cannot be explained. The maximum anticipated design pressure was 488 psi.

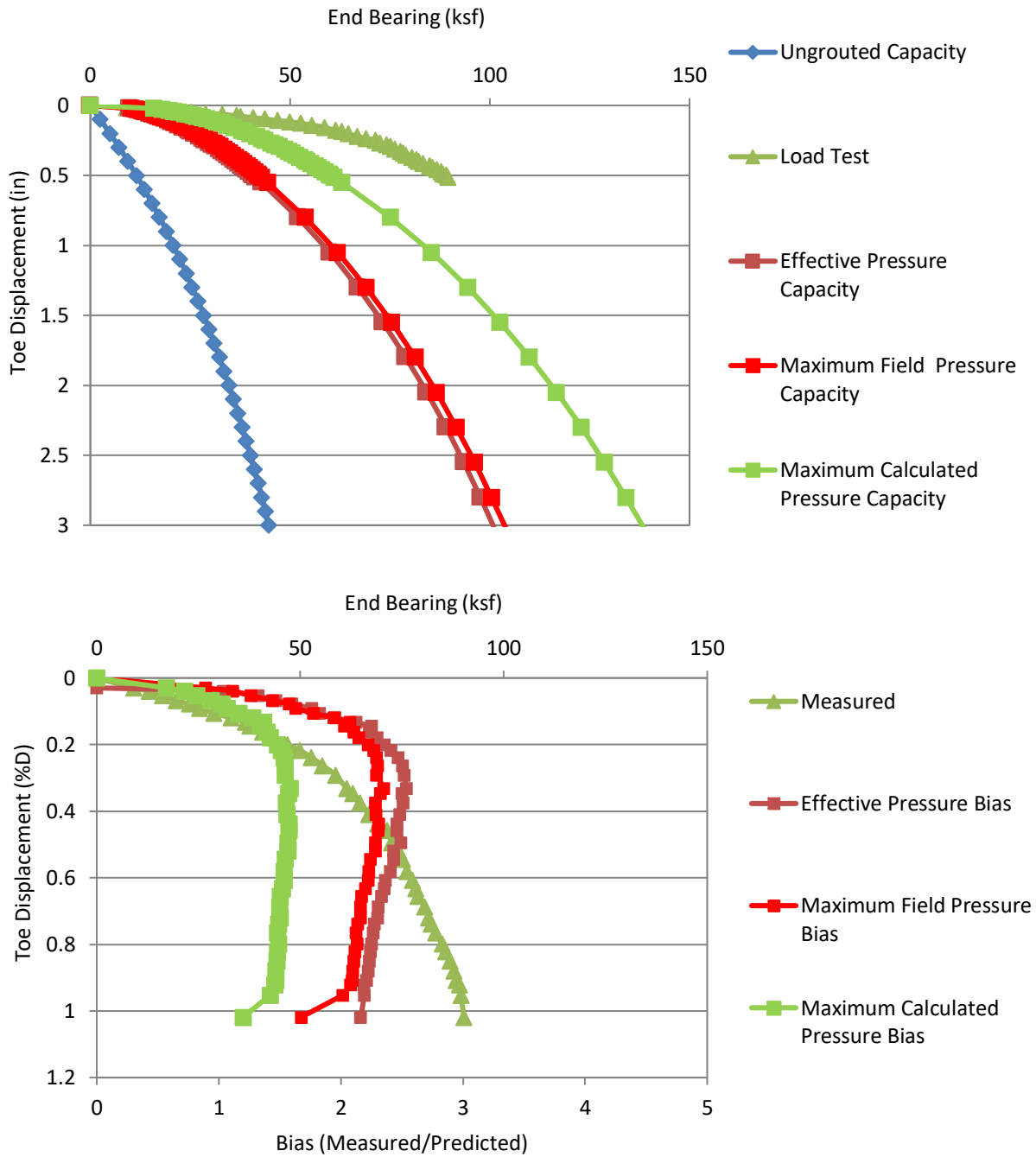


Figure 4.81 Data set 27 predicted/design and load test response (top); bias vs disp. (bottom).

4.2.28 Data Set 28, Gilmerton Bridge Replacement, S-1

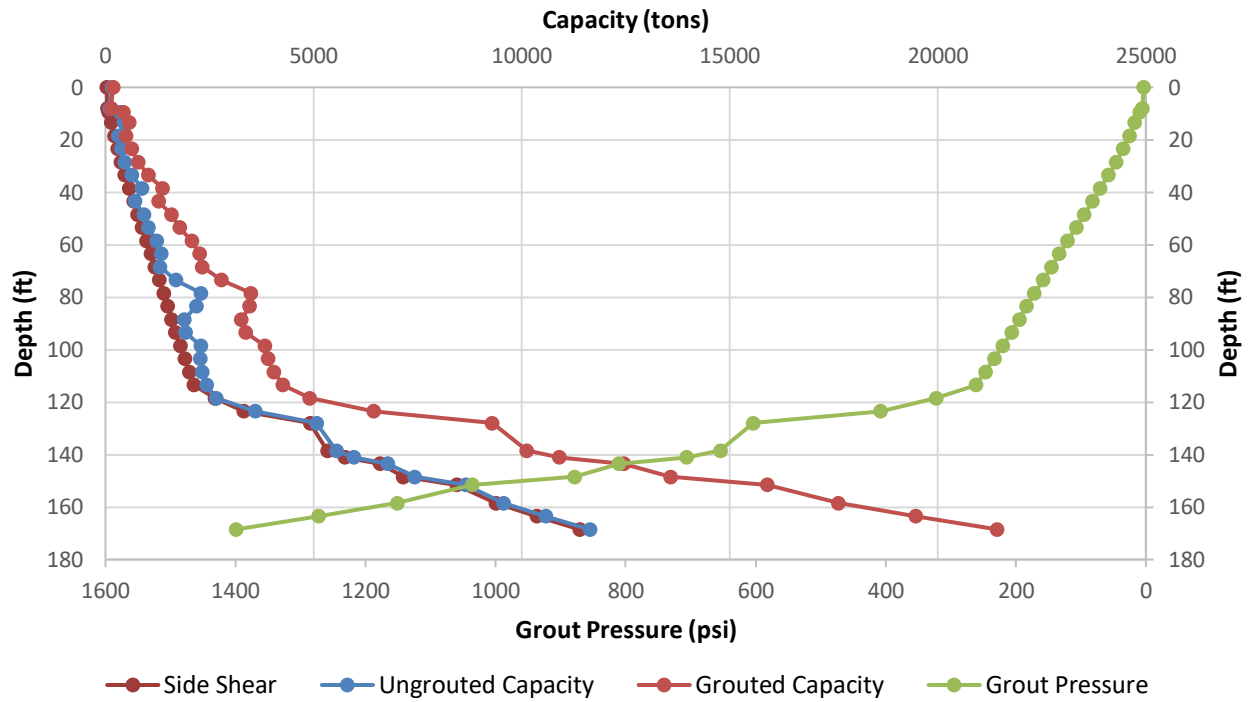


Figure 4.82 Data set 28 design curves.

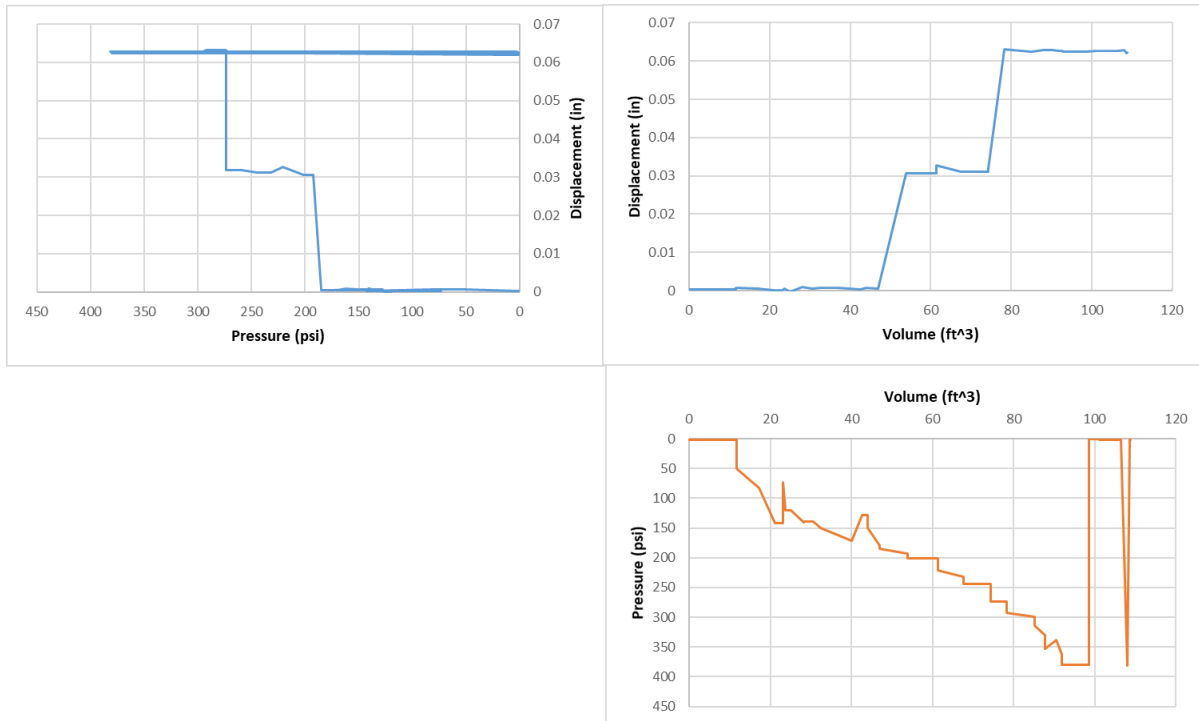


Figure 4.83 Data set 28 grout tri-axis plots.

Figure 4.84 shows the tri-axis plots for data set 28. Similar to data set 27, the normal pressure vs volume response makes this data usable despite the small and irregular uplift displacement response. A second circuit may have been used or a second attempt to grout the same circuit is shown as a spike in pressure in both the pressure vs. volume and pressure vs. displacement plots. Effective and maximum pressures were taken to be 380 psi. Maximum anticipated design pressure was 260 psi.

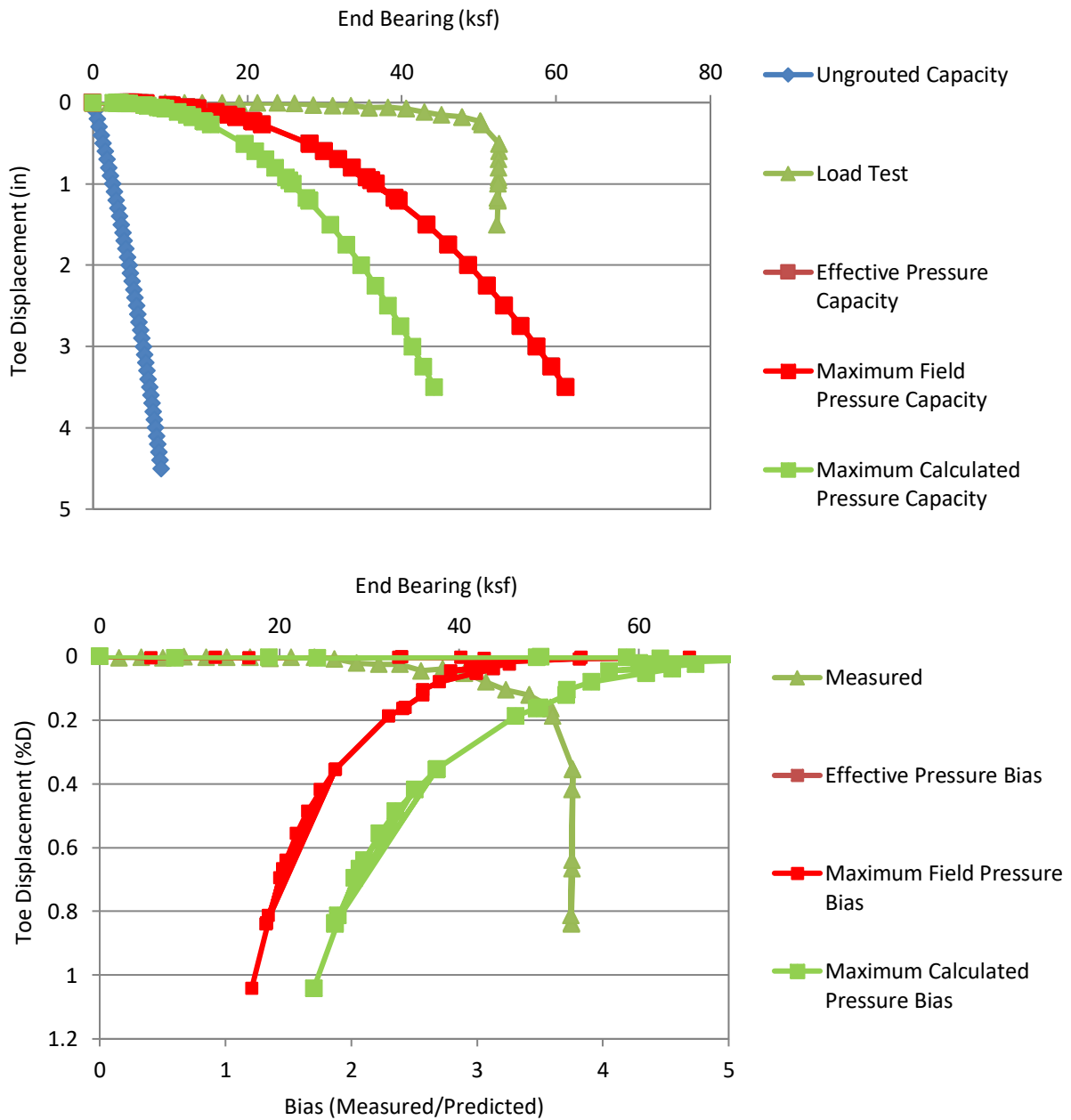


Figure 4.84 Data set 28 predicted/design and load test response (top); bias vs disp. (bottom).

4.2.29 Data Set 29, Peninsula Condominium

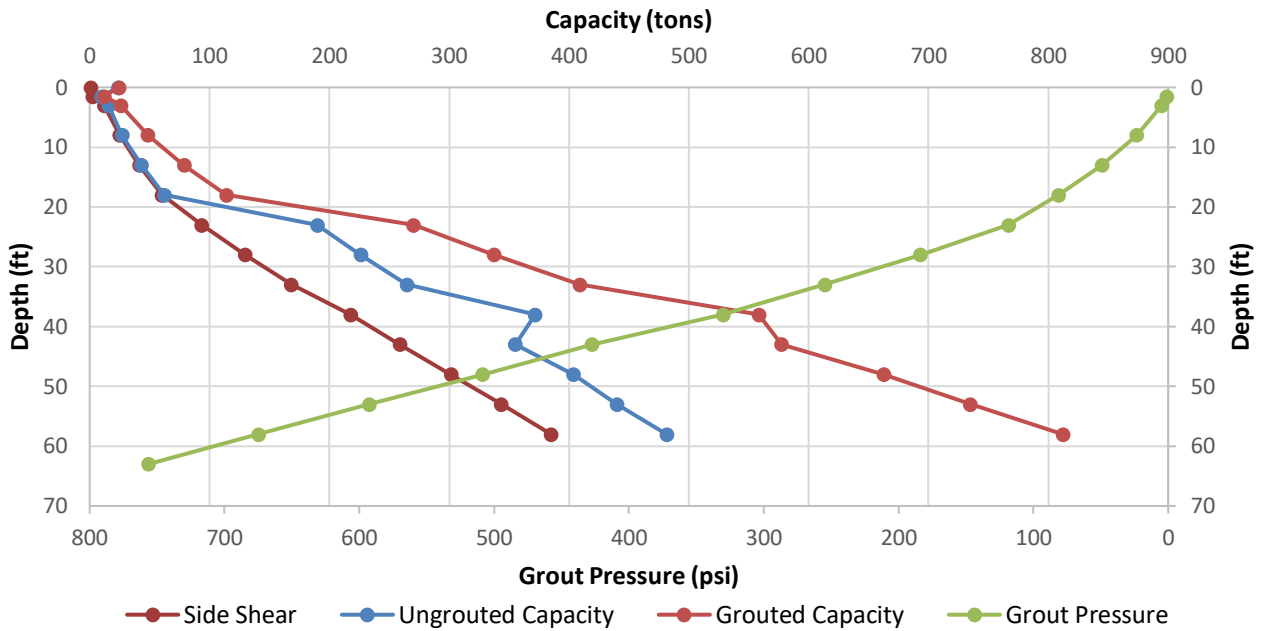


Figure 4.85 Data set 29 design curves.

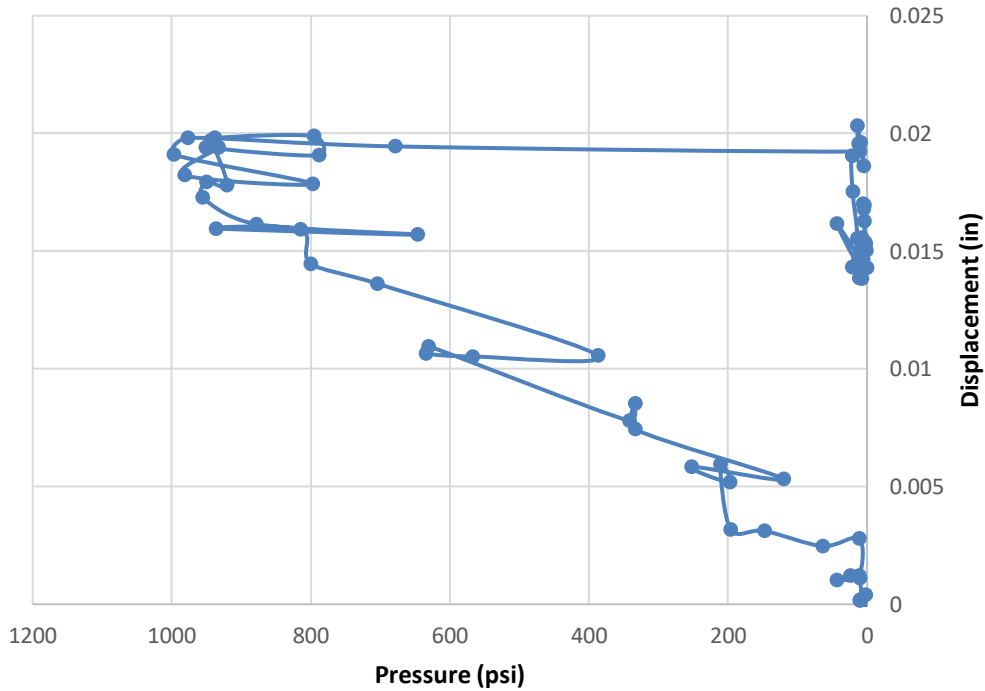


Figure 4.86 Data set 29 pressure vs disp. plot.

No volume data was available for this site, but the pressure vs. displacement plot appears to be normal. Figure 4.87 shows the pressure versus displacement graph. Had irregularities in this plot been present, the lack of volume data would make it impossible to troubleshoot. Maximum pressure

was 997 psi while effective pressure was taken as 935 psi. The maximum anticipated design pressure approximately 710 psi.

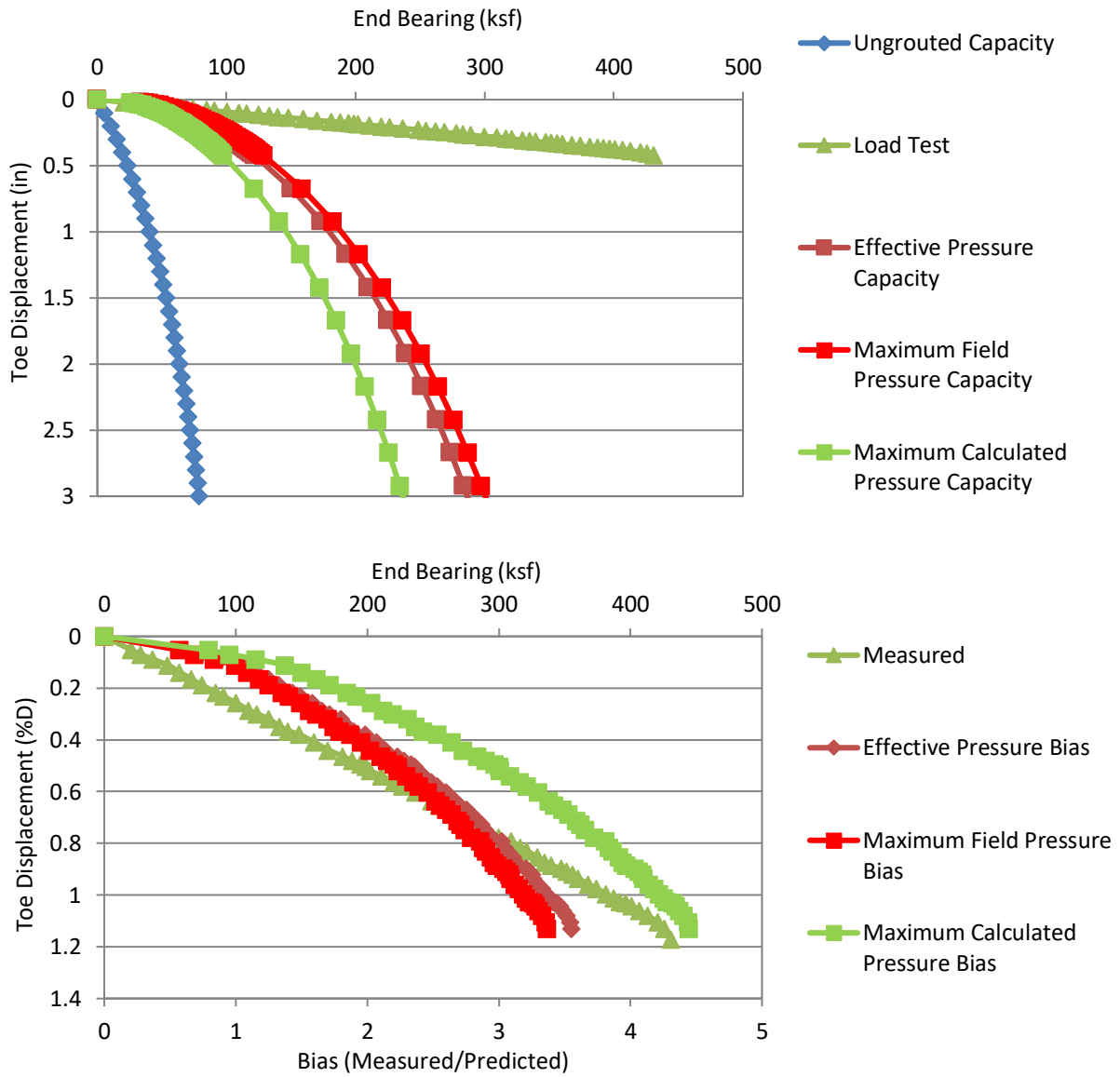


Figure 4.87 Data set 29 predicted/design and load test response (top); bias vs disp. (bottom).

4.2.30 Data Set 30, West Rail Bypass, 41E

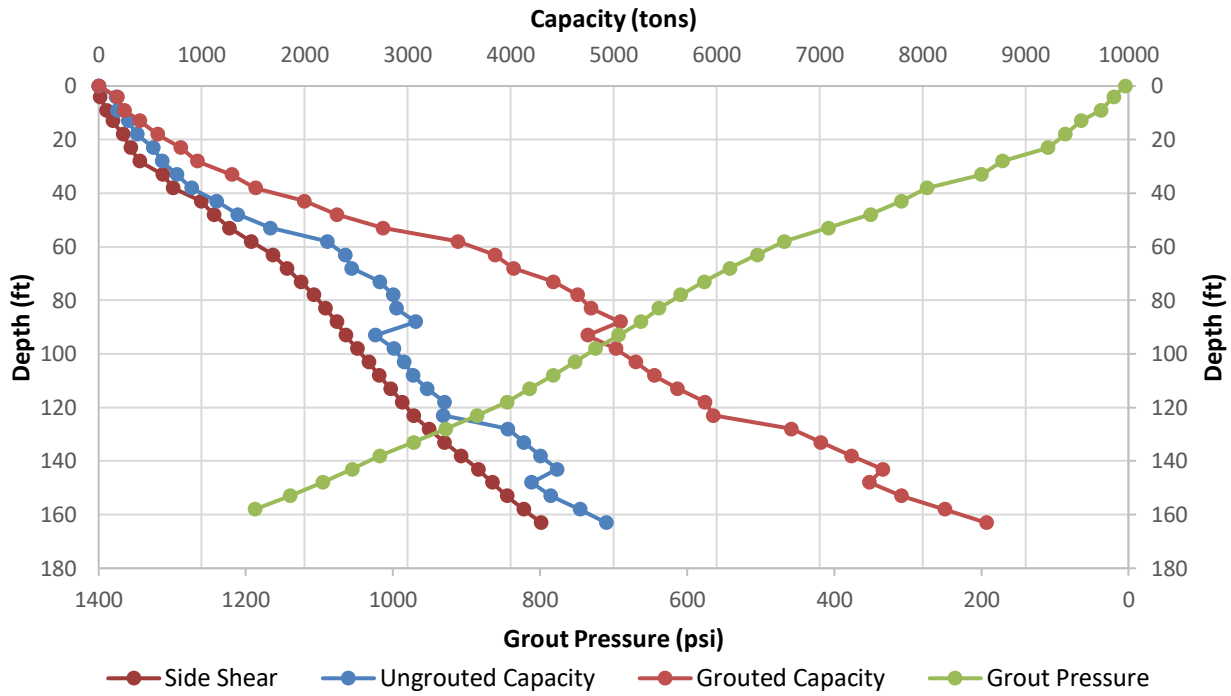


Figure 4.88 Data set 30 design curves.

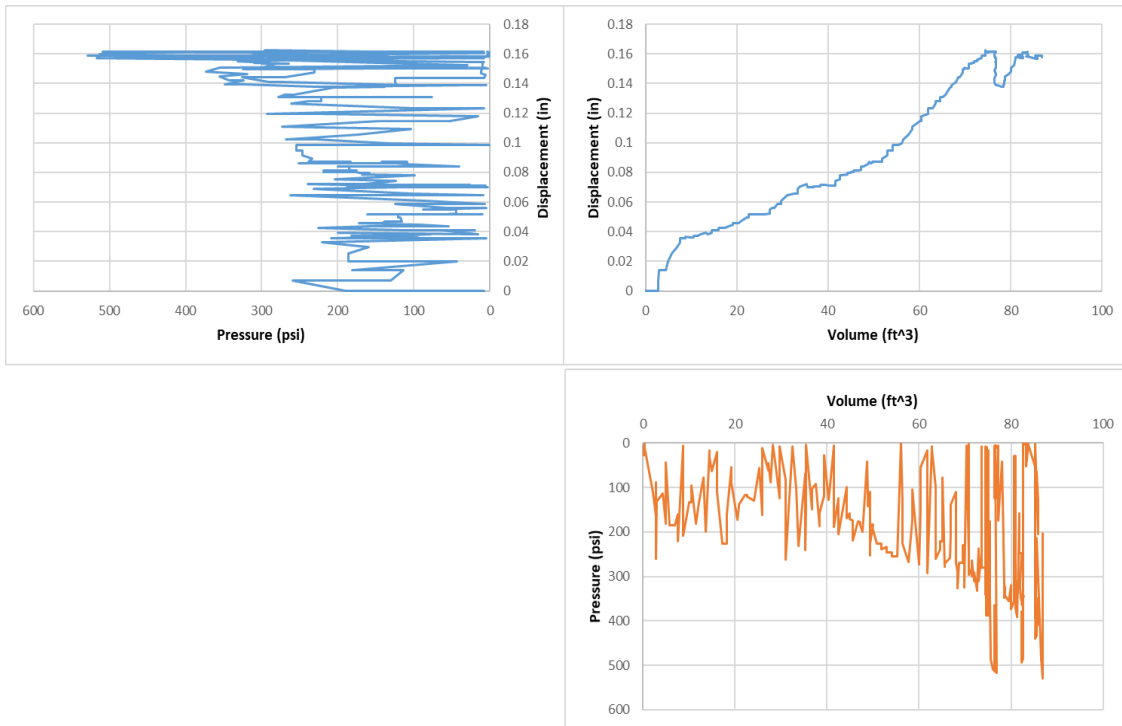


Figure 4.89 Data set 30 tri-axis plots.

Figure 4.90 shows the tri-axis plots for data set 30. Both the pressure vs. volume and volume vs. displacement graphs show horizontal trends supporting end bearing failure or piping. Also, both the pressure vs. volume and pressure vs. uplift graphs show spikes in pressure without an associated uplift or volume increase, which indicates a grout line blockage at the end of the grouting process. Effective pressure could be argued to be 400 or 150 psi. The 400 psi value was legitimately achieved during effective grouting, but was unable to maintain that pressure with additional volume, which suggests a change in soil structure beneath the shaft tip. Just prior to line blockage, 300 psi was being sustained. This value was used as the effective pressure. The maximum field recorded pressure was 530 psi.

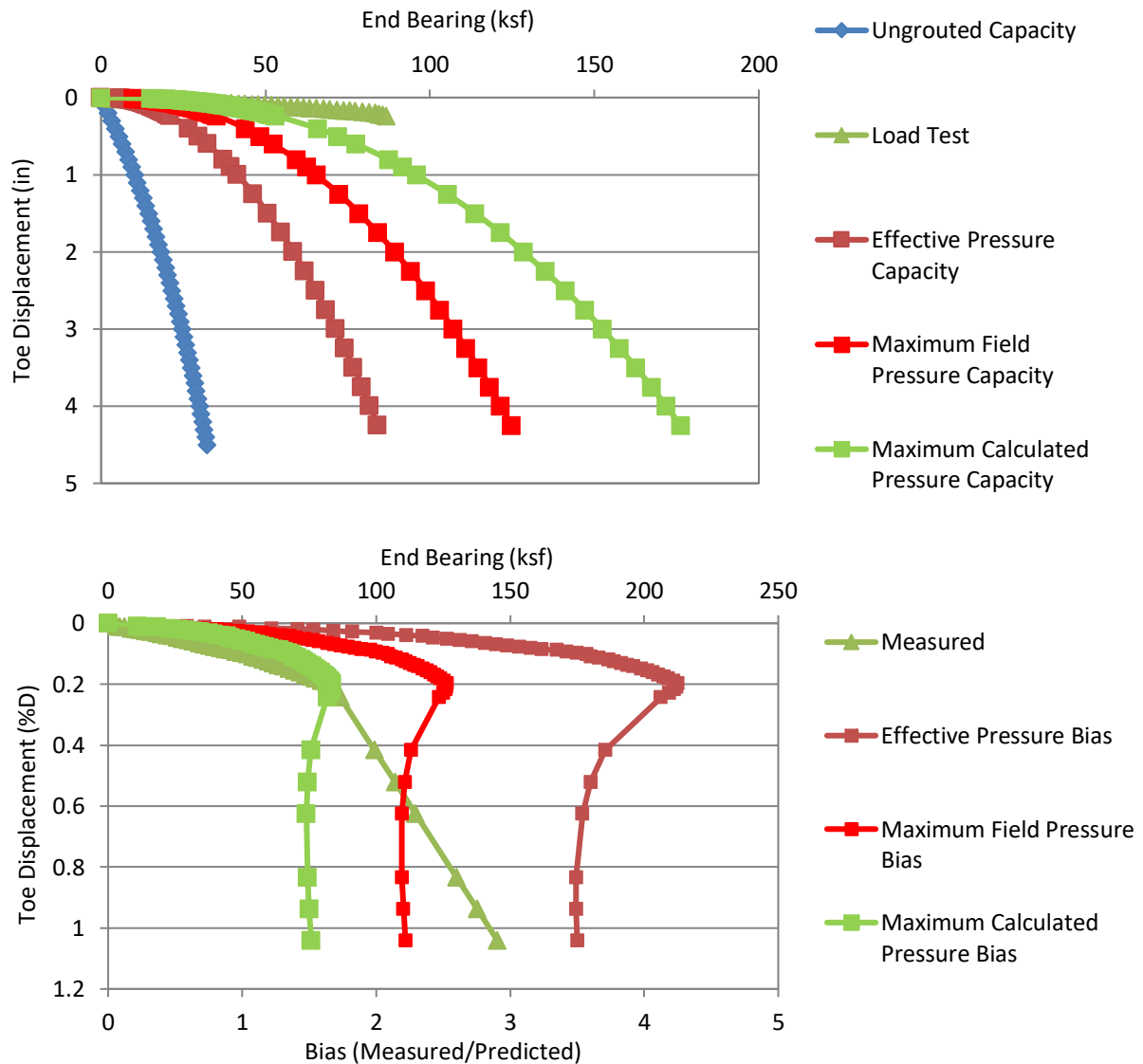


Figure 4.90 Data set 30 predicted/design and load test response (top); bias vs disp. (bottom).

4.2.31 Data Set 31, West Rail Bypass, 41W

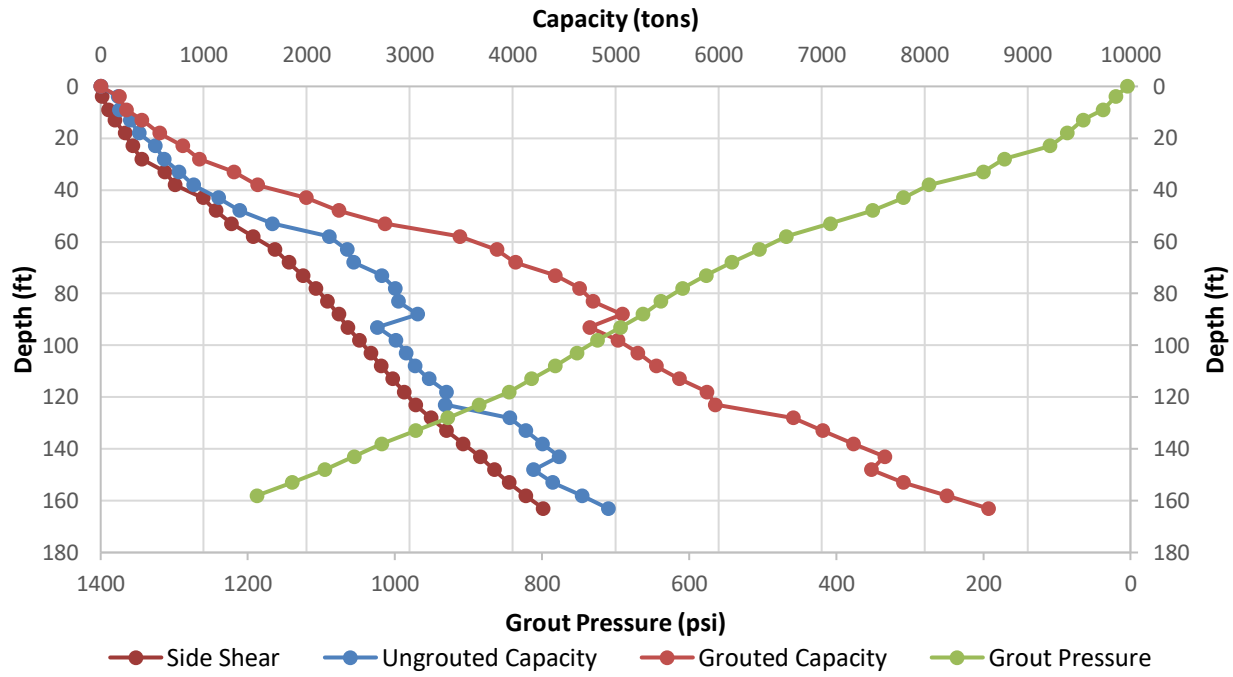


Figure 4.91 Data set 31 design curves.

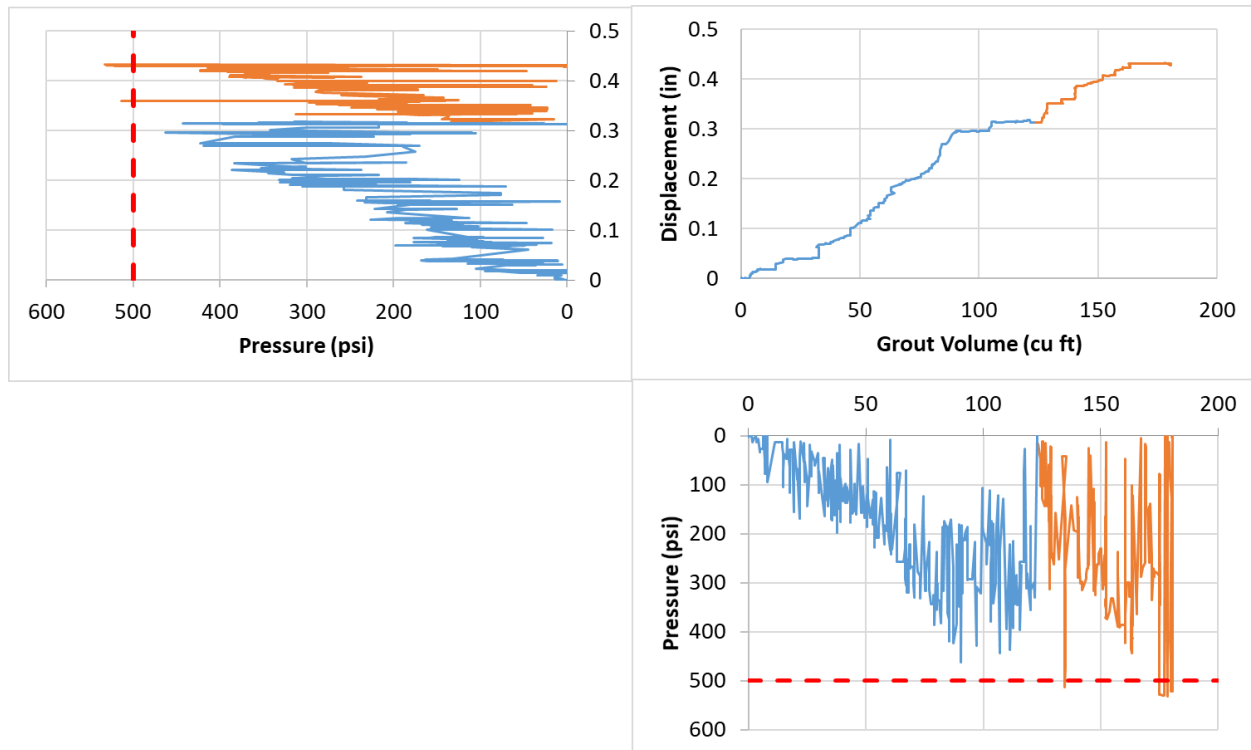


Figure 4.92 Data set 31 tri-axis plots.

Figure 4.93 shows the tri-axis plots for data set 31. Grouting on this shaft was performed in 2 stages; stage 1 shown in orange and stage 2 in blue. Both the pressure vs volume and volume vs. displacement graphs show horizontal trends supporting end bearing failure or piping / migration. Also, both the pressure vs. volume and pressure vs. uplift graphs show spikes in pressure without an associated uplift or volume increase which indicates a grout line blockage at the end of stage 1. Stage 2 had no meaningful effect on the resulting pressure even though it did cause uplift. Effective pressure could be taken as 380 psi but with reduction thereafter, 300 psi was chosen. The maximum field recorded pressure was 513 si.

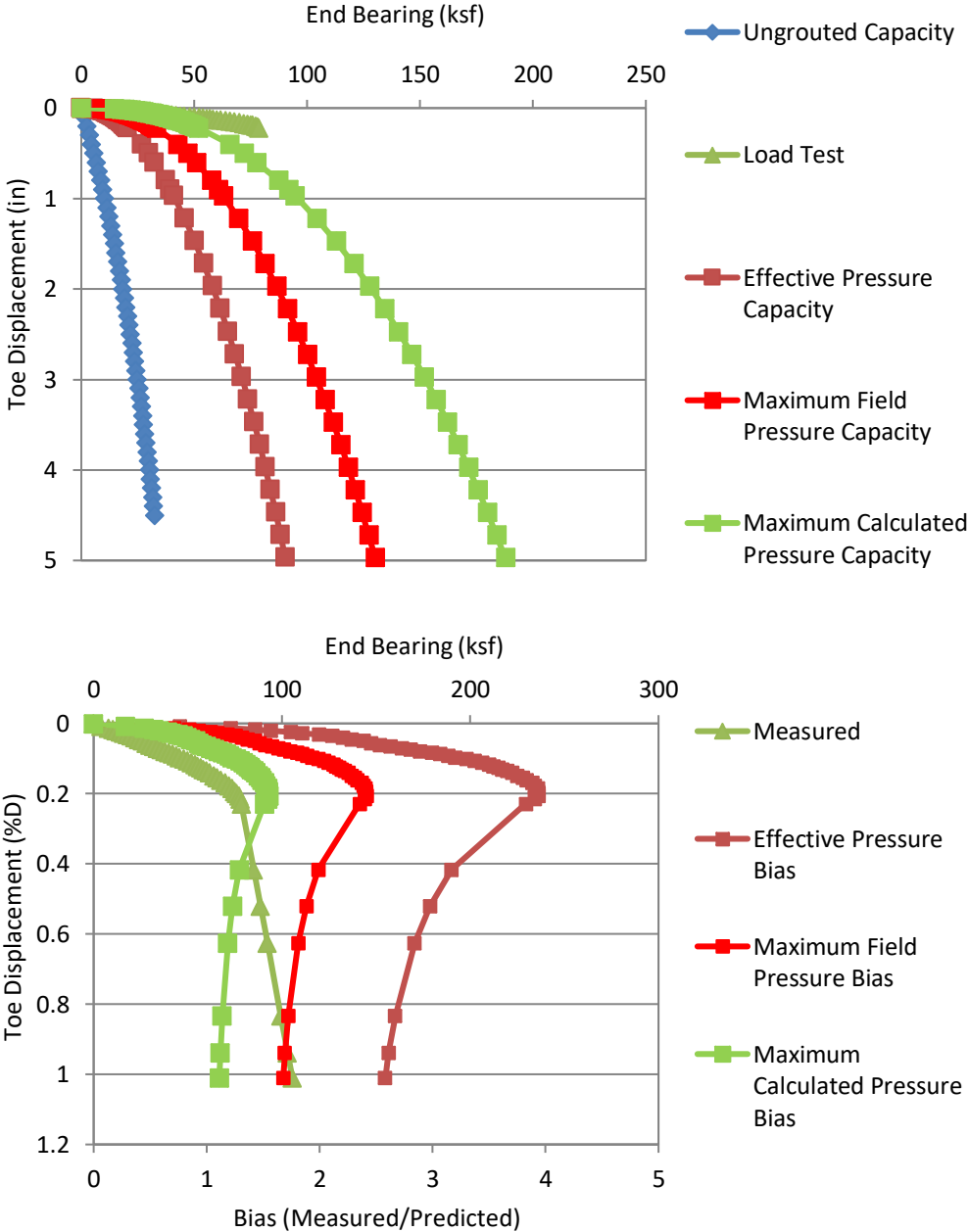


Figure 4.93 Data set 31 Predicted/design and load test response (top); bias vs disp. (bottom)

4.3 Bias Factors

The bias was computed using the measured load, and predicted capacity of the 31 subject shafts at each of 7 different displacements. Therein capacity both measured and predicted is not simply one number but rather a function of shaft displacement. Displacement values were selected on the basis of a function of shaft diameter percentage which normalizes all shaft sizes to a common variable. These values were selected as 0.3, 1, 2, 3, 4, and 5%D. As some designers arbitrarily assume 1 inch to be an acceptable service limit, 1 inch has also been included for each case, but note this is not a truly comparable value when considering the percentage of shaft diameter. Tables 4.2-4.4 summarize the bias values for three grout pressures: effective, maximum field and maximum calculated / design, respectively.

Table 4.2 Shaft bias versus percent displacement for effective pressure.

Data Set	Project	Shaft ID	BIAS						
			1 inch	0.30%	1%	2%	3%	4%	5%
1	Royal Park Bridge	LT-2	2.500	1.324	2.461	2.427	2.109	1.901	1.751
2		LT-3	1.216	1.122	1.216	-	-	-	-
3	PGA	LT-2	0.882	0.510	0.833	0.893	0.858	0.827	-
4	Iowa	TS-4	4.250	5.868	4.531	3.909	3.500	3.091	2.682
5	Gerald Desmond	TP-2	0.886	1.167	0.915	0.846	0.826	0.801	0.789
6		TS-3C	1.431	1.440	1.432	1.370	1.276	1.204	1.161
7	Huey P. Long	TS-1	1.526	1.888	1.439	1.256	1.204	1.194	1.210
8	TXDOT	S-2	1.220	1.551	1.378	1.229	1.117	1.039	0.986
9	Nachez	S-1	2.385	2.640	-	-	-	-	-
10	Clearwater Site I	FJ-1	0.928	1.324	1.314	1.139	1.013	-	-
11		FJ-2	1.341	1.365	1.615	1.408	1.249	1.128	-
12		SP-1	1.080	1.042	1.246	1.207	1.132	1.057	-
13		SP-2	1.016	0.531	0.849	0.935	0.966	-	-
14	Clearwater Site II	FJ-1	1.079	0.412	1.336	1.077	1.010	1.081	1.204
15		SP-1	2.080	1.072	1.861	2.017	2.067	2.070	1.963
16	Flagler	S-1	3.847	1.698	3.387	-	-	-	-
17	WPB Airport	S-1	0.846	0.990	0.964	0.855	0.760	0.685	-
18	Plant Daniel	501	1.403	1.242	1.498	-	-	-	-
19		528	1.470	1.277	1.470	-	-	-	-
20		530	1.590	1.277	1.518	-	-	-	-
21	Southern 80 SR	S-1	4.024	2.570	4.024	-	-	-	-
22		S-2	4.822	2.866	4.329	-	-	-	-
23		S-3		2.700	3.137	-	-	-	-
24	Overland	S-1	4.968	4.851	4.968	-	-	-	-
25		S-2	5.318	6.661	5.318	-	-	-	-
26		S-3	2.290	3.428	2.290	-	-	-	-
27	Carolina Bay	S-1	2.106	2.529	2.106	-	-	-	-
28	Gilmerton	S-1	1.873	2.012	1.210	-	-	-	-
29	Peninsula	S-1	3.533	1.712	3.368	-	-	-	-
30	WestRail	41E	4.248	3.501	3.501	-	-	-	-
31		41W	3.829	3.499	2.580	-	-	-	-
Avg			2.33	2.13	2.27	1.47	1.36	1.34	1.47
STD Dev			1.43	1.50	1.33	0.83	0.74	0.69	0.62
CoV			0.61	0.71	0.59	0.57	0.54	0.51	0.42

Table 4.3 Shaft bias versus percent displacement for maximum field pressure.

Data Set	Project	Shaft ID	BIAS						
			1 inch	0.30%	1%	2%	3%	4%	5%
1	Royal Park Bridge	LT-2	1.892	0.975	1.843	1.845	1.616	1.464	1.354
2		LT-3	0.632	0.536	0.632	-	-	-	-
3	PGA	LT-2	0.626	0.353	0.584	0.632	0.610	0.591	-
4	Iowa	TS-4	2.838	3.619	2.981	2.624	2.369	2.113	1.858
5	Gerald Desmond	TP-2	0.602	0.730	0.614	0.593	0.591	0.580	0.576
6		TS-3C	0.783	0.704	0.792	0.814	0.785	0.756	0.738
7	Huey P. Long	TS-1	0.766	0.873	0.738	0.687	0.680	0.688	0.706
8	TXDOT	S-2	1.220	1.551	1.378	1.229	1.117	1.039	0.986
9	Nachez	S-1	2.385	2.640	-	-	-	-	-
10	Clearwater Site I	FJ-1	0.928	1.324	1.314	1.139	1.013	-	-
11		FJ-2	1.341	1.365	1.615	1.408	1.249	1.128	-
12		SP-1	1.022	0.976	1.172	1.139	1.070	1.000	-
13		SP-2	0.970	0.503	0.807	0.891	0.922	-	-
14	Clearwater Site II	FJ-1	1.079	0.412	1.336	1.077	1.010	1.081	1.204
15		SP-1	1.719	0.860	1.511	1.653	1.703	1.712	1.627
16	Flagler	S-1	3.188	1.377	2.790	-	-	-	-
17	WPB Airport	S-1	0.774	0.891	0.876	0.782	0.698	0.630	-
18	Plant Daniel	501	1.003	0.844	1.065	-	-	-	-
19		528	1.331	1.140	1.331	-	-	-	-
20		530	1.438	1.140	1.374	-	-	-	-
21	Southern 80 SR	S-1	3.809	2.406	3.809	-	-	-	-
22		S-2	3.969	2.299	3.535	-	-	-	-
23		S-3		2.506	2.945	-	-	-	-
24	Overland	S-1	3.644	3.398	3.644	-	-	-	-
25		S-2	2.863	3.201	2.863	-	-	-	-
26		S-3	2.209	3.280	2.209	-	-	-	-
27	Carolina Bay	S-1	2.032	2.427	2.032	-	-	-	-
28	Gilmerton	S-1	1.873	2.012	1.210	-	-	-	-
29	Peninsula	S-1	3.347	1.614	3.190	-	-	-	-
30	WestRail	41E	2.527	2.219	2.219	-	-	-	-
31		41W	2.358	2.174	1.679	-	-	-	-
Avg			1.84	1.62	1.80	1.18	1.10	1.07	1.13
STD Dev			1.04	0.96	0.99	0.56	0.50	0.48	0.46
CoV			0.57	0.59	0.55	0.48	0.45	0.45	0.41

Table 4.4 Shaft bias versus percent displacement for maximum calculated design pressure.

Data Set	Project	Shaft ID	BIAS						
			1 inch	0.30%	1%	2%	3%	4%	5%
1	Royal Park Bridge	LT-2	1.711	0.874	1.661	1.671	1.467	1.331	1.232
2		LT-3	0.538	0.451	0.538	-	-	-	-
3	PGA	LT-2	0.845	0.487	0.797	0.856	0.822	0.794	-
4	Iowa	TS-4	0.687	0.786	0.707	0.642	0.588	0.535	0.481
5	Gerald Desmond	TP-2	0.628	0.767	0.641	0.617	0.614	0.602	0.597
6		TS-3C	0.783	0.704	0.792	0.814	0.785	0.756	0.738
7	Huey P. Long	TS-1	0.500	0.555	0.486	0.463	0.465	0.474	0.489
8	TXDOT	S-2	1.980	3.074	2.407	2.005	1.763	1.607	1.504
9	Nachez	S-1	1.799	1.985	-	-	-	-	-
10	Clearwater Site I	FJ-1	0.876	1.215	1.223	1.068	0.954	-	-
11		FJ-2	1.892	2.286	2.453	2.012	1.741	1.541	-
12		SP-1	1.892	2.110	2.362	2.188	2.000	1.840	-
13		SP-2	1.968	1.207	1.788	1.876	1.886	-	-
14	Clearwater Site II	FJ-1	1.258	0.511	1.600	1.272	1.183	1.260	1.400
15		SP-1	2.279	1.195	2.059	2.221	2.269	2.268	2.148
16	Flagler	S-1	4.106	1.829	3.624	-	-	-	-
17	WPB Airport	S-1	0.995	1.207	1.150	1.006	0.888	0.797	-
18	Plant Daniel	501	1.290	1.126	1.376	-	-	-	-
19		528	5.460	8.118	5.460	-	-	-	-
20		530	6.079	8.118	5.708	-	-	-	-
21	Southern 80 SR	S-1	12.075	12.931	12.075	-	-	-	-
22		S-2	22.032	28.192	23.706	-	-	-	-
23		S-3		13.721	9.585	-	-	-	-
24	Overland	S-1	3.990	3.765	3.990	-	-	-	-
25		S-2	4.121	4.876	4.121	-	-	-	-
26		S-3	1.751	2.487	1.751	-	-	-	-
27	Carolina Bay	S-1	1.432	1.631	1.432	-	-	-	-
28	Gilmerton	S-1	2.677	2.884	1.702	-	-	-	-
29	Peninsula	S-1	4.419	2.195	4.228	-	-	-	-
30	WestRail	41E	1.669	1.515	1.515	-	-	-	-
31		41W	1.514	1.403	1.114	-	-	-	-
Avg			3.11	3.68	3.40	1.34	1.24	1.15	1.07
STD Dev			4.27	5.66	4.65	0.64	0.60	0.58	0.60
CoV			1.37	1.54	1.37	0.48	0.48	0.50	0.56

Figures 4.95 - 4.97 show the resistance factor computed using equation 2.15a for the same three pressures (effective, maximum field, and maximum calculated respectively) all as a function of the reliability index varying from 1 to 4.

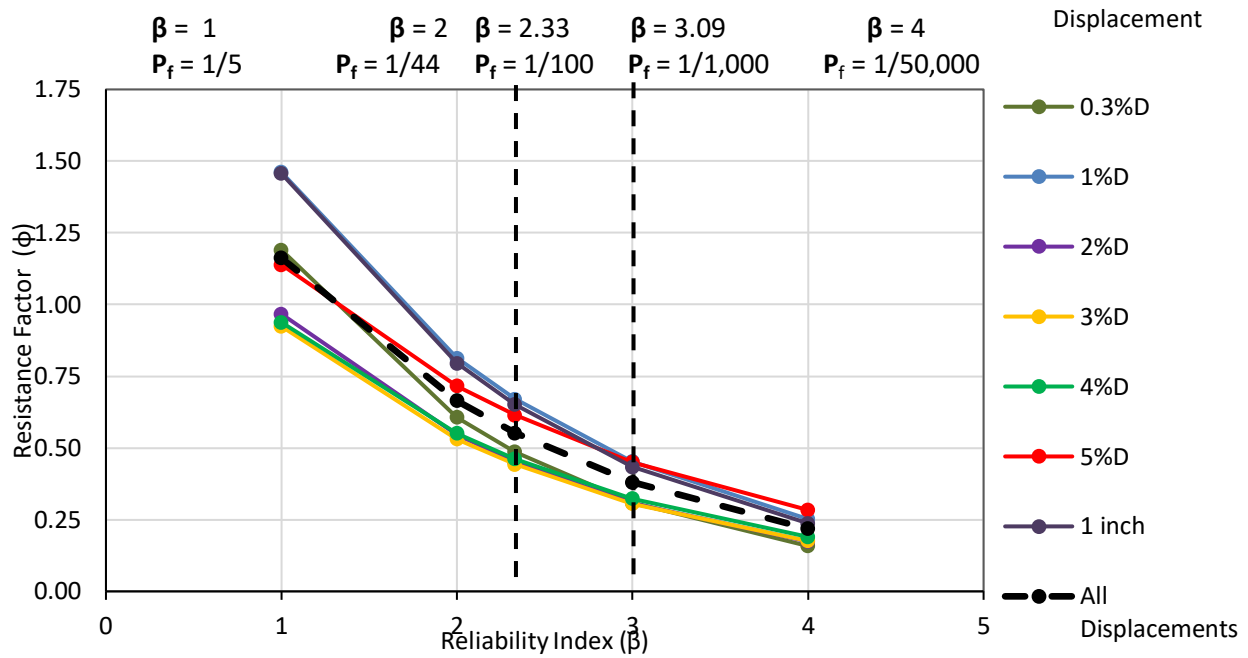


Figure 4.94 Resistance factor vs target reliability graph for effective pressure.

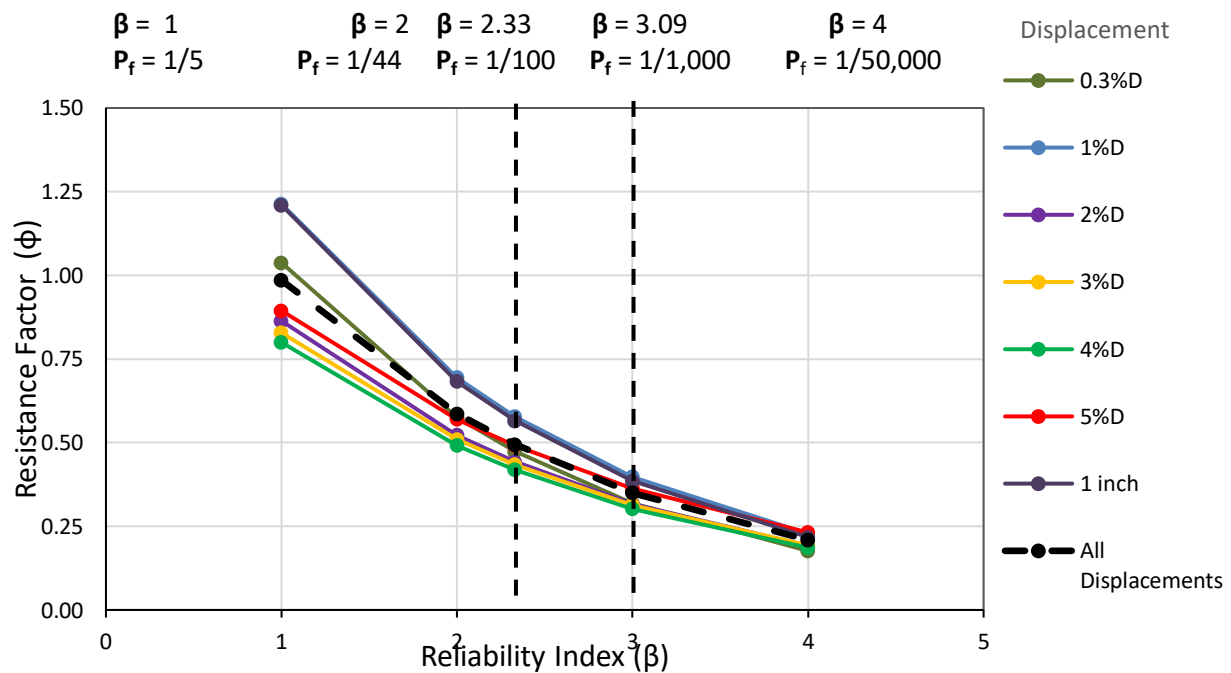


Figure 4.95 Resistance factor vs target reliability graph for maximum field pressure.

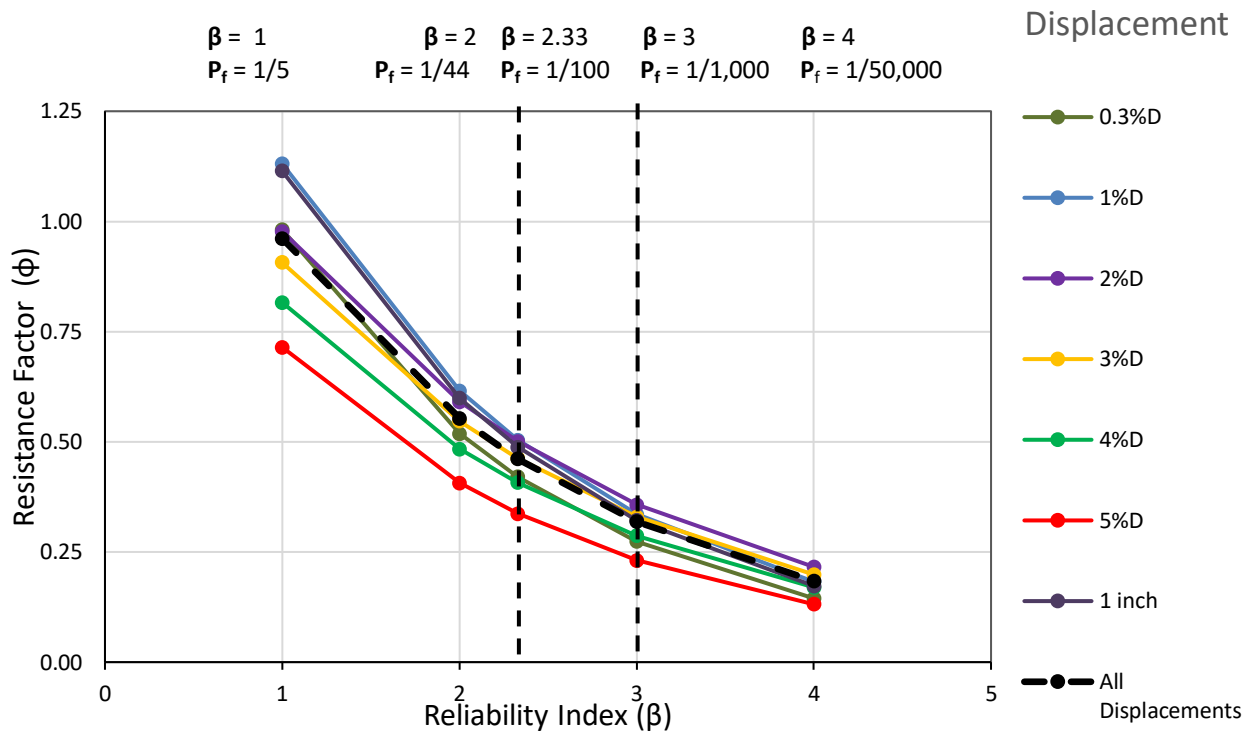


Figure 4.96 Resistance factor vs target reliability graph for maximum calculated pressure.

4.4 Bias Factors FDOT Method

Bias factors were also calculated using the FDOT method which puts a cap on the end bearing at the design grout pressure determined from side shear computations. However, if demonstrated in the field to be higher, then the same effective grouting considerations must be introduced (effective vs max pressure). The resulting bias values have been tabulated below. The bias plots for each data set can be found in appendix C.

Tables 4.5-4.7 summarize the bias values for three design pressures: effective, maximum field and maximum calculated, respectively when using the FDOT method.

Table 4.5 Shaft bias versus percent displacement for effective pressure using an end bearing cap.

Data Set	Project	Shaft ID	BIAS						
			1 inch	0.30%	1%	2%	3%	4%	5%
1	Royal Park Bridge	LT-2	2.636	1.324	2.461	2.818	2.932	3.005	3.045
2		LT-3	1.271	1.122	1.271	-	-	-	-
3	PGA	LT-2	0.995	0.510	0.833	0.945	1.035	1.128	-
4	Iowa	TS-4	4.987	5.868	5.098	5.045	5.114	5.183	5.253
5	Gerald Desmond	TP-2	1.100	1.167	1.019	1.392	1.697	1.910	2.101
6		TS-3C	1.775	1.440	1.895	2.758	3.249	3.597	3.896
7	Huey P. Long	TS-1	1.526	1.888	1.624	2.086	2.497	2.880	3.263
8	TXDOT	S-2	1.735	1.551	1.387	1.710	1.897	2.030	2.147
9	Nachez	S-1	2.385	2.640	-	-	-	-	-
10	Clearwater Site I	FJ-1	1.907	1.324	1.433	1.651	1.827	-	-
11		FJ-2	2.204	1.365	1.835	2.139	2.318	2.471	-
12		SP-1	1.544	1.042	1.246	1.358	1.505	1.597	-
13		SP-2	1.401	0.531	0.849	1.032	1.265	-	-
14	Clearwater Site II	FJ-1	1.817	0.412	1.336	1.312	1.497	1.824	2.239
15		SP-1	3.068	1.072	1.861	2.242	2.744	3.109	3.240
16	Flagler	S-1	3.930	1.698	3.387	-	-	-	-
17	WPB Airport	S-1	1.061	0.990	0.964	1.056	1.136	1.167	-
18	Plant Daniel	501	1.489	1.242	1.534	-	-	-	-
19		528	1.470	1.277	1.470	-	-	-	-
20		530	1.590	1.277	1.537	-	-	-	-
21	Southern 80 SR	S-1	4.368	2.570	4.368	-	-	-	-
22		S-2	5.205	2.866	4.329	-	-	-	-
23		S-3		2.700	3.338	-	-	-	-
24	Overland	S-1	5.094	4.851	5.094	-	-	-	-
25		S-2	6.529	6.661	6.529	-	-	-	-
26		S-3	2.619	3.428	2.619	-	-	-	-
27	Carolina Bay	S-1	2.138	2.529	2.138	-	-	-	-
28	Gilmerton	S-1	1.873	2.012	1.210	-	-	-	-
29	Peninsula	S-1	3.533	1.712	3.368	-	-	-	-
30	WestRail	41E	4.248	3.501	3.501	-	-	-	-
31		41W	3.829	3.499	2.580	-	-	-	-
Avg			2.64	2.13	2.40	1.97	2.19	2.49	3.15
STD Dev			1.49	1.50	1.48	1.07	1.09	1.15	1.07
CoV			0.56	0.71	0.61	0.55	0.50	0.46	0.34

Table 4.6 Shaft bias versus percent displacement for maximum field pressure using end bearing cap.

Data Set	Project	Shaft ID	BIAS						
			1 inch	0.30%	1%	2%	3%	4%	5%
1	Royal Park Bridge	LT-2	1.892	0.975	1.843	2.015	2.094	2.146	2.175
2		LT-3	0.632	0.536	0.632	-	-	-	-
3	PGA	LT-2	0.680	0.353	0.584	0.657	0.708	0.771	-
4	Iowa	TS-4	2.838	3.619	2.981	2.867	2.901	2.935	2.970
5	Gerald Desmond	TP-2	0.622	0.730	0.624	0.788	0.960	1.081	1.189
6		TS-3C	0.783	0.704	0.796	1.103	1.300	1.439	1.559
7	Huey P. Long	TS-1	0.766	0.873	0.738	0.834	0.999	1.152	1.305
8	TXDOT	S-2	1.735	1.551	1.387	1.710	1.897	2.030	2.147
9	Nachez	S-1	2.385	2.640	-	-	-	-	-
10	Clearwater Site I	FJ-1	1.907	1.324	1.433	1.651	1.827	-	-
11		FJ-2	2.204	1.365	1.835	2.139	2.318	2.471	-
12		SP-1	1.439	0.976	1.172	1.272	1.403	1.489	-
13		SP-2	1.323	0.503	0.807	0.975	1.194	-	-
14	Clearwater Site II	FJ-1	1.817	0.412	1.336	1.312	1.497	1.824	2.239
15		SP-1	2.422	0.860	1.511	1.770	2.166	2.454	2.558
16	Flagler	S-1	3.188	1.377	2.790	-	-	-	-
17	WPB Airport	S-1	0.943	0.891	0.876	0.938	1.009	1.036	-
18	Plant Daniel	501	1.003	0.844	1.065	-	-	-	-
19		528	1.331	1.140	1.331	-	-	-	-
20		530	1.438	1.140	1.374	-	-	-	-
21	Southern 80 SR	S-1	4.027	2.406	4.027	-	-	-	-
22		S-2	5.205	2.866	4.329	-	-	-	-
23		S-3	-	2.506	3.044	-	-	-	-
24	Overland	S-1	3.644	3.398	3.644	-	-	-	-
25		S-2	2.863	3.201	2.863	-	-	-	-
26		S-3	2.475	3.280	2.475	-	-	-	-
27	Carolina Bay	S-1	2.034	2.427	2.034	-	-	-	-
28	Gilmerton	S-1	1.873	2.012	1.210	-	-	-	-
29	Peninsula	S-1	3.347	1.614	3.190	-	-	-	-
30	WestRail	41E	2.527	2.219	2.219	-	-	-	-
31		41W	2.358	2.174	1.679	-	-	-	-
Avg			2.06	1.64	1.86	1.43	1.59	1.74	2.02
STD Dev			1.10	0.98	1.06	0.63	0.63	0.68	0.62
CoV			0.53	0.60	0.57	0.44	0.39	0.39	0.31

Table 4.7 Shaft bias versus percent displacement for maximum calculated pressure using end bearing cap.

Data Set	Project	Shaft ID	BIAS						
			1 inch	0.30%	1%	2%	3%	4%	5%
1	Royal Park Bridge	LT-2	1.711	0.874	1.661	1.798	1.863	1.909	1.935
2		LT-3	0.538	0.451	0.538	-	-	-	-
3	PGA	LT-2	0.949	0.487	0.797	0.903	0.987	1.075	-
4	Iowa	TS-4	0.687	0.786	0.707	0.674	0.659	0.643	0.628
5	Gerald Desmond	TP-2	0.660	0.767	0.657	0.835	1.018	1.146	1.261
6		TS-3C	0.783	0.704	0.796	1.103	1.300	1.439	1.559
7	Huey P. Long	TS-1	0.500	0.555	0.486	0.509	0.609	0.702	0.796
8	TXDOT	S-2	4.200	3.074	3.263	4.139	4.592	4.915	5.198
9	Nachez	S-1	1.799	1.985	-	-	-	-	-
10	Clearwater Site I	FJ-1	1.725	1.215	1.315	1.494	1.653	-	-
11		FJ-2	4.407	2.286	3.416	4.277	4.637	4.942	-
12		SP-1	3.398	2.110	2.500	2.946	3.313	3.516	-
13		SP-2	3.502	1.213	1.950	2.558	3.162	-	-
14	Clearwater Site II	FJ-1	2.282	0.511	1.600	1.648	1.880	2.291	2.812
15		SP-1	3.452	1.195	2.059	2.522	3.087	3.497	3.646
16	Flagler	S-1	4.265	1.829	3.624	-	-	-	-
17	WPB Airport	S-1	1.330	1.207	1.150	1.323	1.424	1.462	-
18	Plant Daniel	501	1.325	1.126	1.392	-	-	-	-
19		528	-	-	-	-	-	-	-
20		530	-	-	-	-	-	-	-
21	Southern 80 SR	S-1	-	-	-	-	-	-	-
22		S-2	-	-	-	-	-	-	-
23		S-3	-	-	-	-	-	-	-
24	Overland	S-1	3.990	3.765	3.990	-	-	-	-
25		S-2	4.352	4.876	4.352	-	-	-	-
26		S-3	1.761	2.487	1.761	-	-	-	-
27	Carolina Bay	S-1	1.432	1.631	1.432	-	-	-	-
28	Gilmerton	S-1	2.677	2.884	1.702	-	-	-	-
29	Peninsula	S-1	4.419	2.195	4.228	-	-	-	-
30	WestRail	41E	1.669	1.515	1.515	-	-	-	-
31		41W	1.514	1.403	1.114	-	-	-	-
Avg			2.28	1.66	1.92	1.91	2.16	2.29	2.23
STD Dev			1.39	1.09	1.21	1.22	1.37	1.55	1.57
CoV			0.61	0.66	0.63	0.64	0.63	0.68	0.70

Figures 4.98 - 4.100 show the resistance factor computed using equation 2.15a for the same three pressures (effective, maximum field, and maximum calculated respectively) all as a function of the reliability index varying from 1 to 4.

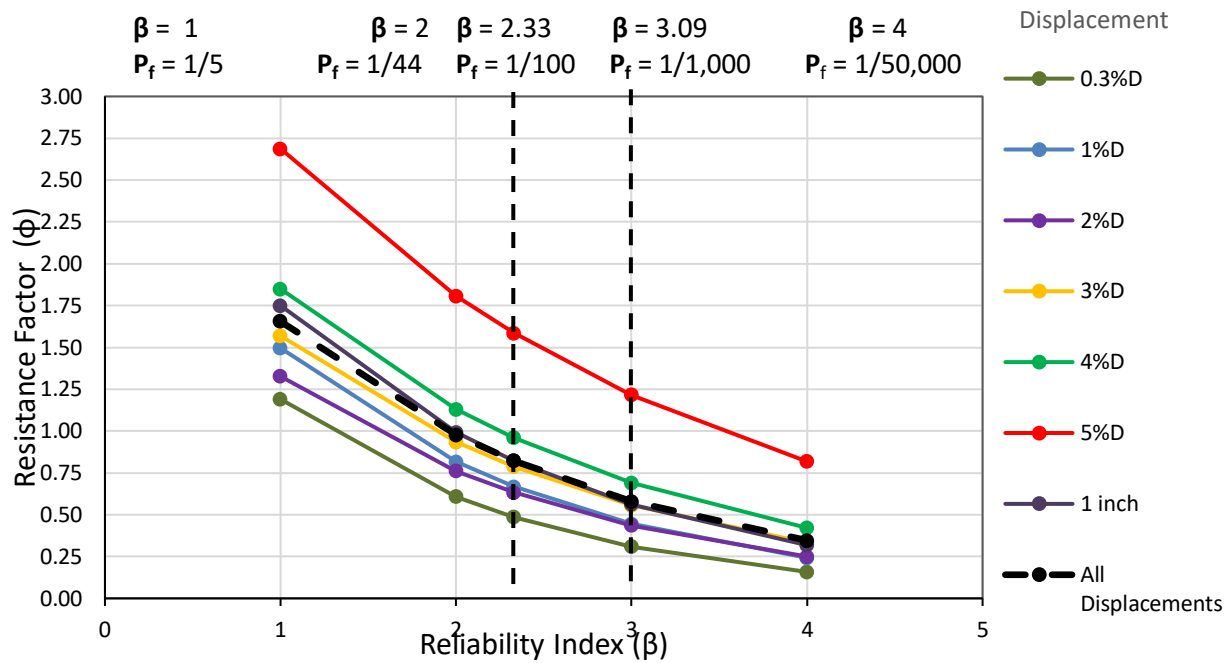


Figure 4.97 Resistance factor vs reliability graph for effective pressure using end bearing cap.

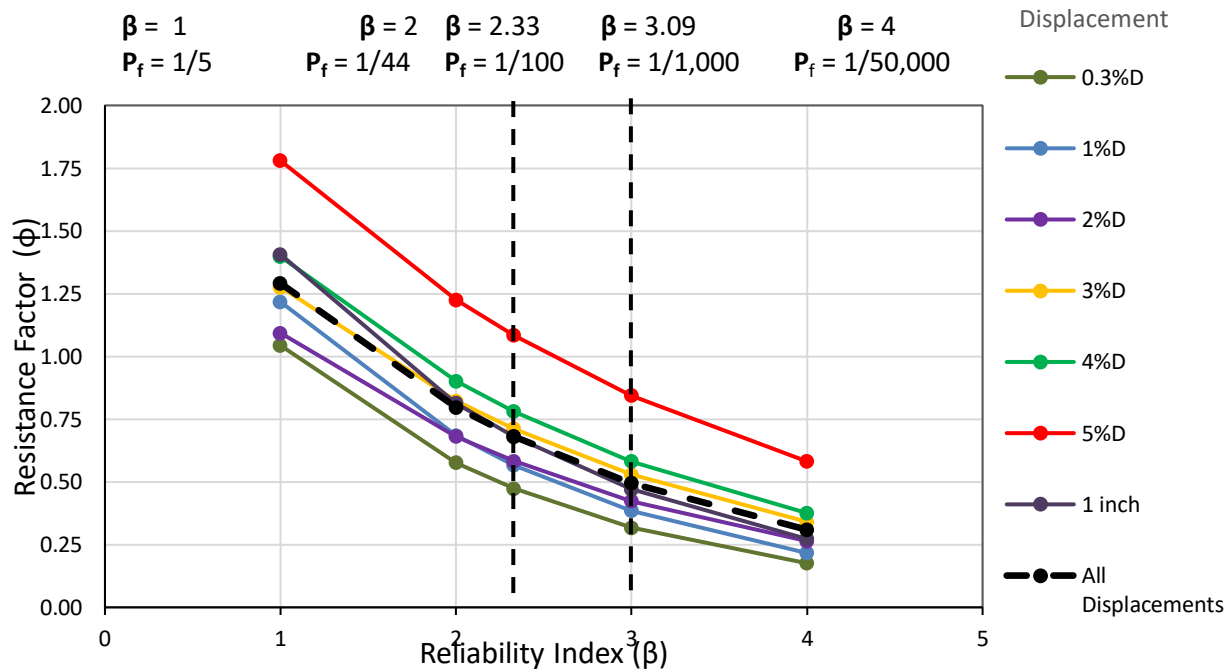


Figure 4.98 Resistance factor vs reliability graph for maximum field pressure using end bearing cap.

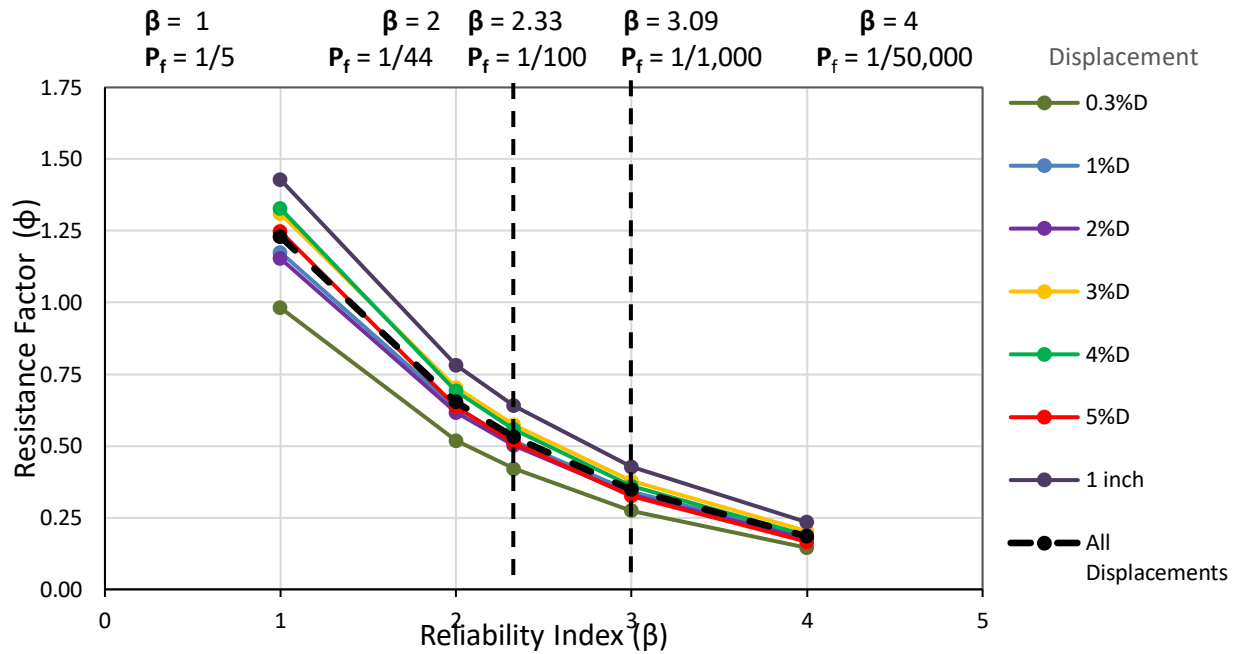


Figure 4.99 Resistance factor vs target reliability graph for maximum calculated pressure using an end bearing cap.

4.5 Chapter Summary

In this chapter the information gathered from 31 data sets was presented. Where possible, all data was shown in tri-axis plot format with each plot analyzed for grouting anomalies. Bias factors were calculated and tabulated for three pressure conditions for both end bearing capped (FDOT method) and uncapped (2006 method) scenarios and the respective resistance factors were presented over the usable range of reliability indices.

Chapter Five: Discussion and Conclusions

5.1 Overview

Postgrouting is the process of injecting high-pressure grout beneath or beside a deep foundation element to improve the load-carrying capacity. While used for precast and cast-in-place piles, this study focused only on cast-in-place drilled shafts and even more specifically, only on end bearing improvements. As the name implies, “post”-grouting is performed post-construction, after the element has been cast and has achieved necessary strength to structurally withstand the high-pressure grout. A significant benefit is realized in reduction of the strain incompatibility between mobilized side shear and end bearing. Therein, a conventional shaft end bearing requires 10 times the amount of displacement to mobilize the same percentage of side shear/friction (i.e., 0.5%D for side shear and 5%D for end bearing). While it is tempting to view postgrouting as a measure to increase quality, it should be more appropriately deemed a construction process that is vulnerable to the same construction-type problems. Hence, the quality of the grouting process can be and should be monitored and be part of routine inspection protocols.

This study introduced quality control and assurance protocols that, if observed, benefit both the contractor and owner with a better understanding of how well or effectively the grouting is being performed or how well it was performed. The simple act of plotting real-time tri-axis plots (discussed in Chapter 2 and 4) helps to identify whether the grouting process has become ineffective or if the grouting is well on its way to successful completion. Further, the pressure at which the system becomes ineffective was shown to be more closely linked to predicted end bearing. So, criteria for acceptance should not only incorporate thresholds for pressure (min), volume (min), or uplift (min or max), but also should demonstrate the inextricable connections between these measurements. When performed correctly, increasing the volume of grout pumped to the bottom of the shaft should be accompanied by a steadily increasing pressure and uplift.

Thirty-one postgrouted and load-tested shafts from eighteen sites were examined for grouting quality, grouting parameters, and load response and compared to predictions using two closely linked design methods: the 2006 method proposed by Mullins et al. and an adaptation of that method described by the FDOT Design Guidelines which caps the end bearing to be no higher than the applied grout pressure. In both methods, the design predictions hinge on imparting the anticipated grout pressure to the entire shaft tip. And, if the design pressure cannot be achieved in the field, a lesser capacity should be expected. Therefore, at the design phase, side shear resistance is estimated, from which the anticipated grout pressure is computed and the reliability of the pressure values (or measurements) in predicting end bearing (via equations) then comes into play. The primary objective of this study was to determine the magnitude of LRFD resistance factors to be used in concert with postgrouted end bearing design methods.

Whether or not the side shear force is sufficient to develop the design grout pressure was not assessed in this study. The designer should recognize the reduced side shear resistance that often accompanies uplift (relative to downward compression) when assessing the anticipated design grout pressure.

5.2 Reliability Index Selection

One of the most important parameters when calculating resistance factors is the target reliability which is controlled by the reliability index (β). The chosen value reflects the acceptable failure ratio which is chosen based on the philosophy of the owner balancing risk and safety; higher values are associated with safer designs (lower failure ratio). In some cases, the failure of one element leads to the failure of the entire structure (fracture critical elements) while in others, multiple load paths (high redundancy) prevent global failure through reliance on the group performance. Therefore, when selecting β values, redundancy, frequency of testing, and quality controls/inspection must be addressed. Typically, β values used for foundations range from 2.33 (driven piles) to 3.00 (little or no testing) which as shown in Figure 5.1 correspond to failure probabilities of 1/100 and approximately 1/1000, respectively.

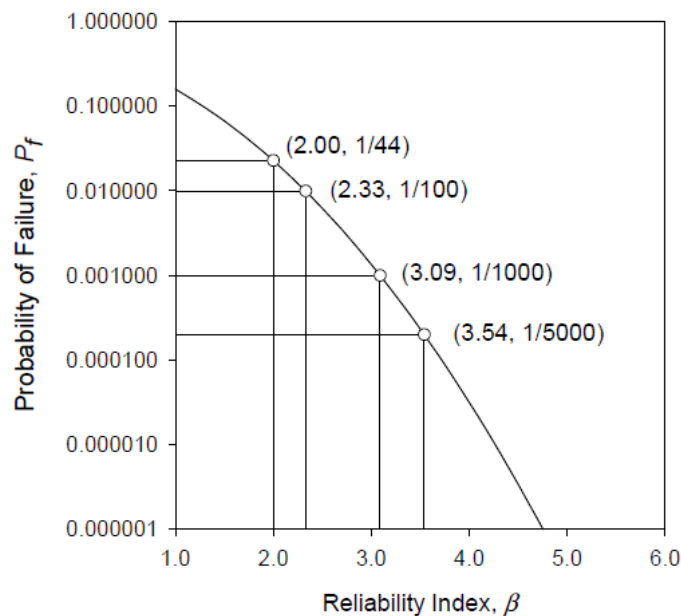


Figure 5.1 Reliability index vs probability of failure (Allen, 2005).

In this study, resistance factors were calculated and plotted for a range of reliability index values from 1 to 4 corresponding to failure ratios of 1 in 5 to 1 in 50,000 (Figure 5.1). Basically, using a β of 1 is too risky while choosing a β of 4 is perhaps too conservative and will incur excessive costs. However, typical values for concrete or steel structural applications use a reliability index of 3.5 (1 in 4,146 failure ratio). For redundant foundation applications, values of 2.33 have been justified by both experience and with the notion that exceeding the design capacity often does not cause failure but rather capacity can increase with more displacement (which is not always true). For non-redundant applications consideration for a higher reliability index (3.0) is justified.

Presently, there is debate as to what is an acceptable amount of end bearing displacement when computing strength limit state resistances. Reese and O'Neill (1988), for instance, presented the now widely used equation for shaft end bearing in sand. He noted an estimated 5%D displacement would be experienced at the point at which 100% of the computed capacity was mobilized and that additional capacity could be expected up to 10-12%D displacements. Bruce (1986) estimated shafts in sand could undergo up to 15%D displacement where more capacity would be progressively

mobilized. To this end, O’Neill also provided a tip capacity reduction factor (a normalized end bearing relationship shown later in Figures 5.4 and 5.6) intended to match the project-specific allowable settlement with the anticipated end bearing. Today, all too often, designers simply sum the maximum equation-predicted capacities from side shear and end bearing without consideration of the strain compatibility or incompatibility. This is not tolerated in structural steel designs where excessive displacements from a yielding section (not ultimate breaking strength) is considered ultimate capacity for gross cross-sectional area computations and where the ultimate steel strength is restricted only to connections. This too could present problems when considering to what degree of settlement a postgrouted shaft should be permitted to undergo without the expectation of unforeseen performance problems.

The act of grouting pre-mobilizes the end bearing soils in some cases to very high levels. Considering that the grout compresses the soil up to and beyond the amounts to which O’Neill and Bruce postulated as upper levels, it may then be prudent to reduce the amount of tolerable settlement in design. Figure 5.2 presents the magnitude of end bearing movement (from the study data) using a simplistic assumption that the volume of grout forms a disk with thickness (in %D) and with the cross-sectional area of the shaft. In reality, cavity expansion theory should be employed which will lessen the magnitude of the grout bulb thickness, but the data suggests the soil moved anywhere from 1 to 200% of the shaft diameter. The very low volumes were probably insufficient to impart meaningful improvement (or the soil did not need improving) and the very high volumes most likely migrated a portion of the grout volume away from the shaft. Nevertheless, with an average of 49%D one must suspect the 10-15%D upper limit has been exceeded. Therefore, one aspect of the study was to determine the resistance factor associated with various amounts of displacement as both the end bearing prediction and load test capacity are dependent on displacement.

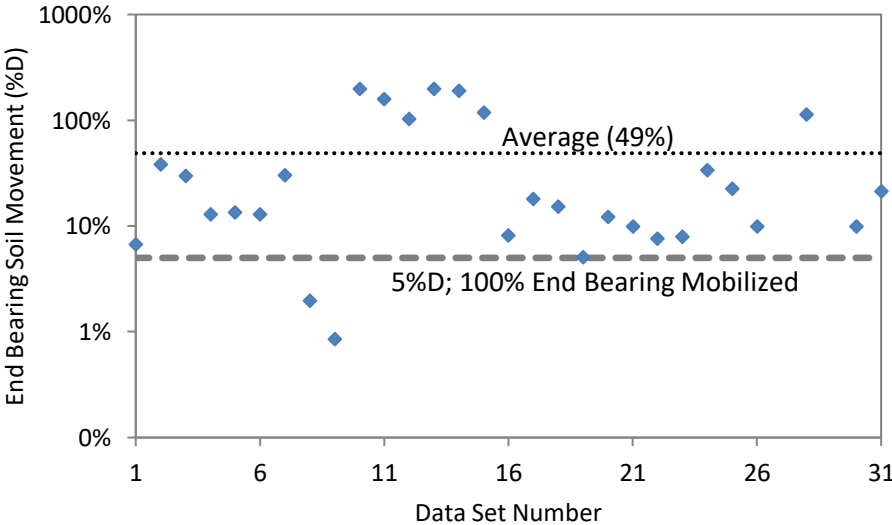


Figure 5.2 End bearing movement from grouting.

While computation of resistance factors was completed for displacement values ranging from 0.3 to 5%D (Chapter 4), Tables 5.1 and 5.2 highlight the resistance factors for 1%D which is similar to the upper limit for side shear (0.5 – 1%D) and for all displacements. Table 5.1 provides resistance factor values for the 2006 design method without an upper bearing capacity limit and Table 5.2

provides values for the FDOT method that caps the computed end bearing to the computed grout pressure. In both cases, a higher resistance factor is assigned to cases for the effective pressure bias criterion. Hence, use of this resistance factor requires verification via tri-axis plots.

Table 5.1 Bias criteria vs resistance factor summary for 1%D and all displacements.

Bias Criteria	Resistance Factor, Phi (ϕ)		Resistance Factor, Phi (ϕ)	
	1% Displacement		All Displacements	
	$\beta = 2.33$	$\beta = 3.00$	$\beta = 2.33$	$\beta = 3.00$
Effective pressure (tri-axis plots)	0.67	0.45	0.55	0.38
Maximum field pressure	0.58	0.40	0.49	0.35
Boring log-calculated pressure	0.23	0.12	0.36	0.24

Table 5.2 Bias criteria vs resistance factor summary using a grout pressure end bearing cap (FDOT method).

Bias Criteria	Resistance Factor, Phi (ϕ)		Resistance Factor, Phi (ϕ)	
	1% Displacement		All Displacements	
	$\beta = 2.33$	$\beta = 3.00$	$\beta = 2.33$	$\beta = 3.00$
Effective pressure (tri-axis plots)	0.67	0.44	0.82	0.58
Maximum field pressure	0.57	0.38	0.68	0.50
Boring log-calculated pressure	0.52	0.34	0.53	0.35

Several observations can be made when reviewing the computed resistance factors:

1. In all cases verification of effective pressure resulted in higher resistance factors confirming a closer agreement between actual and the anticipated performance. This was followed by the maximum field recorded pressure values and a much poorer correlation between boring log predicted pressure and actual.
2. All 31 data sets exhibited at least 0.3%D displacement, but only 8 achieved 5%D (Chapter 4 bias tables). Therefore, when considering the *all displacements* category the data is populated more heavily with smaller displacements (31-0.3%; 30-1.0%, 14-2%; 14-3%; 12-4%; and 8-5%). However, 0.3%D was not included when determining the *all displacements* resistance factor.
3. By limiting the design end bearing to the computed grout pressure, the FDOT method produces progressively higher bias values at higher and higher displacements as the increasing load test data separates from the prediction method (Figure 5.3). This results in progressively higher resistance factor values at larger displacements. This skews the *all displacements* values as a result.
4. The 1%D values for both methods are essentially the same given lower predicted capacity is developed at small displacements and the FDOT limit is not yet active.
5. The relationship between the boring predicted pressure and that applied in the field is poorest resulting in the lowest resistance factors in all categories. Table 5.3 shows the ratios for the various grout pressure values and the CoV values which in part support this finding.

The average bias of the Eff./Des. Ratio (the actual measured to design pressure), while close to 1.0, has the highest variability (CoV = 0.67).

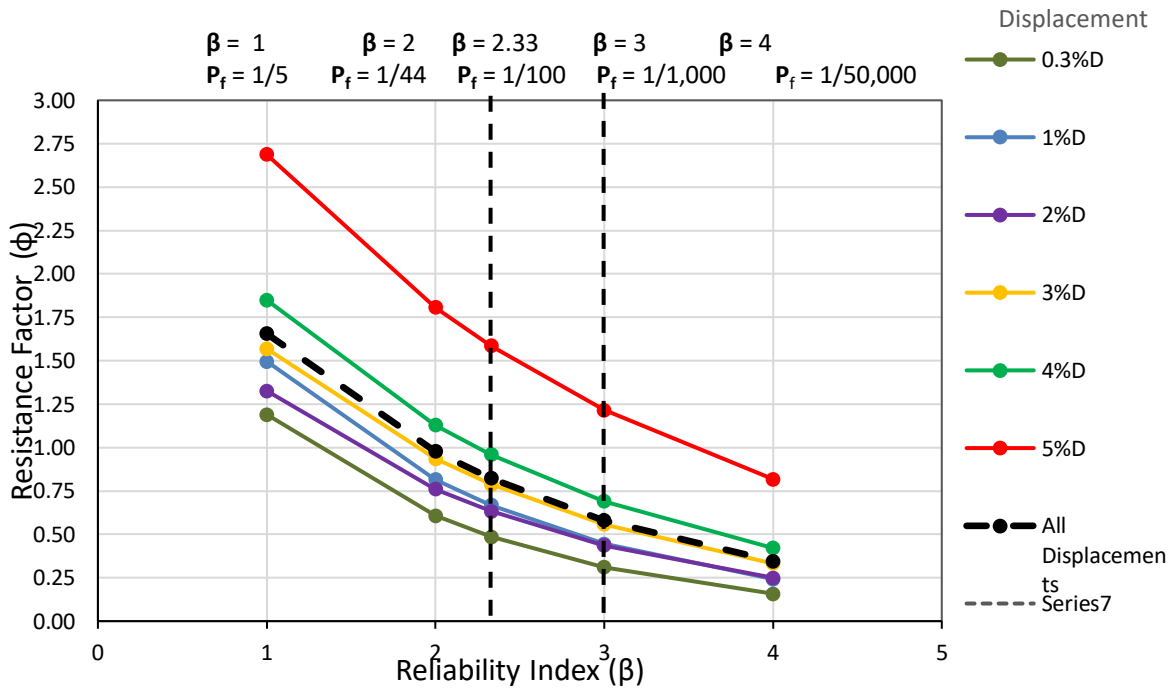
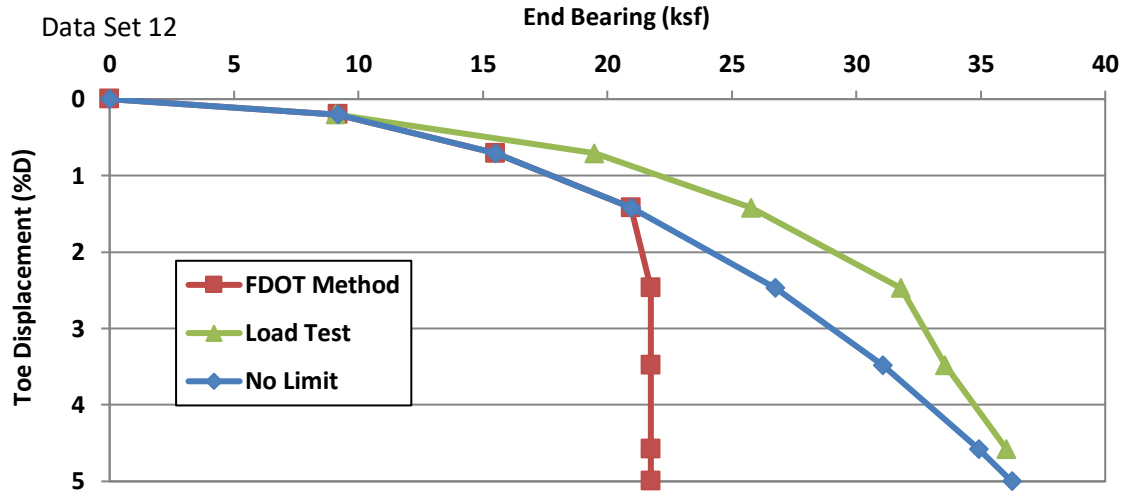


Figure 5.3 Effect of pressure limit on bias and resistance factors.

Table 5.3 Summary of grout pressures and grout pressure ratios.

Data Set	Project	Shaft ID	Effective	Peak	Design	Eff/Des	Eff/Peak	Peak/Des	
1	Royal Park Bridge	LT-2	500	700	787	0.64	0.71	0.89	
2		LT-3	300	700	846	0.35	0.43	0.83	
3	PGA	LT-2	750	1097	787	0.95	0.68	1.39	
4	Iowa	TS-4	80	142	726	0.11	0.56	0.20	
5	Gerald Desmond	TP-2	600	1060	1000	0.60	0.57	1.06	
6		TS-3C	400	1000	1000	0.40	0.40	1.00	
7	Huey P. Long	TS-1	300	750	1230	0.24	0.40	0.61	
8	TXDOT	S-2	230	230	95	2.42	1.00	2.42	
9	Nachez	S-1	320	320	450	0.71	1.00	0.71	
10	Clearwater Site I	FJ-1	80	80	88	0.90	1.00	0.90	
11		FJ-2	70	70	35	2.00	1.00	2.00	
12		SP-1	151	162	69	2.20	0.93	2.36	
13		SP-2	170	180	68	2.50	0.94	2.65	
14	Clearwater Site II	FJ-1	100	100	80	1.26	1.00	1.26	
15		SP-1	90	114	80	1.13	0.79	1.43	
16	Flagler	S-1	700	880	645	1.09	0.80	1.36	
17	WPB Airport	S-1	470	529	375	1.25	0.89	1.41	
18	Plant Daniel	501	700	1097	787	0.89	0.64	1.39	
19		528	700	800	-	-	0.88	-	
20		530	700	800	-	-	0.88	-	
21	Southern 80 SR	S-1	590	640	-	-	0.92	-	
22		S-2	600	765	-	-	0.78	-	
23		S-3	590	647	-	-	0.91	-	
24	Overland	S-1	400	609	541	0.74	0.66	1.13	
25		S-2	300	743	450	0.67	0.40	1.65	
26		S-3	345	365	513	0.67	0.95	0.71	
27	Carolina Bay	S-1	293	308	488	0.60	0.95	0.63	
28	Gilmerton	S-1	380	380	260	1.46	1.00	1.46	
29	Peninsula	S-1	935	997	710	1.32	0.94	1.40	
30	WestRail	41E	300	530	822	0.36	0.57	0.64	
31		41W	300	513	822	0.36	0.58	0.62	
						average	0.99	0.78	1.24
						stdev	0.66	0.21	0.61
						CoV	0.67	0.26	0.49

5.3 Design Equation Refinement

The design equation published by Mullins et al (2006) was based on the linear relationship between the grout pressure index (GPI) and the tip capacity multiplier (TCM) and the non-linear relationship between displacement expressed as the percent of shaft diameters (%D) and TCM. This was determined by computing the TCM and GPI at different points along the load test curves from nine test shafts from five different sites and expressed as a three-dimensional plot (Figure 5.4).

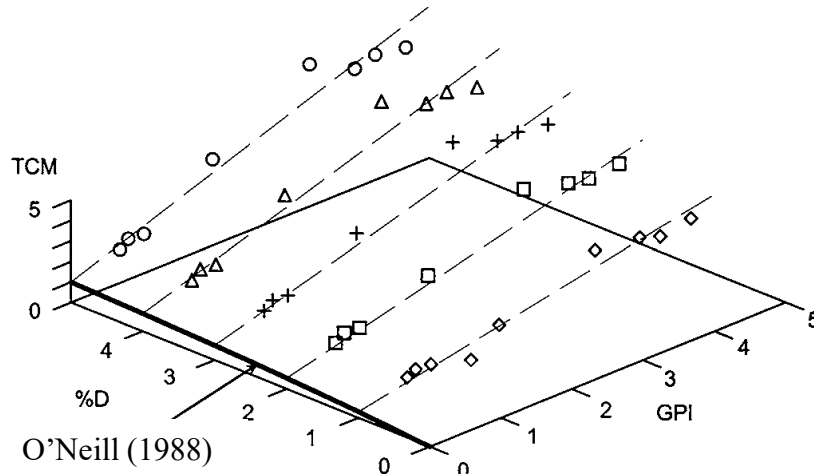


Figure 5.4 TCM defined by linear and non-linear relationships between GPI and %D, respectively (Mullins et al. 2006).

The design equation that resulted from these regressions (Eqn 2.4) was developed by determining the slope of each linear relationship and then by defining a relationship between slope of each line and the respective displacement, in %D. The slope of each line in that publication was expressed as a fitted power function with R^2 of 0.97 (Figure 5.5). This is the same equation as the present FDOT method. The zero-GPI intercepts when plotted versus %D replicated Reese and O'Neill's (1988) trendline for the normalized load transfer in end bearing also shown in AASHTO (2014) and Figure 5.6. Hence, at zero grout pressure the design equation resulted in an end bearing TCM that was the same as an ungrouted shaft.

Simply, TCM is a linear equation ($mx+b$) where x is the grout pressure index (GPI) and where m and b are dependent on %D. Equation 5.1 reorders Eqn 2.4 to show this more clearly. Table 5.3 shows the values of the slope and intercept for each of the lines shown in Figure 5.2.

Table 5.4 Coefficient and intercept values used to define design equation.

%D	1	2	3	4	5
m	0.6944	0.9846	1.1149	1.1923	1.2575
b	0.29	0.53	0.71	0.87	1

$$TCM = 0.713(\%D^{0.364})(GPI) + \frac{\%D}{0.4(\%D)+3.0} \quad (5.1)$$

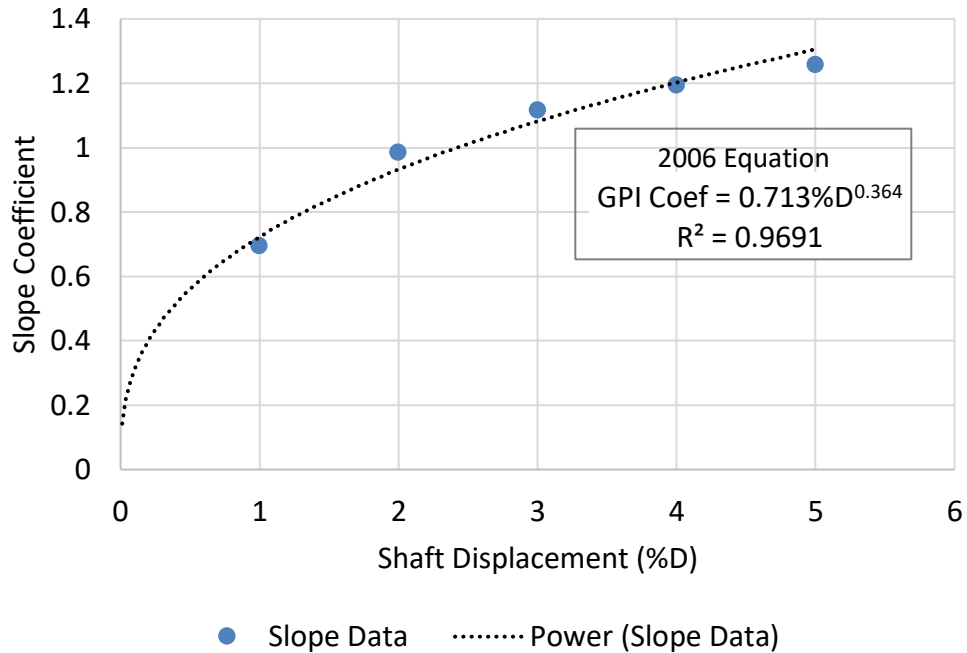


Figure 5.5 Original and refined GPI coefficient determination approaches.

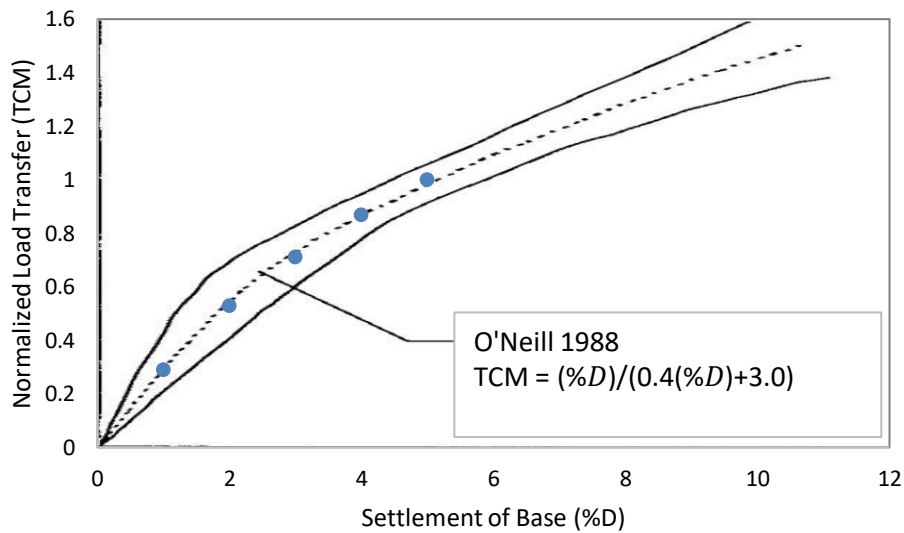
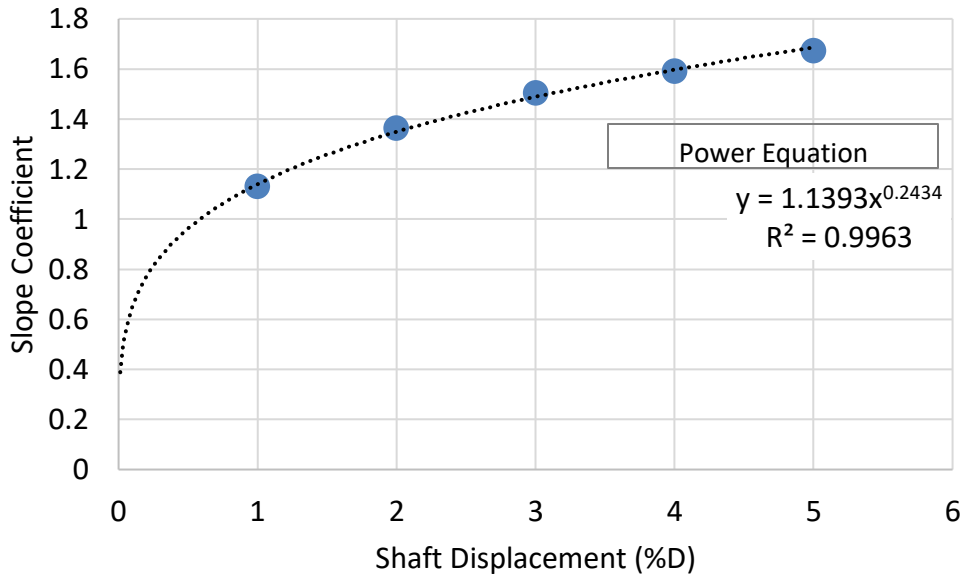


Figure 5.6 TCM intercepts (Table 5.4) match O'Neill design graph (adapted from AASHTO 2014 and Reese and O'Neill 1988).

The collection of more data sets compels the re-evaluation of the original design equation. Using the additional data sets, the same procedure outlined above was replicated to produce a new GPI vs %D relationship which then collectively becomes the GPI coefficient (Figure 5.7). The original intercept values were left the same again as the ungrouted shaft databased used by O'Neill is well accepted. The updated design equation is shown in Equation 5.2.



● Slope Data Power (Slope Data)

Figure 5.7 Updated equation using additional data sets.

$$TCM = 1.14(\%D^{0.243})(GPI) + \frac{\%D}{0.4(\%D)+3.0} \quad 5.2$$

At smaller displacements ($\leq 1\%D$) the updated equation gives higher capacity where the coefficient increased from 0.713 to 1.14. However, at larger displacements the smaller exponent gives lower capacity. In all, the average bias reduced. Table 5.5 shows the resistance factors that result from the updated equation for only the effective pressure bias where no grout pressure limit was applied just to show the effect of the update.

Table 5.5 Resistance factors using updated equation.

Bias Criteria	Resistance Factor, Phi (ϕ)		Resistance Factor, Phi (ϕ)	
	1% Displacement		All Displacements	
	$\beta = 2.33$	$\beta = 3.00$	$\beta = 2.33$	$\beta = 3.00$
Effective pressure (tri-axis plots)	0.45	0.30	0.42	0.29

The average bias (1.29) is improved (closer to 1.0) for the 31-shaft database which implies the updated equation better predicts (on average) the end bearing capacity; the CoV (0.59) did not improve markedly making the newer expression no better than the original equation. The higher bias stemming from the original design equation (1.74) coupled with a similar CoV value (0.62) results in a higher resistance factor. Technically, the original equation with the higher resistance factor or use of the updated equation with the lower resistance factor result in the same probability of failure (and design capacity). Therefore, it is recommended no change be made to the existing equation and the resistance factors computed Table 5.1 or 5.2 are appropriately safe.

5.4 Recommendations

Ultimate capacity of driven piles is predicted on the basis of the Davisson method which either caps both end bearing and side shear dependent on the elastic shortening of the pile head (displacement based) or by assigning 100% side shear along with only one-third of the ultimate predicted capacity. In both cases, there is an attempt to match the side shear and end bearing capacities that develop simultaneously at the same displacement (strain compatible). For shafts, worldwide, there is a continued practice of assigning ultimate capacity under the strength limit state umbrella which unwittingly allows indefensible mismatches in the actual shaft performance from side shear and end bearing for a given displacement. Where postgrouting minimizes this incompatibility, it is unwise (and perhaps unsafe) to assume more capacity from end bearing that stems from displacements that allow the side shear to go into a reduced residual state.

5.4.1 Limit the Design End Bearing Displacement

The rationale for limiting the computed postgrouted unit end bearing to the computed grout pressure (FDOT method) is somewhat simplistic paralleling some of the original design philosophies of the 1970s when no rational design procedure had been developed. With both methods (Mullins et al., 2006 and FDOT) being mostly toe displacement dependent, a more reasonable restriction is to limit the end bearing capacity to smaller displacements that align with known maximum side shear movement or 1%D. When considering the computed resistance factors for limited and unlimited approaches, there is no difference in resistance factor ($\phi = 0.67$ rounded down to the nearest 0.05 use 0.65) at strain compatible displacements (1%D). This should be qualified to only be used for redundant shaft / foundation configurations as a reliability index of 2.33 was used therein. For non-redundant shaft foundations that are postgrouted a significantly reduced resistance factor should be applied ($\phi = 0.45$). Table 5.5 shows the same resistance factors are computed for the Mullins et al. (2006) and FDOT design methods at a displacement of 1%D.

Table 5.6 Comparison of resistance factors by design method.

Bias Criteria	2006 Method (No Limit)		FDOT Method (w/limit)	
	1%D Displacement		1%D Displacement	
	$\beta = 2.33$	$\beta = 3.00$	$\beta = 2.33$	$\beta = 3.00$
Effective pressure (tri-axis plots)	0.67	0.45	0.67	0.44

The conservatism associated with the grout pressure limited end bearing prediction method (FDOT method) at larger displacement (Table 5.2 *all displacements*) resulted in an unusually high resistance factor (0.82) when compared to other FDOT or AASHTO design methods when not employing a load test (Chapter 2). However, allowing larger displacements defeats the strain compatibility restrictions/compliance discussed above and is not recommended. The original design method (Tables 5.1 and 5.6) resulted in a lower and more reasonable resistance factor (0.65) again

when compared to other design methods. Table 5.7 shows the existing FDOT resistance factor values updated to include postgrouted end bearing.

Table 5.7 FDOT resistance factor values including postgrouted end bearing.

Loading	Design Method	Construction QC Method	Resistance Factor	
			Redundant	Non-redundant
Compression	For soil: FHWA alpha or beta method	Specifications	0.6	0.5
	For rock socket: McVay's method neglecting end bearing	Specifications	0.6	0.5
	For rock socket: McVay's method including 1/3 end bearing	Specifications	0.55	0.45
	<i>Post grouted end bearing resistance in sand</i>	<i>Tri-axis grouting verification</i>	<i>0.65*</i>	<i>0.45*</i>
	For rock socket: McVay's method	Statnamic Load Testing	0.7	0.6
	For rock socket: McVay's method	Static Load Testing	0.75	0.65

*with 1%D end bearing displacement limit

5.4.2 New FDOT Design Equation

Using a revised end bearing limit based on 1%D displacement in lieu of the grout pressure limit a more functional rationale for the limit can be imposed. With the value of %D set to 1%, Equations 2.4 and 5.1 are simplified to become

$$TCM = 0.713(GPI) + 0.3 \quad 5.3$$

and where the present design example in the Soils and Foundation Handbook would be replaced to show the total shaft capacity to be the side shear force plus the 1%D end bearing capacity.

The design example in Appendix D of the Soils and Foundation Handbook is replicated in Appendix D of this report using the recommended, new FDOT design equation (Eqn 5.3).

5.4.3 Field Inspection Requirements

Tri-axis plots. The underlying premise of this study was that strict monitoring of grout pressure, grout volume, and shaft uplift along with the simultaneous evaluation of tri-axis plots provides the necessary insight and justification to declare how well (effectively) the grouting has been performed. The design pressure must be verified via inspection records and the inspector-determined effective grout pressure MUST meet or exceed the design pressure in order to justify the use of the 0.65 resistance factor. Peak field-measured grout pressure was found to 28% higher

than the verified effective pressure; office-calculated grout pressure was 24% higher than the effective pressure. This resulted in lower resistance factors when ignoring field effectiveness and an even lower resistance factor with no verification / inspection.

Strain gauges. In cases where the shaft design has more side shear resistance than necessary to resist the design grout pressure, it is reasonable to expect little to no uplift during grouting. Without an indication of global movement, mobilization of both the end bearing and side shear cannot be verified. Therefore, other methods to assess the global toe load should include use of strain gages located in close proximity to the toe of the shaft (within 3 to 4 ft). Strain gages should be used in groups of four nearest the toe (fewer gages per level are reasonable at other upper levels to control costs but with the risk of loss from reduced redundancy). Unfortunately, as the toe level gages cannot be exactly at the toe, the measured strain at the time of grouting does not indicate the load coming from the grout pressure times grouted area; rather the strain indicates the toe force minus the side shear associated with the 3 to 4 feet of separation between the grouting force and the strain gage level. Nevertheless, the gages do provide a mechanism to assess when active grouting is occurring and if increases in pressure are felt as increases in strain. Further, the magnitude of strain in the individual gages can be used to assess whether or not the grouting is loading the full area and/or if the grout bulb is eccentric to the centroid of the shaft cross section.

In the state of Florida, FDOT requires the use of four strain gages at the toe to verify grout bulb distribution, but these measurements should be used in the tri-axis plots to augment or replacement uplift measurements. Augmenting means the uplift graphs have dual axis plots; replacement refers to cases where the uplift measurements show zero or near zero movement. Figure 5.8 shows tri-axis plots prepared for a shaft that exhibited no uplift and where the strain data replaced the uplift data. The peak field measured pressure was almost 700 psi, but when considering the strain measurements and the presence of force causing the strain, it is clear that increases in pressure were not reflected by the strain gauges above a pressure of approximately 275 psi. In fact, the strain continued to decrease regardless of subsequent grouting attempts with other grouting circuits (3 circuit sleeve port system).

Strain measurements have additional value in the form of showing the center of the grout bulb if the strain measurements are interpreted using Equation 5.4.

$$e = \frac{E_{comp} S (\epsilon_i - \epsilon_{avg})}{P A_{grout} - \pi D L_{seg} f_s} \quad 5.4$$

Where,

e is the eccentricity measured in units of length

E_{comp} is the composite elastic modulus; prorated modulus of the steel and concrete areas,

P is the grout pressure,

A_{grout} is assumed to be the area of the shaft,

D is the shaft diameter,

L is the distance between the shaft bottom and the strain gage level (e.g., 3-4 ft),

f_s is the unit side shear in the lower level,

S is the section modulus of the uncracked section,

ϵ_i is the strain measured on one side of the shaft, and ϵ_{avg} is the average strain from all gages.

Figures 5.9 and 5.10 show the application of Equation 5.4 with strain from two opposing gauges where the center of grout force was located 400mm (16 in) off-center below a 2100mm (7 ft) diameter shaft (Mullins, 2015). This was verified via thermal integrity sensors continuously monitoring the shaft temperature as the grout cured (Figure 5.11).

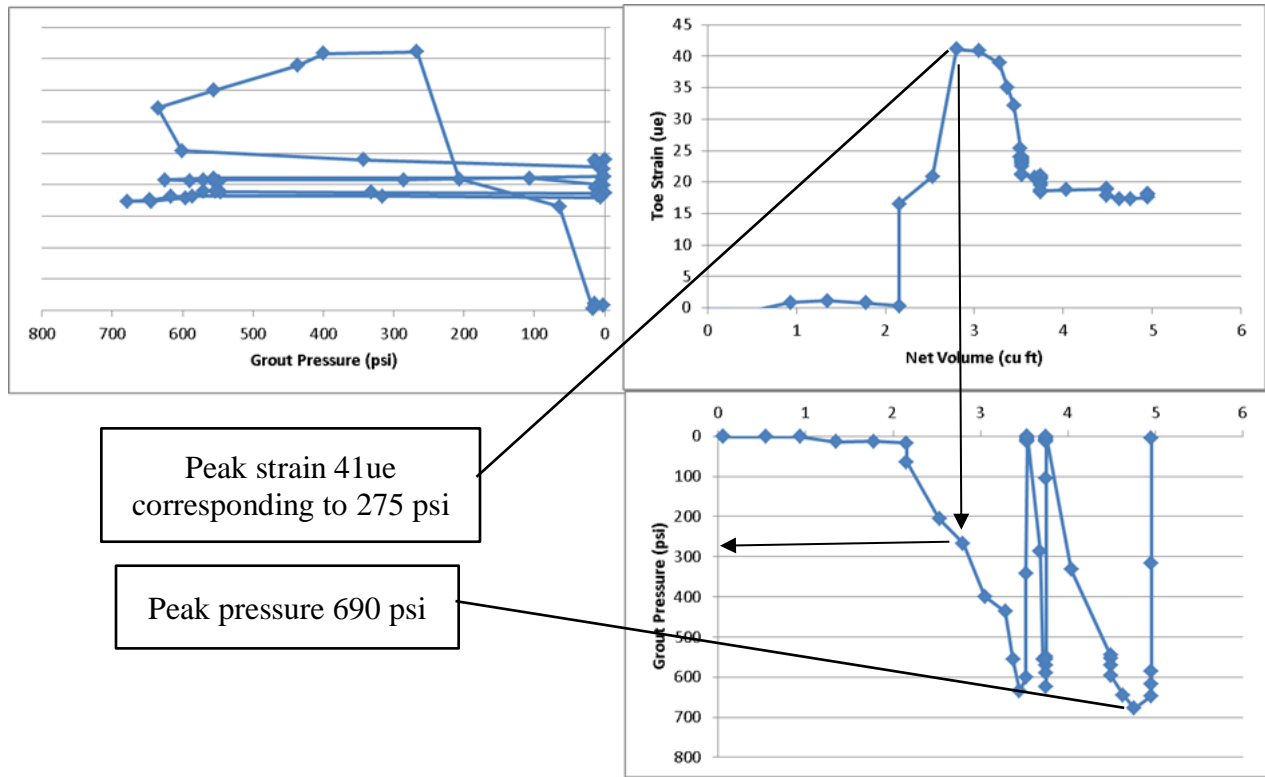


Figure 5.8 Tri-axis plots using strain gauge instead of uplift measurements.

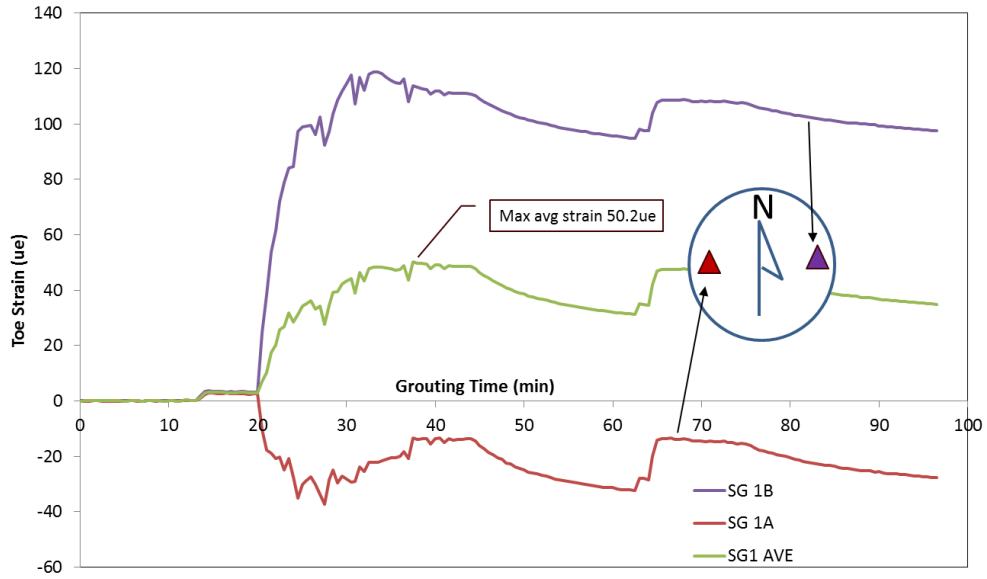


Figure 5.9 Eccentric grout bulb formation noted by strain gauges.

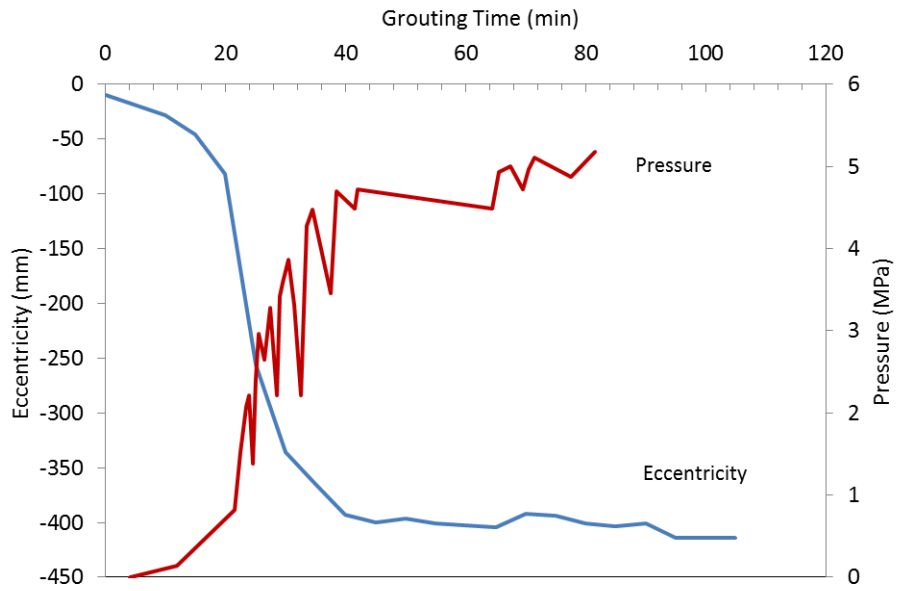


Figure 5.10 Eccentricity as a function of grouting time.

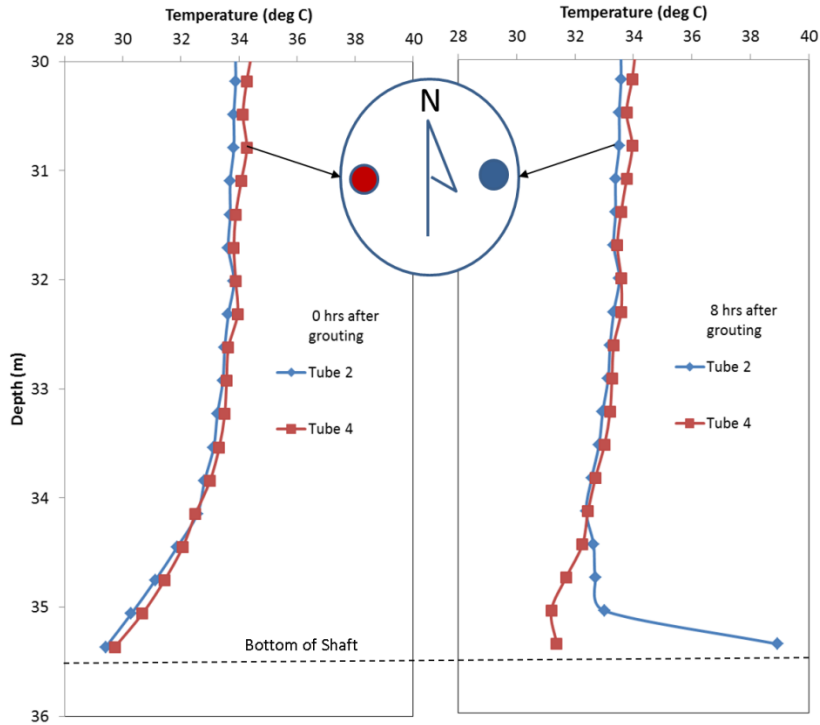


Figure 5.11 Thermal integrity profile near toe of shaft showing more cement on one side.

5.5 Limitations

Stage grouting is a practice that cannot be eliminated as there are numerous scenarios whereby unforeseen equipment malfunctions or soil cavities are experienced. However, the resistance factors determined in this study were based on the FDOT Method and the precursor method developed in 2006 (Mullins et al., 2006) which are based on single stage grouting. As a result, extension of these resistance factors to projects where stage grouting is performed may not be appropriate unless the grouting performance is verified to continue with the same effectiveness both via continued strain gauge measurements and tri-axis plot trends. The true conditions that result from stage grouting vary between scenarios and therefore require a thorough review to fully understand the net effectiveness.

References

- AASHTO. (2014). *LRFD Bridge Design Specifications, Seventh Edition, U.S. Customary Units*, American Association of State Highway and Transportation Officials, Washington, DC. ISBN: 978-1-56051-592-0.
- AASHTO. (2010). *LRFD Bridge Design Specifications, Fifth Edition*, American Association of State Highway and Transportation Officials, Washington, DC.
- AbdelSalam, S.S. Ng, K. W., Sritharan, S., Suleiman, M.T., and Roling, M. (2012). *Development of LRFD Design Procedures for Bridge Piles in Iowa – Volume III: Recommended Resistance Factors with Consideration of Construction Control and Setup*, IHRB Project No. TR-584. Institute for Transportation, Iowa State University, Ames, IA.
- Baker, A.C. and Broadrick, R.L., (1997). *Compaction Grouting, a twenty year update and a vision for the 21st century*, Proceedings Florida/South Florida Section Annual Meeting, Clearwater, FL, September.
- Bolognesi, A. J. L. and Moretto, O. (1973). *Stage Grouting Preloading of Large Shafts in Sand*, Proceedings of 8th ICSMFE, Moscow.
- Bittner, R., Safaqaq, O., Zhang, X. and Jensen, O. (2007). *Design and Construction of the Sutong Bridge Foundations*, DFI Journal, Deep Foundations Institute, Vol. 1, No. 1, November, pp. 2-18.
- Brown, D.A., Turner, J.P., and Castelli, R.J., (2010). *Drilled Shafts: Construction Procedures and LRFD Design Methods*, Publication No. FHWA-NHI-10-016; GEC No. 10, FHWA, Washington, DC.
- Bruce, D.A. (1986). *Enhancing the Performance of Large Diameter Shafts by Grouting, Part 1*, Ground Engineering, Vol. 19, May, Minerva Press, Essex, England.
- Bruce, D.A. (1986). *Enhancing the Performance of Large Diameter Shafts by Grouting, Part 2*, Ground Engineering, Vol. 19, July, Minerva Press, Essex, England.
- Bruce, D. A., Nufer, P. J., and Triplett, R. E. (1995). *Enhancement of Caisson Capacity by Micro-Fine Cement Grouting - a recent case history*, ASCE Special Publication 57, Verification of Geotechnical Grouting.
- Dapp, S.D. (1998). *Interviews with engineers during load testing on the My Thuan Bridge, Mekong Delta, Vietnam.*”
- Dapp, S. and Mullins, G. (2002). *Pressure-Grouting Drilled Shaft Tips: Full-Scale Research Investigation for Silty and Shelly Sands*, Deep Foundations 2002: An International Perspective on Theory, Design, Construction, and Performance, ASCE Geo Institute, GSP No. 116, Vol. I, pp. 335-350.

- Dapp, S. D. (2002). *Pressure Grouting of Drilled Shafts in Sands*, Ph.D. Dissertation, University of South Florida, Tampa, Florida.
- Dapp, S. and Brown, D. (2010). *Evaluation of Base Grouted Drilled Shafts at the Audubon Bridge*, GeoFlorida 2010: Advances in Analysis, Modeling & Design, ASCE (GSP 199).
- Domone, P. L. J., and Jefferis, S. A. (1994). *Structural Grouts*, Chapman and Hall, New York, New York.
- FDOT. (2017). *Structures Design Guidelines, FDOT Structures Manual, Vol. 1*, Florida Department of Transportation, Tallahassee, FL.
- FDOT. (2019). *Soils and Foundation Handbook, Appendix D*, Florida Department of Transportation, Tallahassee, FL.
- FHWA. (1998). *Load and Resistance Factor Design (LRFD) for Highway Bridge Substructures*, FHWA-HI-98-0002, National Highway Institute, Federal Highway Administration, Washington, D.C.
- FHWA. (1999). *Drilled Shafts: Construction Procedures and Design Methods*, O'Neill, M.W. and Reese, L.C., FHWA-IF-99-025, Federal Highway Administration, Washington, D.C.
- Fellenius, B.H., (2002). *Discussion of "Side Resistance in Piles and Drilled Shafts" by Michael W. O'Neill*, Journal of Geotechnical and Geoenvironmental Engineering, American Society of Civil Engineers, Vol. 128, No. 5, 450-450.
- Flemming, W. G. K. (1993). *The Improvement of Shaft Performance by Base Grouting*, Proceedings of the Institution of Civil Engineers, London.
- Gouvenot, D. and Gabiax, F. D. (1975). *A New Foundation Technique using Shafts Sealed by Concrete under High Pressure*, Proceedings, Seventh Annual Offshore Technical Conference.
- Gunaratne, M., Mullins, G., and Wasman, S. (2019). *Re-evaluation of LRFD Resistance Factors for Driven Piles*, Final Report, FDOT Project BDV-25-977-53, Tallahassee, FL,
- Gunaratne, M. (ed), (2014). *The Foundation Engineering Handbook, Second Edition*, CRC Press, Taylor & Francis Group, Boca Raton, FL.
- Gunaratne, M. (ed), (2010). *The Foundation Engineering Handbook*, CRC Press, Taylor & Francis Group, Boca Raton, FL.
- Green, D.; Ng, Kam W., Dunker, K.; Sritharan, S.; and Nop, M. (2012). *Development of LRFD Procedures for Bridge Piles in Iowa-Volume IV: Design Guide and Track Examples*, IHRB Project No's. TR-573, TR-583, and TR-584. Institute for Transportation, Iowa State University, Ames, IA.

- Littlejohn, G. S., Ingle, J., and Dadasbilge, K. (1983). *Improvement in Base Resistance of Large Diameter Piles Founded in Silty Sand*, Proceedings, Eighth European Conference on Soil Mechanics and Foundation Engineering, Helsinki, May.
- Lizzi, F., Viggiani, C., and Vinale, F. (1983). *Some Experience with Pre-Loading Cells at the Base of Large Diameter Bored Piles*, Proceedings of the 7th Asian Regional Conference on Soil Mechanics and Foundation Engineering, Haifa, Israel
- Luna, R. (2014). *Evaluation of Pile Load Tests for use in Missouri LRFD Guidelines*, Report No. MATC-MS&T: 192. Missouri Department of Transportation, Missouri University of Science and Technology, MO.
- Mayne, P.W., (2002). *Discussion of "Side Resistance in Piles and Drilled Shafts" by Michael W. O'Neill.*, Journal of Geotechnical and Geoenvironmental Engineering, Vol. 128, No. 5, 450-450. American Society of Civil Engineers.
- McVay, M.C., Ellis D.E., Birgisson, B., Consolazio, G.R., Putcha, S. and Lee, S.M. (2003). *Load and Resistance Factor Design, Cost and Risk*, Transportation Research Record, 1849, Paper No. O3-3189.
- McVay, M., Bloomquist, D. and Thiyyakkandi, S., (2014). *Field Testing of Jet-Grouted Piles and Drilled Shafts*, Final Report, FDOT Contract No.: BDK75-977-41.
- McVay, M.C., D. Bloomquist, and K.T. Tran. (2013). *Embedded Data Collector (EDC) Evaluation Phase II – Comparison with Instrumented Static Load Tests*, Final Report, FDOT Contract No.: BDK75 977-24, Tallahassee, FL.
- McVay, M. and Wasman, S. (2015). *Embedded Data Collector (EDC) Phase II Load and Resistance Factor Design (LRFD)*, Final Report, FDOT Contract No.: BDV31 977-13, Tallahassee, FL.
- Mojabe, M.S., and Duffin, M. J. (1991). *Large Diameter, Rock Socket, Base Grouted Piles in Bristol*, Proceedings of the 4th International Conference on Piling and Deep Foundations, Stresa, Italy, April
- Mullins, G. (1999). *Interviews with engineers during load testing on the Taipei Financial Center*, Taipei, Taiwan.
- Mullins, G. (2015). *Construction QA/QC Methods for Postgrouting Drilled Shafts*, J. Perform. Constr. Facil. , 10.1061/(ASCE)CF.1943-5509.0000827 , 04015085.
- Mullins, G., Dapp, S., and Lai, P. (2000). *Pressure-Grouting Drilled Shaft Tips in Sand*, New Technological and Design Developments in Deep Foundations, American Society of Civil Engineers, Denver, Colorado.

- Mullins, G. and Winters, D. (2004). *Postgrouting Drilled Shaft Tips - Phase II Final Report*, Final Report submitted Florida Department of Transportation, Tallahassee, Florida, June.
- Mullins, G. and O'Neill, M. (2003). *Pressure Grouting Drilled Shaft Tips - A Full-Scale Load Test Program*, Research Report, University of South Florida, Tampa, Florida, May.
- Mullins, G., Dapp, S., Frederick, E., and Wagner, R. (2001). *Pressure Grouting Drilled Shaft Tips - Phase I Final Report*, Final Report submitted Florida Department of Transportation, Tallahassee, Florida, December.
- Mullins, G., Dapp, S., and Lai, P. (2000). *New Technological and Design Developments in Deep Foundations, Pressure-Grouting Drilled Shaft Tips in Sands*, American Society of Civil Engineers, Denver, Colorado.
- Mullins, G., Winters, D., and Dapp, S., (2008). *Closure to "Predicting End Bearing Capacity of Postgrouted Drilled Shafts in Cohesionless Soils"*, ASCE Journal of Geotechnical and GeoEnvironmental Engineering, Vol. 134, No. 3, p. 413.
- Mullins, G., Winters, D., and Dapp, S. (2006). *Predicting End Bearing Capacity of Postgrouted Drilled Shafts in Cohesionless Soils*, ASCE Journal of Geotechnical and GeoEnvironmental Engineering, Vol. 132, No. 4. pp. 478-487 .
- Ng, K. W., Suleiman, M.T., Sritharan, S., Roling, M., and AbdelSalam, S.S. (2011a). *Development of LRFD Design Procedures for Bridge Piles in Iowa – Soil Investigation and Full-Scaled Pile Tests*, Final Report Vol. II. IHRB Project No. TR-583. Institute for Transportation, Iowa State University, Ames, IA.
- O'Neill, M. W., (2001). *Side Resistance in Piles and Drilled Shafts (The Thirty-Fourth Karl Terzaghi Lecture)*, Journal of Geotechnical and Geoenvironmental Engineering, Vol. 127, No. 1, 3-16. American Society of Civil Engineers.
- O'Neill, M.W., and Reese, L.A., (1999). *Drilled shafts: Construction procedures and design methods*, Publication FHWA-IF-99-025, FHWA, Washington, D.C.
- Piccione, M., Carletti, G., and Diamanti, L. (1984). *The Piled Foundations of the Al Gazira Hotel in Cairo*, Proceedings of the International Conference on Advances in Piling and Ground Treatment for Foundations, Institution of Civil Engineers, London, UK.
- Reese, L.C., and O'Neill, M.W. (1988). *Field Load Tests of Drilled Shafts*, Proceedings International Seminar on Deep Foundations on Bored and Auger Shafts, Van Impe (ed.), Balkama, Rotterdam, June, pp. 145-192.
- Reese, L.C. and O'Neill, M.W. (1988). *Drilled Shafts: Construction and Design*, FHWA, Publication No. HI-88-042, Washington, D.C.

- Roling, M.J., Sritharan, S., and Suleiman, M.T. (2010). *Development of LRFD design procedures for Bridge Piles in Iowa – An Electronic Database for Pile Load Tests in Iowa (PILOT-Iowa)*, Final Report Vol. I. IHRB Project No. TR-573, TR-583 and TR-584. Institute for Transportation, Iowa State University, Ames, IA.
- Santosuossa, M., Rizzi, G., Diamanti, L. (1991). *Construction of Pile Foundation of the Postal Citadel in the Direction Center of Naples*, Proceedings of the 4th International Conference on Piling and Deep Foundations, Stresa, Italy, April
- Schmertmann, J. and Hayes, J. (1997). *The Osterberg Cell and Bored Pile Testing – A Symbiosis*, The Third International Geotechnical Engineering Conference, Cairo, Egypt, January 5-8.
- Sliwinski, Z. J., and Flemming, W. G. K. (1984). *The Integrity and Performance of Bored Piles*, Proceedings of the International Conference on Advances in Piling and Ground Treatment for Foundations, Institution of Civil Engineers, London, UK.
- Sliwinski, Z. J., and Philpot, T. A. (1980). *Conditions for Effective End Bearing of bored Cast in Situ Piles*, Proceedings of Recent Developments in the Design and Construction of Piles, Institute of Civil Engineers, London, UK.
- Stocker, M.F. (1983). *The influence of post grouting on the load bearing capacity of bored piles*, Proceedings, *Eighth European Conference on Soil Mechanics and Foundation Engineering*, Helsinki, May.
- Stuckmeyer, M. G., and Luna, R. (2014). *Two Driven Pile Load Tests for use in Missouri LRFD Guidelines*, Master's Thesis 7279, Department of Civil, Architectural and Environmental Engineering, Missouri University of Science and Technology, MO.
- Troughton, V. M. and Platis, A. (1989). *The Effects of Changes in Effective Stress on a Base Grouted Pile in Sand*, Proceedings of the International Conference on Piling and Deep Foundations, London, UK, May.
- TRB. (2004). *Load and Resistance Factor Design (LRFD) for Deep Foundations*, NCHRP 507, Transportation Research Board, Washington, D.C.,
- Vesic', A. S., (1967). *Ultimate Loads and Settlements of Deep Foundations in Sand*, Proceedings of a Symposium Held at Duke University, April 5/6, 1965, sponsored by National Science Foundation and Duke University, Published by Duke University, Durham, N.C.
- Winters, D. (2014). *Selected Topics in Foundation Design, Quality Assurance, and Remediation*, Ph.D. Dissertation, University of South Florida, Tampa, Florida.
- Yu, X, Abu-Farsakh, M.Y., Yoon, S., Tsai, C., and Zhang, Z., (2012). *Implementation of LRFD of Drilled Shafts in Louisiana*, Journal of Infrastructure Systems, ASCE, Vol. 18, No. 2.

Boring Number: LT-3 Ground Surface Elevation: -3.51 m Water Table Elevation: 0.00 m						
Elevation (m)	Depth (m)	SPT-N	Soil Type	Rock Coring Information		
				qu (kPa)	qs (kPa)	Recovery %
-3.96	0.46	0	3			
-4.72	1.22	39	3			
-5.49	1.98	16	3			
-6.25	2.74	50	3			
-9.30	5.79	23	3			
-10.06	6.55	40	3			
-10.82	7.32	25	3			
-11.58	8.08	23	3			
-12.34	8.84	40	3			
-13.11	9.60	39	3			
-13.87	10.36	53	3			
-14.63	11.13	50	3			
-17.68	14.17	25	3			
-18.44	14.94	15	3			
-19.20	15.70	2	3			
-19.96	16.46	0	3			
-20.73	17.22	6	3			
-21.49	17.98	5	3			
-22.25	18.75	15	3			
-23.01	19.51	10	3			
-23.77	20.27	26	3			
-24.54	21.03	44	3			
-25.30	21.79	68	3			
-26.06	22.56	14	3			
-26.82	23.32	31	3			
-27.58	24.08	49	3			
-28.35	24.84	79	3			
-29.11	25.60	47	3			
-29.87	26.37	30	3			
-30.63	27.13	17	3			
-31.39	27.89	32	3			
-32.16	28.65	21	3			
-32.92	29.41	20	3			
-33.68	30.18	25	3			
-34.44	30.94	18	3			
-35.05	31.55	38	3			

Figure A.2 Data set 2 soil information.

LOG OF BORING NO. TS-4										Page 2 of 2	
CLIENT Longfellow Drilling Inc.					PROJECT Broadway Viaduct						
SITE Council Bluffs, IA											
GRAPHIC LOG	DESCRIPTION	DEPTH, ft.	USCS SYMBOL	SAMPLES				TESTS			
				NUMBER	TYPE	RECOVERY, in.	SPT - N ** BLOWS / ft.	WATER CONTENT, %	DRY UNIT WT pcf	UNCONFINED STRENGTH, psf	
	<p>FINE TO COARSE SAND with silt and gray lean clay Brown, medium dense</p> <p>Trace gray fat clay layer, trace gravel at about 63.5 feet</p> <p>Trace lignite, trace sandy clay, trace gravel below about 68.5 feet</p>	60	SP 12	SS	18	10					
				HS							
			65	SP 13	SS	18	19				
					HS						
			70	SP 14	SS	18	8				
					HS						
			75	SP 15	SS	14	11				
					HS						
			80	SP 16	SS	18	15				
					HS						
		85	SP 17	SS	15	14					
				HS							
		90	SP 18	SS	15	19					
	BOTTOM OF BORING										

The stratification lines represent the approximate boundary lines between soil and rock types: in-situ, the transition may be gradual.

*Calibrated Hand Penetrometer
**CME Automatic Hammer


WATER LEVEL OBSERVATIONS, ft								BORING STARTED		3-26-10	
WL	20	WD						BORING COMPLETED		3-26-10	
WL								RIG	96	FOREMAN	JM
WL								APPROVED DAM	JOB # 05105037		

Figure A.4b Data set 4 soil information

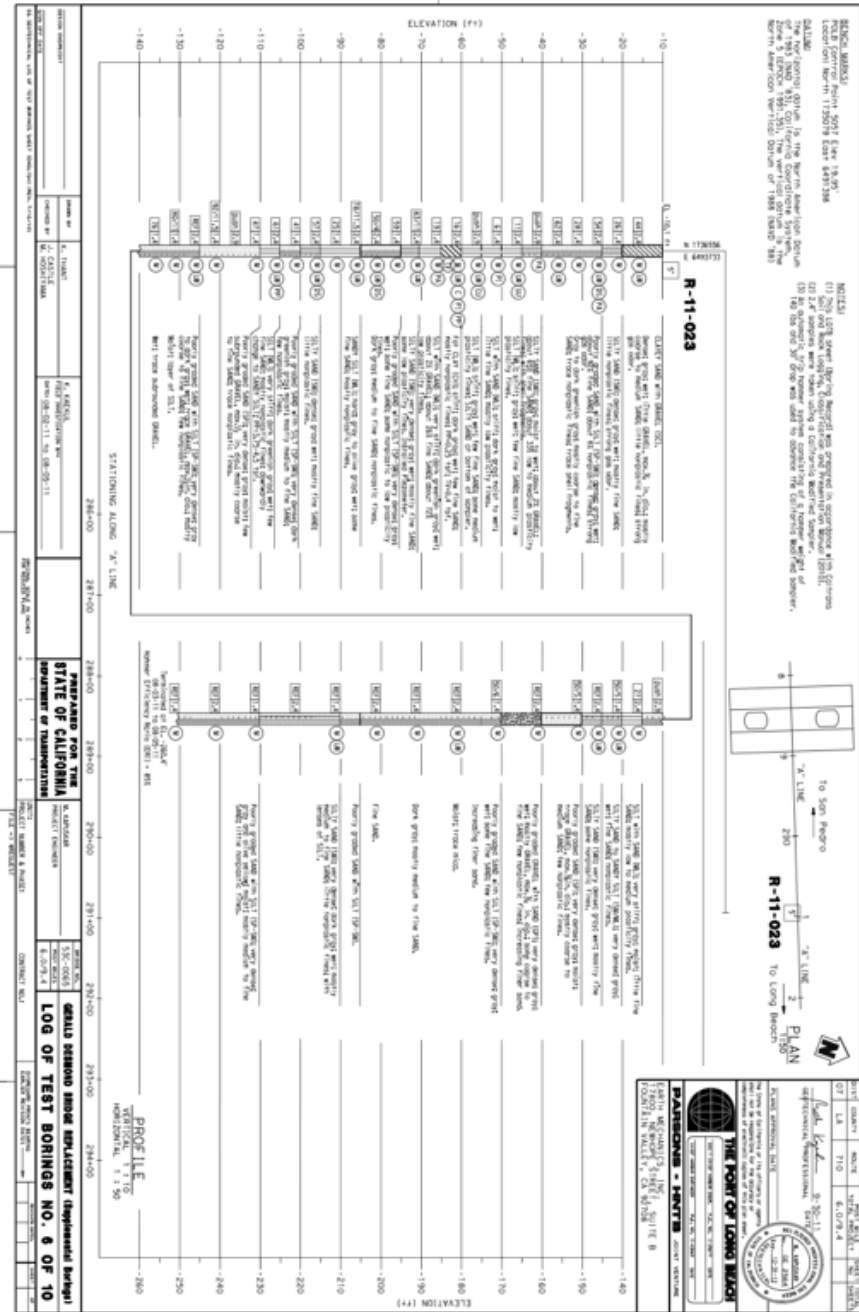


Figure A.5 Data set 5 soil information

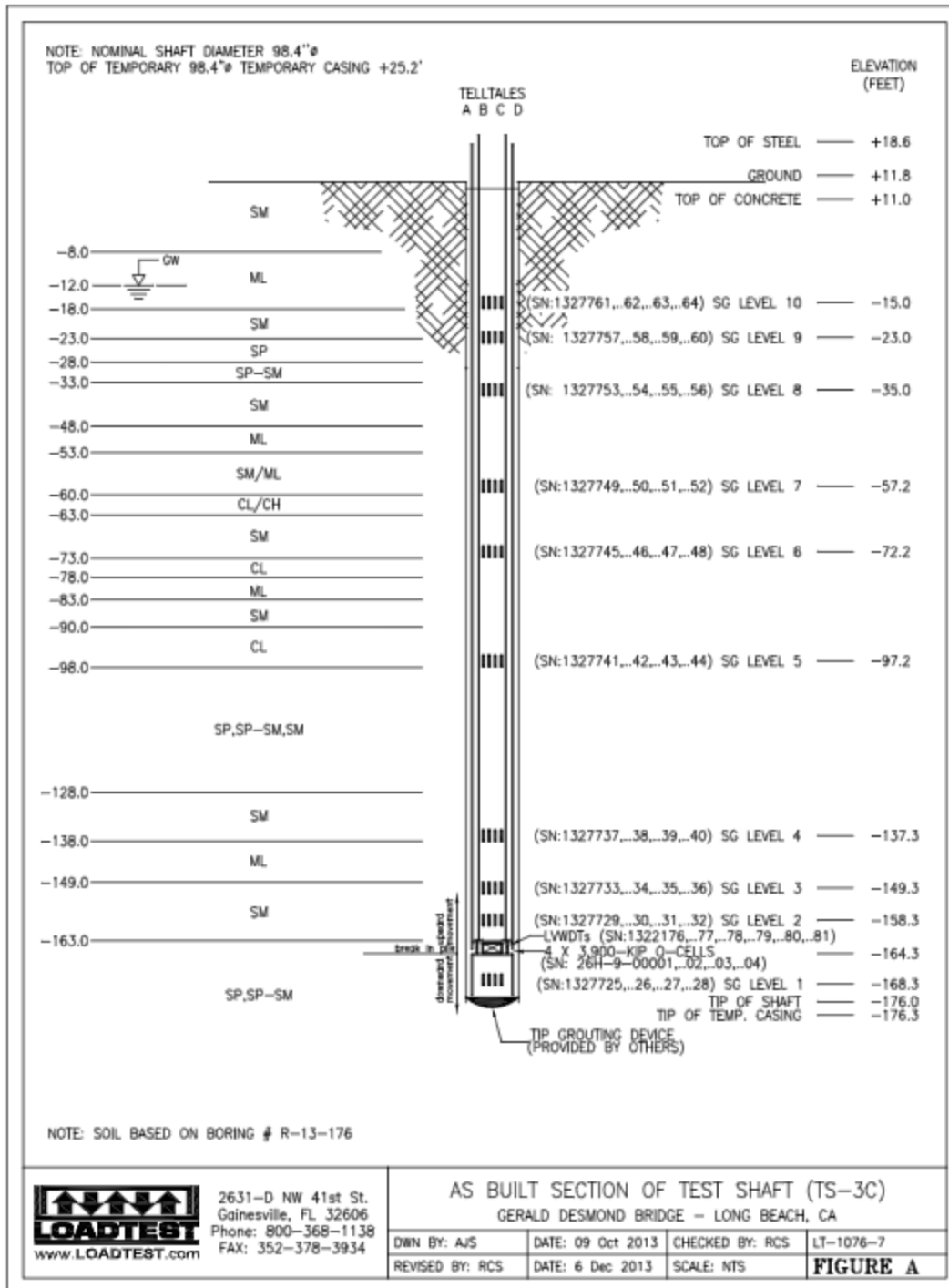


Figure A.6 Data set 6 soil information

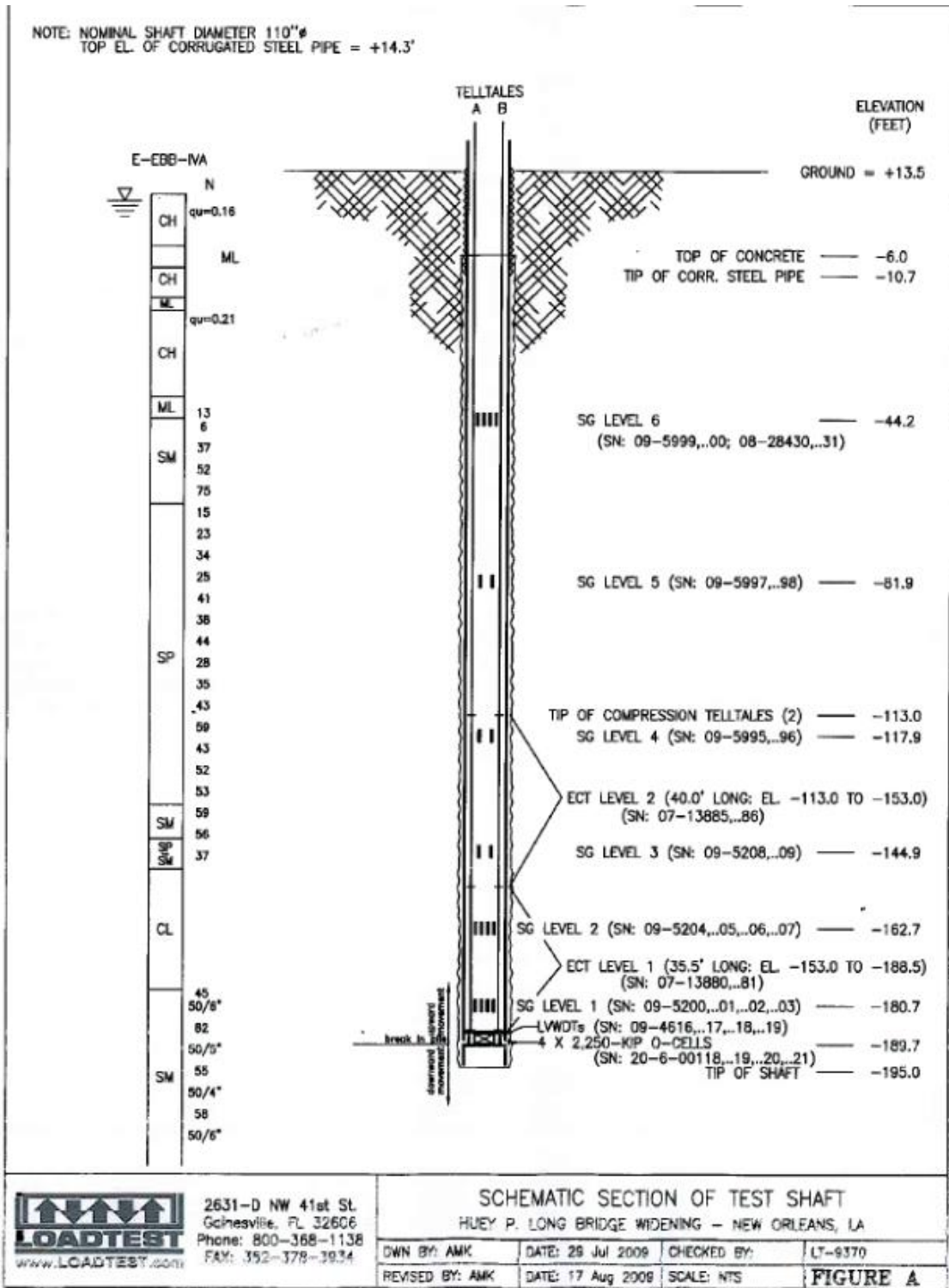


Figure A.7 Data set 7 soil information

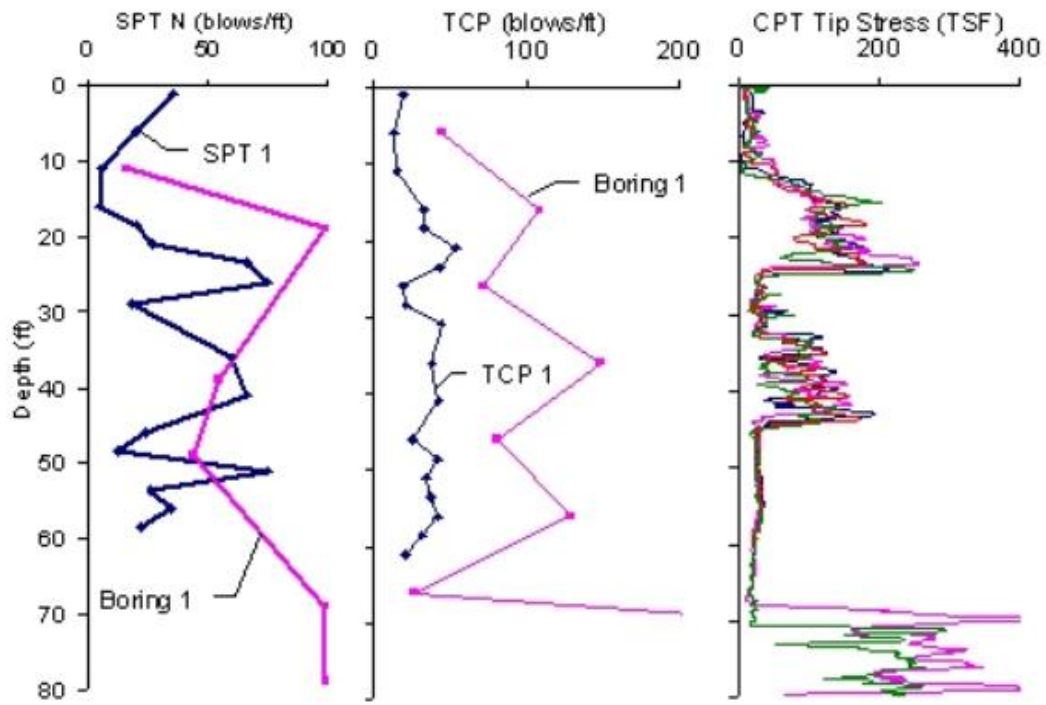


Figure A.8 Data set 8 soil information

Project Name:	Nachez						
Project Location:	Nachez, MS						
Geo Engineer:	Wilbur Smith						
Boring No:	B-1						
Pile Length (ft):	75						
Pile Diameter (ft)	6						
Elevation (NAD)	98.1						
Water Table Depth (ft)	0						
Effective Grout pressure (psi)	120						
q grouted	99.60						
γ_D	1.3889						
TCM (ungROUTED)	0.3906						

Soil Type	
1	Clay
2	Silt
3	Sand

Elevation (ft)	Depth, Z (ft)	Z avr (ft)	Δ Z (ft)	Δ A (ft ²)	N	Soil Classification from SPT	Soil Type
98.1	0						
96.6	1.5	3.25	1.5	28.274	3	Silt	2
93.1	5	7.0	3.5	65.973	27	Silt	2
89.1	9	11.5	4	75.398	17	Sand	3
84.1	14	16.5	5	94.248	2	Silt	2
79.1	19	21.5	5	94.248	10	Sand	3
74.1	24.0	26.5	5	94.248	44	Sand	3
69.1	29	31.5	5	94.248	50	Sand	3
64.1	34	36.5	5	94.248	20	Sand	3
59.1	39	41.5	5	94.248	74	Sand	3
54.1	44	46.5	5	94.248	50	Sand	3
49.1	49	51.5	5	94.248	83	Sand	3
44.1	54	56.5	5	94.248	21	Sand	3
39.1	59	29.5	5	94.248	50	Sand	3

Figure A.9 Data set 9 soil information

Project Name: Clearwater
 Project Location: Clearwater, FL
 Geo Engineer: S1-FJ1
 Boring No: CPT FJ1
 Pile Length (ft): 15
 Pile Diameter (ft) 2
 Elevation (NAD) 0
 Water Table Depth (ft) 0
 Effective Grout pressure (psi) 20 2.88 ksf
 q grouted 43.90
 perm disp (in) 1
 %D 4.1667
 TCM (ungrouted) 0.8929

Elevation (ft)	Depth, Z (ft)	Z avr (ft)	Δ Z (ft)	Δ A (ft ²)	Qc (tsf)	Qc (bar)	FR(%)	N	Soil Classification from SPT
0	0								
-0.25	0.25	0.375	0.25	1.5708	0.0022	0.0022	0.1462	0.0147	SAND
-0.5	0.5	0.6	0.25	1.5708	0.0069	0.0066	0.318	0.0208	SAND
-0.75	0.75	0.9	0.25	1.5708	0.025	0.024	0.3891	0.0617	SAND
-1	1	1.1	0.25	1.5708	0.1109	0.1065	0.5095	0.209	SAND
-1.25	1.25	1.4	0.25	1.5708	0.1411	0.1354	0.7794	0.1738	SAND
-1.5	1.5	1.6	0.25	1.5708	0.168	0.1612	0.752	0.2144	SAND
-1.75	2	1.9	0.25	1.5708	0.1534	0.1473	0.6248	0.2357	SAND
-2	2	2.1	0.25	1.5708	0.1366	0.1311	0.6475	0.2025	SAND
-2.25	2	2.4	0.25	1.5708	0.1116	0.1072	0.8185	0.1309	SAND
-2.5	3	2.6	0.25	1.5708	0.0636	0.061	1.2623	0.0483	CLAY
-2.75	2.75	2.9	0.25	1.5708	0.0347	0.0333	1.1354	0.0293	CLAY
-3	3	3.1	0.25	1.5708	0.0122	0.0117	0.9331	0.0126	SAND
-3.25	3.25	3.4	0.25	1.5708	0.0463	0.0445	0.6079	0.0731	SAND
-3.5	3.5	3.6	0.25	1.5708	0.0685	0.0658	0.5803	0.1133	SAND
-3.75	3.75	3.9	0.25	1.5708	0.0547	0.0525	0.9245	0.0568	SAND
-4	4	4.1	0.25	1.5708	0.0434	0.0417	1.641	0.0254	CLAY
-4.25	4.25	4.4	0.25	1.5708	0.0321	0.0308	1.0689	0.0288	CLAY
-4.5	4.5	4.6	0.25	1.5708	0.0231	0.0222	0.7452	0.0298	SAND
-4.75	4.75	4.9	0.25	1.5708	0.0231	0.0222	0.4448	0.0499	SAND
-5	5	5.1	0.25	1.5708	0.0203	0.0195	0.3905	0.05	SAND
-5.25	5.25	5.4	0.25	1.5708	0.0282	0.027	0.3905	0.0693	SAND
-5.5	5.5	5.6	0.25	1.5708	0.0798	0.0766	0.4336	0.1766	SAND
-5.75	5.75	5.9	0.25	1.5708	0.0908	0.0872	0.4336	0.201	SAND
-6	6	6.1	0.25	1.5708	0.0978	0.0938	0.4293	0.2186	SAND
-6.25	6.25	6.4	0.25	1.5708	0.0991	0.0952	0.5504	0.1729	SAND
-6.5	6.5	6.6	0.25	1.5708	0.095	0.0912	0.5504	0.1657	SAND
-6.75	6.75	6.9	0.25	1.5708	0.0837	0.0803	0.6445	0.1246	SAND
-7	7	7.1	0.25	1.5708	0.074	0.071	0.3944	0.18	SAND
-7.25	7.25	7.4	0.25	1.5708	0.0522	0.0501	0.2173	0.2306	SAND
-7.5	7.5	7.6	0.25	1.5708	0.0424	0.0407	0.0908	0.4485	SAND
-7.75	7.75	7.9	0.25	1.5708	0.0295	0.0283	0.0109	2.5946	SAND
-8	8	8.1	0.25	1.5708	0.0295	0.0283	0.0109	2.5946	SAND
-8.25	8.25	8.4	0.25	1.5708	0.0221	0.0212	0.0078	2.7163	SAND
-8.5	8.5	8.6	0.25	1.5708	0.0221	0.0212	0.0078	2.7163	SAND
-8.75	8.75	8.9	0.25	1.5708	0.0221	0.0212	0.0228	0.9293	SAND
-9	9	9.1	0.25	1.5708	0.0171	0.0165	0.0983	0.1674	SAND
-9.25	9.25	9.4	0.25	1.5708	0.0181	0.0174	0.0537	0.3239	SAND

Figure A10a Data set 10 soil information

Project Name: Clearwater
 Project Location: Clearwater, FL
 Geo Engineer: S1-FJ1
 Boring No: CPT FJ1
 Pile Length (ft): 15
 Pile Diameter (ft): 2
 Elevation (NAD): 0
 Water Table Depth (ft): 0
 Effective Grout pressure (psi): 20 2.88 ksf
 q grouted: 43.90
 perm disp (in): 1
 %D: 4.1667
 TCM (ungrouted): 0.8929

Elevation (ft)	Depth, Z (ft)	Z avr (ft)	Δ Z (ft)	Δ A (ft ²)	Qc (tsf)	Qc (bar)	FR(%)	N	Soil Classification from SPT
-9.5	9.5	9.6	0.25	1.5708	0.0195	0.0187	0.0537	0.3491	SAND
-9.75	9.75	9.9	0.25	1.5708	0.0281	0.027	0.0537	0.502	SAND
-10	10	10.1	0.25	1.5708	0.0335	0.0322	0.0379	0.8485	SAND
-10.25	10.25	10.4	0.25	1.5708	0.0432	0.0414	0.0379	1.0935	SAND
-10.5	10.5	10.6	0.25	1.5708	0.0432	0.0414	0.0379	1.0935	SAND
-10.75	10.75	10.9	0.25	1.5708	0.0457	0.0439	0.917	0.0479	SAND
-11	11	11.1	0.25	1.5708	0.0457	0.0439	0.917	0.0479	SAND
-11.25	11.25	11.4	0.25	1.5708	0.0457	0.0439	0.0012	36.584	SAND
-11.5	11.5	11.6	0.25	1.5708	0.0457	0.0439	0.0012	36.584	SAND
-11.75	11.75	11.9	0.25	1.5708	0.0266	0.0255	1.6748	0.0152	CLAY
-12	12	12.1	0.25	1.5708	0.0266	0.0255	1.6748	0.0152	CLAY
-12.25	12.25	12.4	0.25	1.5708	0.0207	0.0199	1.6748	0.0119	CLAY
-12.5	12.5	12.6	0.25	1.5708	0.0156	0.015	0.0591	0.2531	SAND
-12.75	12.75	12.9	0.25	1.5708	0.0156	0.015	1.6766	0.0089	CLAY
-13	13	13.1	0.25	1.5708	0.0257	0.0247	1.6766	0.0147	CLAY
-13.25	13.25	13.4	0.25	1.5708	0.0257	0.0247	0.0239	1.0327	SAND
-13.5	13.5	13.6	0.25	1.5708	0.0181	0.0174	0.0239	0.7262	SAND
-13.75	13.75	13.9	0.25	1.5708	0.0181	0.0174	0.1417	0.1225	SAND
-14	14	14.1	0.25	1.5708	0.0194	0.0187	0.1417	0.1316	SAND
-14.25	14.25	14.4	0.25	1.5708	0.0207	0.0199	0.3616	0.0551	SAND
-14.5	14.5	14.6	0.25	1.5708	0.0207	0.0199	0.5316	0.0375	SAND
-14.75	14.75	14.9	0.25	1.5708	0.0213	0.0204	0.3785	0.054	SAND
-15	15	15.1	0.25	1.5708	0.0329	0.0316	0.3785	0.0835	SAND
-15.25	15.25	15.4	0.25	1.5708	0.0329	0.0316	0.2758	0.1146	SAND
-15.5	15.5	15.6	0.25	1.5708	0.0454	0.0435	0.569	0.0765	SAND
-15.75	15.75	15.9	0.25	1.5708	0.0421	0.0404	0.6153	0.0657	SAND
-16	16	16.1	0.25	1.5708	0.029	0.0279	0.5876	0.0474	SAND
-16.25	16.25	16.4	0.25	1.5708	0.0233	0.0223	0.9567	0.0234	SAND
-16.5	16.5	16.6	0.25	1.5708	0.0151	0.0145	0.7306	0.0199	SAND
-16.75	16.75	16.9	0.25	1.5708	0.0071	0.0068	0.7306	0.0093	SAND
-17	17	17.1	0.25	1.5708	0.0107	0.0103	0.0408	0.2527	SAND
-17.25	17.25	17.4	0.25	1.5708	0.009	0.0087	0.0799	0.1084	SAND
-17.5	17.5	17.6	0.25	1.5708	0.0104	0.01	0.0799	0.1252	SAND
-17.75	17.75	17.9	0.25	1.5708	0.0119	0.0114	0.0799	0.1429	SAND
-18	18	18.1	0.25	1.5708	0.0029	0.0028	0.0799	0.0345	SAND
-18.25	18.25	18.4	0.25	1.5708	0.0029	0.0028	0.0425	0.0648	SAND
-18.5	18.5	18.6	0.25	1.5708	0.0026	0.0025	0.0425	0.0594	SAND
-18.75	18.75	18.9	0.25	1.5708	0.0026	0.0025	0.036	0.0701	SAND
-19	19	19.1	0.25	1.5708	0.0014	0.0013	0.036	0.0373	SAND
-19.25	19.25	19.4	0.25	1.5708	0.0014	0.0013	0.1808	0.0074	SAND
-19.5	19.5	19.6	0.25	1.5708	0.0014	0.0013	0.5229	0.0026	SAND
-19.75	19.75	19.9	0.25	1.5708	0.0014	0.0013	0.2239	0.006	SAND
-20	20	20.1	0.25	1.5708	0.0014	0.0013	0.2239	0.006	SAND

Figure A.10b Data set 10 soil information

Project Name: Clearwater
 Project Location: Clearwater, FL
 Geo Engineer: SI-F12
 Boring No: CPT F12
 Pile Length (ft): 15
 Pile Diameter (ft): 2
 Elevation (NAVD): 0
 Water Table Depth (ft): 0
 Effective Grout pressure (psf) 15 2.16 ksf
 q grouted 2.09
 perm disp (in) 1
 %O 4.1667
 TCM (ungrouted) 0.8925

Elevation (ft)	Depth, Z (ft)	Z _{avr} (ft)	Δ Z (ft)	Δ A (ft ²)	Q _c (tsf)	Q _c (bar)	FR(%)	N	Soil Classification from SPT
0	0								
-0.25	0.25	0.375	0.25	1.5708	0.0285	0.013622	0.0769	0.1771	SAND
-0.5	0.50	0.6	0.25	1.5708	0.0285	0.013622	0.2852	0.0478	SAND
-0.75	0.75	0.9	0.25	1.5708	0.0599	0.028662	0.3486	0.0822	SAND
-1	1.00	1.1	0.25	1.5708	0.1145	0.05483	0.2942	0.1864	SAND
-1.25	1.25	1.4	0.25	1.5708	0.2967	0.142047	0.2534	0.5606	SAND
-1.5	1.50	1.6	0.25	1.5708	0.3017	0.144465	0.362	0.399	SAND
-1.75	1.75	1.9	0.25	1.5708	0.2006	0.096027	0.5658	0.1697	SAND
-2	2.00	2.1	0.25	1.5708	0.1575	0.075414	0.5159	0.1462	SAND
-2.25	2.25	2.4	0.25	1.5708	0.1446	0.069237	0.7196	0.0962	SAND
-2.5	2.50	2.6	0.25	1.5708	0.0976	0.046709	0.6607	0.0707	SAND
-2.75	2.75	2.9	0.25	1.5708	0.1278	0.061188	0.4026	0.152	SAND
-3	3.00	3.1	0.25	1.5708	0.0499	0.023907	0.7204	0.0332	SAND
-3.25	3.25	3.4	0.25	1.5708	0.0758	0.036771	0.6108	0.0594	SAND
-3.5	3.50	3.6	0.25	1.5708	0.0433	0.020747	0.4568	0.0454	SAND
-3.75	3.75	3.9	0.25	1.5708	0.0498	0.023845	0.2485	0.096	SAND
-4	4.00	4.1	0.25	1.5708	0.051	0.024429	0.1352	0.1807	SAND
-4.25	4.25	4.4	0.25	1.5708	0.051	0.024429	0.1533	0.1593	SAND
-4.5	4.50	4.6	0.25	1.5708	0.0324	0.015495	0.108	0.1435	SAND
-4.75	4.75	4.9	0.25	1.5708	0.0276	0.013206	0.1804	0.0732	SAND
-5	5.00	5.1	0.25	1.5708	0.0324	0.015519	0.0491	0.3164	SAND
-5.25	5.25	5.4	0.25	1.5708	0.0212	0.010127	0.0491	0.2065	SAND
-5.5	5.50	5.6	0.25	1.5708	0.0189	0.009054	0.0491	0.1846	SAND
-5.75	5.75	5.9	0.25	1.5708	0.0215	0.010295	0.0444	0.2319	SAND
-6	6.00	6.1	0.25	1.5708	0.0188	0.009021	0.1349	0.0669	SAND
-6.25	6.25	6.4	0.25	1.5708	0.0632	0.030266	0.3024	0.1001	SAND
-6.5	6.50	6.6	0.25	1.5708	0.0731	0.034883	0.3034	0.1157	SAND
-6.75	6.75	6.9	0.25	1.5708	0.0811	0.038837	0.3069	0.1266	SAND
-7	7.00	7.1	0.25	1.5708	0.0895	0.042864	0.3023	0.1418	SAND
-7.25	7.25	7.4	0.25	1.5708	0.0895	0.042864	0.5677	0.0755	SAND
-7.5	7.50	7.6	0.25	1.5708	0.0915	0.043822	0.5677	0.0772	SAND
-7.75	7.75	7.9	0.25	1.5708	0.0774	0.05707	0.3701	0.1002	SAND
-8	8.00	8.1	0.25	1.5708	0.0565	0.027049	0.5014	0.0539	SAND
-8.25	8.25	8.4	0.25	1.5708	0.0529	0.025334	0.5466	0.0463	SAND
-8.5	8.50	8.6	0.25	1.5708	0.0529	0.025334	0.4379	0.0579	SAND
-8.75	8.75	8.9	0.25	1.5708	0.0529	0.025334	0.1888	0.1342	SAND
-9	9.00	9.1	0.25	1.5708	0.0245	0.011722	0.0846	0.1385	SAND
-9.25	9.25	9.4	0.25	1.5708	0.0245	0.011722	0.0209	0.5608	SAND
-9.5	9.50	9.6	0.25	1.5708	0.022	0.010564	0.0209	0.5045	SAND
-9.75	9.75	9.9	0.25	1.5708	0.0423	0.020254	0.0209	0.9691	SAND
-10	10.00	10.1	0.25	1.5708	0.0635	0.030391	0.0211	1.441	SAND
-10.25	10.25	10.4	0.25	1.5708	0.0218	0.010438	0.0256	0.4085	SAND
-10.5	10.50	10.6	0.25	1.5708	0.0253	0.012119	0.0256	0.4743	SAND
-10.75	10.75	10.9	0.25	1.5708	0.0395	0.018933	0.0256	0.741	SAND
-11	11.00	11.1	0.25	1.5708	0.029	0.013876	0.0256	0.5431	SAND
-11.25	11.25	11.4	0.25	1.5708	0.029	0.0139	0.0256	0.544	SAND
-11.5	11.50	11.6	0.25	1.5708	0.029	0.0139	0.0256	0.544	SAND
-11.75	11.75	11.9	0.25	1.5708	0.029	0.0139	0.0117	1.186	SAND
-12	12.00	12.1	0.25	1.5708	0.031	0.014824	0.3332	0.0445	SAND
-12.25	12.25	12.4	0.25	1.5708	0.0253	0.01205	0.2517	0.048	SAND
-12.5	12.50	12.6	0.25	1.5708	0.0203	0.00973	-0.007	-1.495	SAND
-12.75	12.75	12.9	0.25	1.5708	0.0257	0.012301	0.0071	1.7399	SAND
-13	13.00	13.1	0.25	1.5708	0.0294	0.014096	-0.016	-0.902	SAND
-13.25	13.25	13.4	0.25	1.5708	0.0294	0.014096	0.0296	0.4759	SAND
-13.5	13.50	13.6	0.25	1.5708	0.0282	0.013522	-0.029	-0.462	SAND
-13.75	13.75	13.9	0.25	1.5708	0.0273	0.013048	-0.029	-0.445	SAND
-14	14.00	14.1	0.25	1.5708	0.025	0.011947	-0.029	-0.408	SAND
-14.25	14.25	14.4	0.25	1.5708	0.0342	0.016352	-0.029	-0.558	SAND
-14.5	14.50	14.6	0.25	1.5708	0.022	0.010524	-0.016	-0.663	SAND
-14.75	14.75	14.9	0.25	1.5708	0.022	0.010524	-0.02	-0.515	SAND
-15	15.00	15.1	0.25	1.5708	0.0301	0.014422	0.287	0.0502	SAND
-15.25	15.25	15.4	0.25	1.5708	0.0289	0.01288	-0.003	-3.836	SAND
-15.5	15.50	15.6	0.25	1.5708	0.0226	0.010817	0.0247	0.4377	SAND
-15.75	15.75	15.9	0.25	1.5708	0.0255	0.012715	-0.002	-4.906	SAND
-16	16.00	16.1	0.25	1.5708	0.042	0.020101	0.079	0.2545	SAND

Figure A.11 Data set 11 soil information

Project Name: Clearwater									
Project Location: Clearwater, FL									
Geo Engineer: S1-SP1									
Boring No: CPT SP1									
Elevation (ft)	Depth, Z (ft)	Z avr (ft)	Δ Z (ft)	Δ A (ft ²)	Qc (tsf)	Qc (bar)	FR(%)	N	Soil Classification from SPT
0	0								
-0.75	0.75	0.875	0.75	4.712	0.035	0.017	0.34	0.049	SAND
-1	1.00	1.1	0.25	1.571	0.079	0.038	0.338	0.112	SAND
-1.25	1.25	1.4	0.25	1.571	0.085	0.041	0.658	0.062	SAND
-1.5	1.50	1.6	0.25	1.571	0.144	0.069	0.54	0.128	SAND
-1.75	1.75	1.9	0.25	1.571	0.209	0.1	0.54	0.185	SAND
-2	2.00	2.1	0.25	1.571	0.242	0.116	0.329	0.353	SAND
-2.25	2.25	2.4	0.25	1.571	0.122	0.058	0.258	0.227	SAND
-2.5	2.50	2.6	0.25	1.571	0.099	0.048	0.67	0.071	SAND
-2.75	2.75	2.9	0.25	1.571	0.121	0.058	0.529	0.109	SAND
-3	3.00	3.1	0.25	1.571	0.151	0.072	0.536	0.135	SAND
-3.25	3.25	3.4	0.25	1.571	0.149	0.071	0.465	0.153	SAND
-3.5	3.50	3.6	0.25	1.571	0.094	0.045	0.465	0.096	SAND
-3.75	3.75	3.9	0.25	1.571	0.064	0.031	0.465	0.066	SAND
-4	4.00	4.1	0.25	1.571	0.037	0.018	0.447	0.039	SAND
-4.25	4.25	4.4	0.25	1.571	0.022	0.011	0.445	0.024	SAND
-4.5	4.50	4.6	0.25	1.571	0.034	0.016	0.143	0.115	SAND
-4.75	4.75	4.9	0.25	1.571	0.07	0.034	0.208	0.161	SAND
-5	5.00	5.1	0.25	1.571	0.07	0.034	0.208	0.161	SAND
-5.25	5.25	5.4	0.25	1.571	0.082	0.039	0.343	0.115	SAND
-5.5	5.50	5.6	0.25	1.571	0.089	0.043	0.343	0.125	SAND
-5.75	5.75	5.9	0.25	1.571	0.089	0.043	0.385	0.111	SAND
-6	6.00	6.1	0.25	1.571	0.071	0.034	0.385	0.088	SAND
-6.25	6.25	6.4	0.25	1.571	0.071	0.034	0.425	0.08	SAND
-6.5	6.50	6.6	0.25	1.571	0.053	0.025	0.469	0.054	SAND
-6.75	6.75	6.9	0.25	1.571	0.032	0.015	0.606	0.025	SAND
-7	7.00	7.1	0.25	1.571	0.032	0.015	0.441	0.034	SAND
-7.25	7.25	7.4	0.25	1.571	0.032	0.015	0.161	0.094	SAND
-7.5	7.50	7.6	0.25	1.571	0.032	0.015	0.02	0.756	SAND
-7.75	7.75	7.9	0.25	1.571	0.032	0.015	0.02	0.756	SAND
-8	8.00	8.1	0.25	1.571	0.018	0.008	0.02	0.421	SAND
-8.25	8.25	8.4	0.25	1.571	0.03	0.014	0.383	0.037	SAND
-8.5	8.50	8.6	0.25	1.571	0.042	0.02	0.013	1.598	SAND
-8.75	8.75	8.9	0.25	1.571	0.029	0.014	0.102	0.134	SAND
-9	9.00	9.1	0.25	1.571	0.029	0.014	0.04	0.346	SAND
-9.25	9.25	9.4	0.25	1.571	0.029	0.014	0.576	0.024	SAND
-9.5	9.50	9.6	0.25	1.571	0.046	0.022	0.071	0.311	SAND
-9.75	9.75	9.9	0.25	1.571	0.046	0.022	0.575	0.039	SAND
-10	10.00	10.1	0.25	1.571	0.035	0.017	0.575	0.029	SAND
-10.25	10.25	10.4	0.25	1.571	0.035	0.017	0.006	2.767	SAND
-10.5	10.50	10.6	0.25	1.571	0.035	0.017	0.006	2.767	SAND
-10.75	10.75	10.9	0.25	1.571	0.035	0.017	0.083	0.201	SAND
-11	11.00	11.1	0.25	1.571	0.035	0.017	0.416	0.04	SAND
-11.25	11.25	11.4	0.25	1.571	0.035	0.017	0.015	1.085	SAND
-11.5	11.50	11.6	0.25	1.571	0.041	0.02	0.015	1.275	SAND
-11.75	11.75	11.9	0.25	1.571	0.013	0.006	0.118	0.054	SAND
-12	12.00	12.1	0.25	1.571	0.049	0.023	0.118	0.199	SAND
-12.25	12.25	12.4	0.25	1.571	0.069	0.033	0.048	0.689	SAND
-12.5	12.50	12.6	0.25	1.571	0.069	0.033	0.158	0.209	SAND
-12.75	12.75	12.9	0.25	1.571	0.059	0.028	0.108	0.259	SAND
-13	13.00	13.1	0.25	1.571	0.044	0.021	0.108	0.196	SAND
-13.25	13.25	13.4	0.25	1.571	0.044	0.021	0.035	0.607	SAND
-13.5	13.50	13.6	0.25	1.571	0.041	0.019	0.035	0.556	SAND
-13.75	13.75	13.9	0.25	1.571	0.041	0.019	0.099	0.197	SAND
-14	14.00	14.1	0.25	1.571	0.041	0.019	0.099	0.197	SAND
-14.25	14.25	14.4	0.25	1.571	0.038	0.018	0.099	0.186	SAND
-14.5	14.50	14.6	0.25	1.571	0.04	0.019	0.045	0.422	SAND
-14.75	14.75	14.9	0.25	1.571	0.029	0.014	0.045	0.311	SAND
-15	15.00	15.1	0.25	1.571	0.026	0.012	0.157	0.078	SAND
-15.25	15.25	15.4	0.25	1.571	0.026	0.012	0.498	0.025	SAND
-15.5	15.50	15.6	0.25	1.571	0.035	0.017	0.659	0.025	SAND
-15.75	15.75	15.9	0.25	1.571	0.026	0.012	0.748	0.016	SAND
-16	16.00	16.1	0.25	1.571	0.026	0.012	0.839	0.015	SAND
-16.25	16.25	16.4	0.25	1.571	0.021	0.01	0.839	0.012	SAND

Figure A.12 Data set 12 soil information

Project Name: Clearwater									
Project Location: Clearwater, FL									
Geo Engineer: S1-SP2									
Boring No: CPT SP2									
Elevation (ft)	Depth, Z (ft)	Z avr (ft)	Δ Z (ft)	Δ A (ft ²)	Qc (tsf)	Qc (bar)	FR(%)	N	Soil Classification from SPT
0	0								
-0.5	0.50	0.625	0.5	3.142	0.045	0.022	0.099	0.218	SAND
-0.75	0.75	0.9	0.25	1.571	0.116	0.055	0.467	0.119	SAND
-1	1.00	1.1	0.25	1.571	0.216	0.103	0.467	0.221	SAND
-1.25	1.25	1.4	0.25	1.571	0.203	0.097	0.43	0.226	SAND
-1.5	1.50	1.6	0.25	1.571	0.254	0.122	0.297	0.409	SAND
-1.75	1.75	1.9	0.25	1.571	0.254	0.122	0.297	0.409	SAND
-2	2.00	2.1	0.25	1.571	0.248	0.119	0.454	0.262	SAND
-2.25	2.25	2.4	0.25	1.571	0.243	0.116	0.454	0.256	SAND
-2.5	2.50	2.6	0.25	1.571	0.235	0.113	0.454	0.248	SAND
-2.75	2.75	2.9	0.25	1.571	0.258	0.124	0.361	0.342	SAND
-3	3.00	3.1	0.25	1.571	0.121	0.058	0.431	0.134	SAND
-3.25	3.25	3.4	0.25	1.571	0.218	0.104	0.382	0.273	SAND
-3.5	3.50	3.6	0.25	1.571	0.271	0.13	0.442	0.294	SAND
-3.75	3.75	3.9	0.25	1.571	0.161	0.077	0.436	0.177	SAND
-4	4.00	4.1	0.25	1.571	0.112	0.054	0.656	0.082	SAND
-4.25	4.25	4.4	0.25	1.571	0.086	0.041	0.793	0.052	SAND
-4.5	4.50	4.6	0.25	1.571	0.096	0.046	0.64	0.072	SAND
-4.75	4.75	4.9	0.25	1.571	0.096	0.046	0.371	0.124	SAND
-5	5.00	5.1	0.25	1.571	0.11	0.053	0.256	0.206	SAND
-5.25	5.25	5.4	0.25	1.571	0.11	0.053	0.501	0.105	SAND
-5.5	5.50	5.6	0.25	1.571	0.034	0.016	0.374	0.043	SAND
-5.75	5.75	5.9	0.25	1.571	0.121	0.058	0.374	0.155	SAND
-6	6.00	6.1	0.25	1.571	0.113	0.054	0.415	0.13	SAND
-6.25	6.25	6.4	0.25	1.571	0.09	0.043	0.415	0.104	SAND
-6.5	6.50	6.6	0.25	1.571	0.09	0.043	0.437	0.099	SAND
-6.75	6.75	6.9	0.25	1.571	0.074	0.035	0.458	0.077	SAND
-7	7.00	7.1	0.25	1.571	0.055	0.026	0.497	0.053	SAND
-7.25	7.25	7.4	0.25	1.571	0.055	0.026	0.325	0.081	SAND
-7.5	7.50	7.6	0.25	1.571	0.033	0.016	0.075	0.21	SAND
-7.75	7.75	7.9	0.25	1.571	0.033	0.016	0.039	0.408	SAND
-8	8.00	8.1	0.25	1.571	0.033	0.016	0.039	0.408	SAND
-8.25	8.25	8.4	0.25	1.571	0.025	0.012	0.039	0.315	SAND
-8.5	8.50	8.6	0.25	1.571	0.025	0.012	0.042	0.289	SAND
-8.75	8.75	8.9	0.25	1.571	0.025	0.012	0.042	0.289	SAND
-9	9.00	9.1	0.25	1.571	0.056	0.027	0.042	0.633	SAND
-9.25	9.25	9.4	0.25	1.571	0.056	0.027	0.012	2.162	SAND
-9.5	9.50	9.6	0.25	1.571	0.056	0.027	0.012	2.162	SAND
-9.75	9.75	9.9	0.25	1.571	0.056	0.027	0.012	2.162	SAND
-10	10.00	10.1	0.25	1.571	0.056	0.027	0.012	2.162	SAND
-10.25	10.25	10.4	0.25	1.571	0.037	0.018	0.012	1.428	SAND
-10.5	10.50	10.6	0.25	1.571	0.037	0.018	0.052	0.337	SAND
-10.75	10.75	10.9	0.25	1.571	0.037	0.018	0.052	0.337	SAND
-11	11.00	11.1	0.25	1.571	0.043	0.02	0.052	0.391	SAND
-11.25	11.25	11.4	0.25	1.571	0.043	0.02	0.052	0.391	SAND
-11.5	11.50	11.6	0.25	1.571	0.043	0.02	0.037	0.552	SAND
-11.75	11.75	11.9	0.25	1.571	0.056	0.027	0.037	0.722	SAND
-12	12.00	12.1	0.25	1.571	0.056	0.027	0.037	0.722	SAND
-12.25	12.25	12.4	0.25	1.571	0.056	0.027	0.038	0.712	SAND
-12.5	12.50	12.6	0.25	1.571	0.037	0.018	0.038	0.476	SAND
-12.75	12.75	12.9	0.25	1.571	0.046	0.022	0.038	0.59	SAND
-13	13.00	13.1	0.25	1.571	0.046	0.022	0.064	0.347	SAND
-13.25	13.25	13.4	0.25	1.571	0.046	0.022	0.085	0.26	SAND
-13.5	13.50	13.6	0.25	1.571	0.061	0.029	0.085	0.342	SAND
-13.75	13.75	13.9	0.25	1.571	0.061	0.029	0.085	0.342	SAND
-14	14.00	14.1	0.25	1.571	0.045	0.022	0.07	0.31	SAND
-14.25	14.25	14.4	0.25	1.571	0.045	0.022	0.09	0.24	SAND
-14.5	14.50	14.6	0.25	1.571	0.075	0.036	0.09	0.4	SAND
-14.75	14.75	14.9	0.25	1.571	0.098	0.047	0.189	0.248	SAND
-15	15.00	15.1	0.25	1.571	0.09	0.043	0.189	0.227	SAND
-15.25	15.25	15.4	0.25	1.571	0.072	0.034	0.189	0.182	SAND
-15.5	15.50	15.6	0.25	1.571	0.06	0.029	0.189	0.151	SAND
-15.75	15.75	15.9	0.25	1.571	0.06	0.029	0.189	0.151	SAND
-16	16.00	16.1	0.25	1.571	0.06	0.029	0.189	0.151	SAND
-16.25	16.25	16.4	0.25	1.571	0.06	0.029	0.061	0.469	SAND

Figure A.13 Data set 13 soil information

STATE OF FLORIDA DEPARTMENT OF TRANSPORTATION
FIELD BORING LOG

FORM 475-018-B
MATERIALS - 1293

Page 1 of Page 2

Project: USF Type: POST GRANT Boring #: B-3 Elevator: _____ Type Soil penet: CRME 75
 Bridge #: N/A Station #: N/A Other: N/A County: Pinellas U.O.T.S.: 23867
 ELEVATION BASED ON NECCI MARK Township: _____ Range: _____ East Footing: _____
 Description: SET for Post Grant research Water Table Elevation: _____ Type Hammer: Auto
 Drilled By: Randy Johnson Logged By: Randy Johnson Boring started: _____ Boring completed: _____
 Date/Time Started: 07/20/07 Date/Time Completed: 07/20/07 2:45P Water Table Measured: _____
 Water Table Measured Station: N/A Other: N/A Monitor GMR: N/A Water Table Depth: _____

DEPTH (English) SAMPLE		RPT ELEVATIONS	MATERIAL DESCRIPTION	SAMPLES			REMARKS
FROM	TO			NO.	IN	W	
0.0						NO ground sample taken due to rocks, trash	
1.5	1.5	8	med brn Sand 7/16" silty	1			
		5	med brn Sand 7/16" silty				
		7	med brn Sand 7/16" silty	2	13 1/2	75	
3.0	3.0	5	med brn Sand w/scrubs			STRATA CHANGE @ 3.0'	
		8	med brn Sand w/scrubs				
		10	med brn Sand w/scrubs	3	13 1/2	75	
4.5	4.5	3	med brn Sand loose			STRATA CHANGE @ 4.5'	
		3	med brn Sand loose				
		4	med brn Sand loose	4	13 1/2	75	
6.0	6.0	2	med brn Sand loose			STRATA CHANGE @ 6.0'	
		2	med brn Sand loose				
		2	med brn Sand loose	5	12	100	
7.5	7.5	1	SAME				
		1	SAME				
		2	SAME	6	9	50	
9.0	9.0	1	med brn Sand			STRATA CHANGE @ 9.0'	
		1	very loose, wet				
		1	SAME	7	13 1/2	75	
10.5	10.5	0	SAME			(1st blow pushed tube 12")	
		1	SAME	8	7	50	
12.0	12.0	1	SAME			(weight of hammer pushed tube 12")	
		1	SAME	9	12	100	
13.5	13.5	0	med brn Sand 7/16" silty			STRATA CHANGE @ 13.5'	
		2	med brn Sand 7/16" silty				
15.0	15.0	3	med brn Sand 7/16" silty	10	13 1/2	75	

Figure A.14a Data set 14 soil information

STATE OF FLORIDA DEPARTMENT OF TRANSPORTATION
FIELD BORING LOG

FORM 625-04-13
MATERIALS-1895

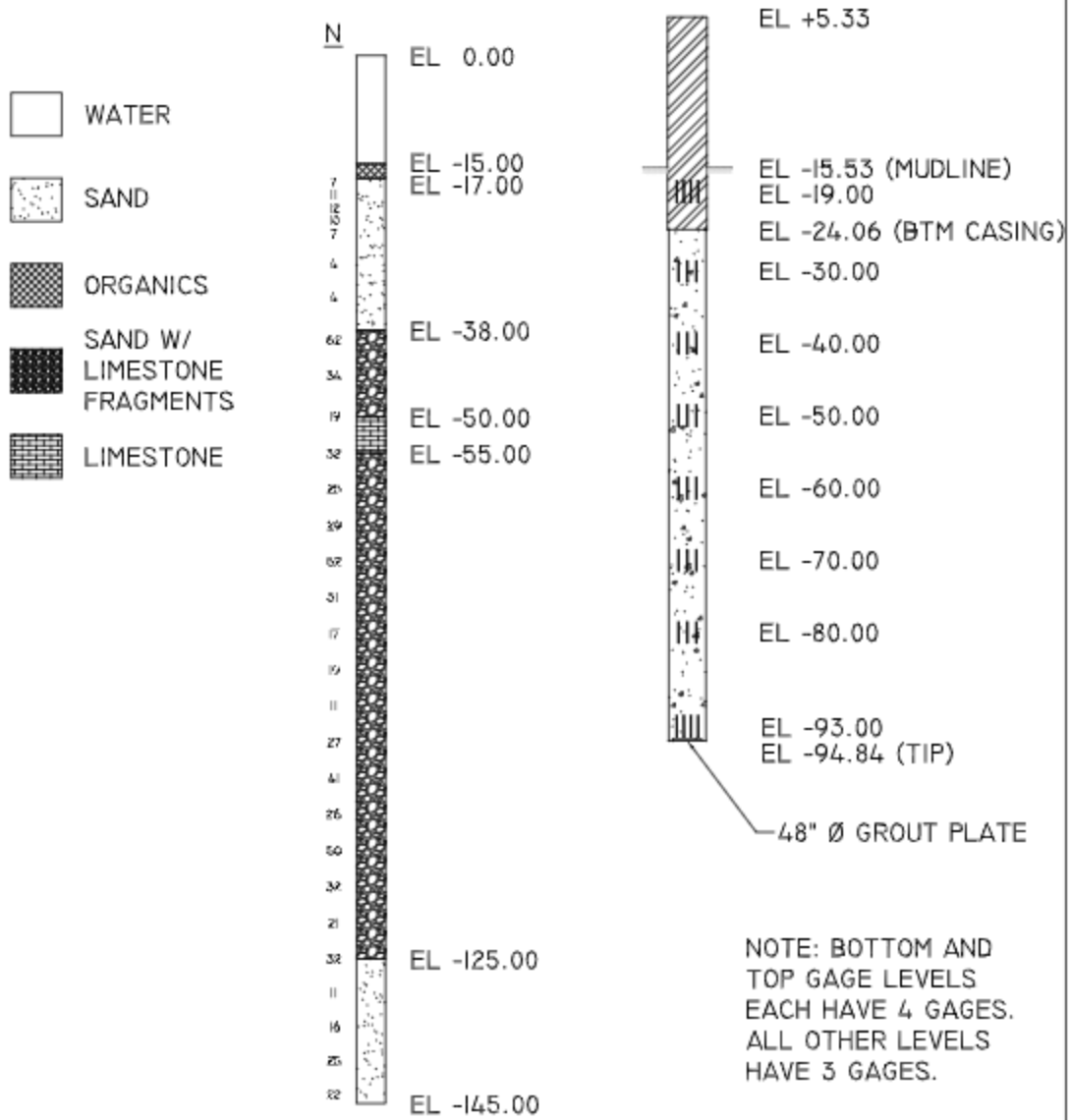
Page 1 of Page 2

Project No. 125F SP Post Locat Boring No. B-4 Iteration: _____ Type Equip. used: 6" P.C.T.S.
 Bridge No. N/A Section No. N/A Other: ETA County: Pinellas D.O.T. No. 23067
 ELEVATION BASED ON BENCH MARK _____ Township: Acush Range: _____ East Section _____
 Description: SP Post Locat research
 Drilled By: Carlton / Stueck Logged By: Rich Campbell Water Table Elevation: _____ Type Hammer: _____
 Date/Time Started: 5/1/00 Date/Time Completed: 5/1/00 Boring type: _____
 Water Table Elevation: Surface, N/A Other: N/A Monitor GWT: N/A Water Table Depth: _____

DEPTH (English) SAMPLE		FEET BLOWS	MATERIAL DESCRIPTION	SAMPLES			REMARKS
FROM	TO			NO.	IN.	%	
0.0		1				no sound sample taken due to rocks & trash	
	1.5			1			
1.5		5	Dark brown sand, T/Silt				
		5	iron med. coarse, moist				
	3.0	5		2	18	100	
3.0		4					
		7	NO RECOVERY				
	4.5	11		3	0	0	
4.5		7	Dark Sand w/ rocks med. coarse, moist			STRATA CHANGE @ 4.5'	
		5					
	6.0	6		4	4 1/2	25	
6.0		2	same (very loose)				
		1					
	7.5	2		5	13 1/2	75	
7.5		4	NO RECOVERY				
		3					
	9.0	1		6	0	0	
9.0		4	med. brown sand very loose, moist			(weight of hammer pushed tube 12")	
		1		7	18	100	
10.5		1	SAME			(weight of hammer pushed tube 6")	
		1					
	12.0	1		8	18	100	
12.0		4	gray sand T/Silt very loose, moist			(weight of hammer pushed tube 12")	
		2		9	13 1/2	75	
13.5		2				STRATA CHANGE @ 12.5'	
13.5		2	gray sand, loose moist			in spoon (weight of rod pushed spoon 6")	
		3		10	13 1/2	75	
15.0						STRATA CHANGE @ 13.5'	

Figure A.15a Data set 15 soil information

TEST SHAFT 2 SCHEMATIC DRAWING INSTRUMENTATION LAYOUT



APPLIED FOUNDATION TESTING, INC.

FLAGLER MEMORIAL BRIDGE

Figure A.16 Data set 16 soil information

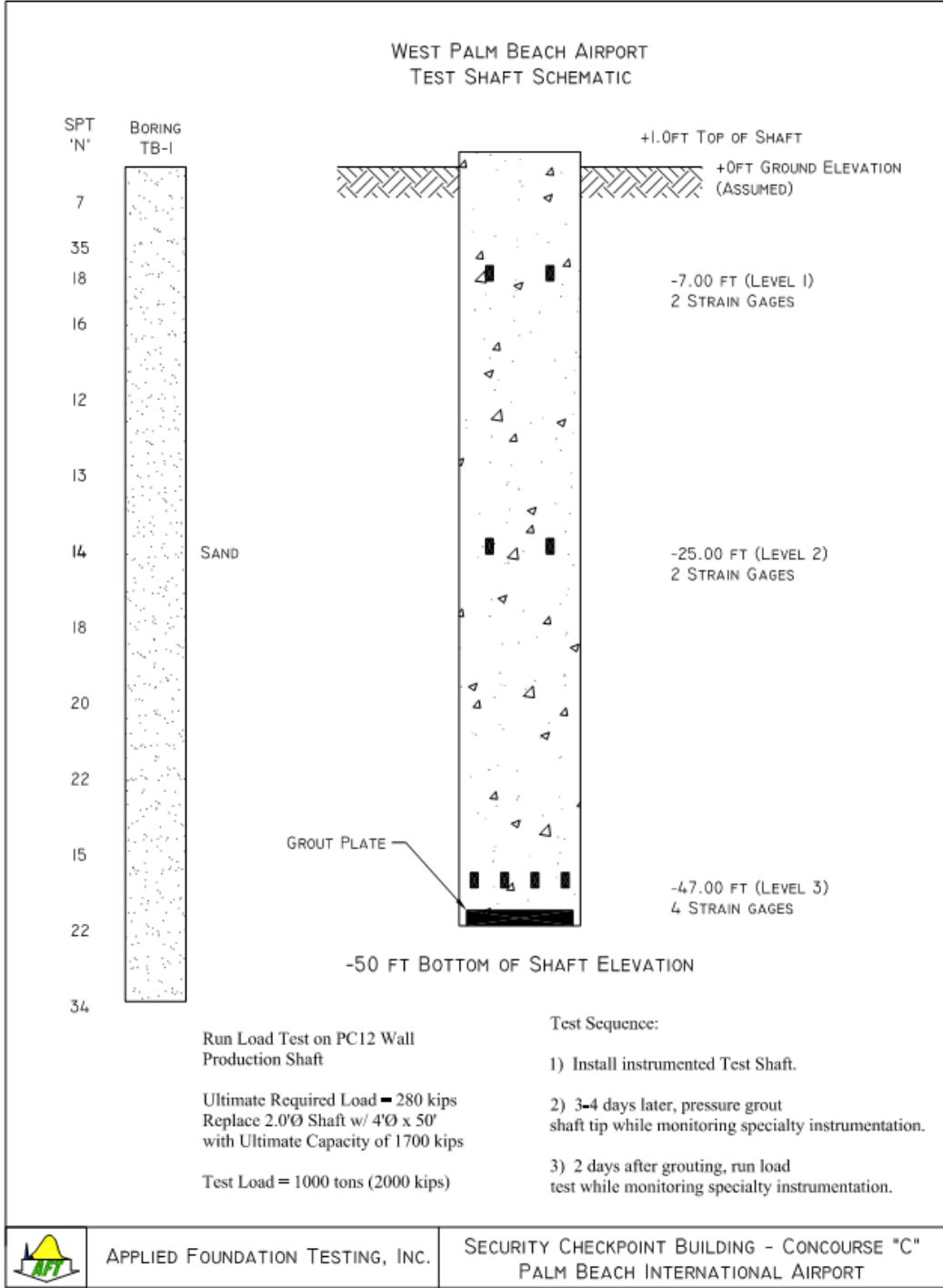


Figure A.17 Data set 17 soil information

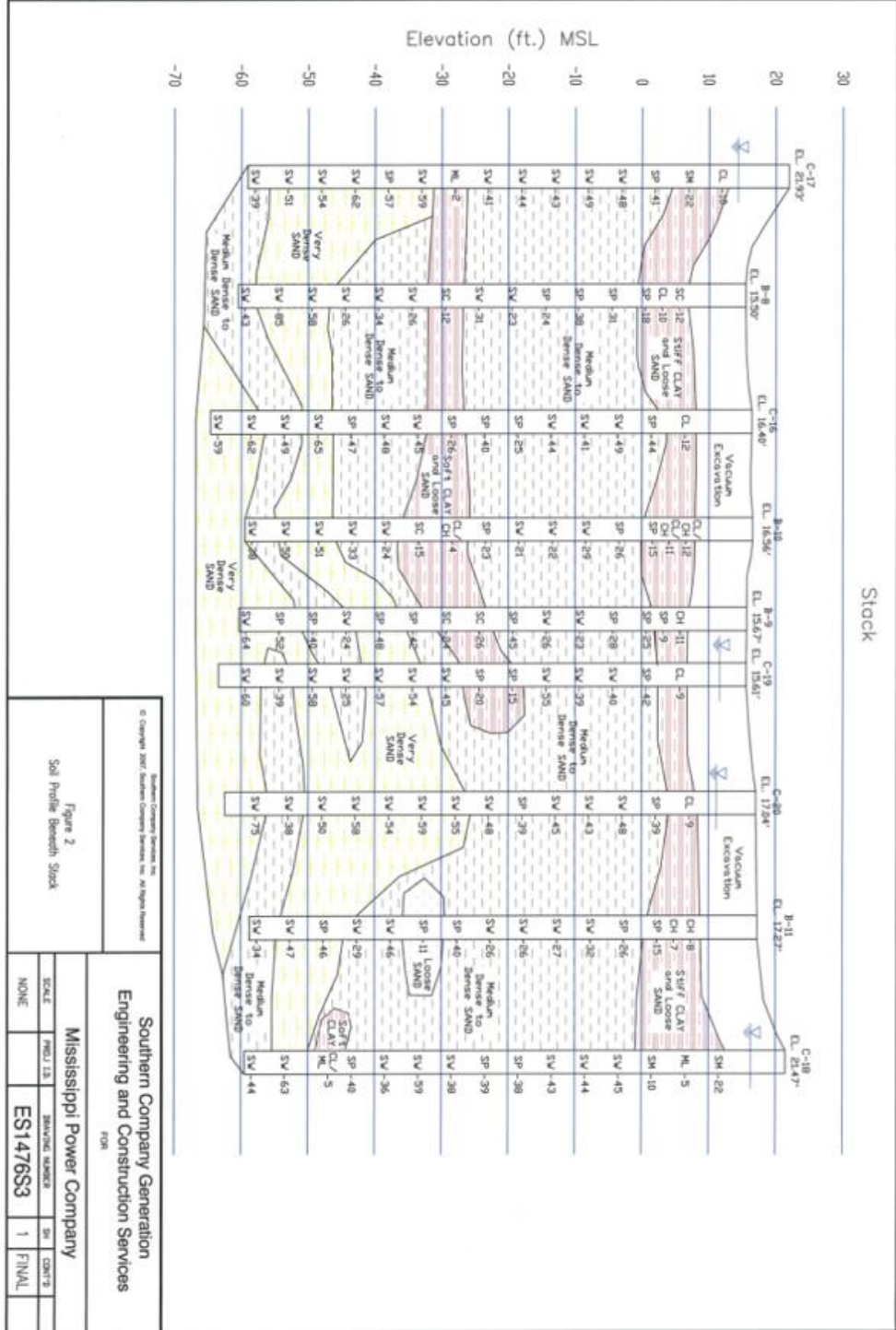


Figure 2
Soil Profile beneath Stock

Southern Company Services, Inc.
 Engineering and Construction Services

FOR
Mississippi Power Company

SCALE	PROJ. I.S.	REVISION NUMBER	BY	DATE
NONE		ES1476S3	1	FINAL

© Copyright 2007, Southern Company Services, Inc. All Rights Reserved.

Figure A.18 Data set 18 soil information

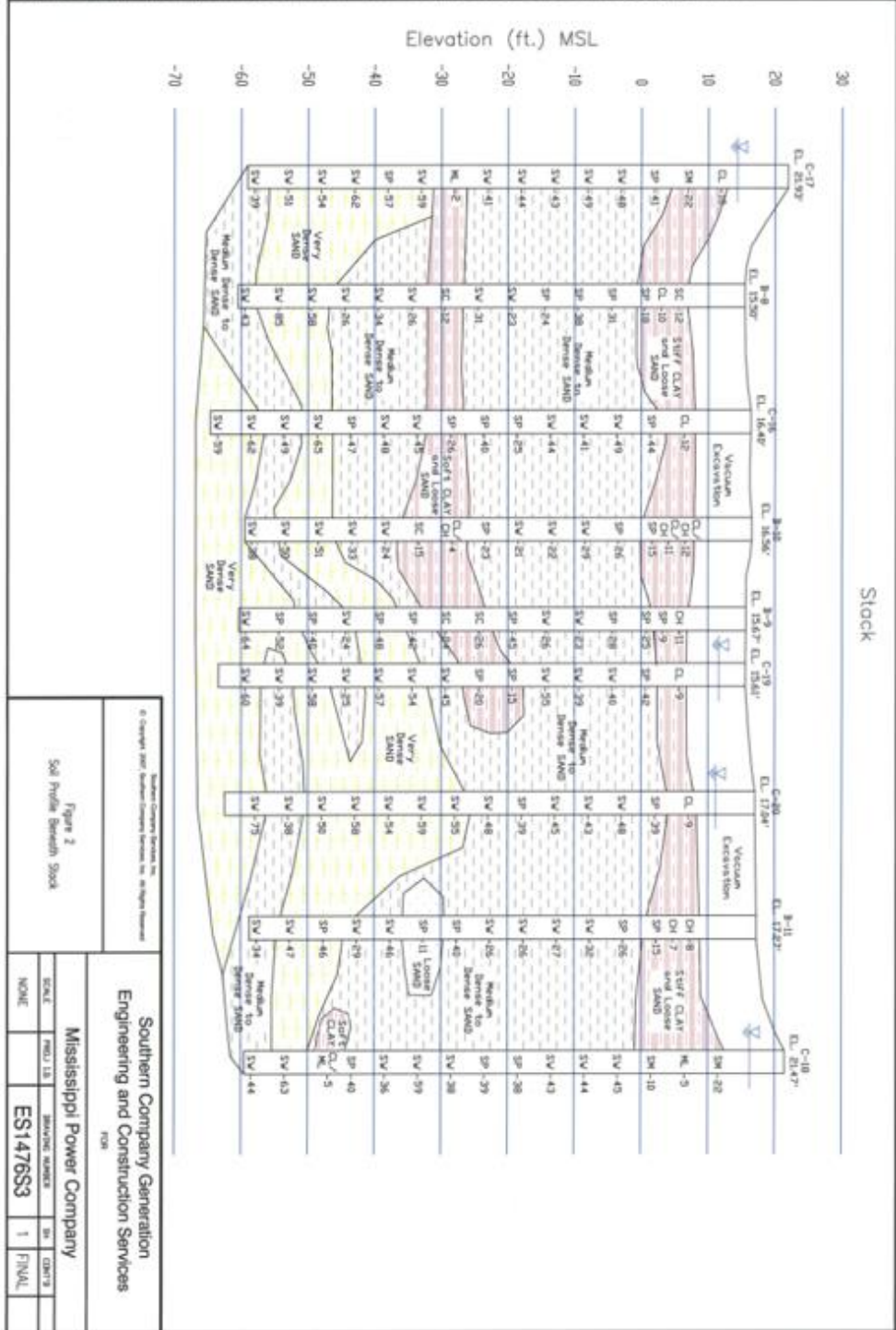


Figure A.19 Data set 19 soil information

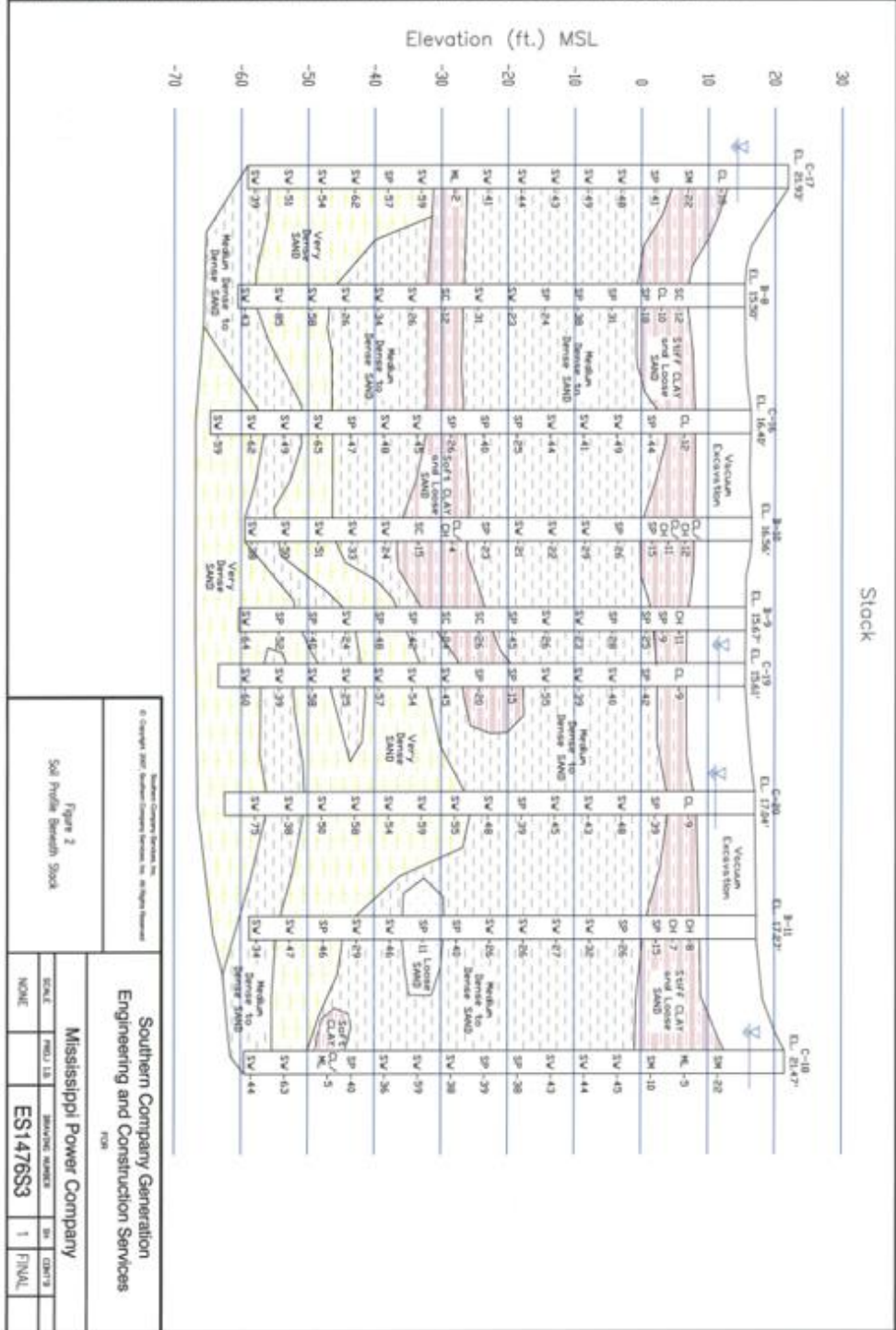
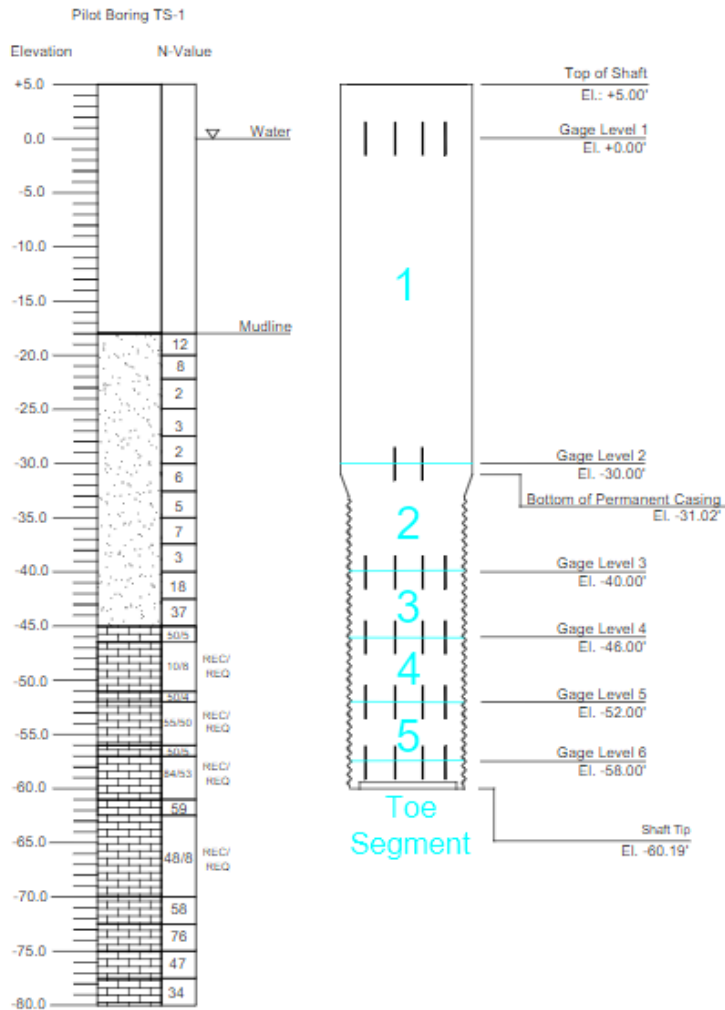


Figure A.20 Data set 20 soil information

TS-1 - As-Built



Applied Foundation Testing
2345 Success DR
Odessa, Florida 33556

Title: STATNAMIC TEST SHAFT - 1

Project Name: SR-80 SOUTHERN BLVD

AFT Project #: 118033

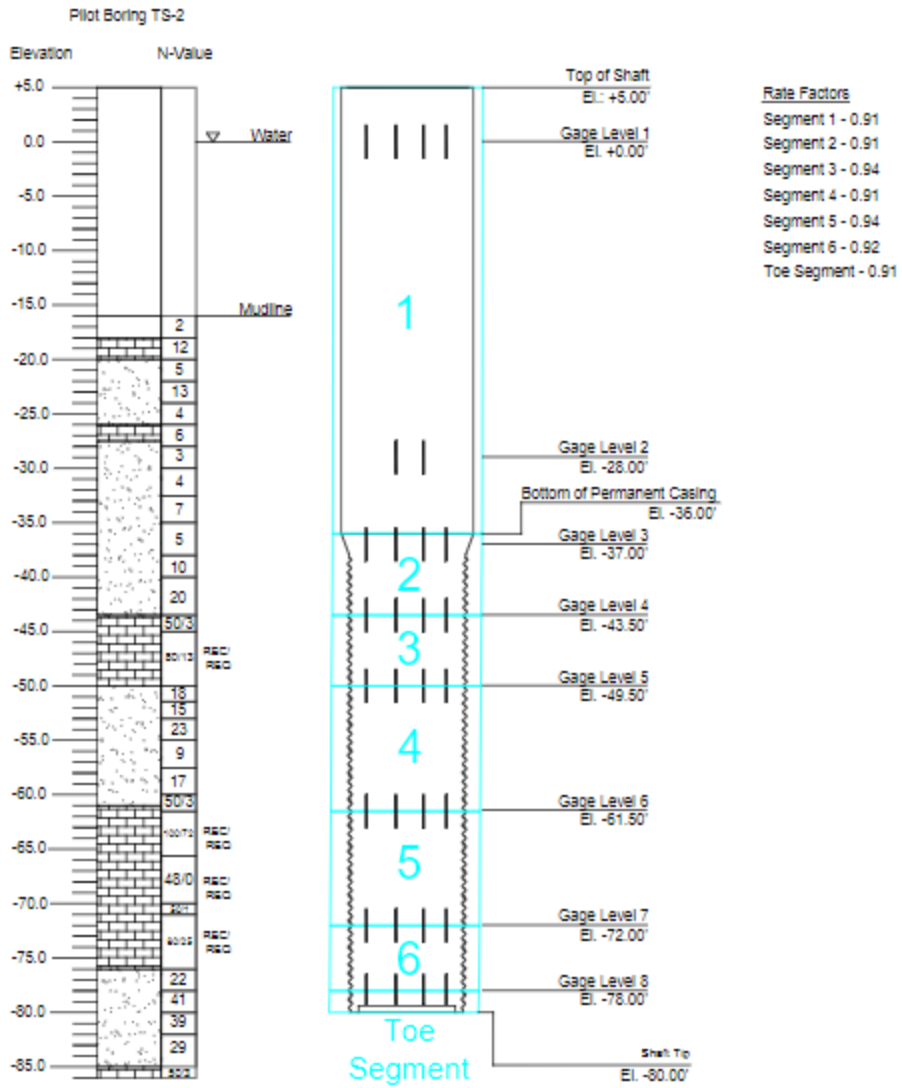
Author: WKC 11/06/18

Rev: JDN 11/14/18

Figure: 1

Figure A.21 Data set 21 soil information

TS-2 - As-Built



Applied Foundation Testing
2345 Success DR
Odessa, Florida 33556

Title: STATNAMIC TEST SHAFT - 2

Project Name: SR-80 SOUTHERN BLVD

AFT Project #: 118033

Author: JMT

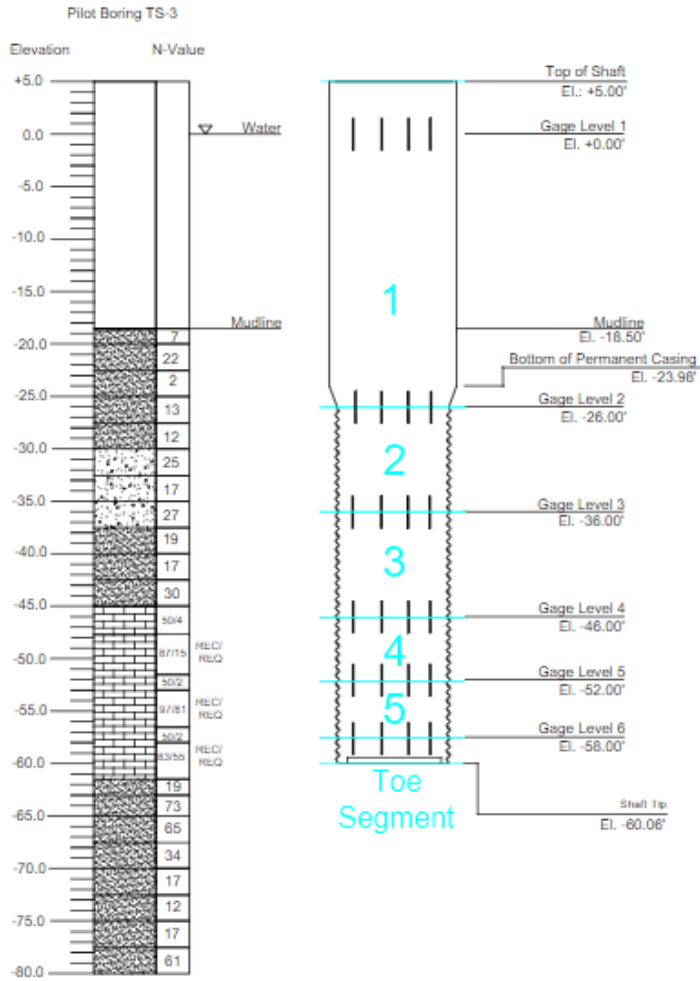
10/30/2018

Rev:

Figure: 1

Figure A.22 Data set 22 soil information

TS-3 - As-Built



Applied Foundation Testing
2345 Success DR
Odessa, Florida 33556

Title: STATNAMIC TEST SHAFT - 3

Project Name: SR-80 SOUTHERN BLVD

AFT Project #: 118033

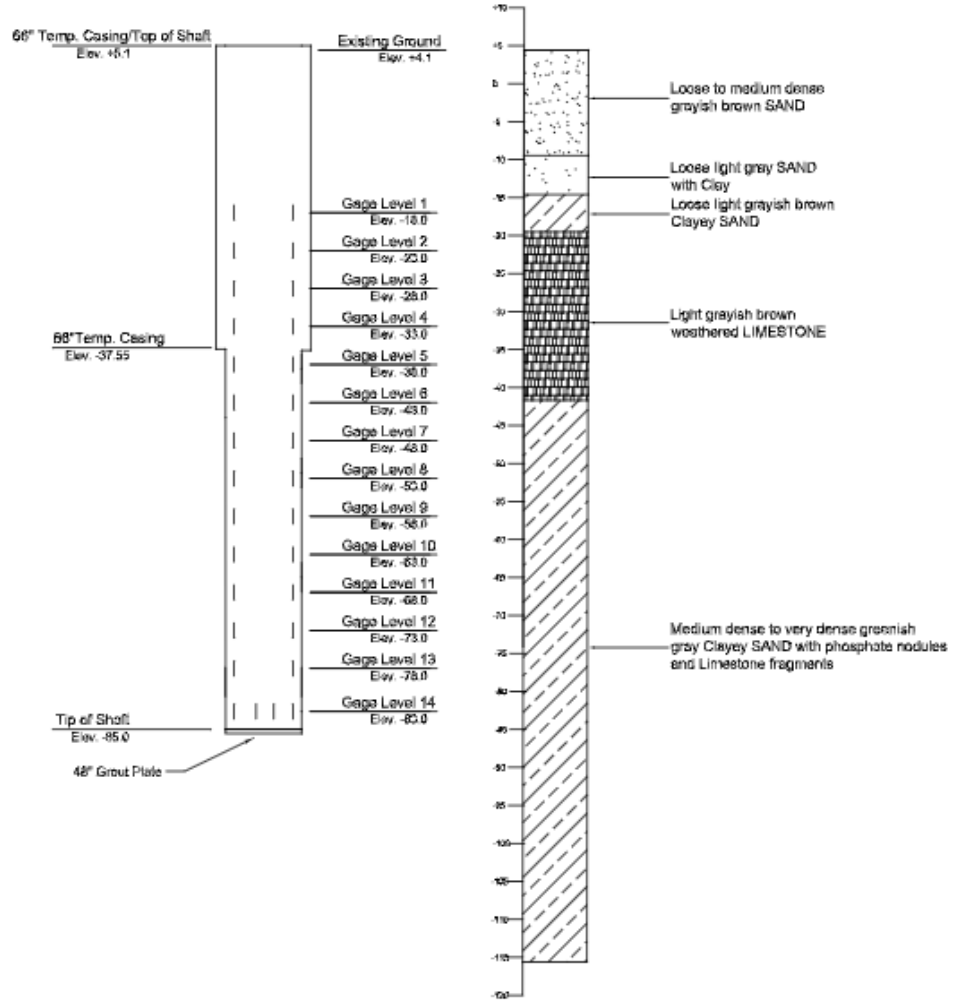
Author: WKC 11/08/18

Rev:

Figure: 1

Figure A.23 Data set 23 soil information

60" Test Pile 1 Schematic




	Applied Foundation Testing, Inc.	Client:	Archer Western	Project:	Overland Bridge	Drawn by:	JAE
---	----------------------------------	---------	----------------	----------	-----------------	-----------	-----

Figure A.24 Data set 24 soil information

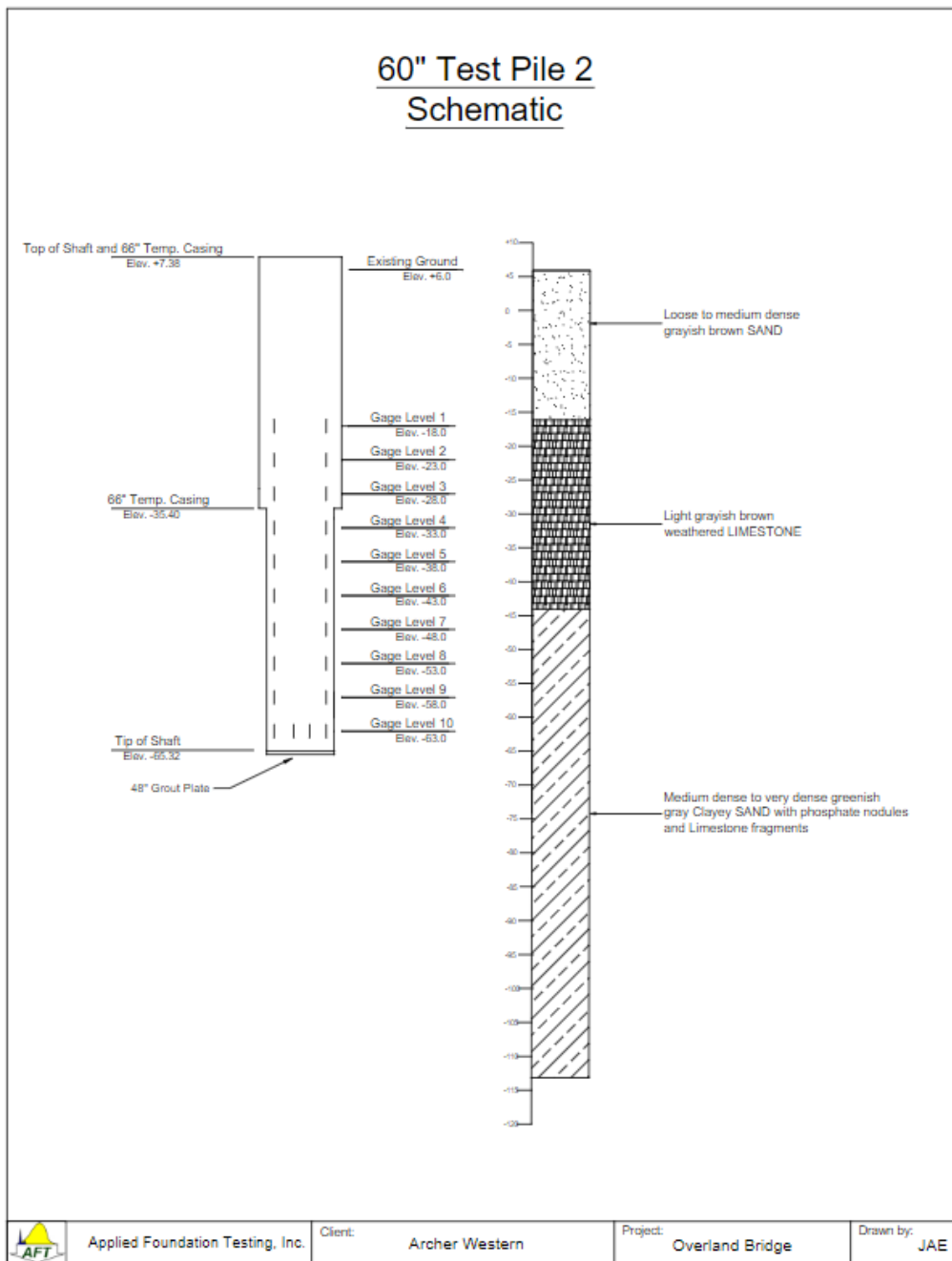
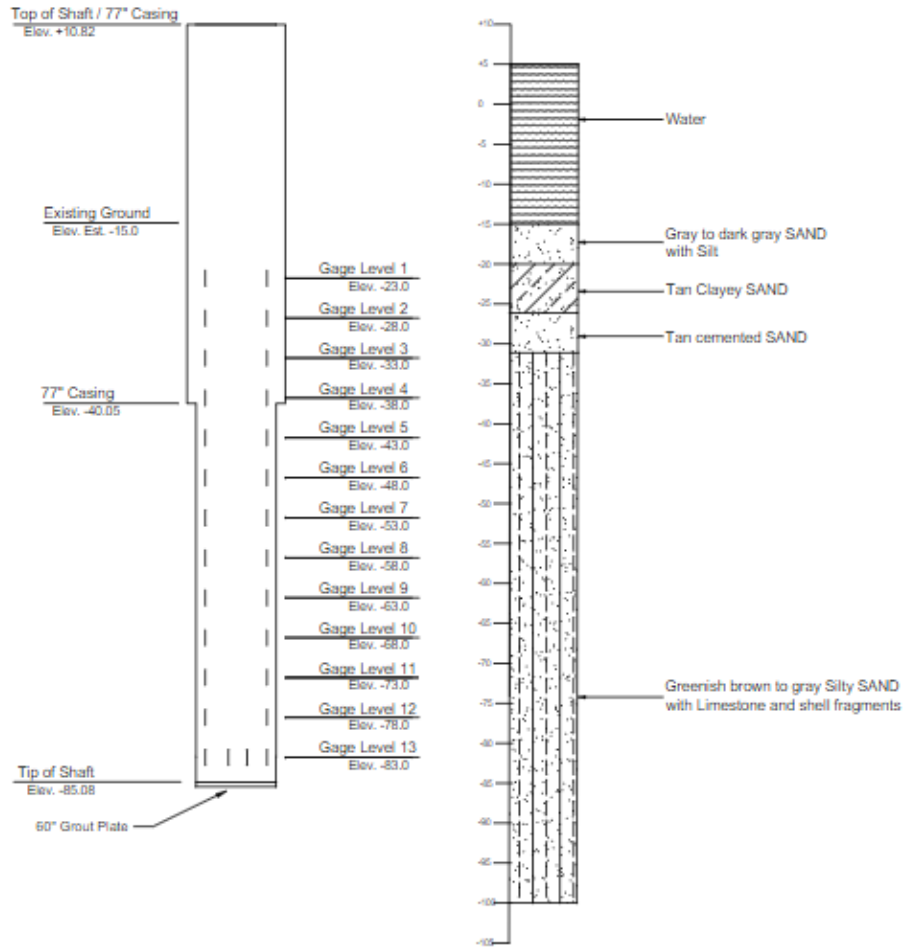


Figure A.25 Data set 25 soil information

72" Test Pile 3 Schematic



Applied Foundation Testing, Inc.

Client:

Archer Western

Project:

Overland Bridge

Drawn by:

JAE

Figure A.26 Data set 26 soil information

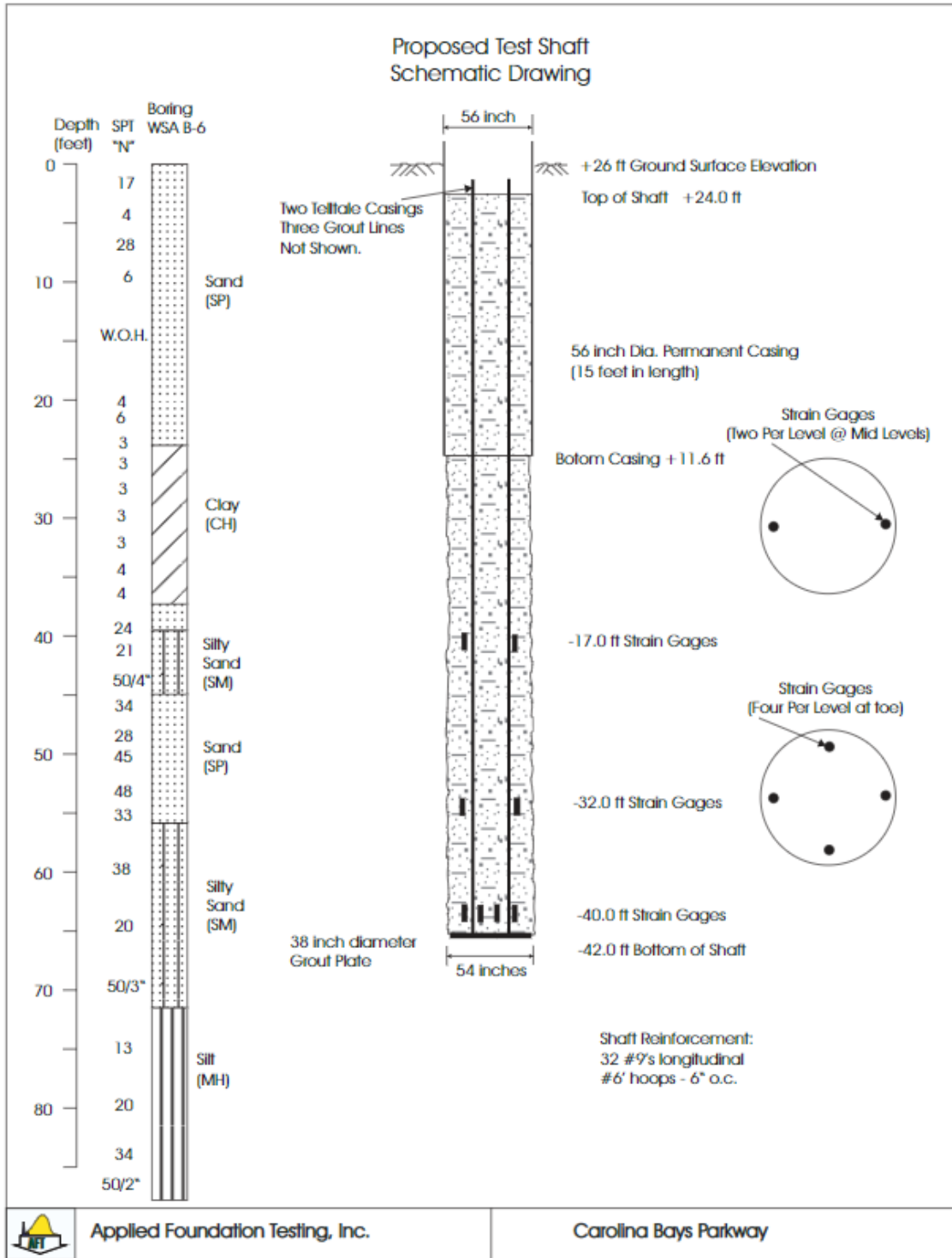


Figure A.27 Data set 27 Soil information

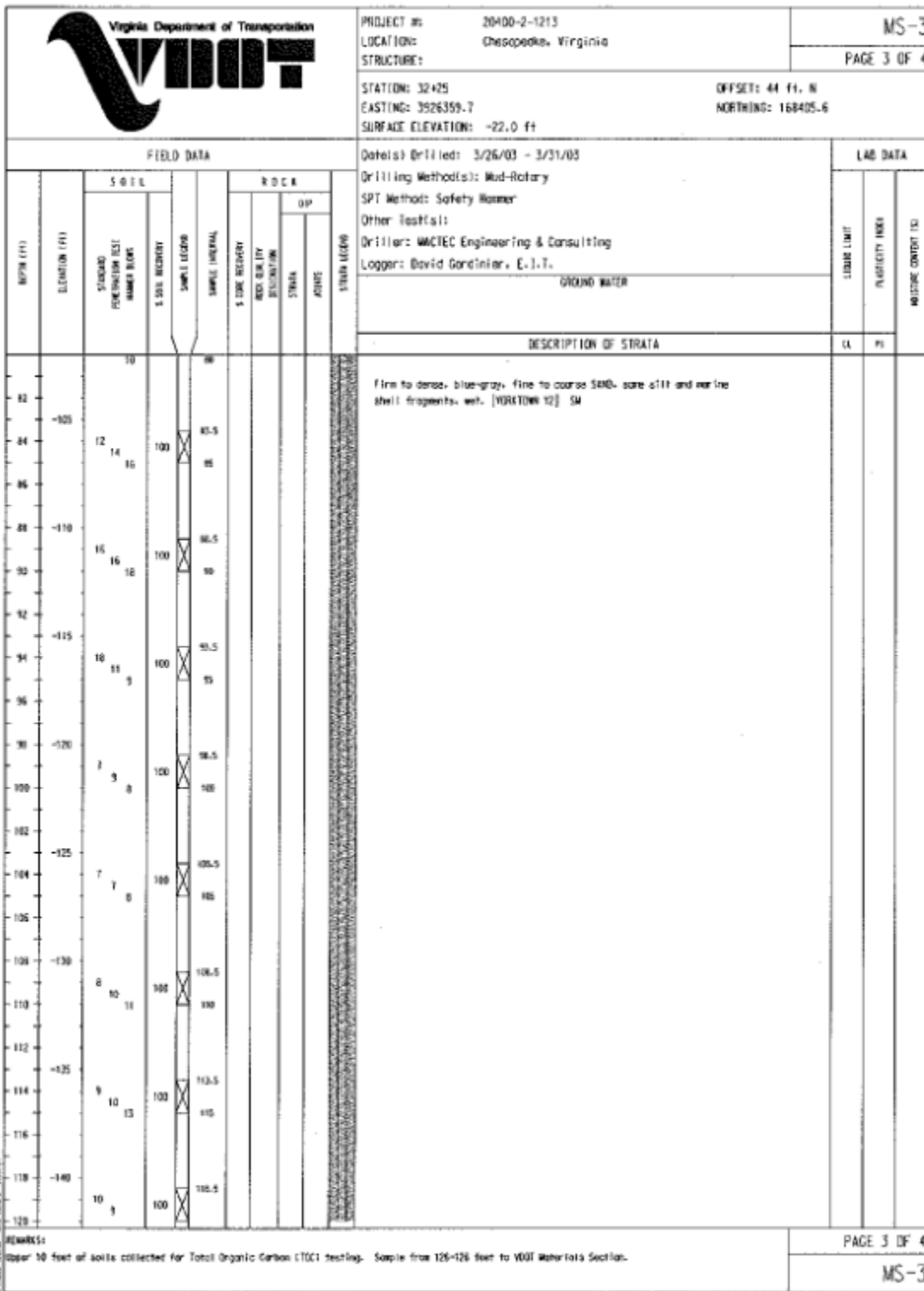


Figure A.28c Data set 28 soil information

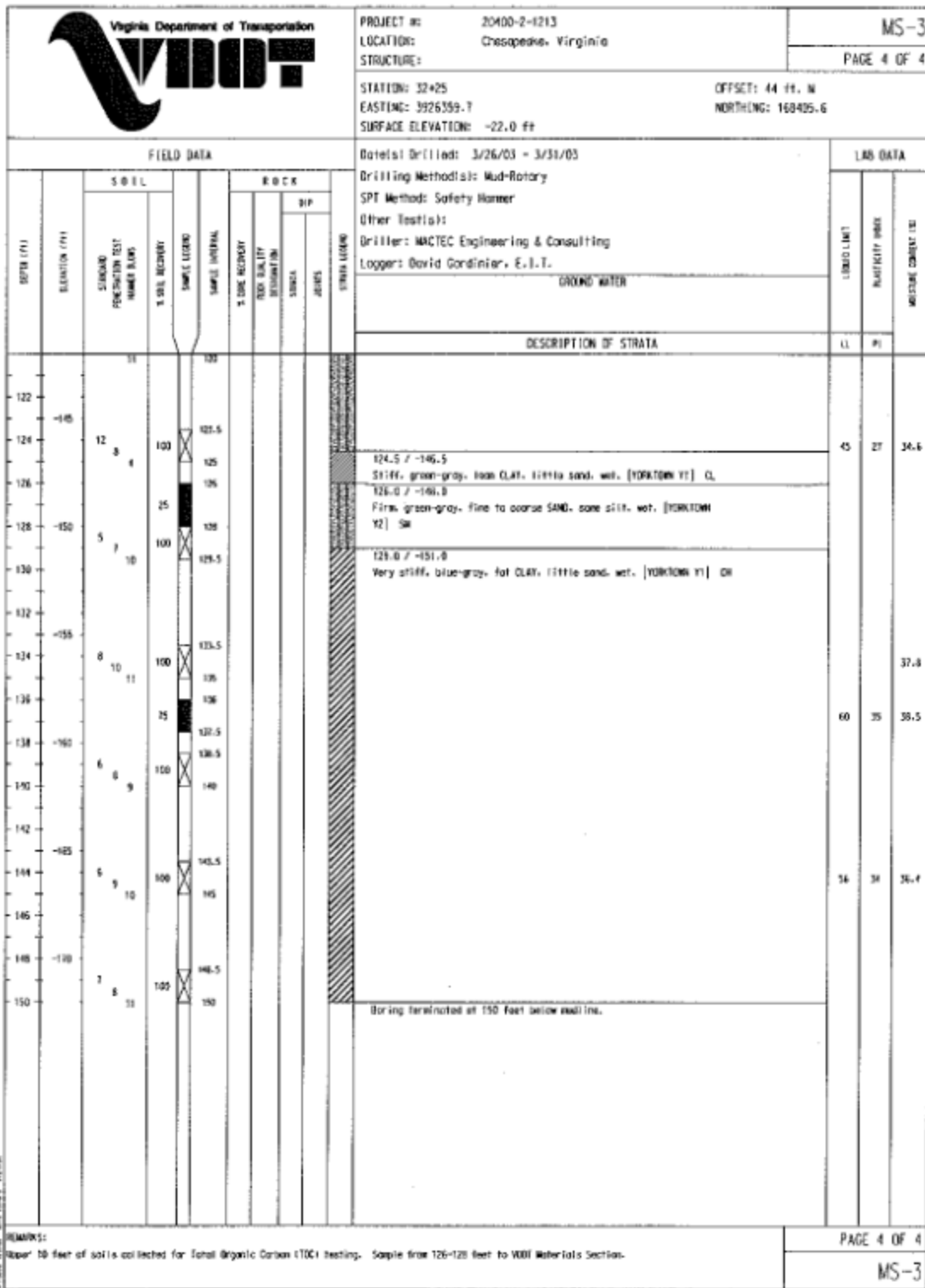


Figure A.28d Data set 28 soil information

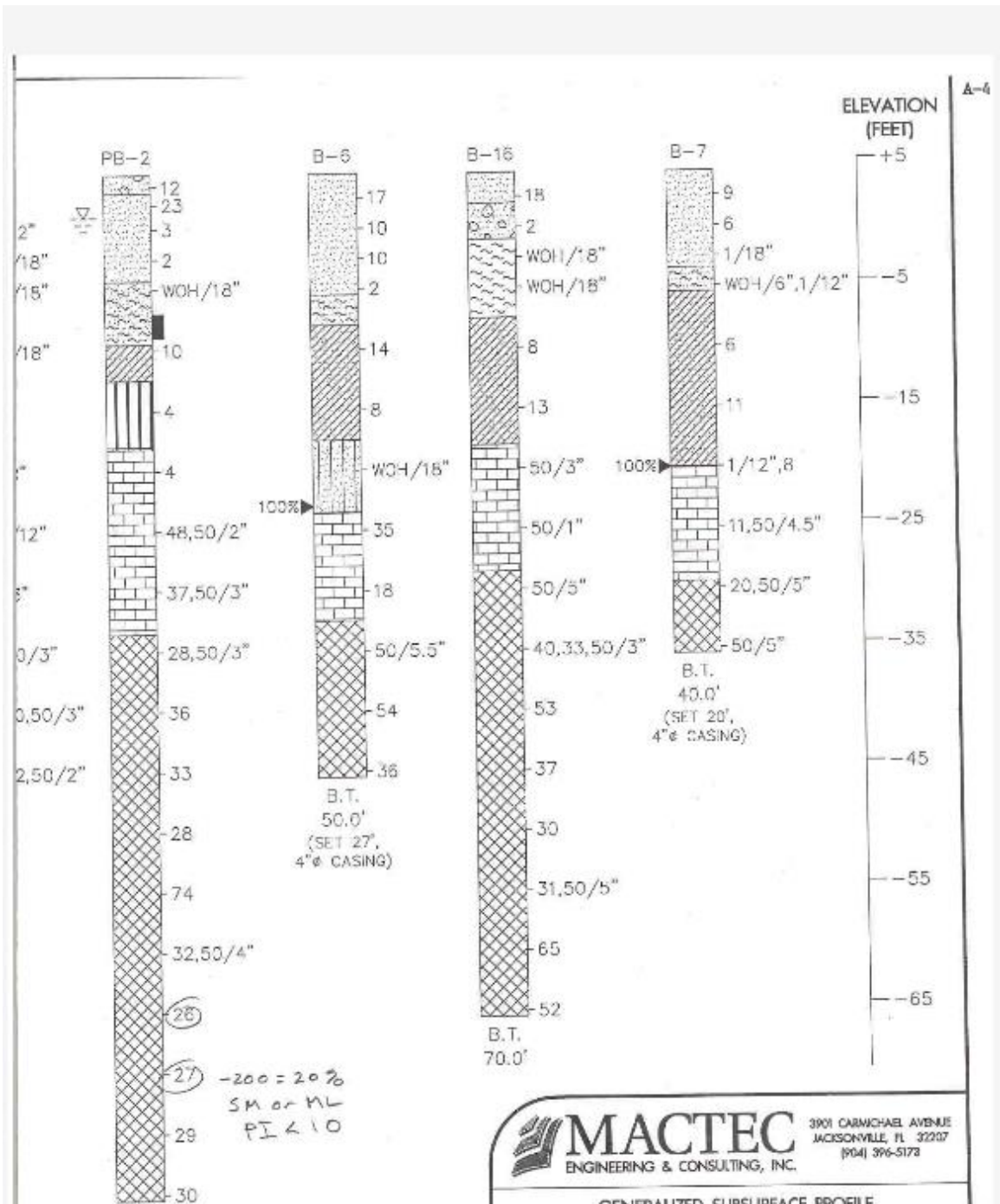


Figure A.29b Data set 29 soil information

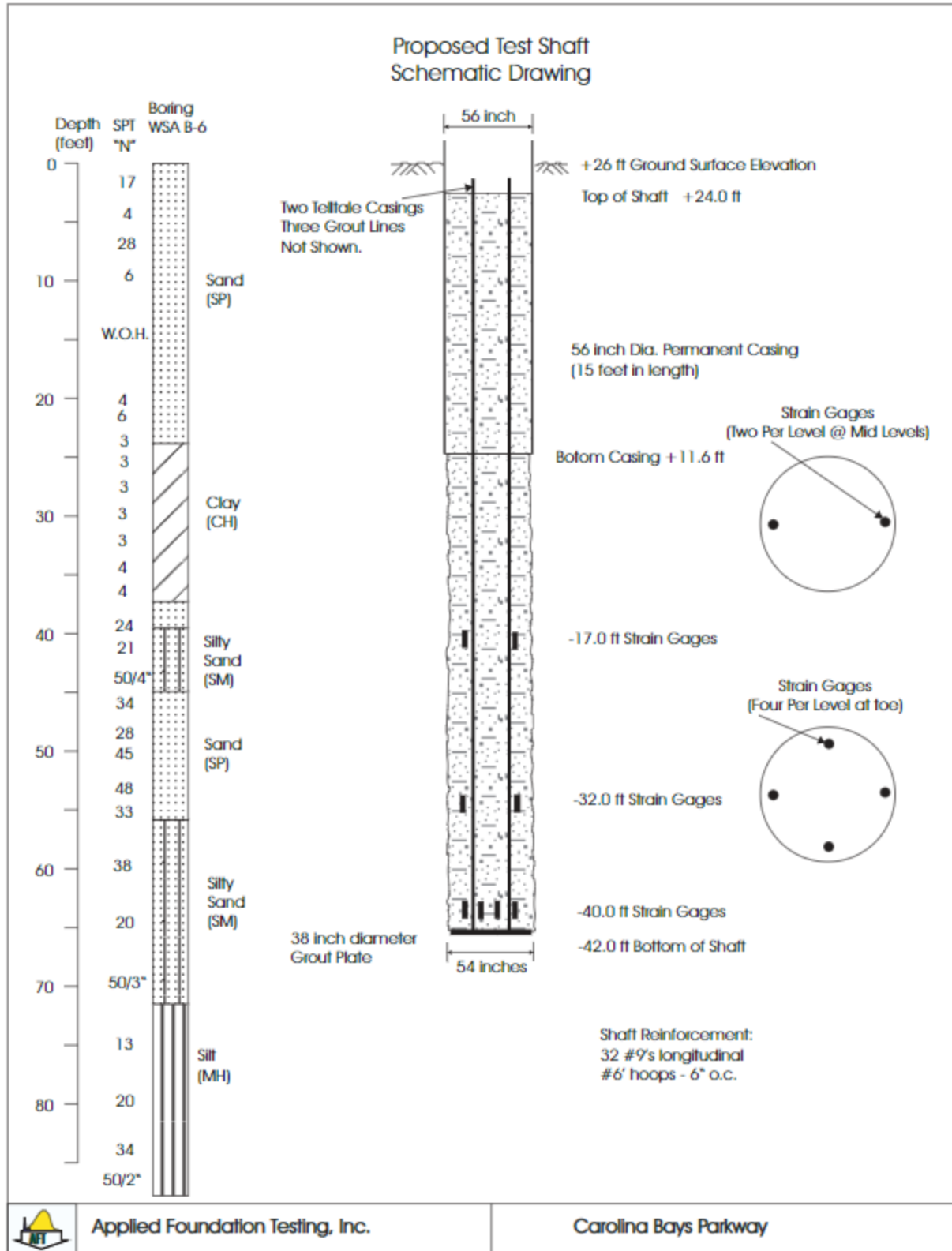


Figure A.30 Data set 30 soil information

APPENDIX B – LOAD TEST RESULTS

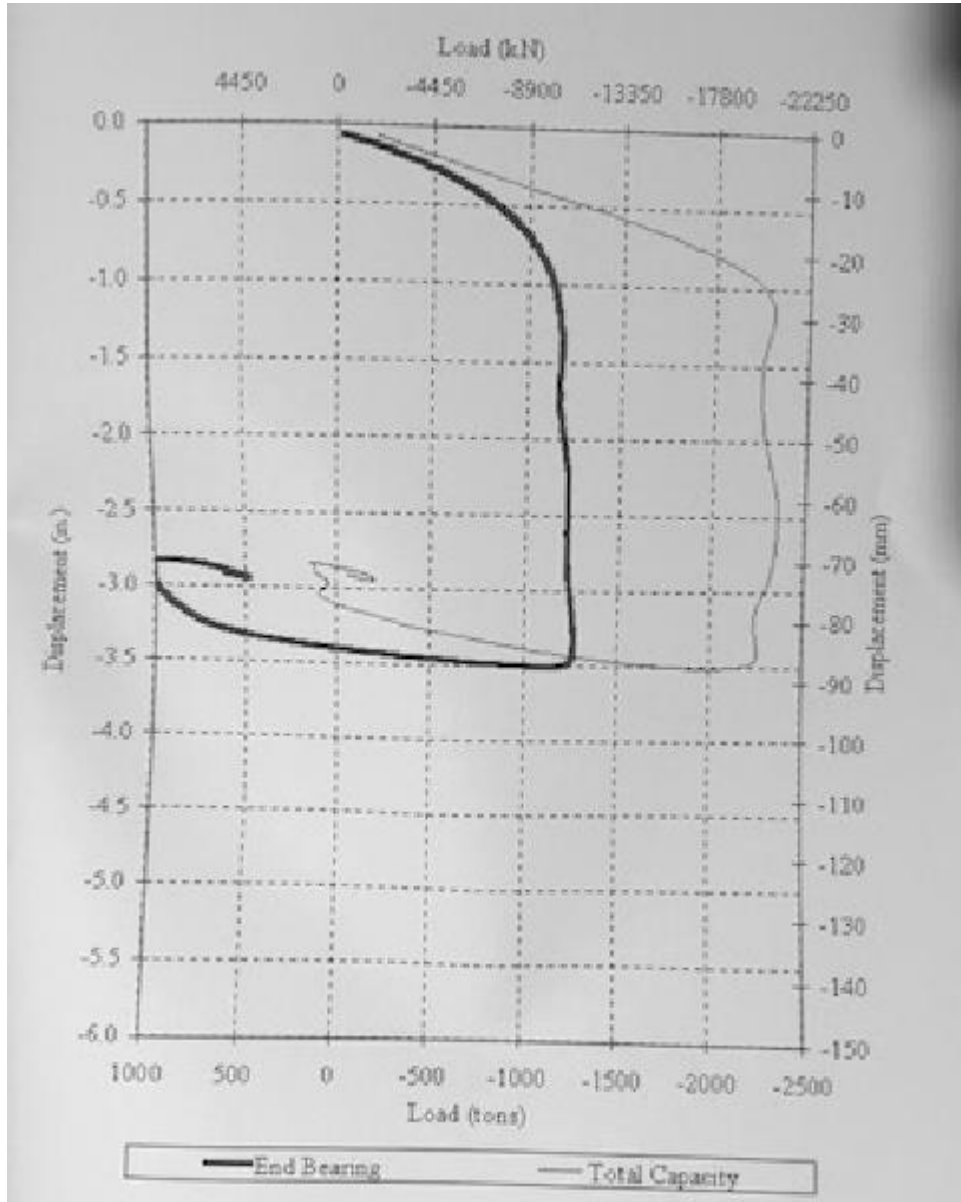


Figure B.1 Data set 1 load test results

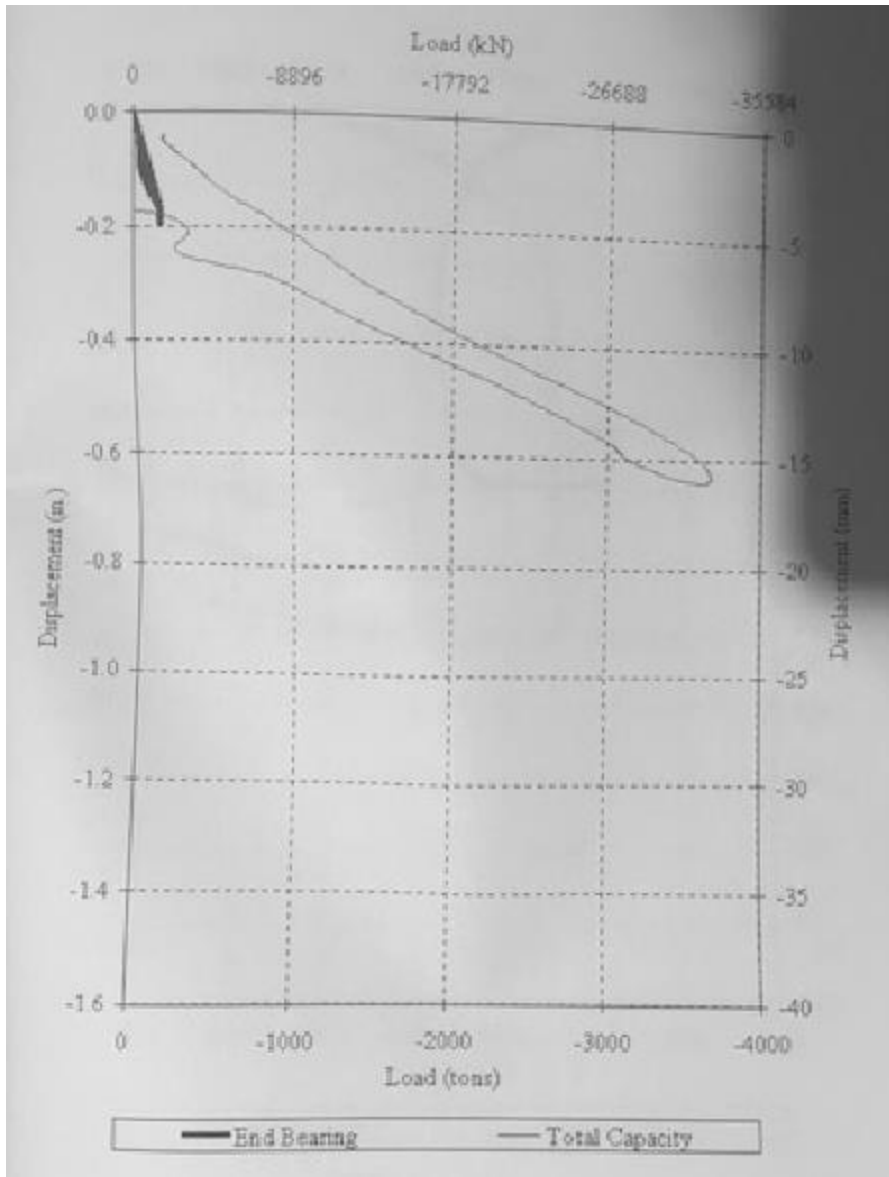


Figure B.2 Data set 2 load test results

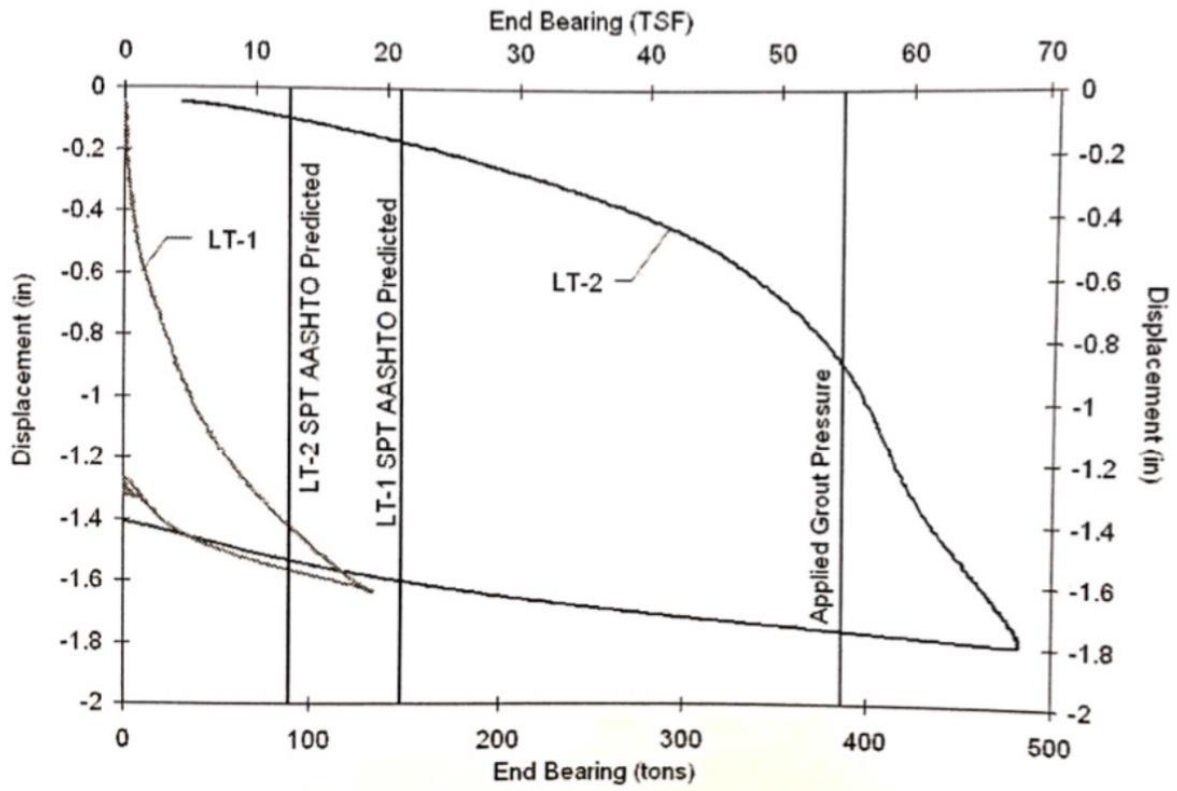


Figure B.3 Data set 3 load test results



Osterberg Cell Load vs. Displacement Plots

Broadway Viaduct - Council Bluffs, IA - TS 4

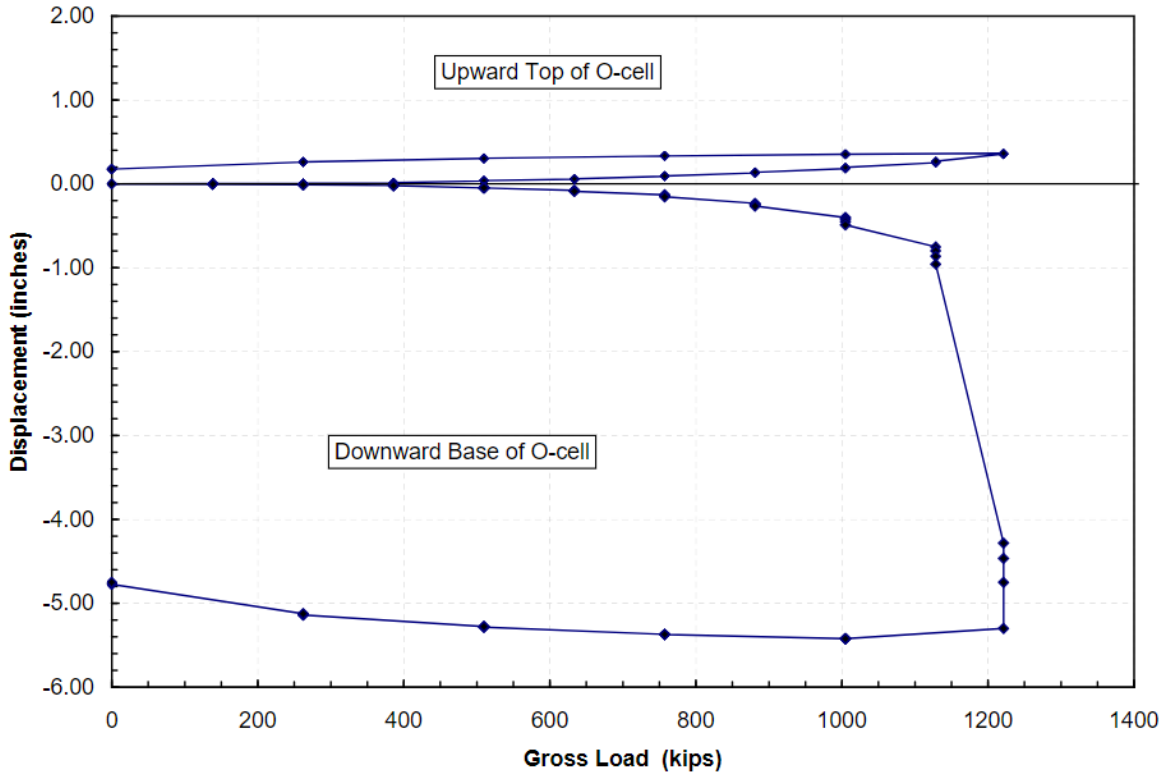


Figure B.4 Data set 4 load test results



Osterberg Cell Load-Displacement

TS-2B - Gerald Desmond Bridge - Long Beach, CA

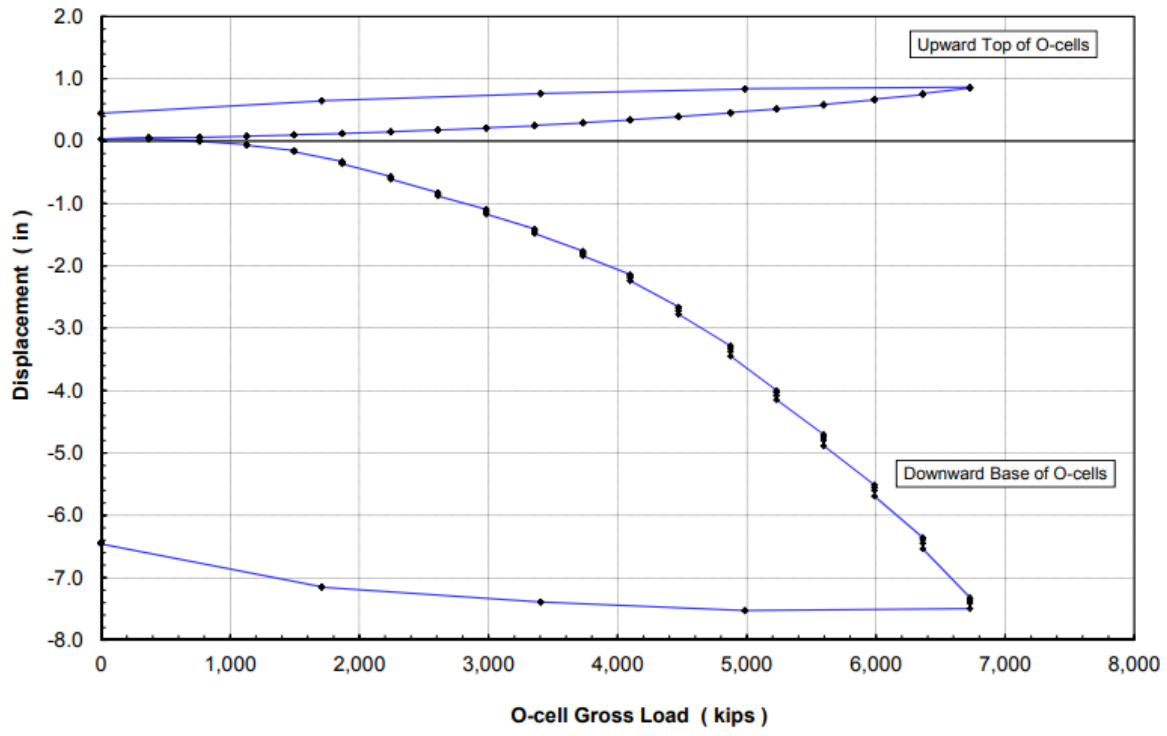


Figure B.5 Data set 5 load test results



Osterberg Cell Load-Displacement

TS-3C - Gerald Desmond Bridge - Long Beach, CA

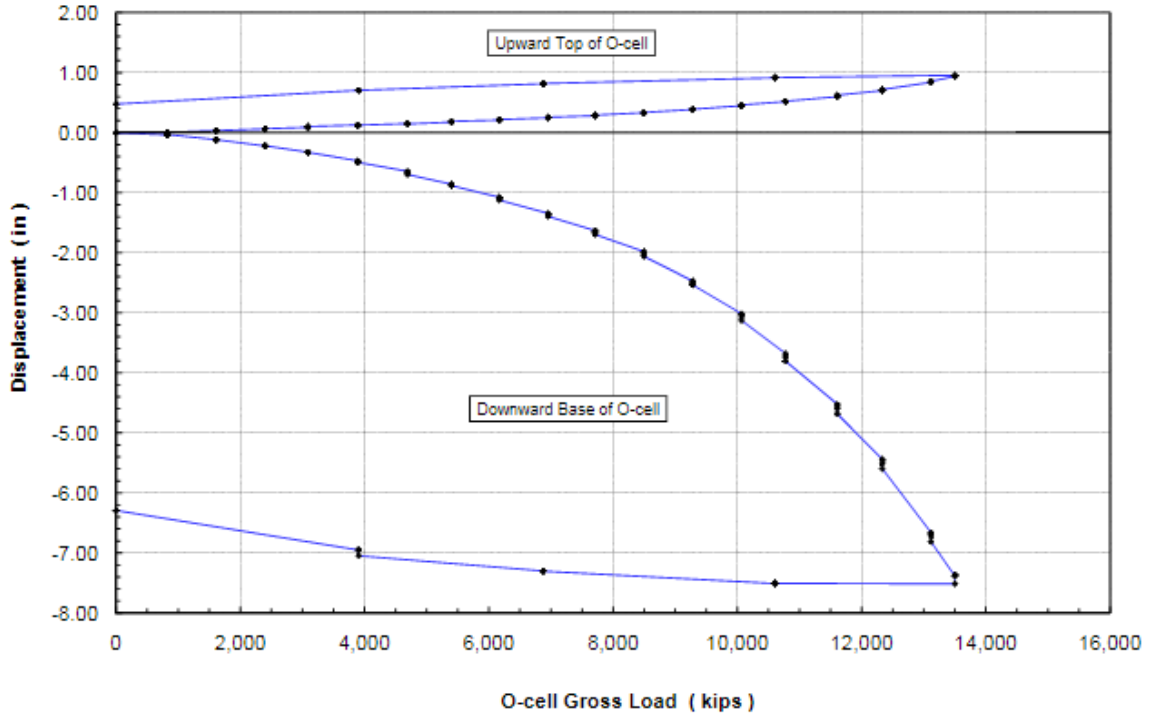


Figure B.6 Data set 6 load test results

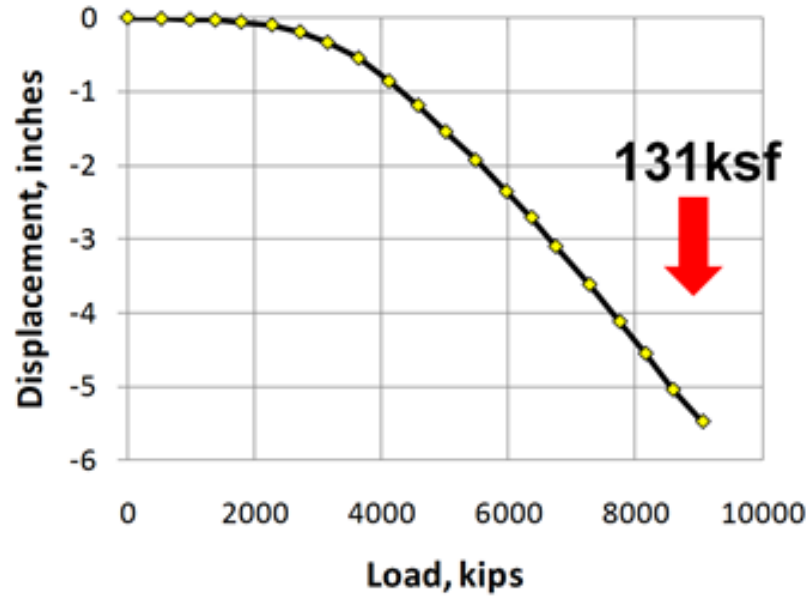


Figure B.7 Data set 7 load test results

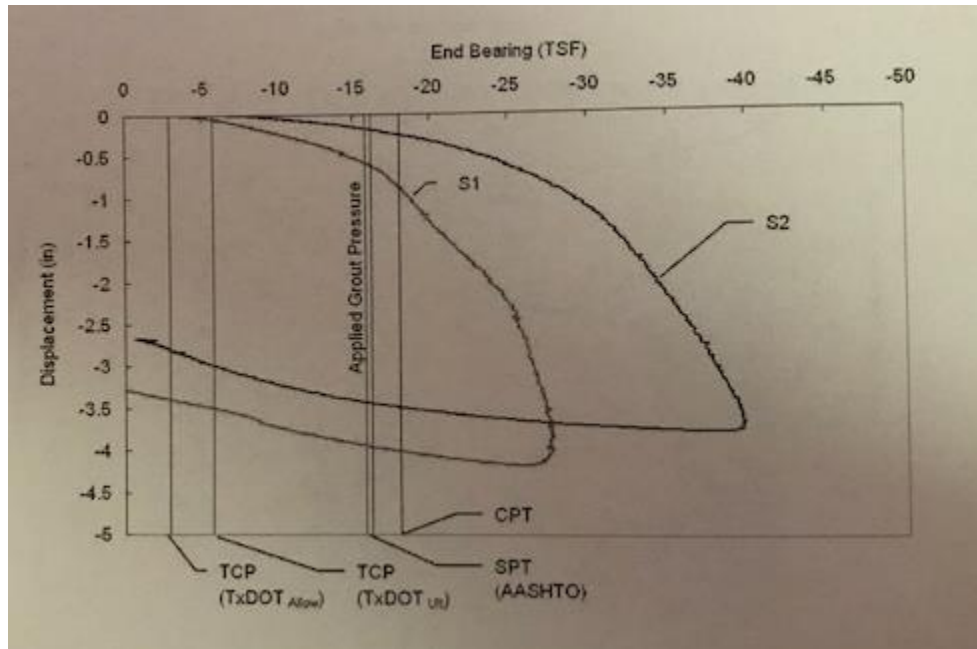


Figure B.8 Data set 8 load test results

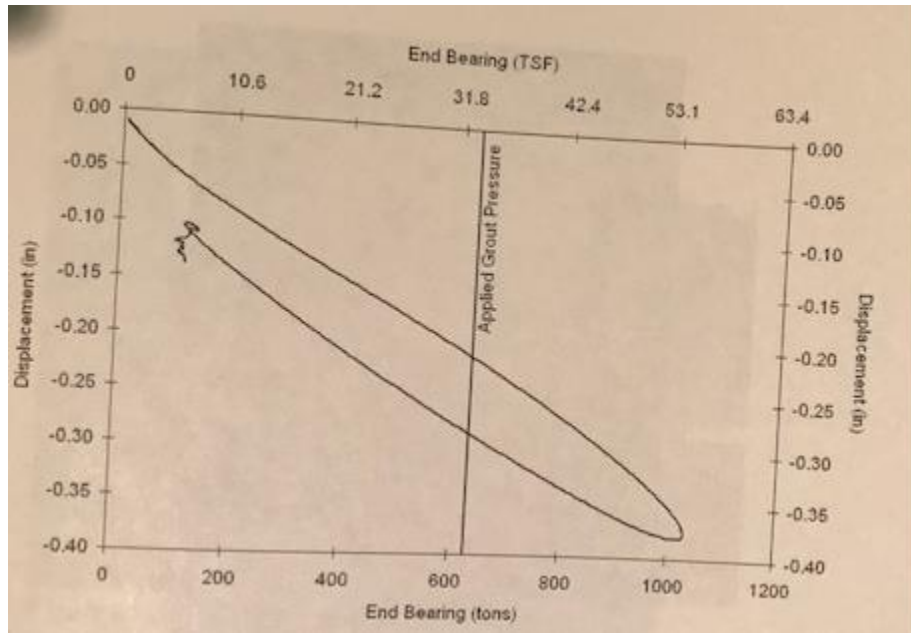


Figure B.9 Data set 9 load test results

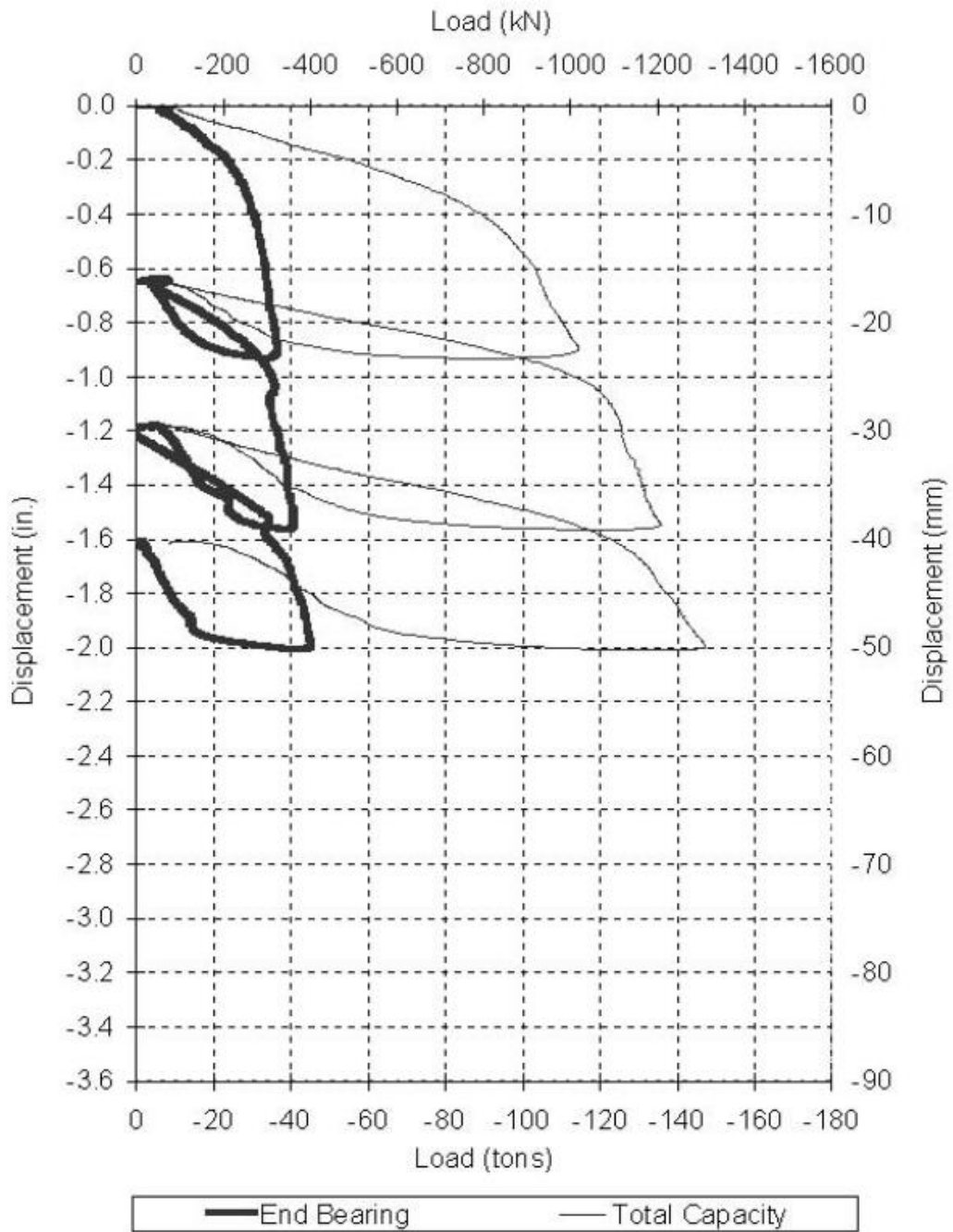


Figure B.10 Data set 10 load test results

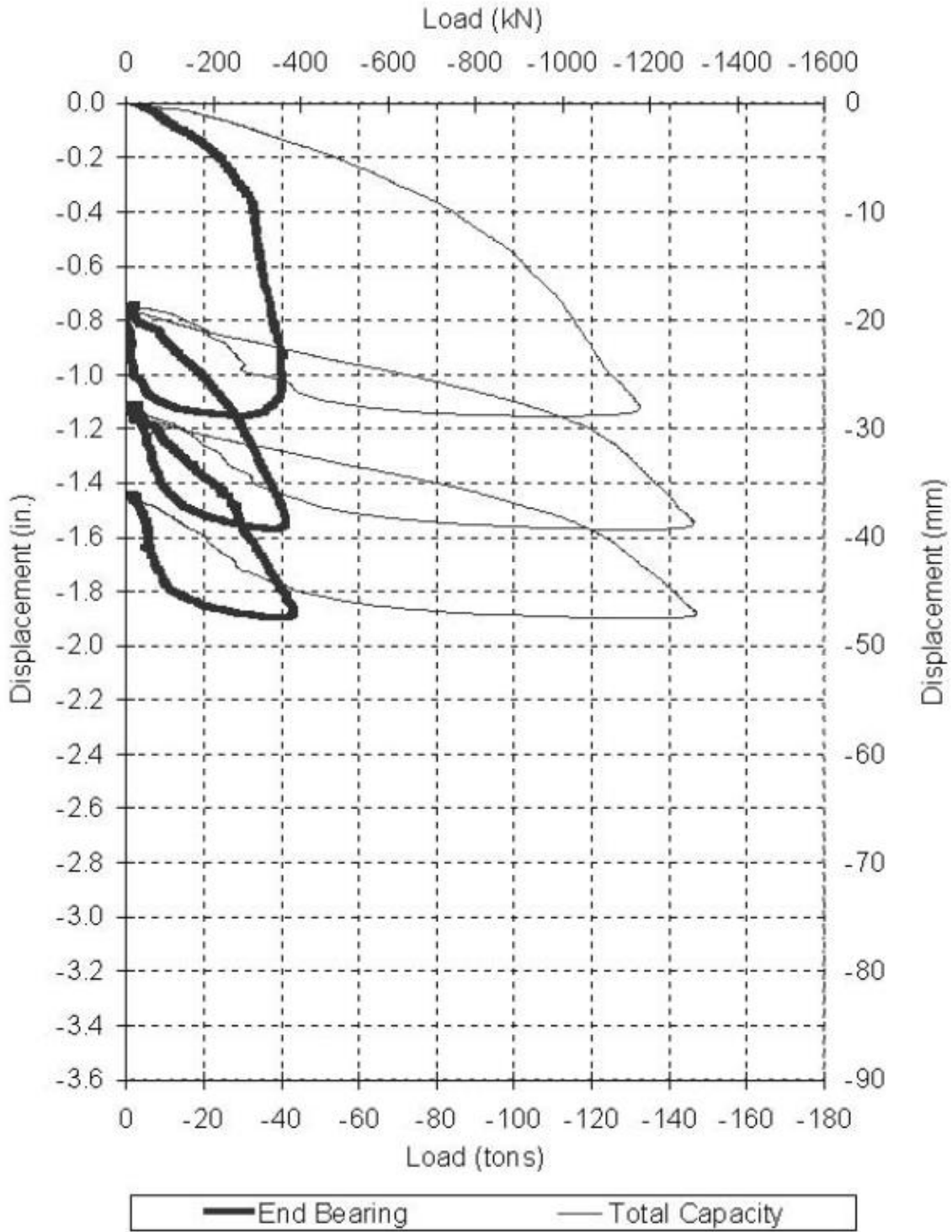


Figure B.11 Data set 11 load test results

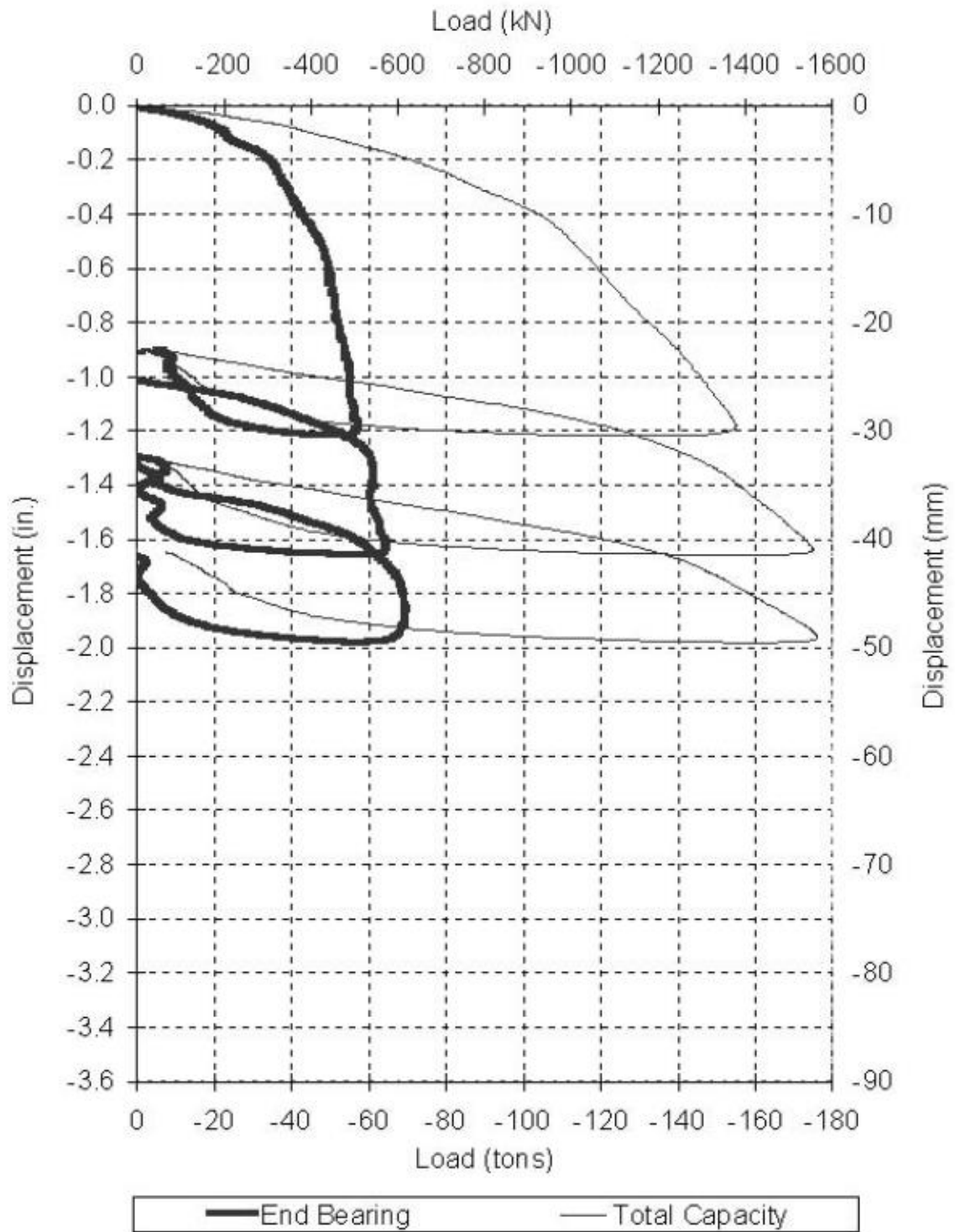


Figure B.12 Data set 12 load test results

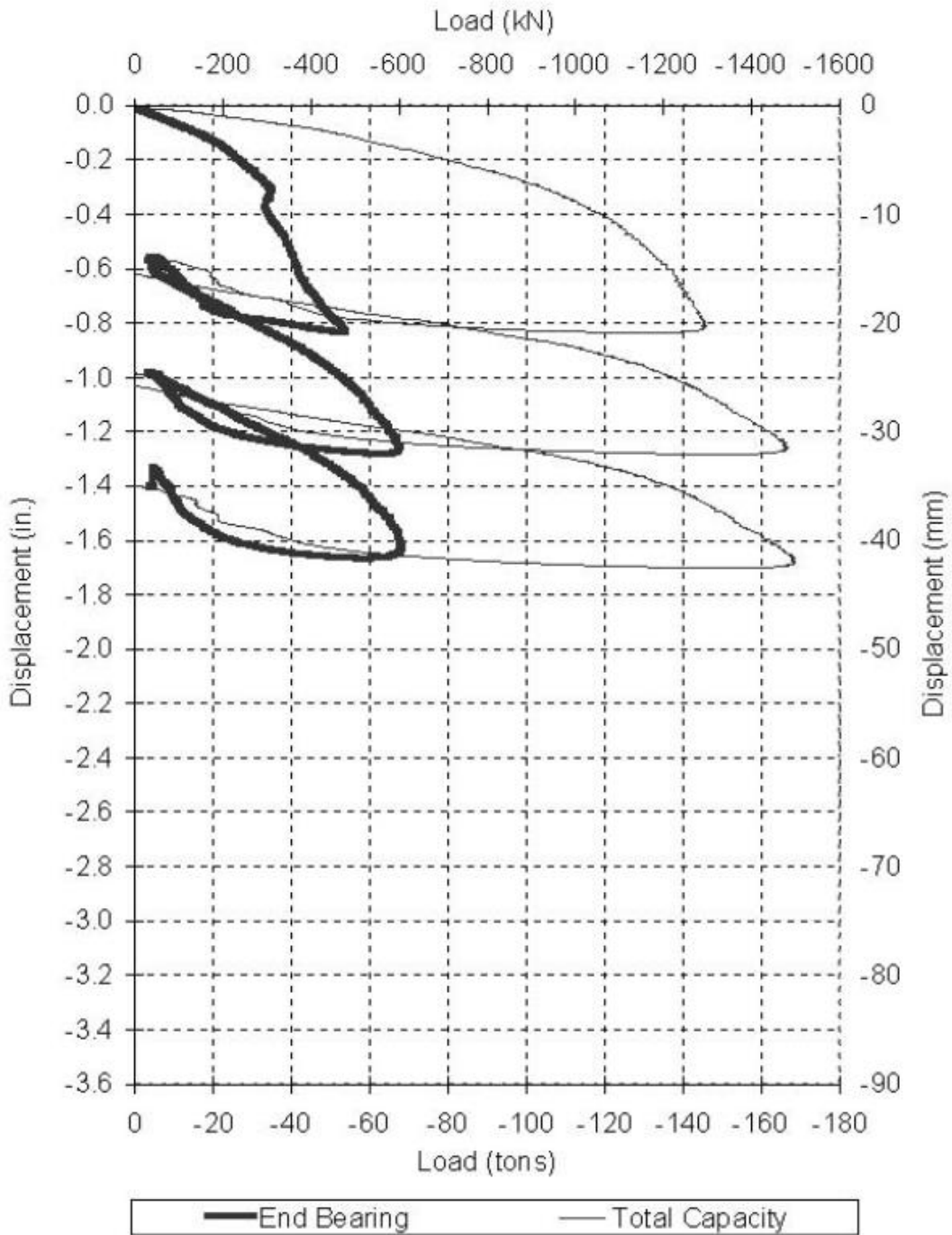
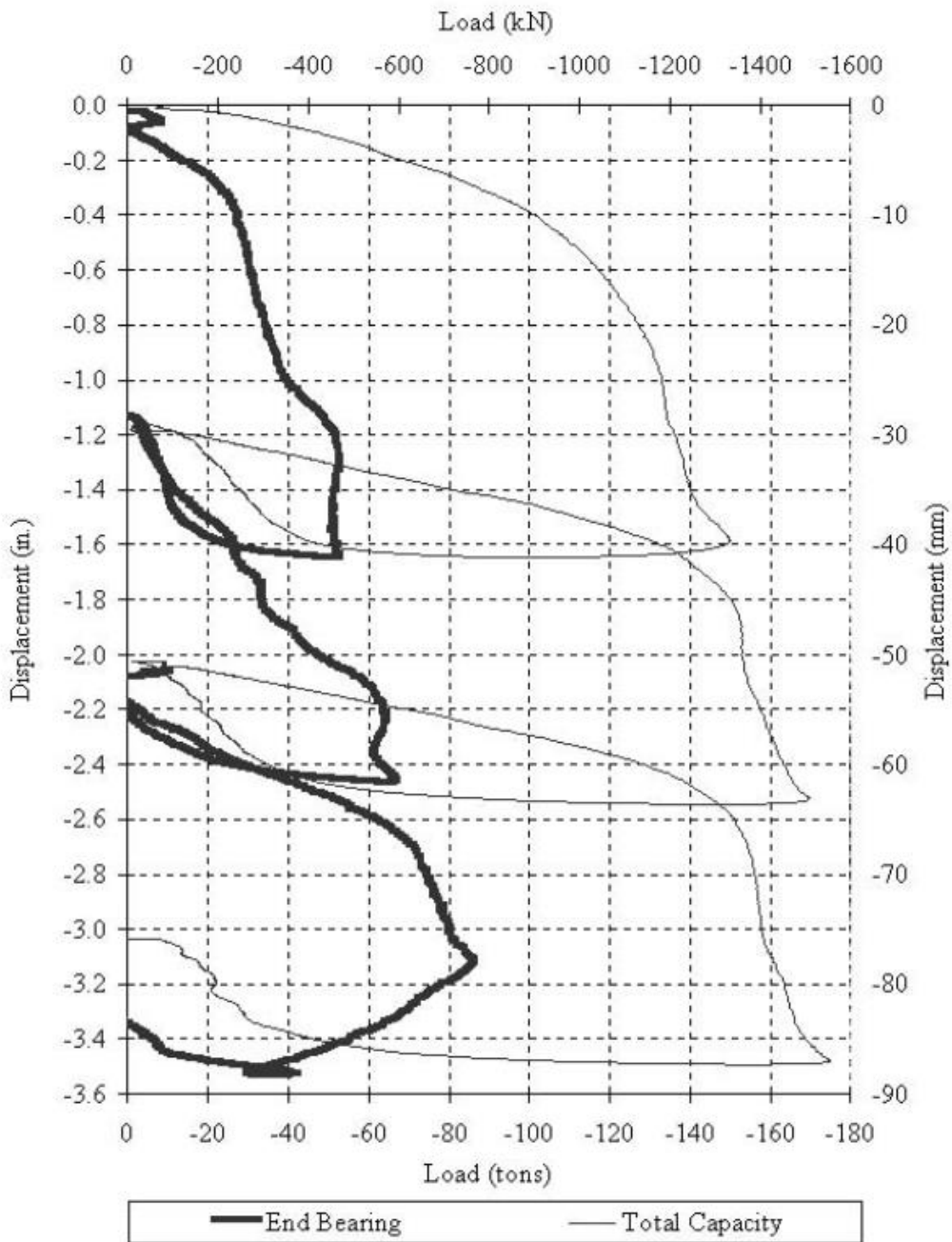


Figure B.13 Data set 13 load test results



FigureB.14 Data set 14 load test results

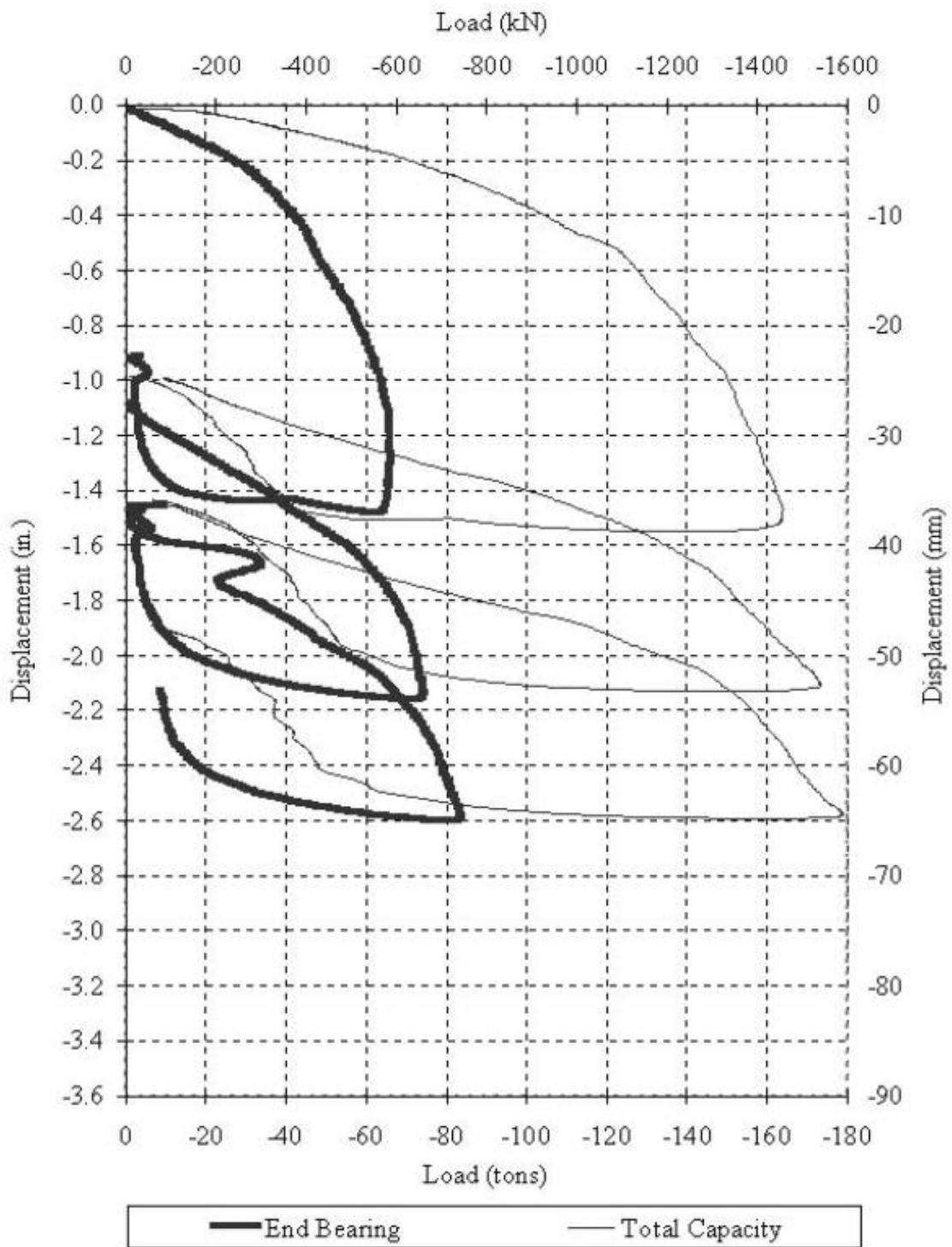
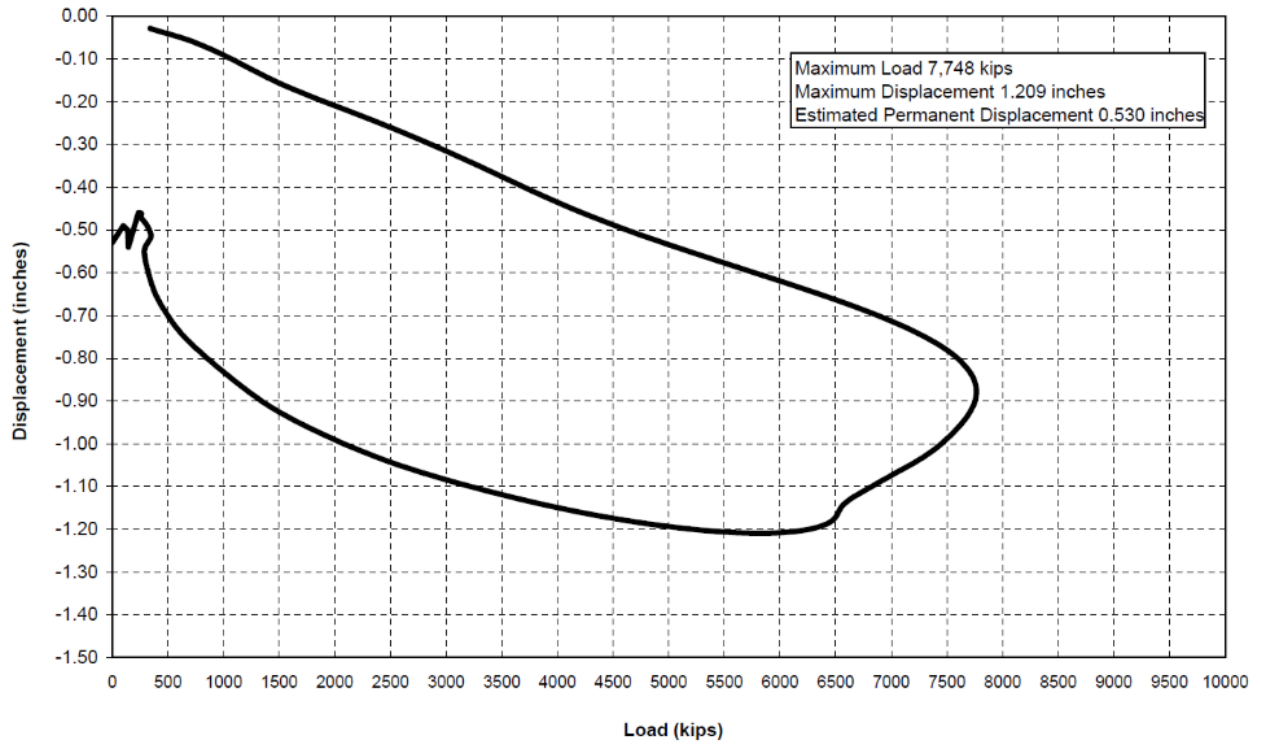


Figure B.15 Data set 15 load test results

Load vs. Displacement from Statnamic Test
Segmental Unloading Point (SUP) w/REF
TS-2, Flagler Memorial Bridge, Palm Beach Co., Florida



FigureB.16 Data set 16 load test results

Top and Toe Load vs. Shaft Top Displacement from Statnamic Test
West Palm Beach International Airport, Terminal C

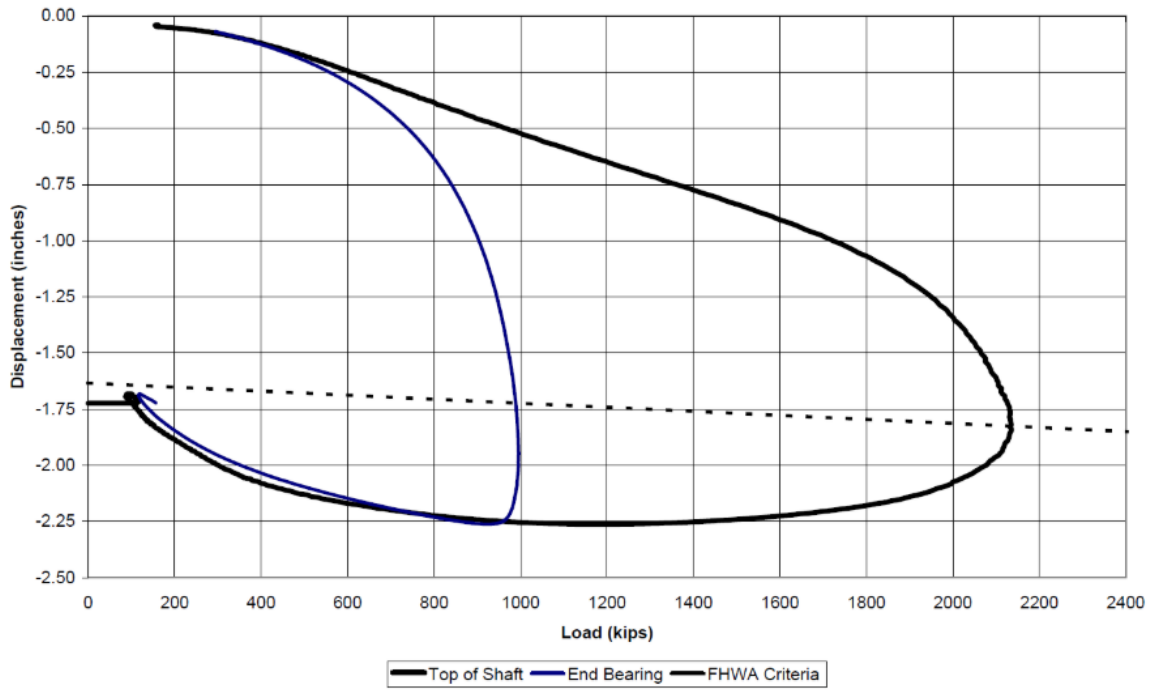


Figure B.17 Data set 17 load test results

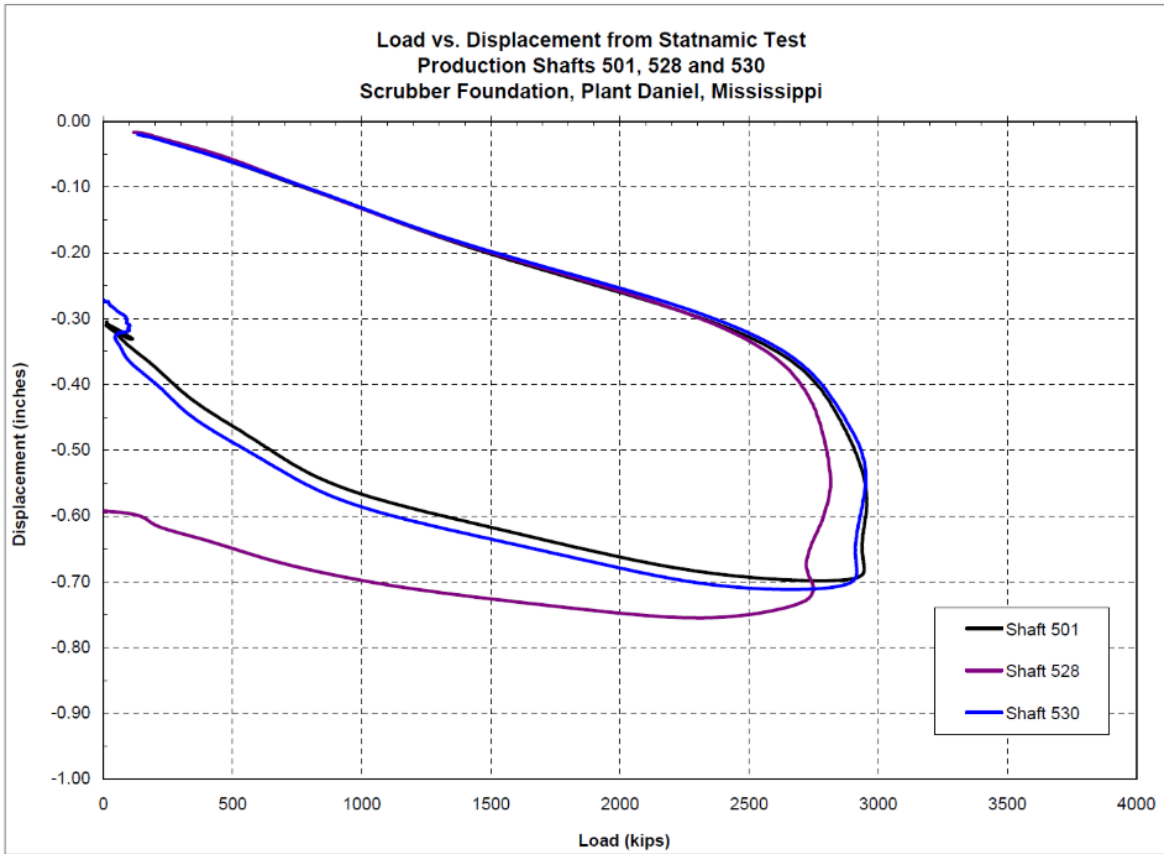


Figure B.18 Data set 18 load test results

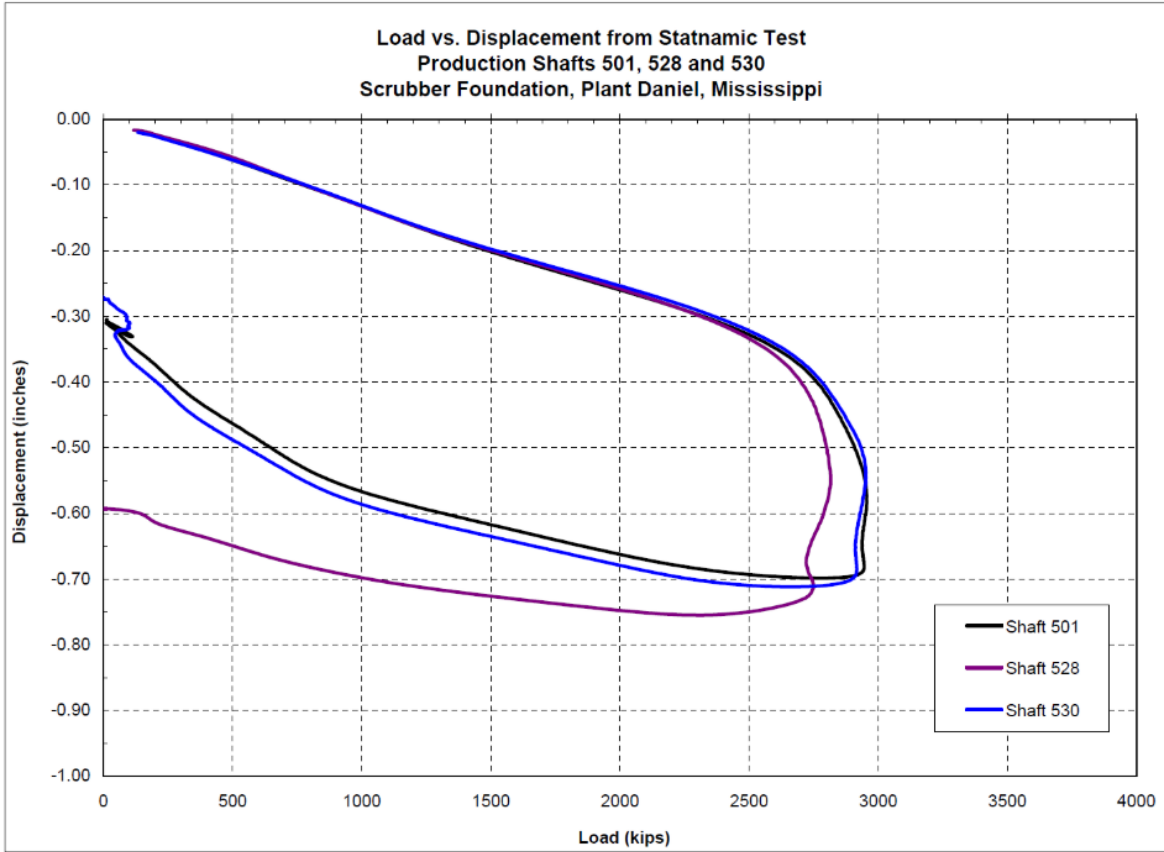


Figure B.19 Data set 19 load test results

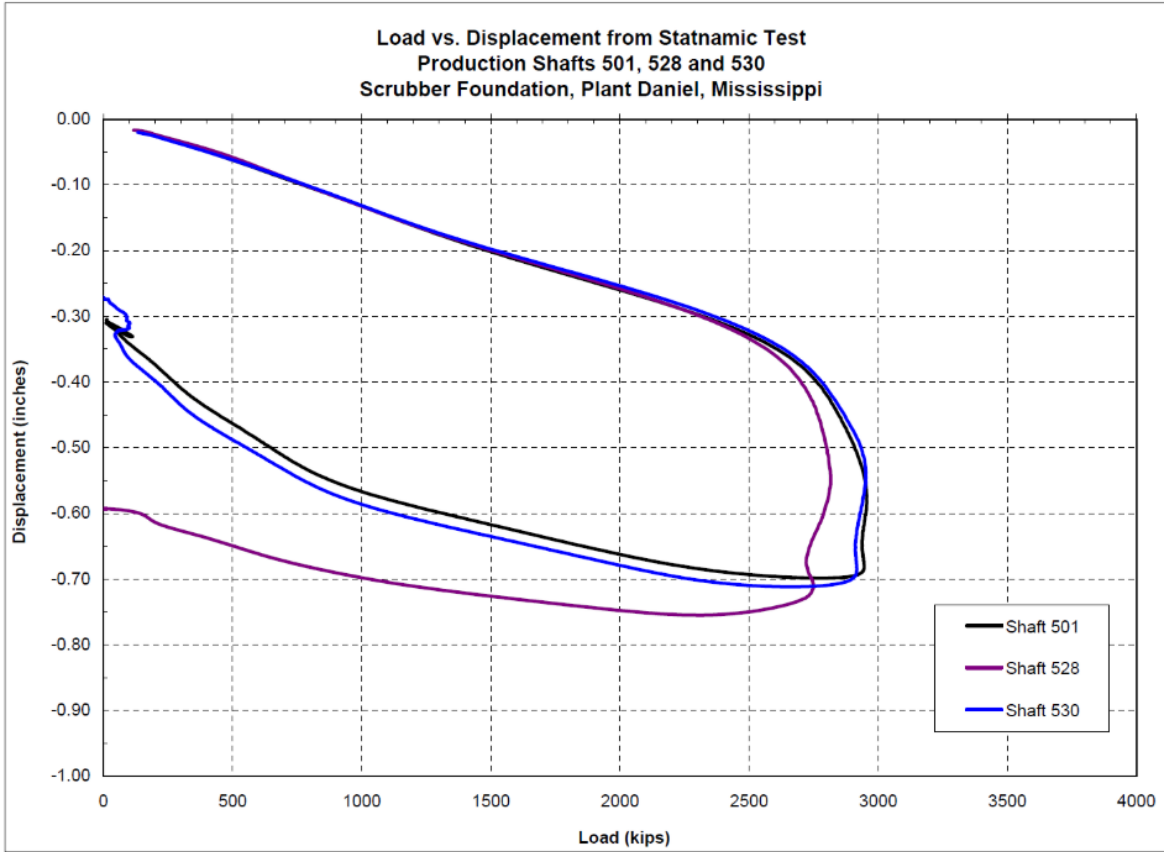


Figure B.20 Data set 20 load test results

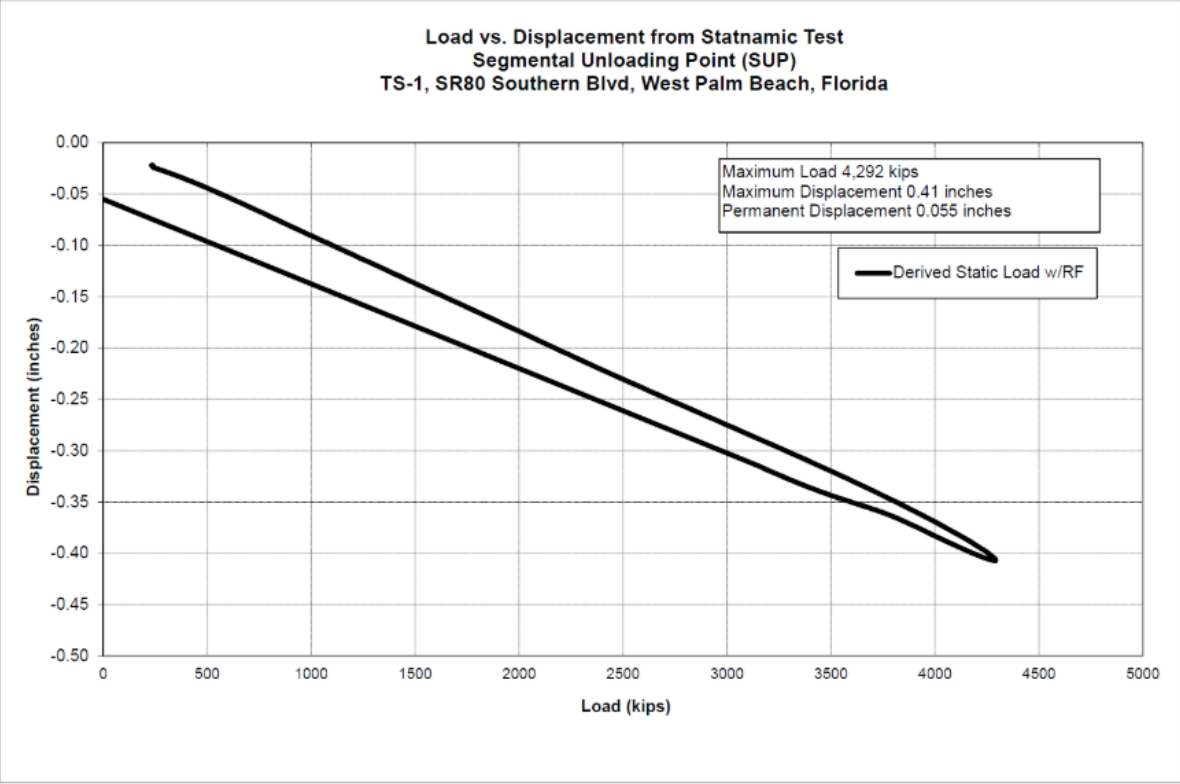


Figure B.21 Data set 21 load test results

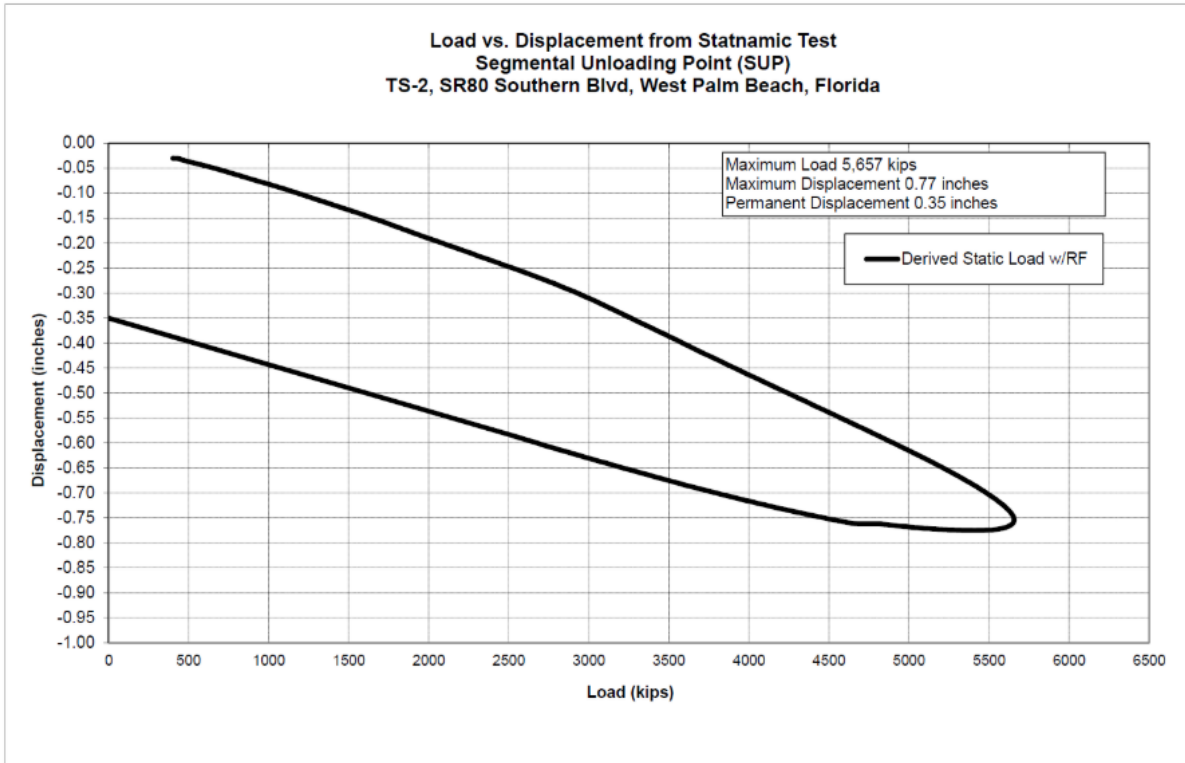


Figure B.22 Data set 22 load test results

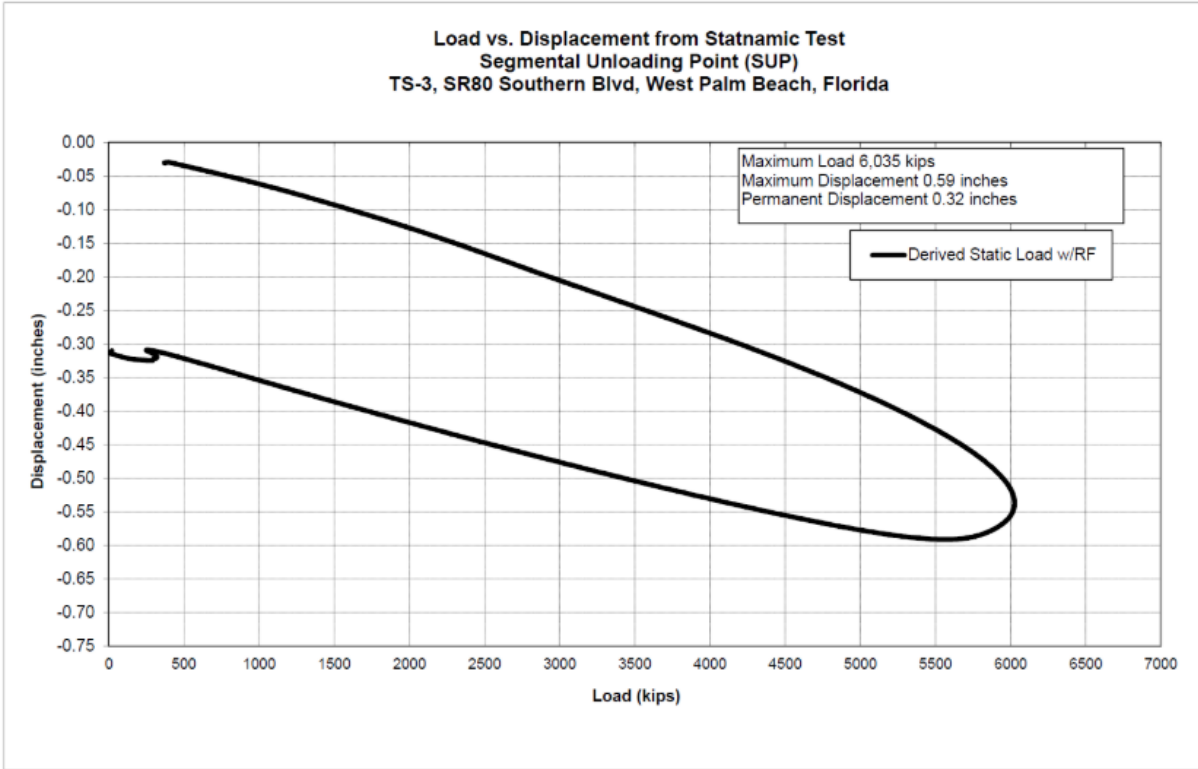


Figure B.23 Data set 23 load test results

Load vs. Displacement from Statnamic Test
TS-1
I-95 Overland Bridge, Jacksonville, Florida

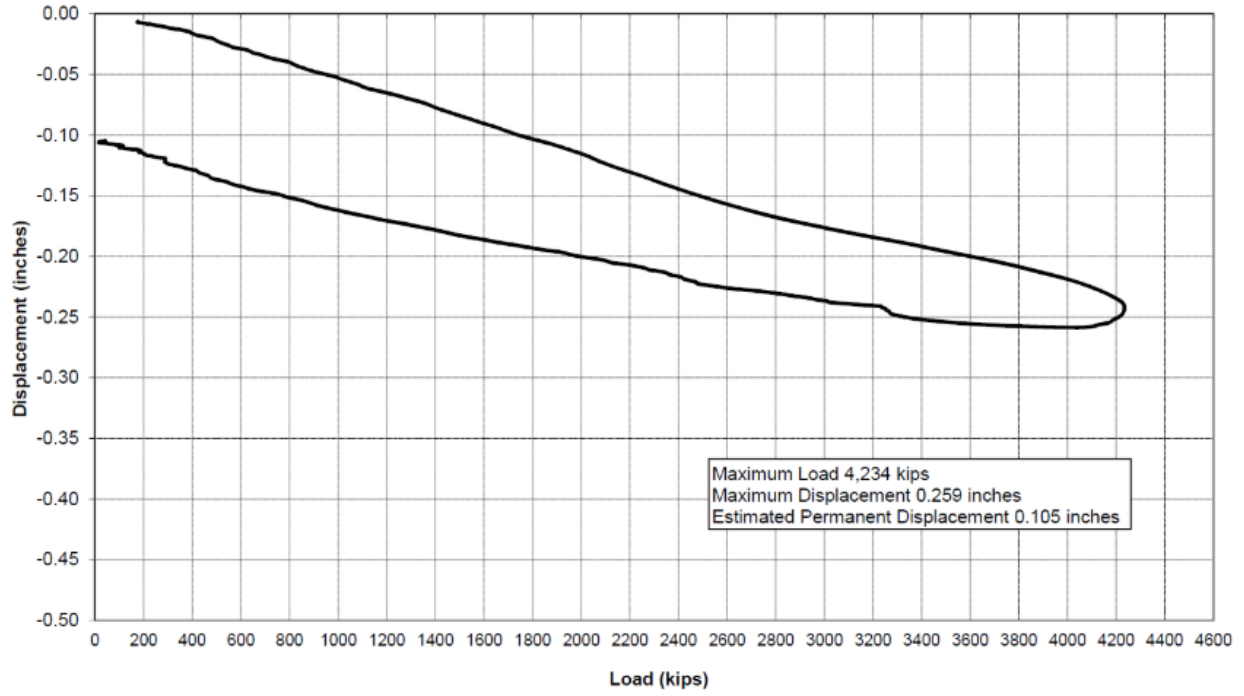


Figure B.24 Data set 24 load test results

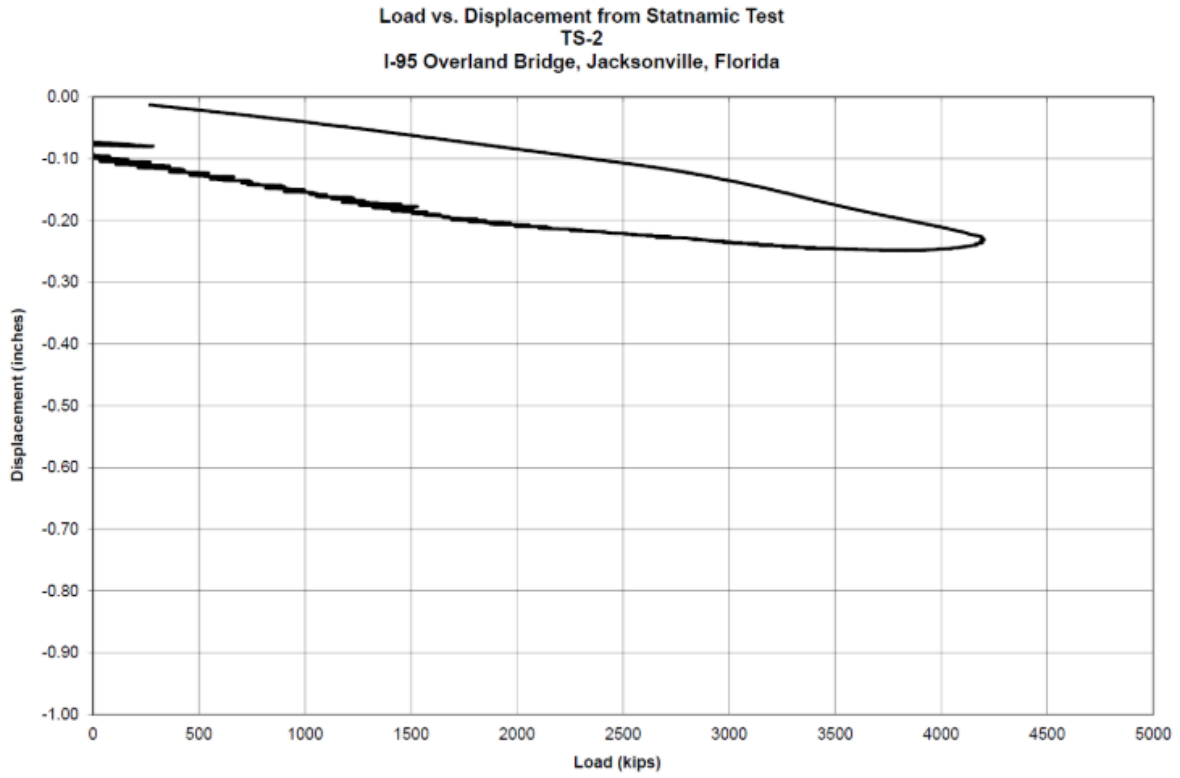


Figure B.25 Data set 25 load test results

Load vs. Displacement from Statnamic Test
TS-3
I-95 Overland Bridge, Jacksonville, Florida

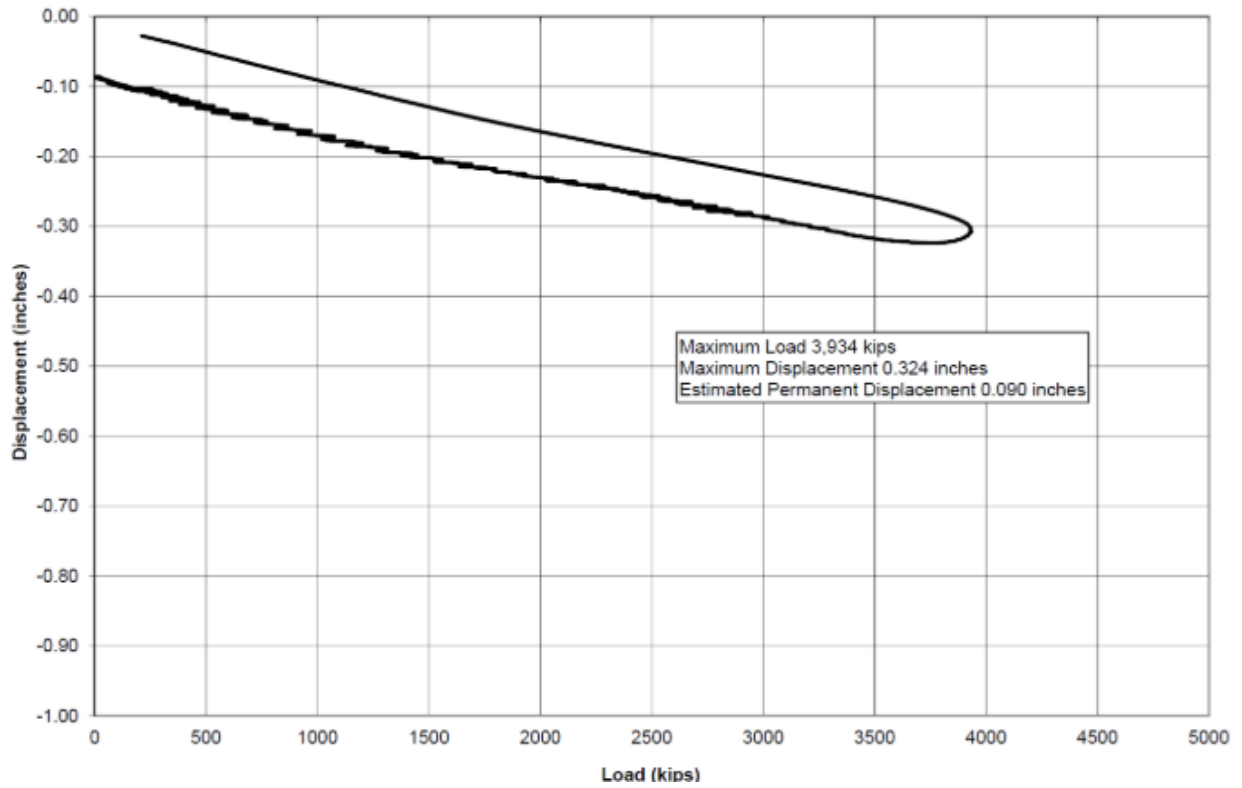


Figure B.26 Data set 26 load test results

Top and Toe Load vs. Top Displacement from Statnamic Test
TS-1, Carolina Bays Parkway

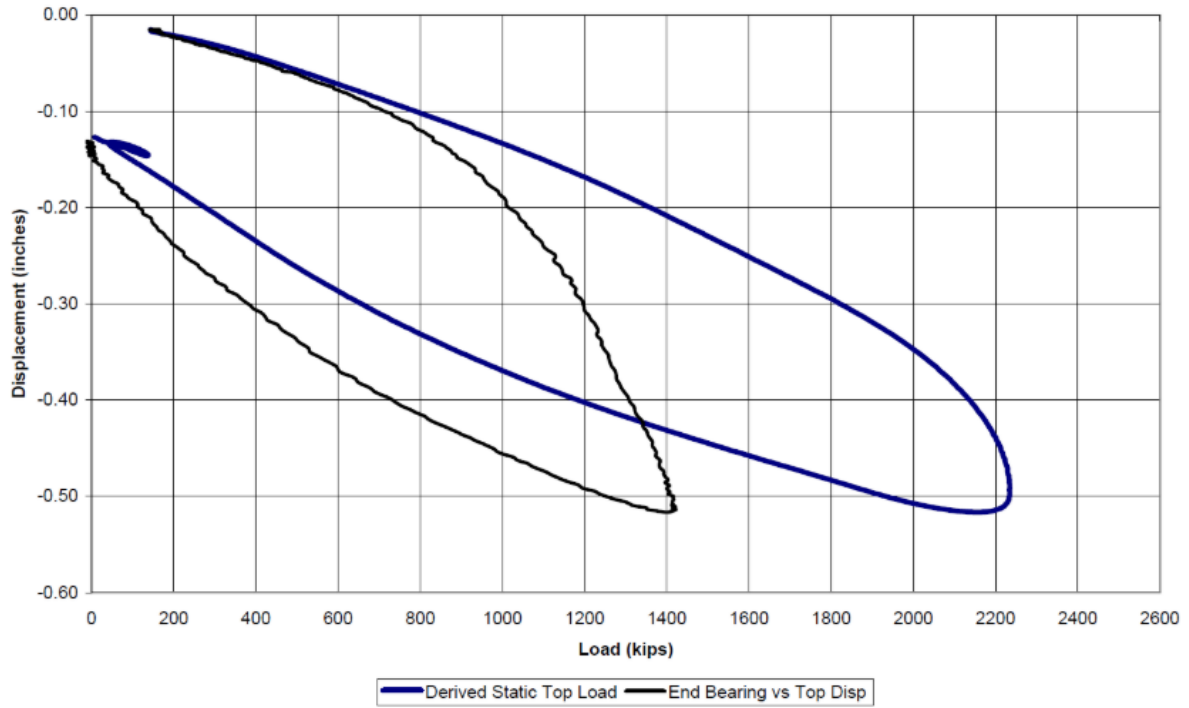


Figure B.27 Data set 27 Load test results



Osterberg Cell Load vs. Displacement Plots Gilmerton Bridge - Chesapeake, VA - Pier 9 SW R

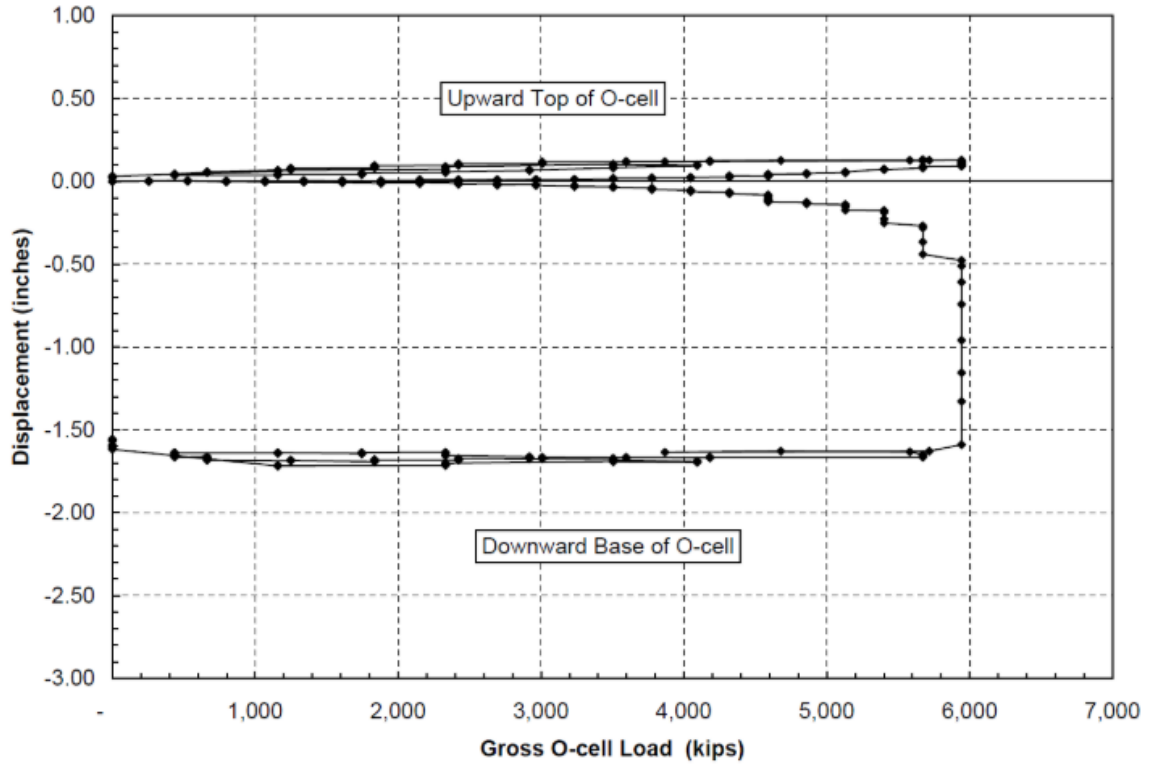


Figure B.28 Data set 28 load test results

Load vs. Displacement
Test Shaft 1
Peninsula Condominiums

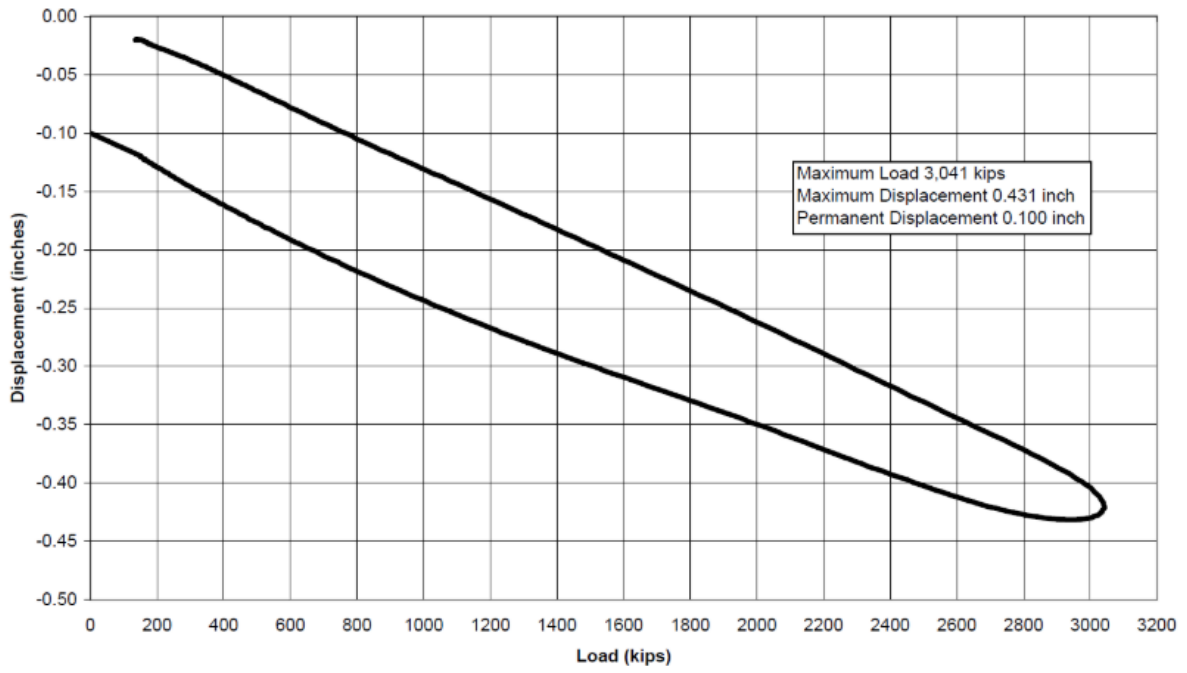


Figure B.29 Data set 29 load test results

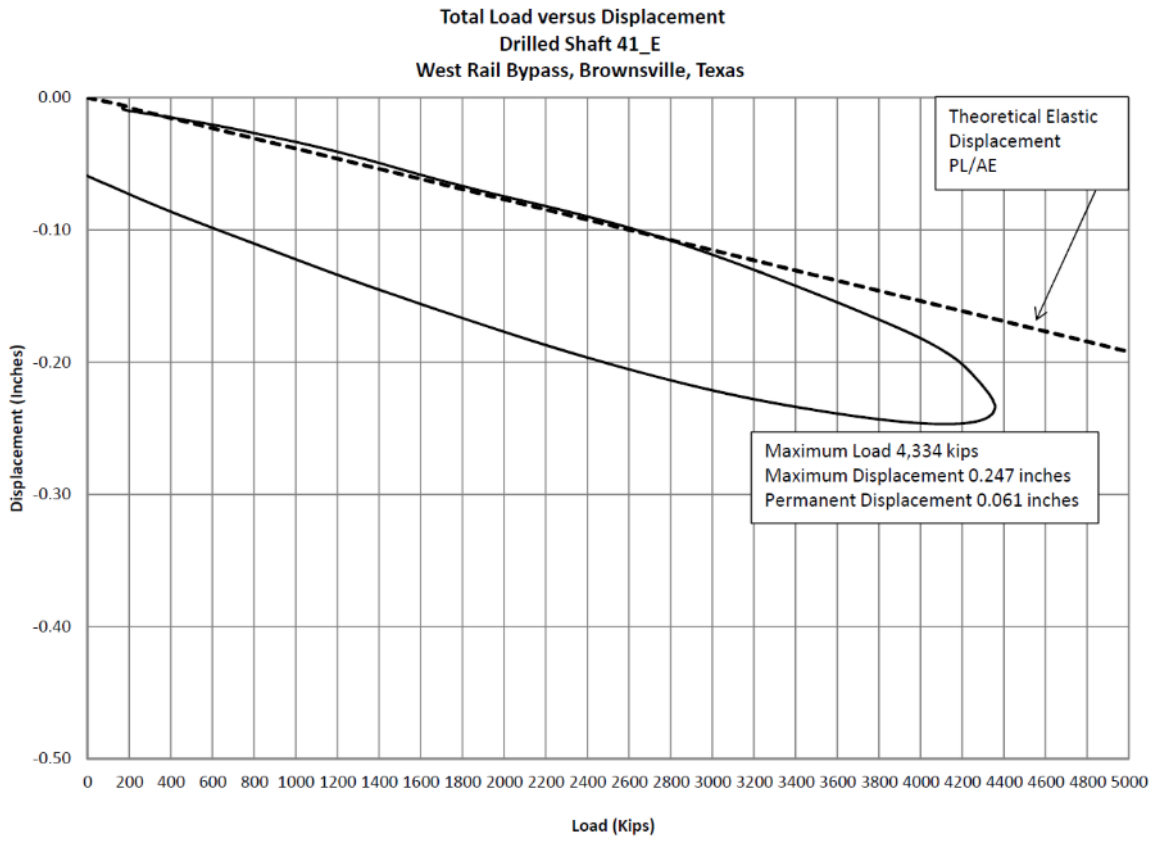


Figure B.30 Data set 30 load test results

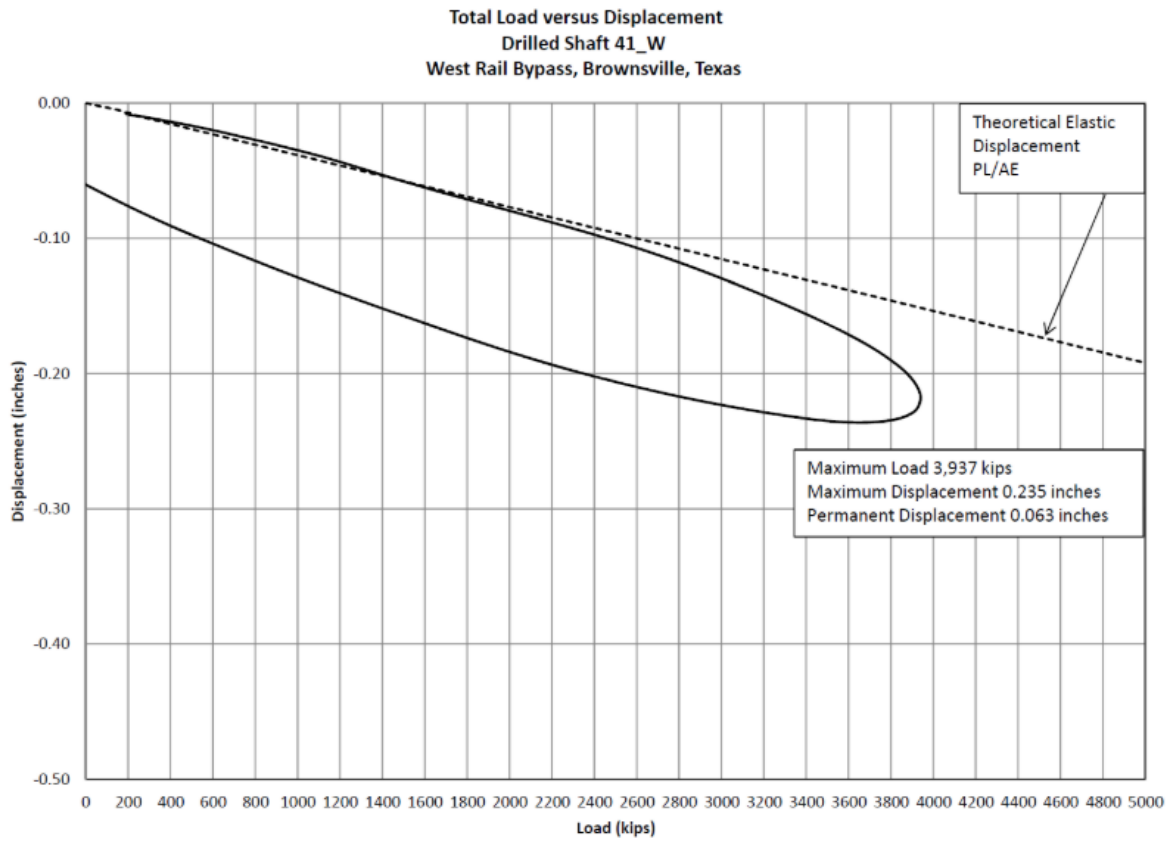


Figure B.31 Data set 31 load test results

APPENDIX C FDOT METHOD BIAS FACTOR PLOTS

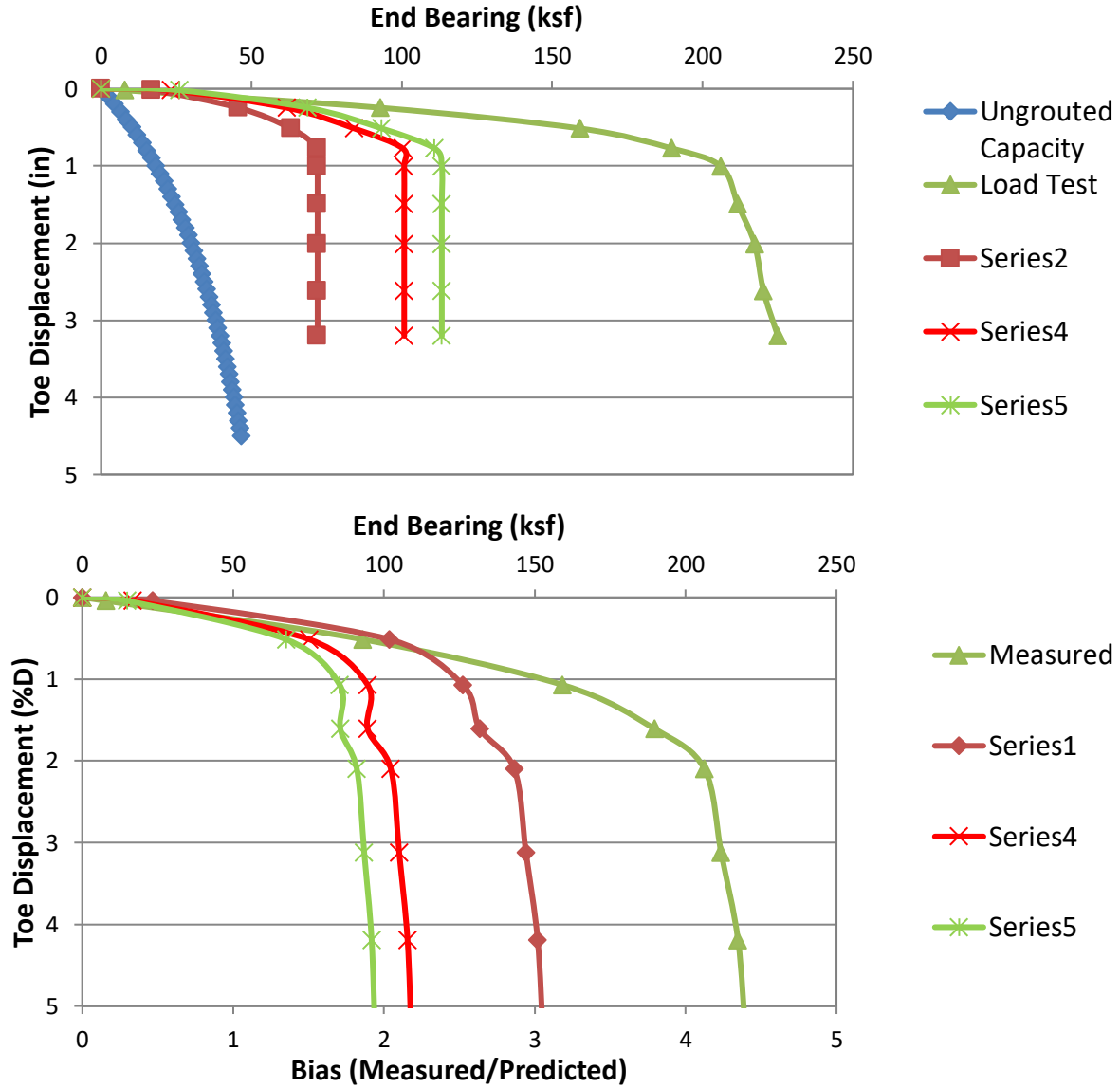


Figure C.1 Data set 1 predicted/design and load test response (top); bias vs disp. (bottom).

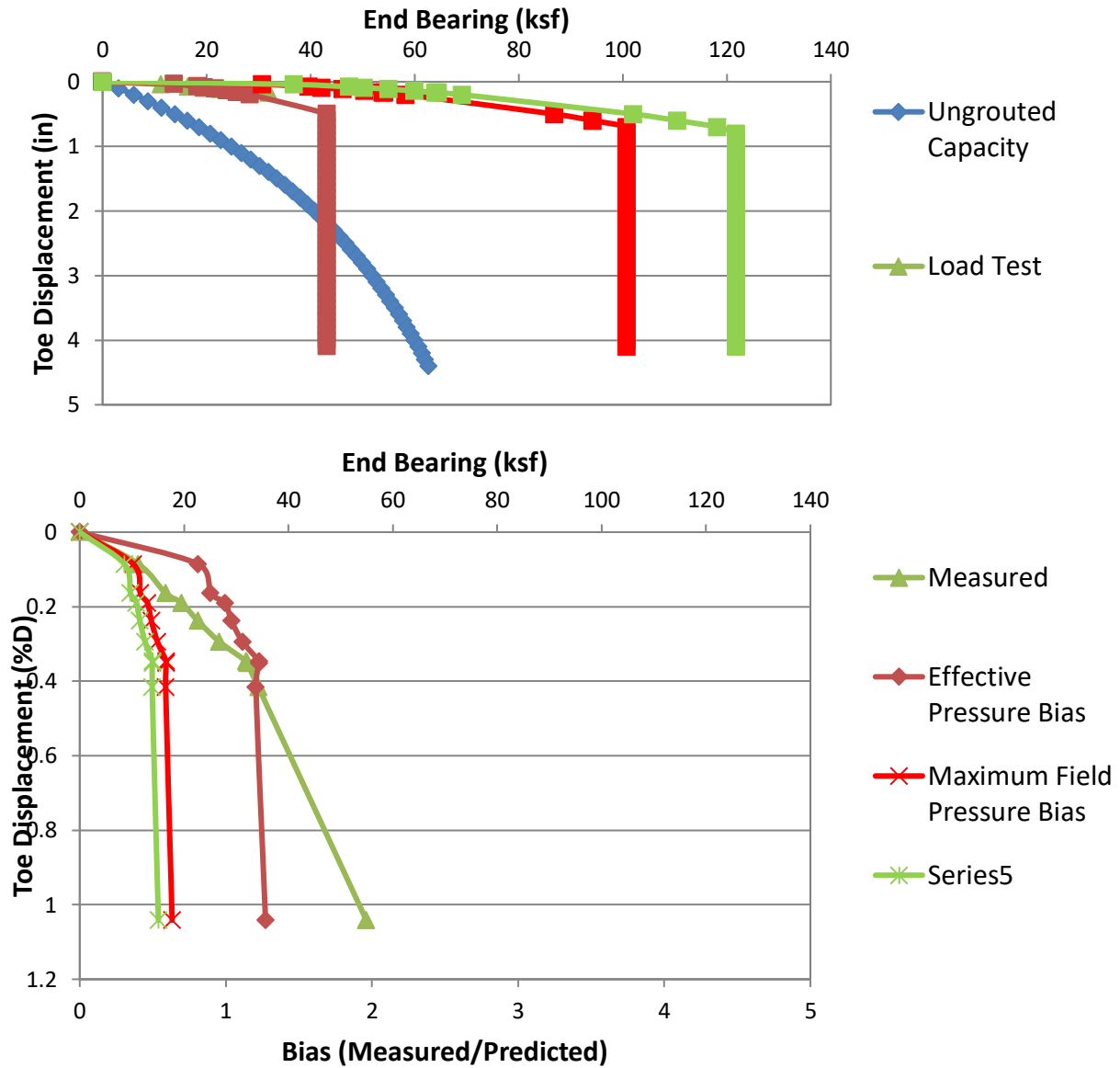


Figure C.2 Data set 2 predicted/design and load test response (top); bias vs disp. (bottom)

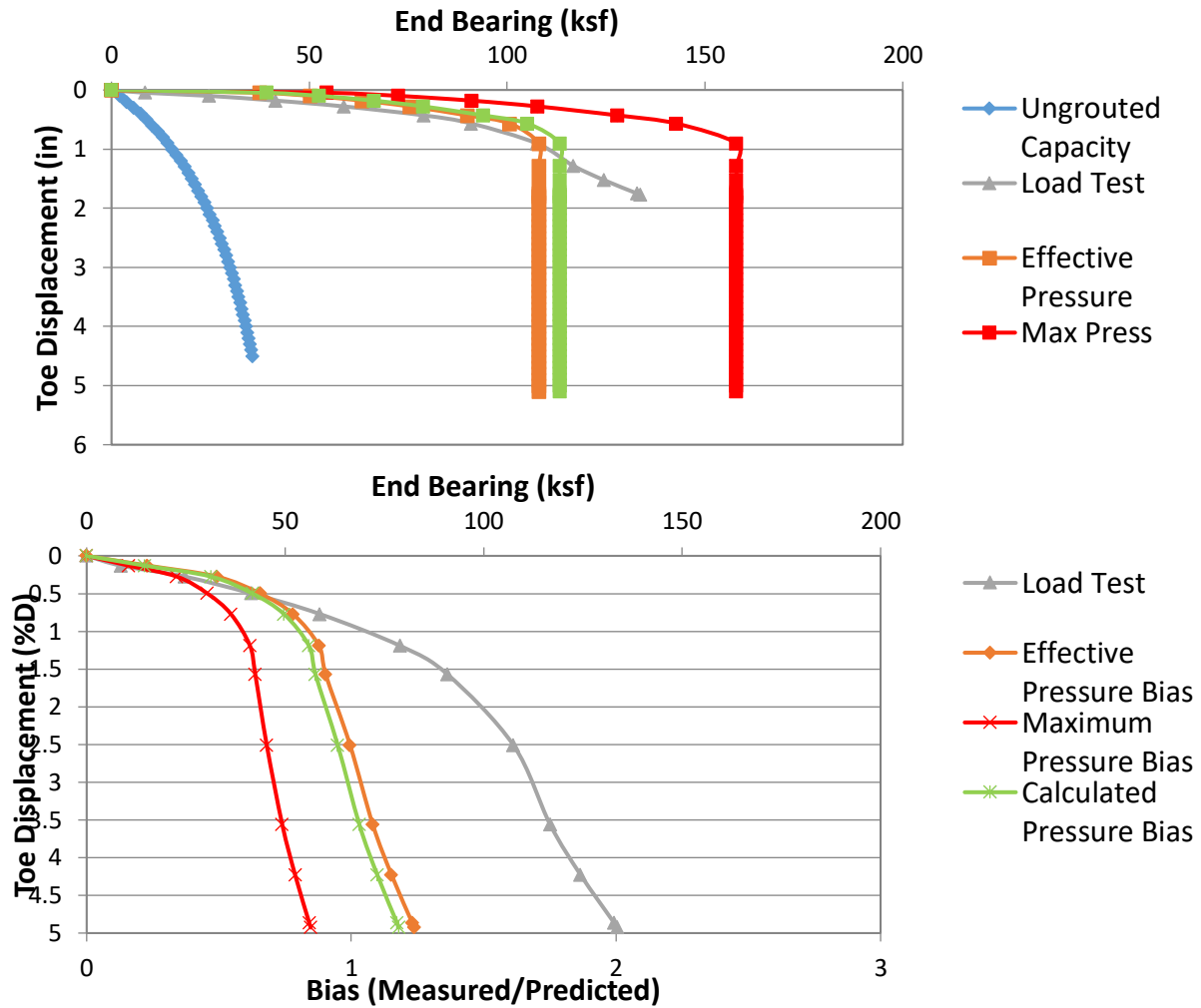


Figure C.3 Data set 3 predicted/design and load test response (top); bias vs disp. (bottom)

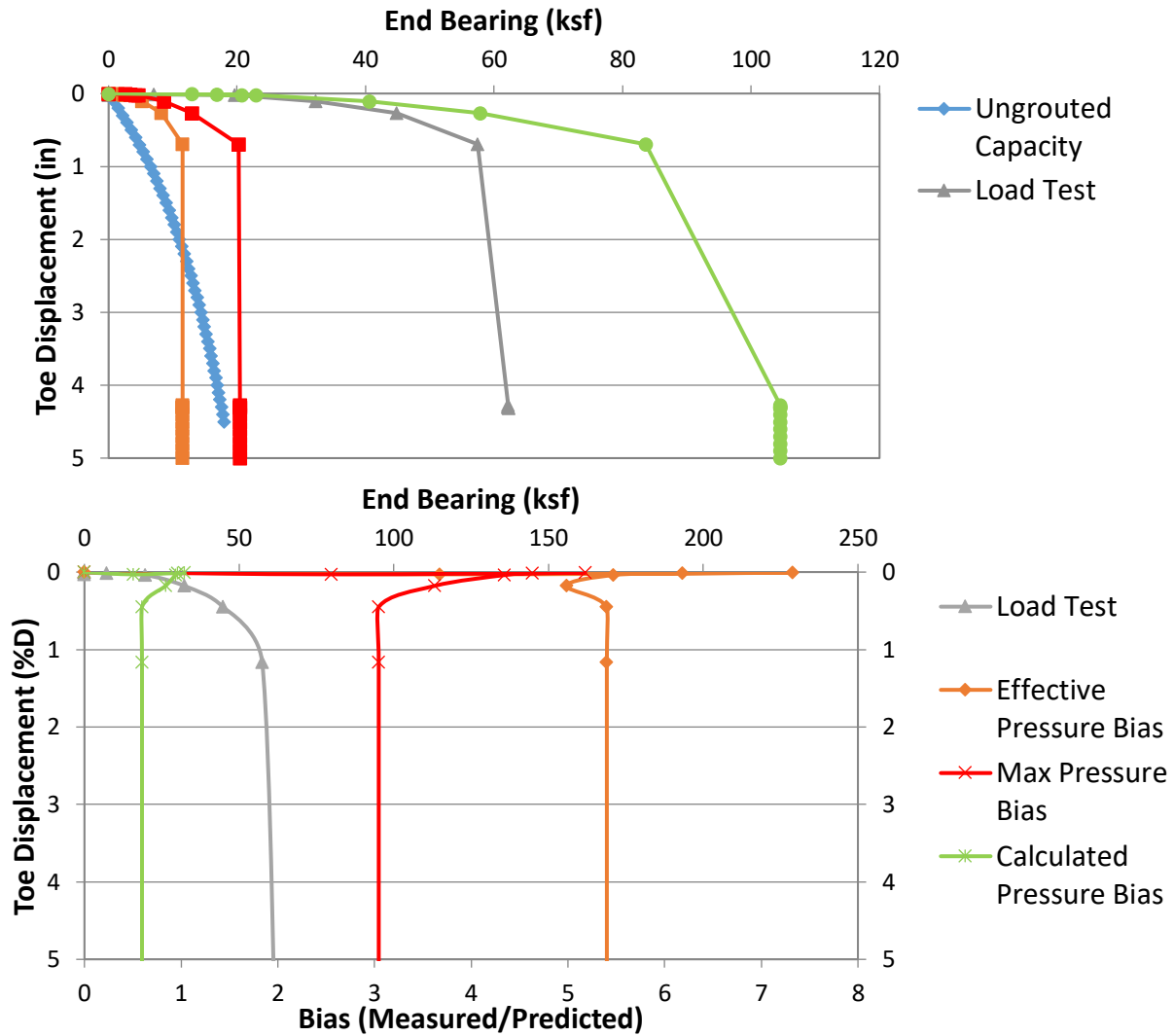


Figure C.4 Data set 4 predicted/design and load test response (top); bias vs disp. (bottom)

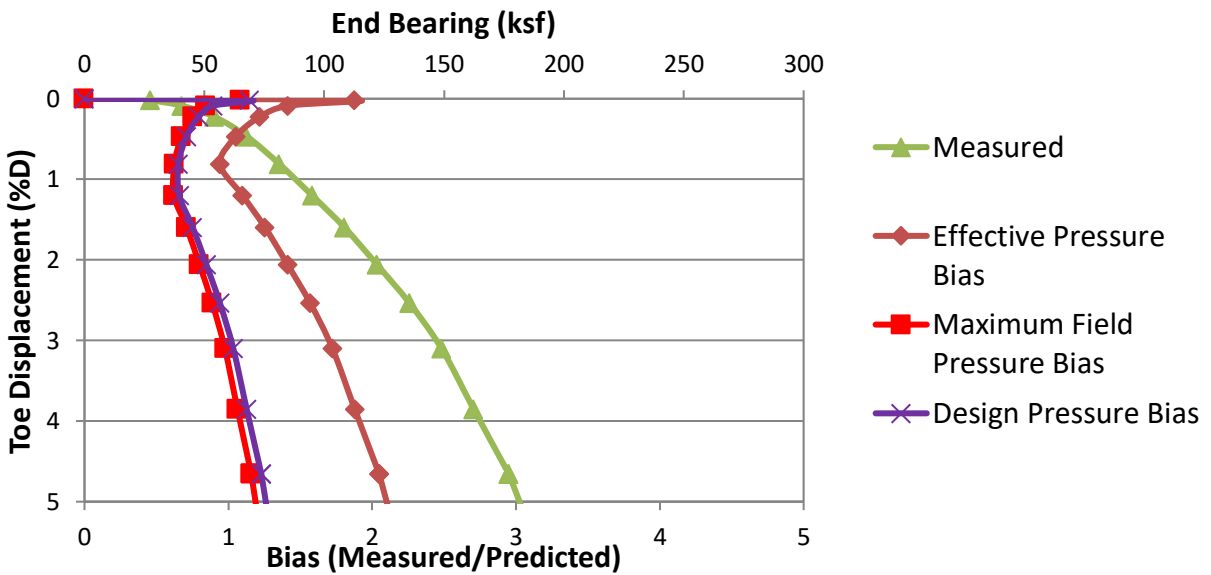
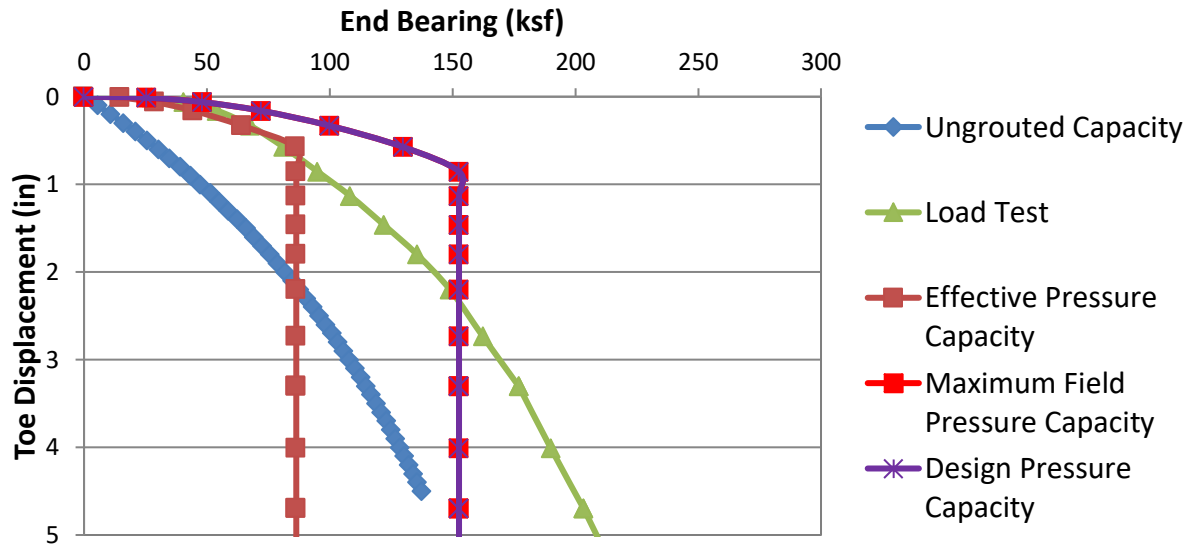


Figure C.5 Data set 5 Predicted/design and load test response (top); bias vs disp. (bottom)

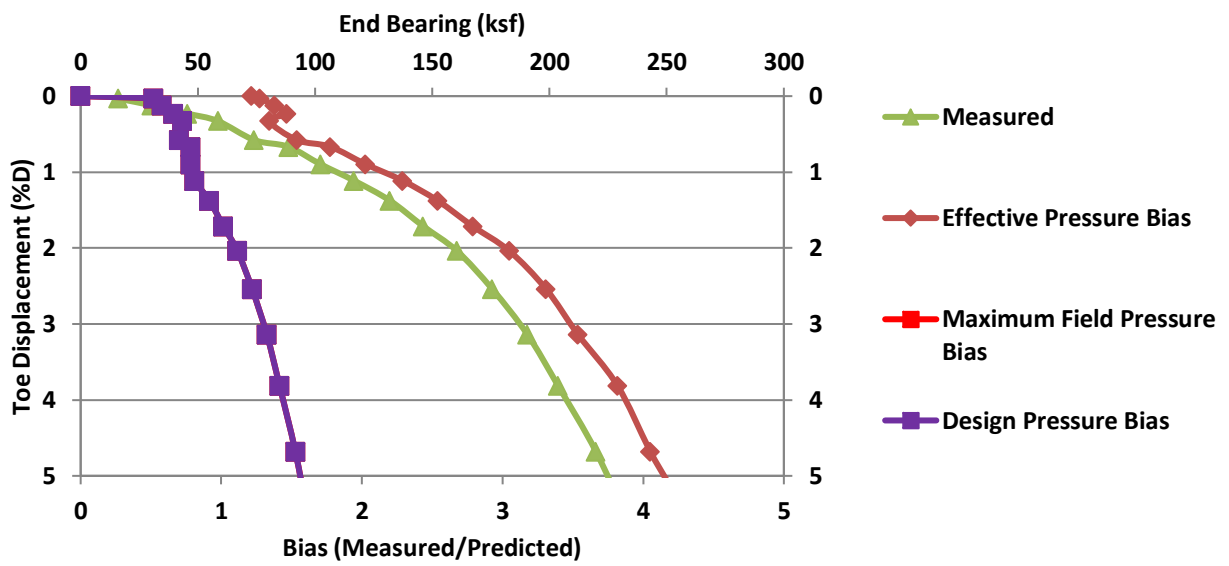
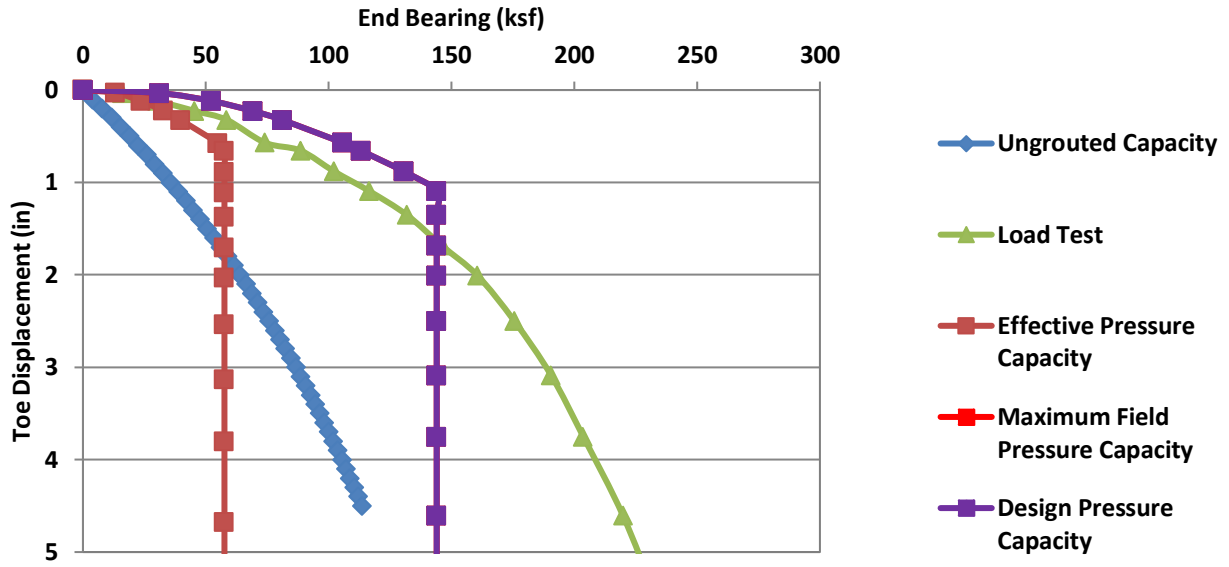


Figure C.6 Data set 6 predicted/design and load test response (top); bias vs disp. (bottom)

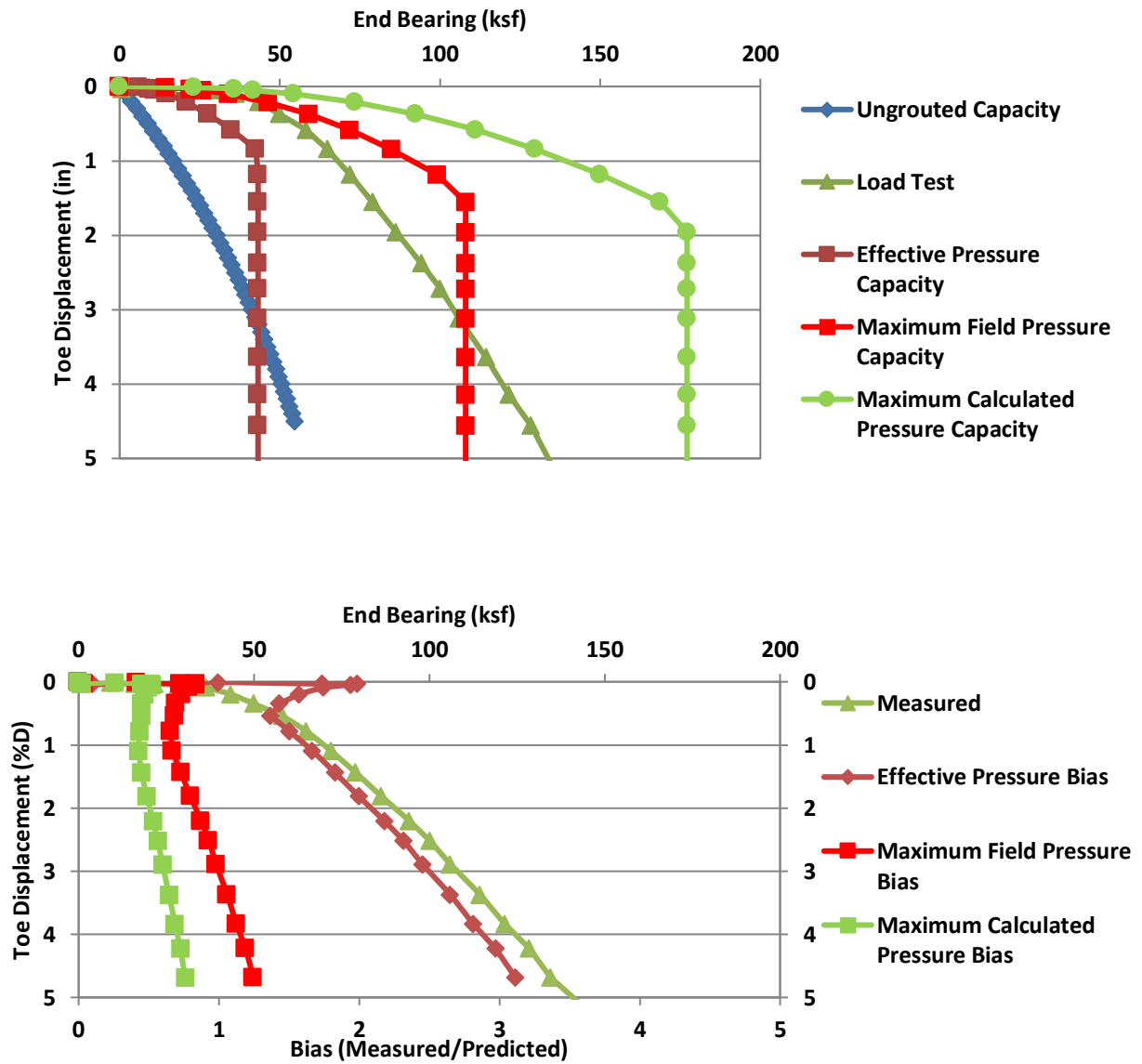


Figure C.7 Data set 7 predicted/design and load test response (top); bias vs disp. (bottom)

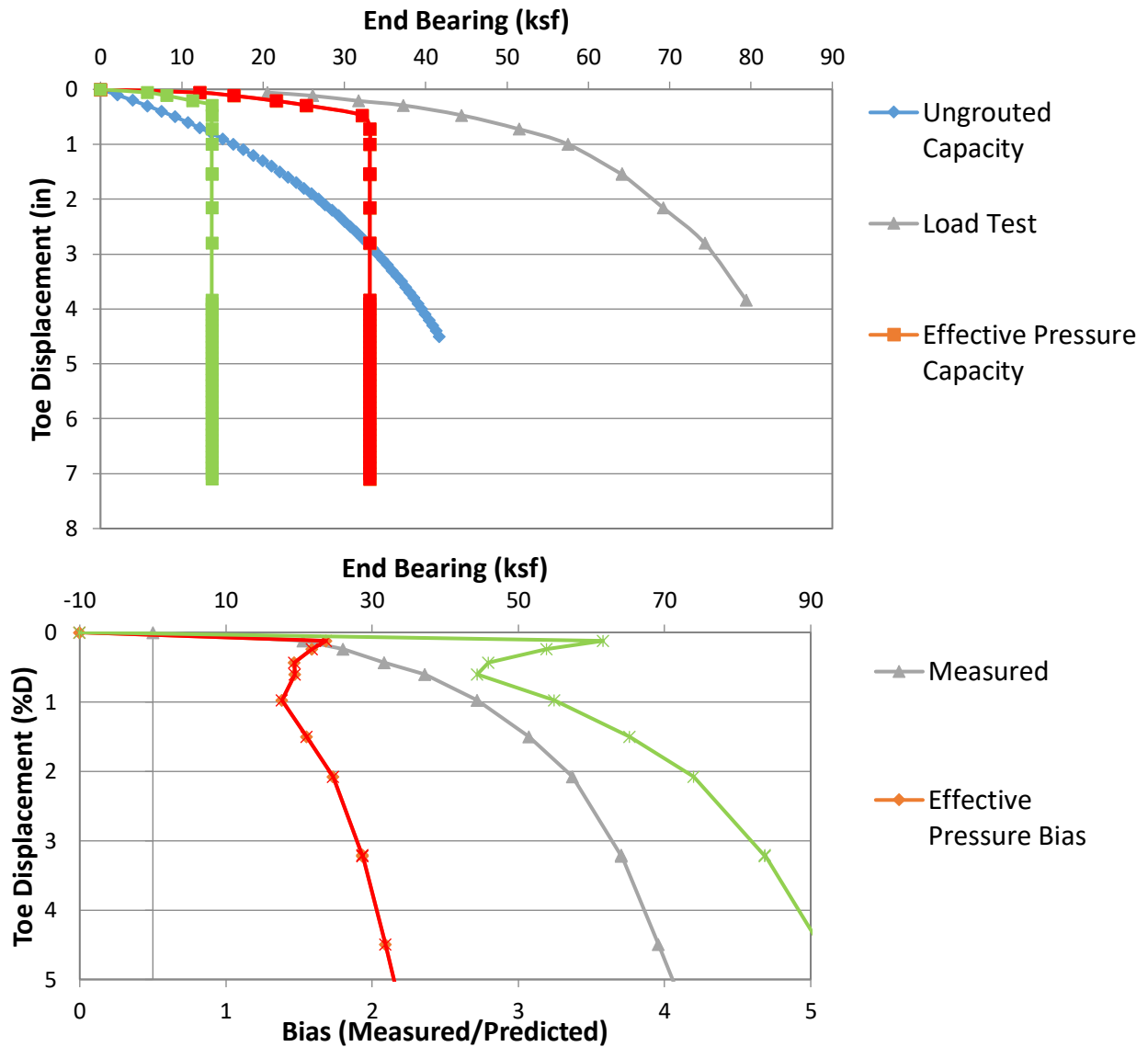


Figure C.8 Data set 8 predicted/design and load test response (top); bias vs disp. (bottom)

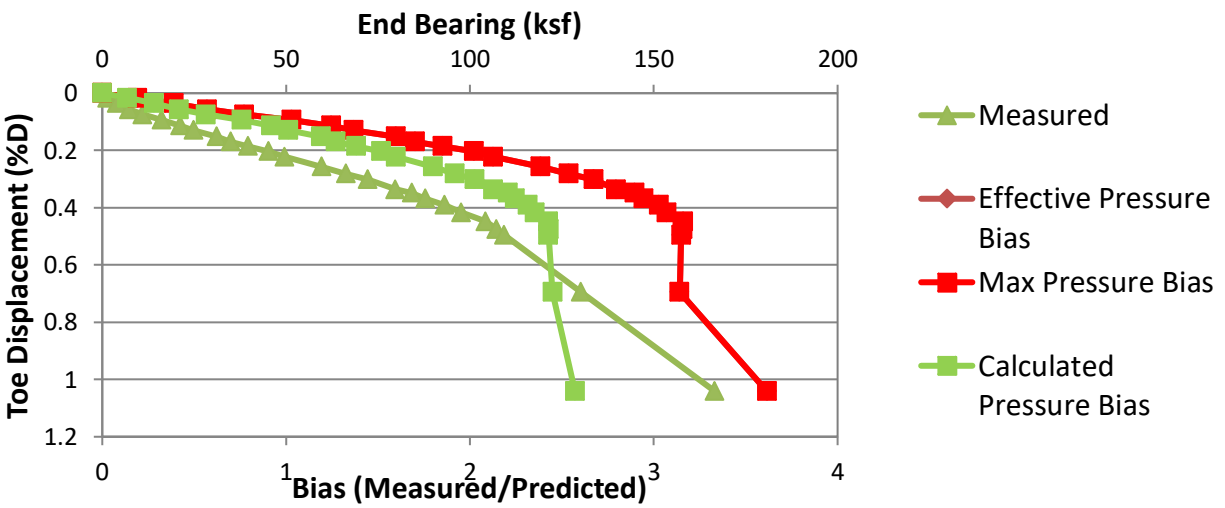
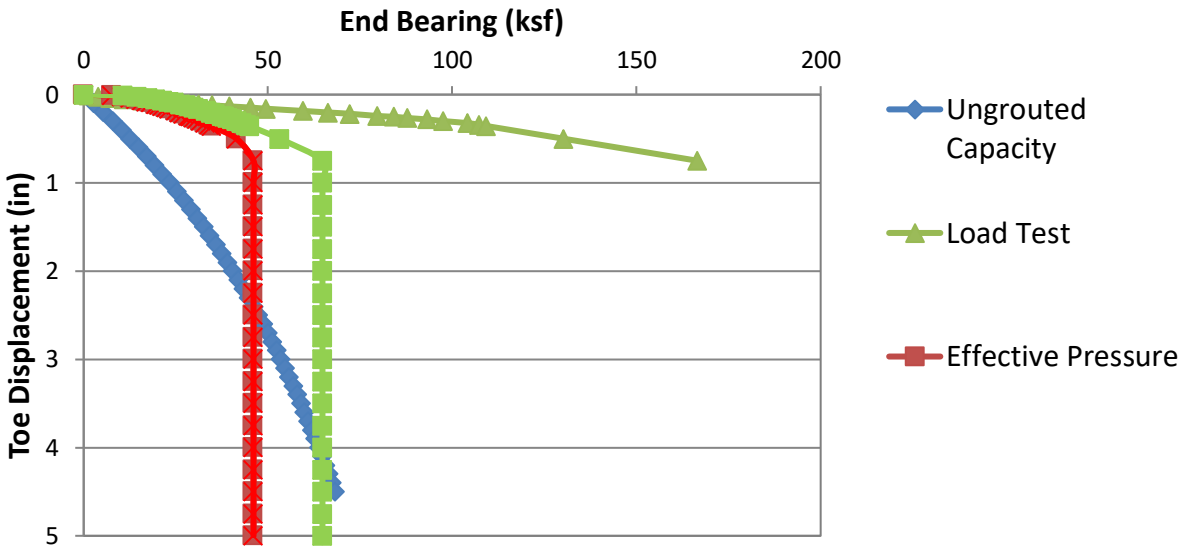


Figure C.9 Data set 9 predicted/design and load test response (top); bias vs disp. (bottom)

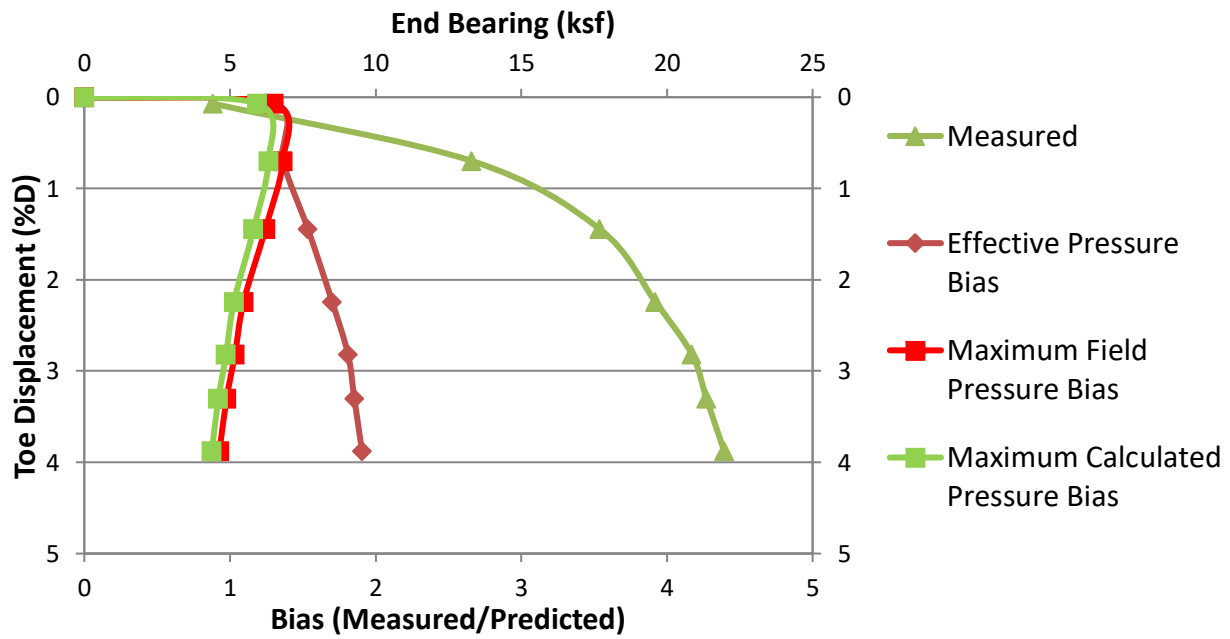
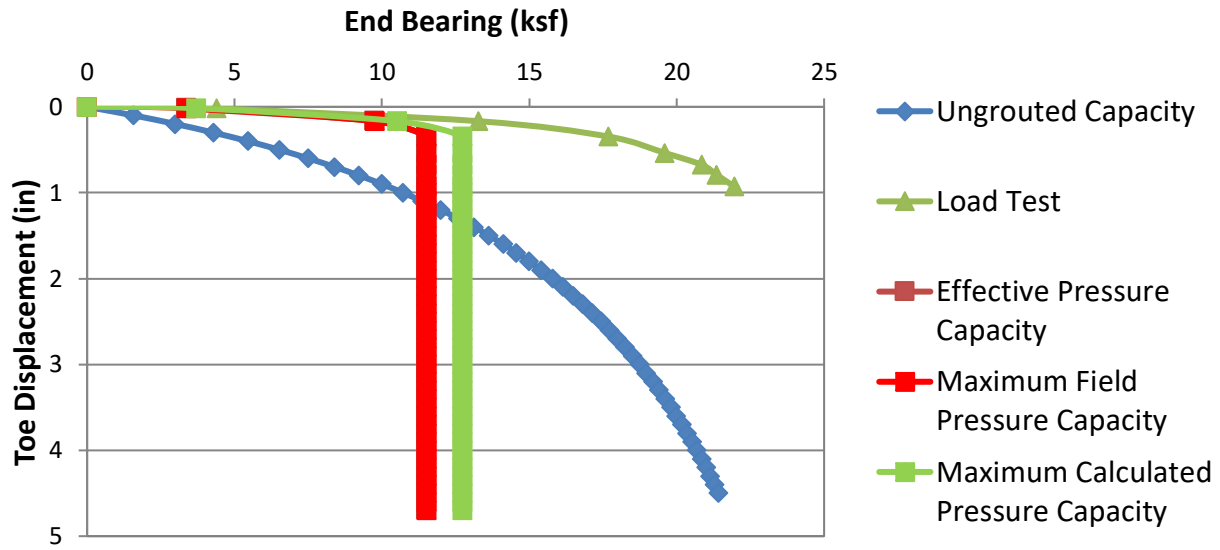


Figure C.10 Data set 10 predicted/design and load test response (top); bias vs disp. (bottom)

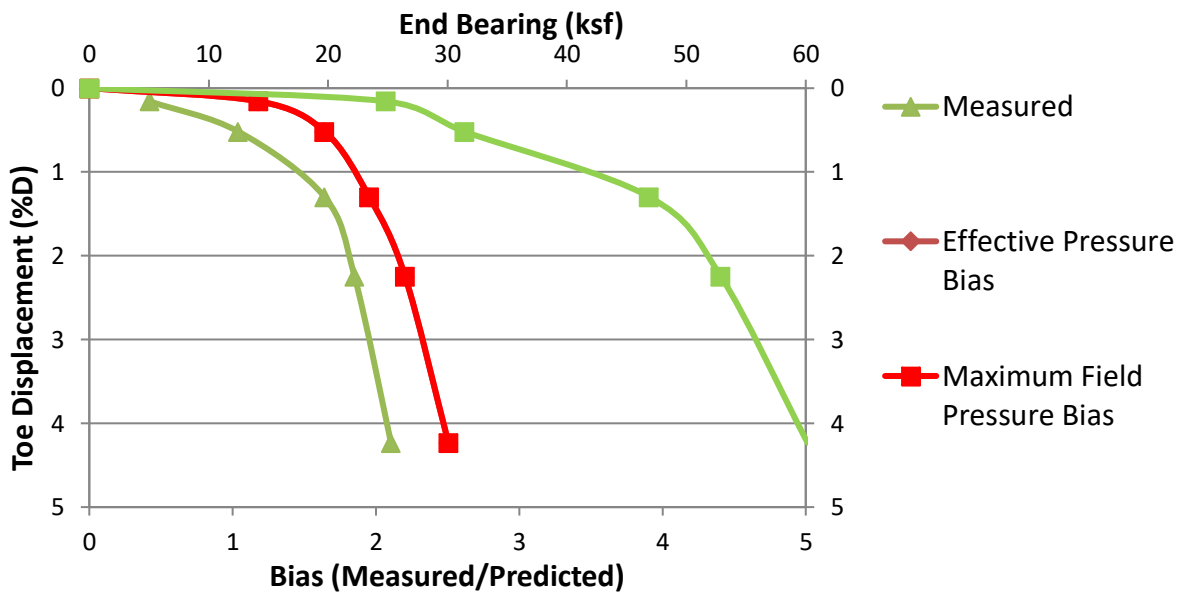
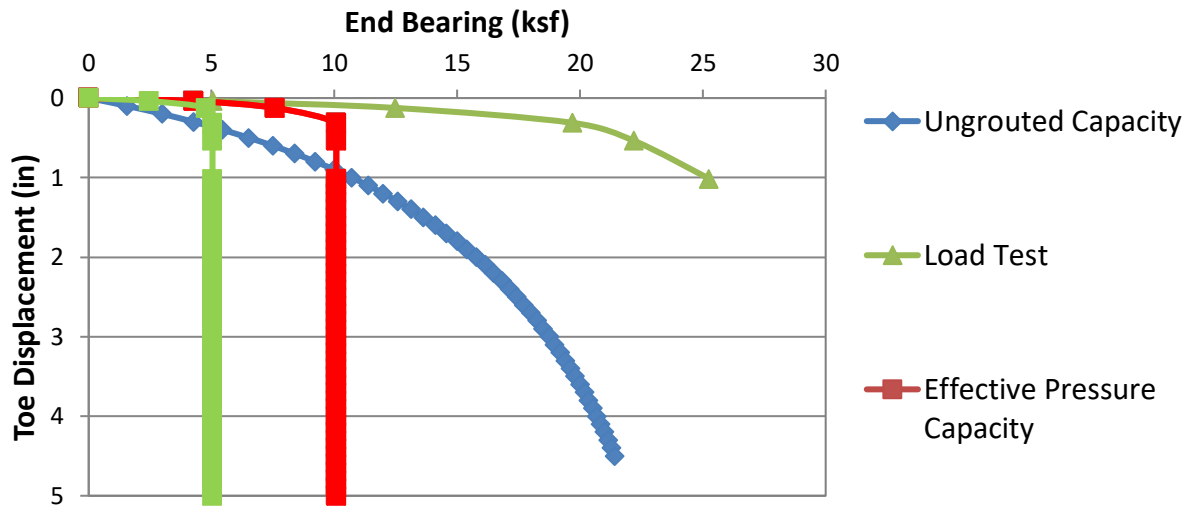


Figure C.11 Data set 11 predicted/design and load test response (top); bias vs disp. (bottom)

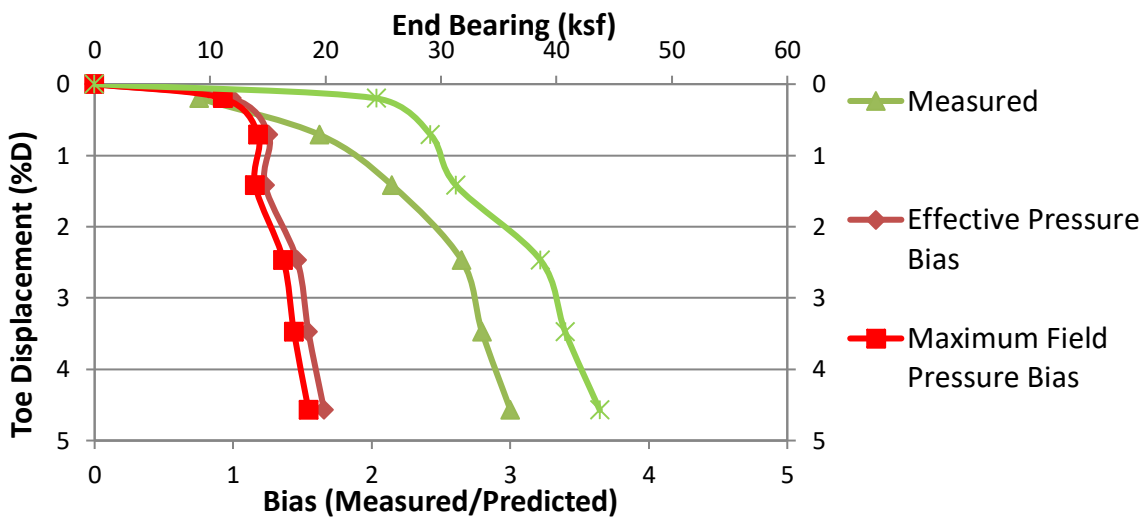
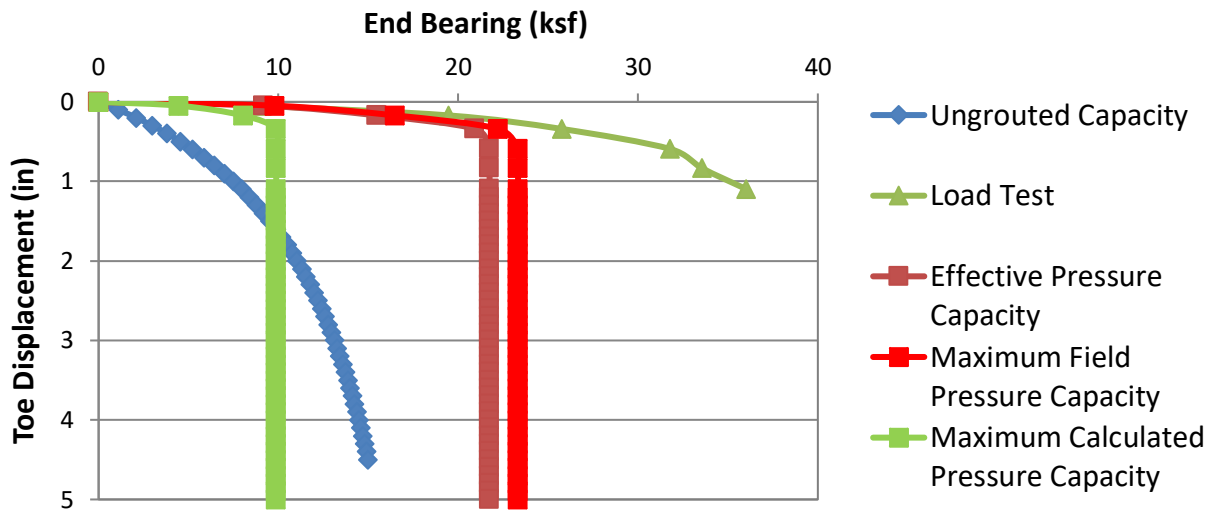


Figure C.12 Data set 12 predicted/design and load test response (top); bias vs disp. (bottom)

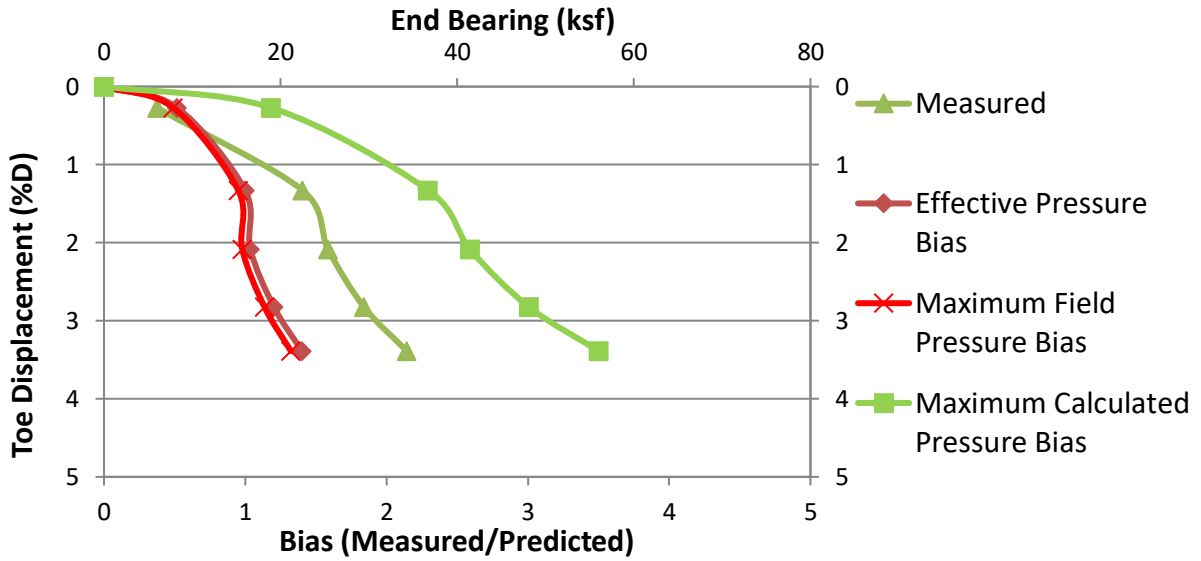
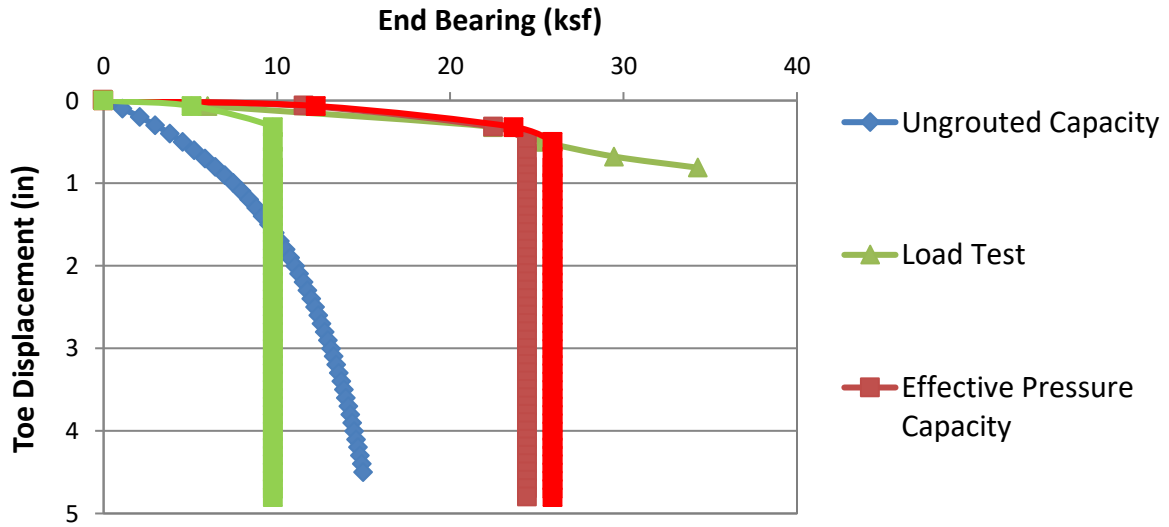


Figure C.13 Data set 13 predicted/design and load test response (top); bias vs disp. (bottom)

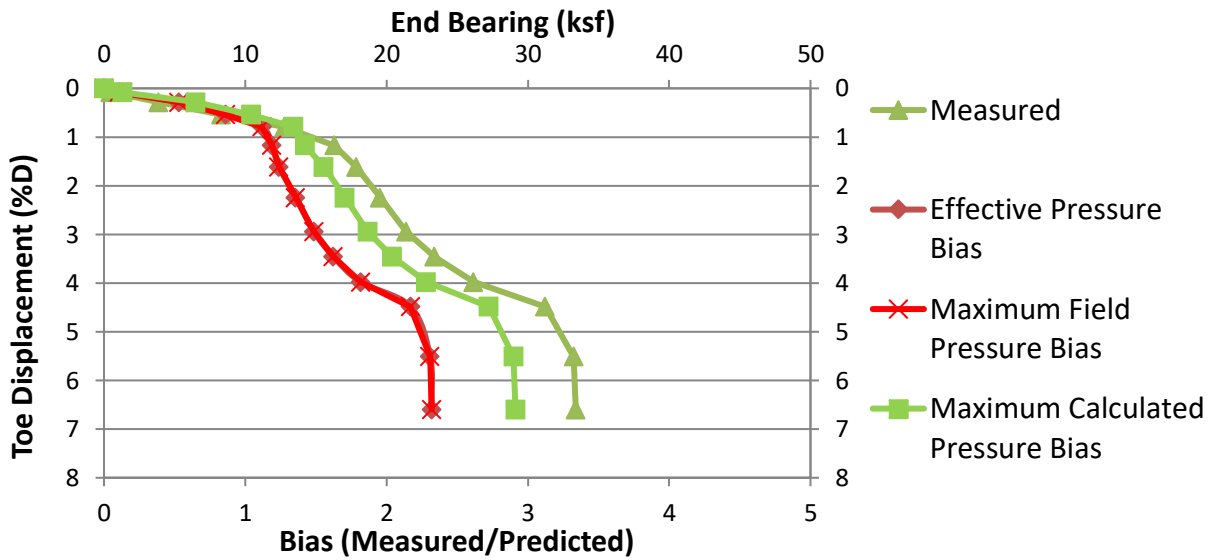
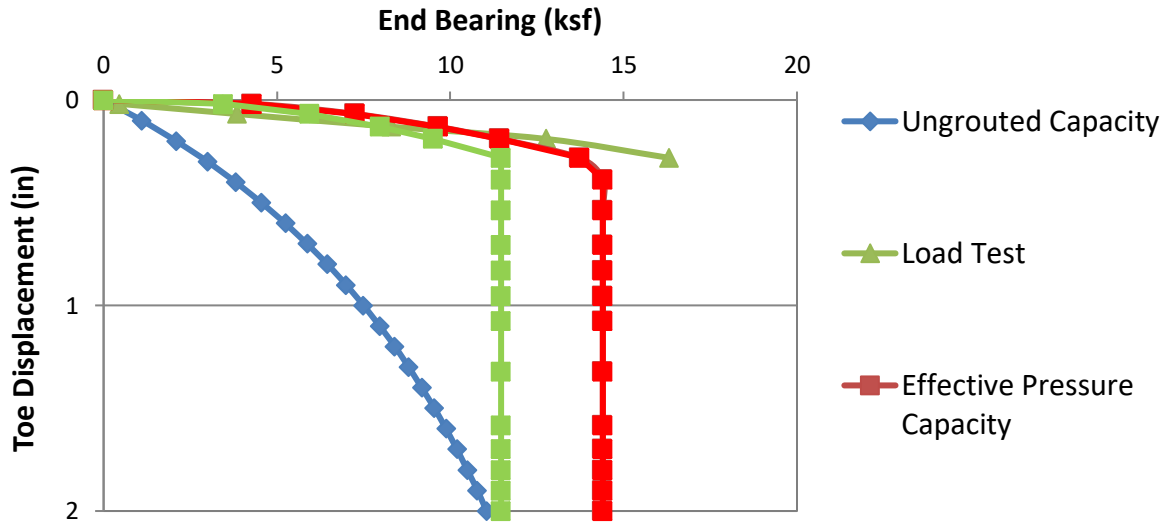


Figure C.14 Data set 14 predicted/design and load test response (top); bias vs disp. (bottom)

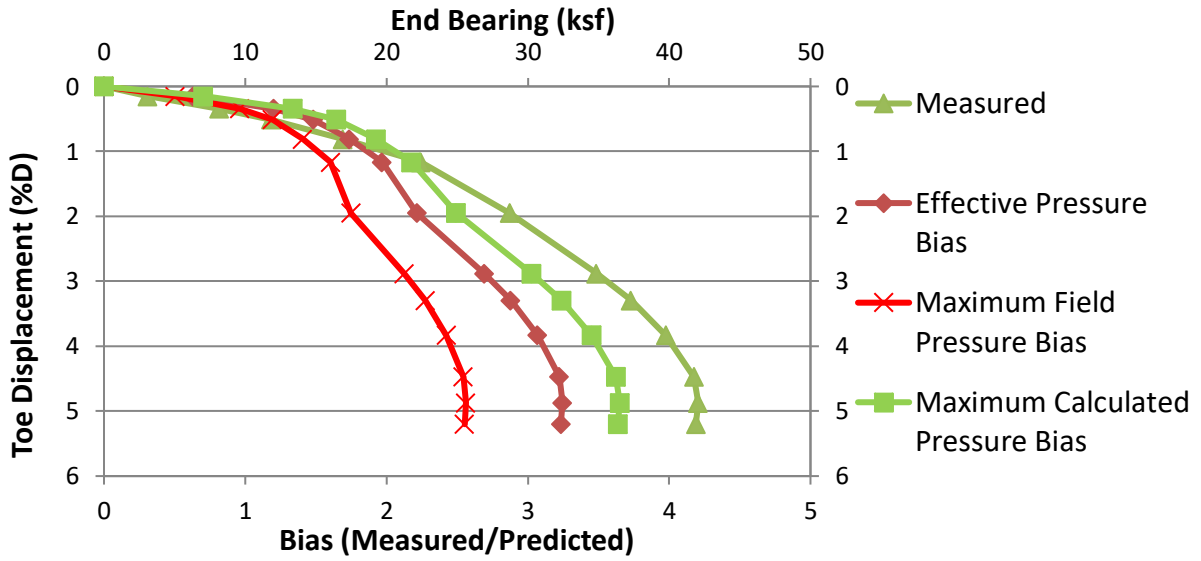
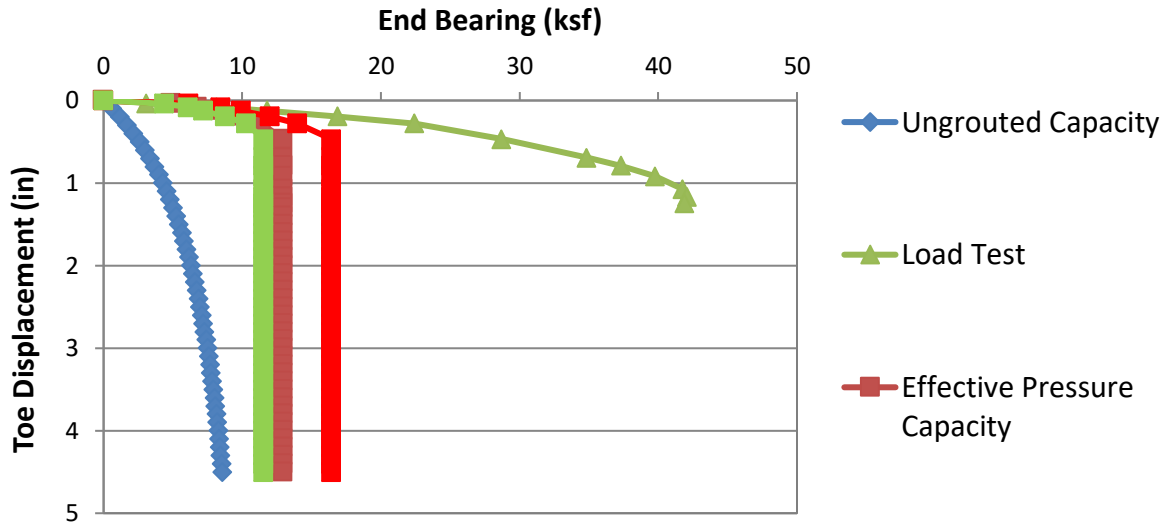
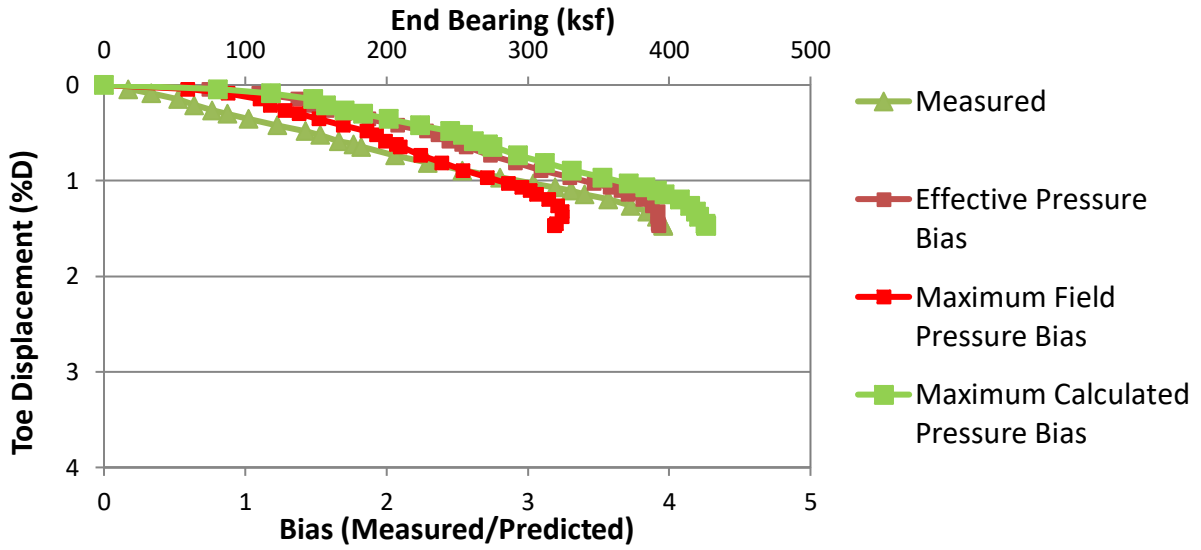
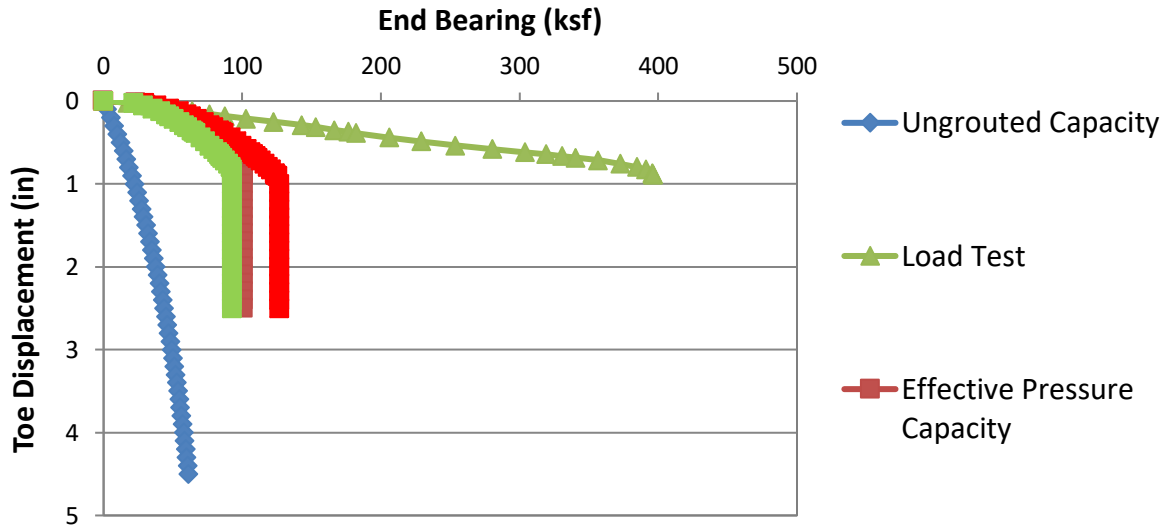


Figure C.15 Data set 15 predicted/design and load test response (top); bias vs disp. (bottom)



FigureC.16 Data set 16 predicted/design and load test response (top); bias vs disp. (bottom)

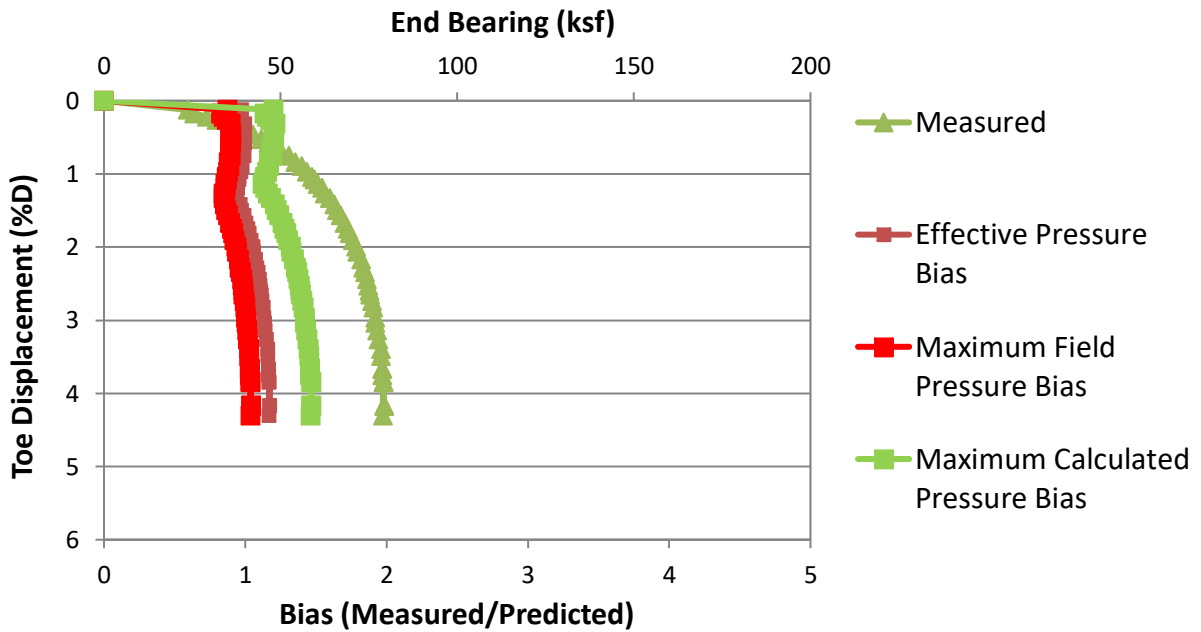
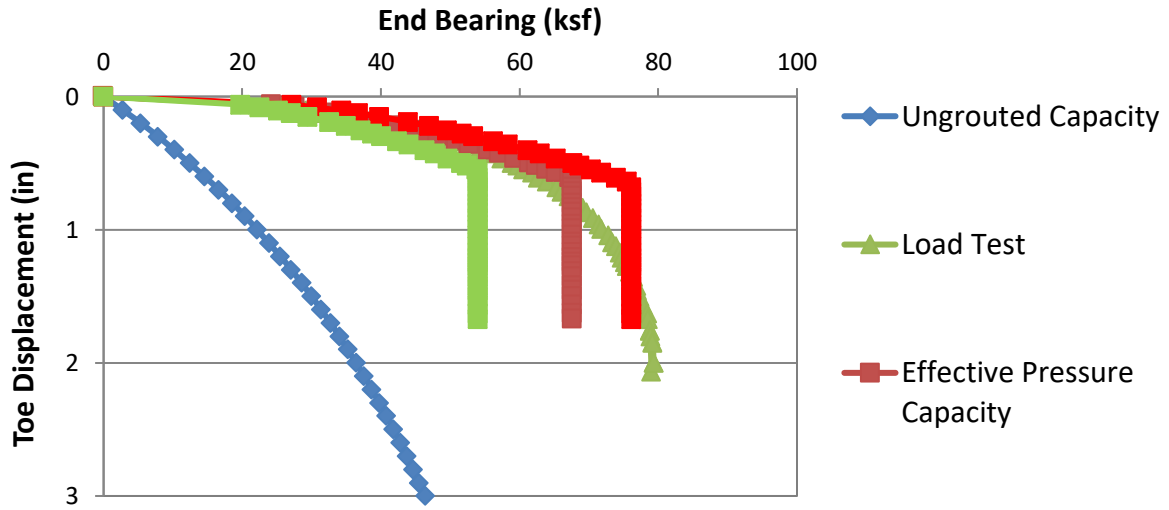


Figure C.17 Data set 17 predicted/design and load test response (top); bias vs disp. (bottom)

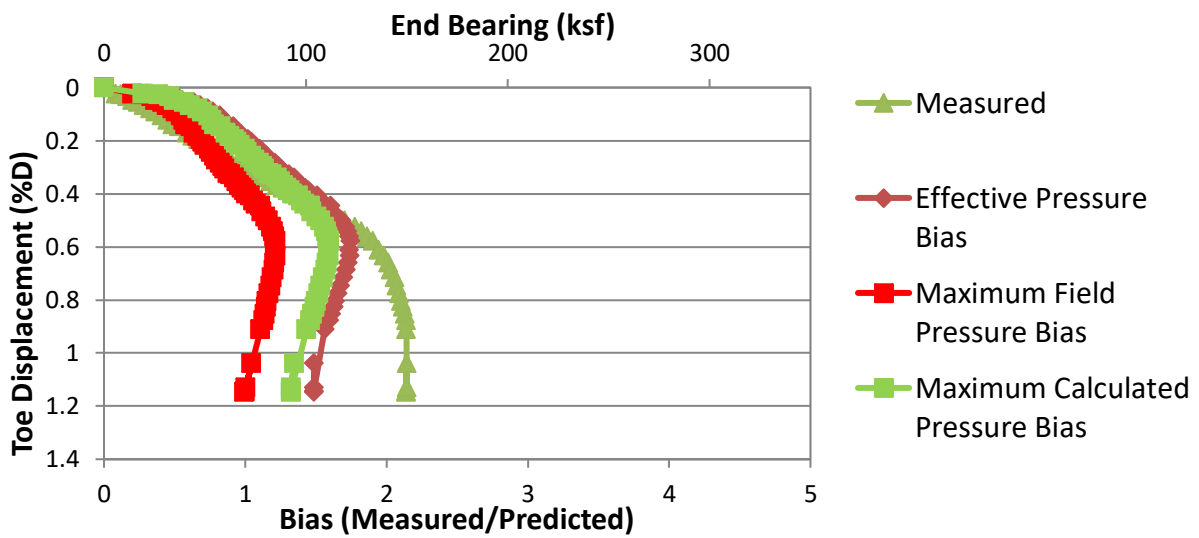
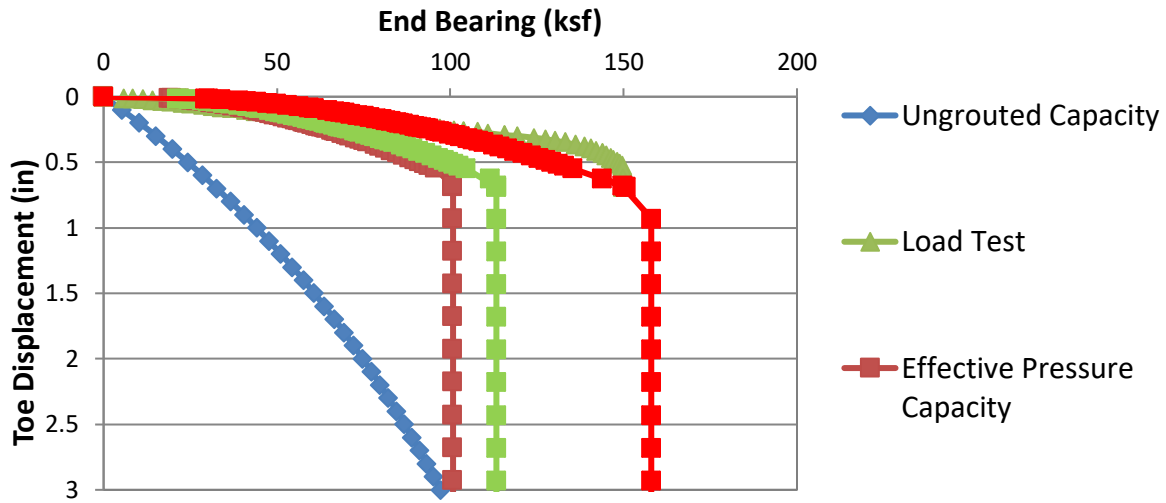


Figure C.18 Data set 18 predicted/design and load test response (top); bias vs disp. (bottom)

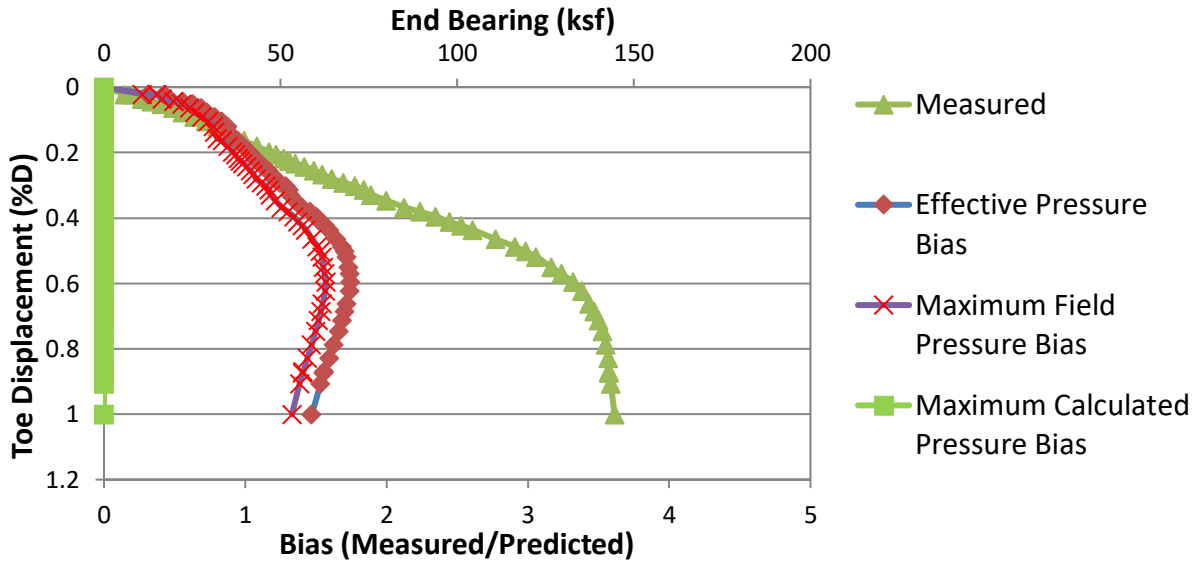
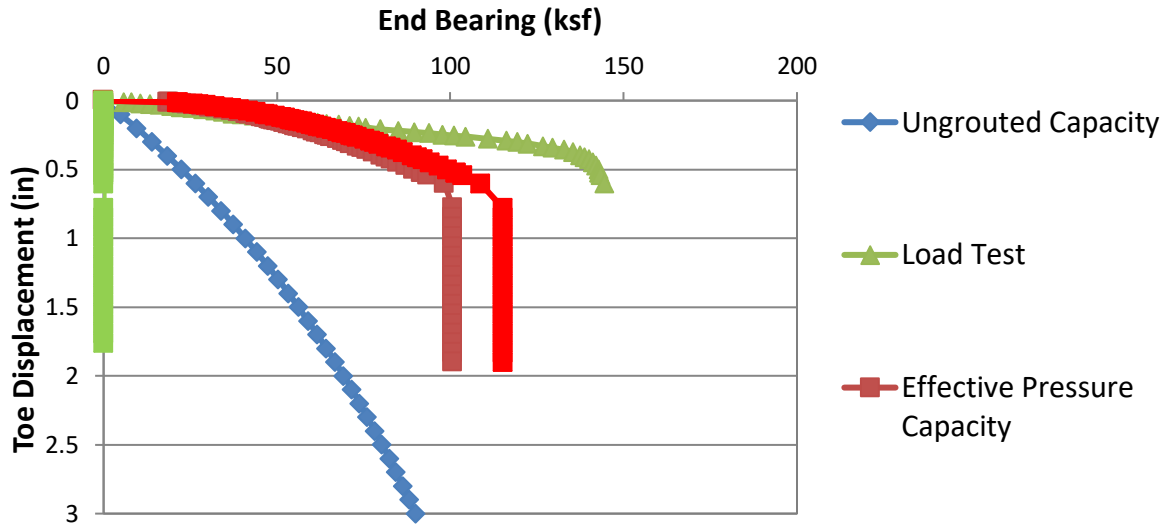


Figure C.19 Data set 19 predicted/design and load test response (top); bias vs disp. (bottom)

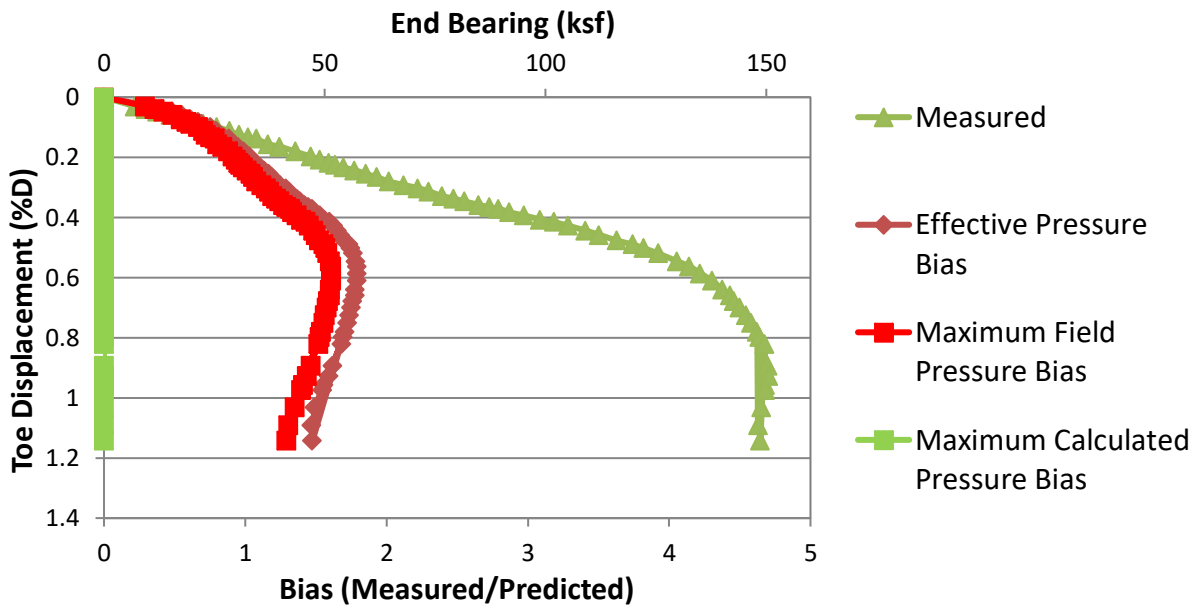
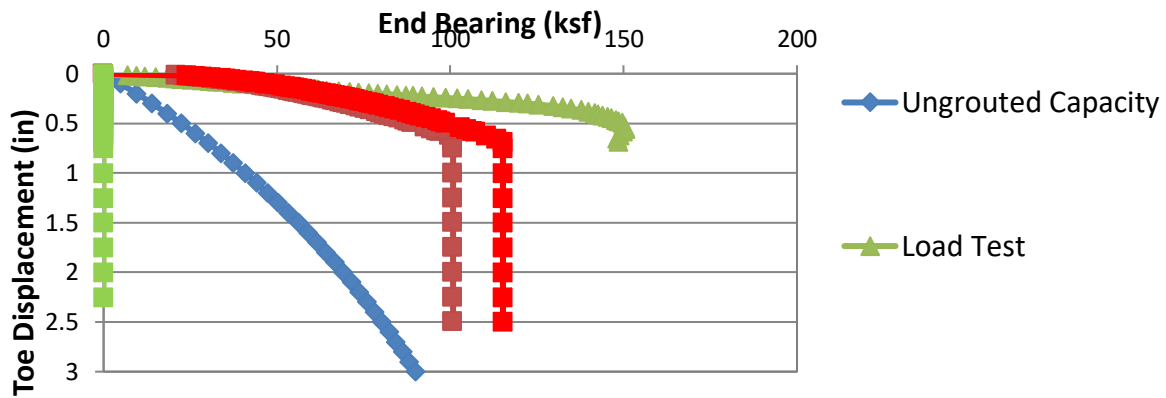


Figure C.20 Data set 20 predicted/design and load test response (top); bias vs disp. (bottom)

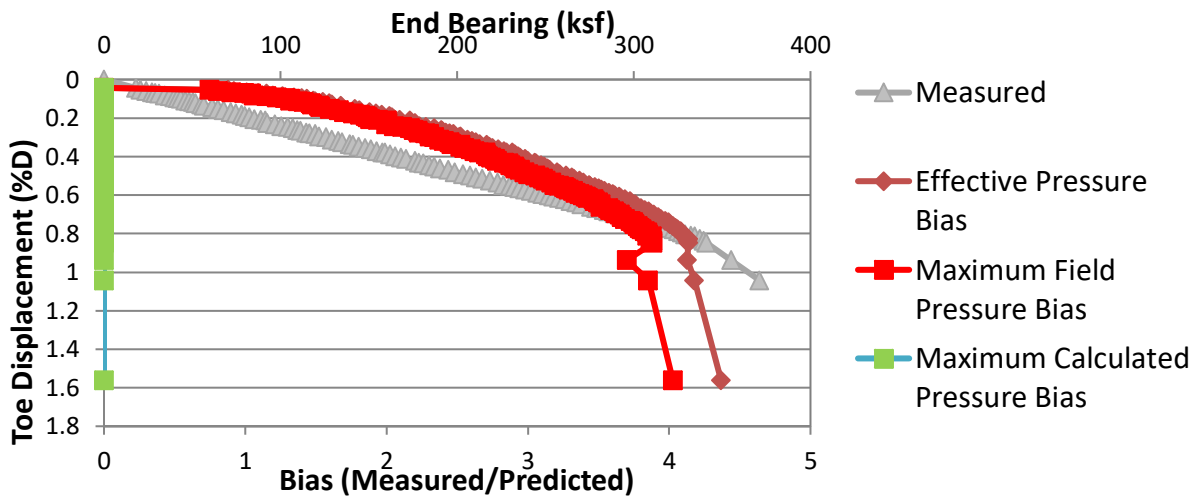
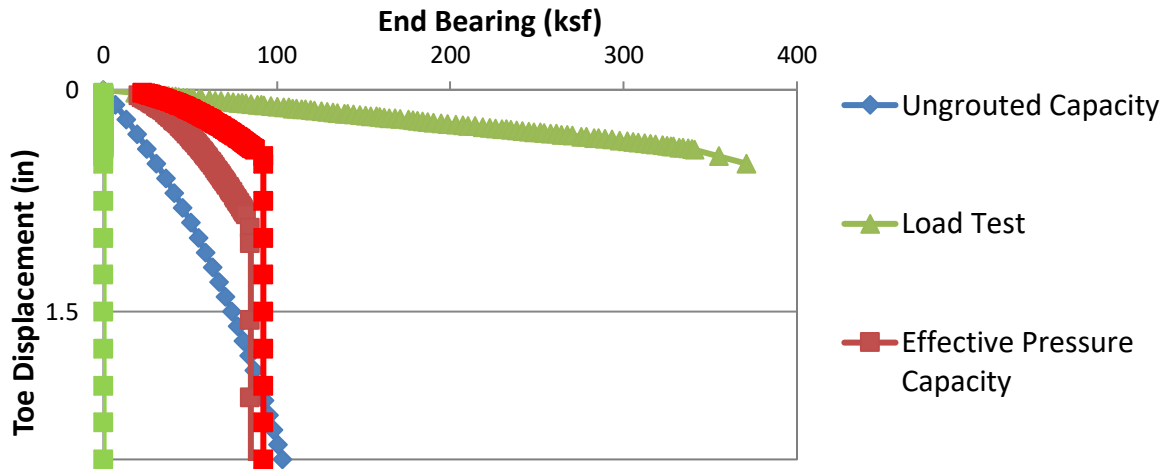


Figure C.21 Data set 21 predicted/design and load test response (top); bias vs disp. (bottom)

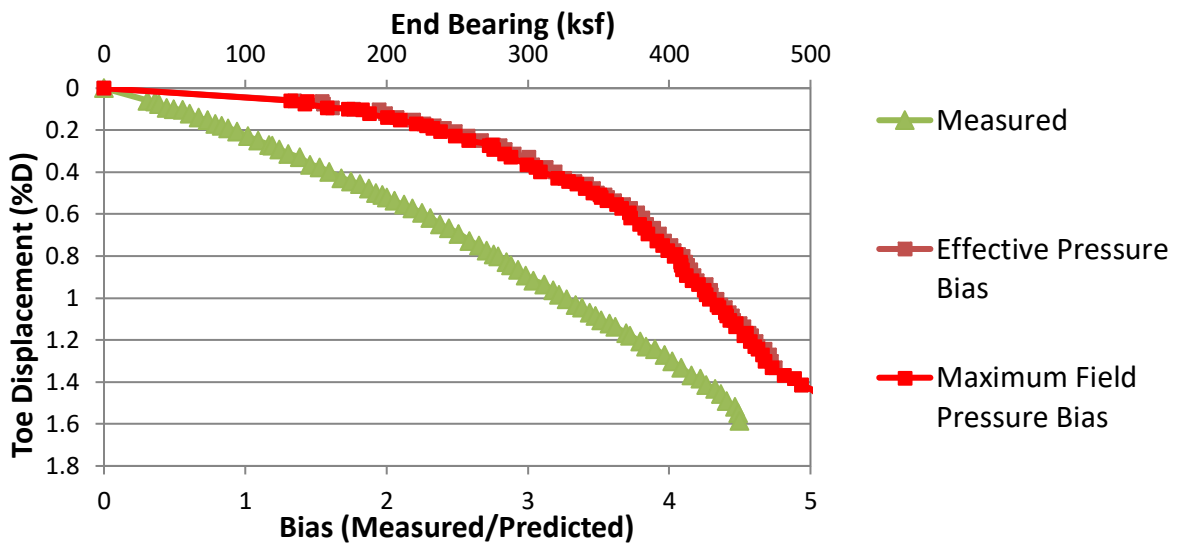
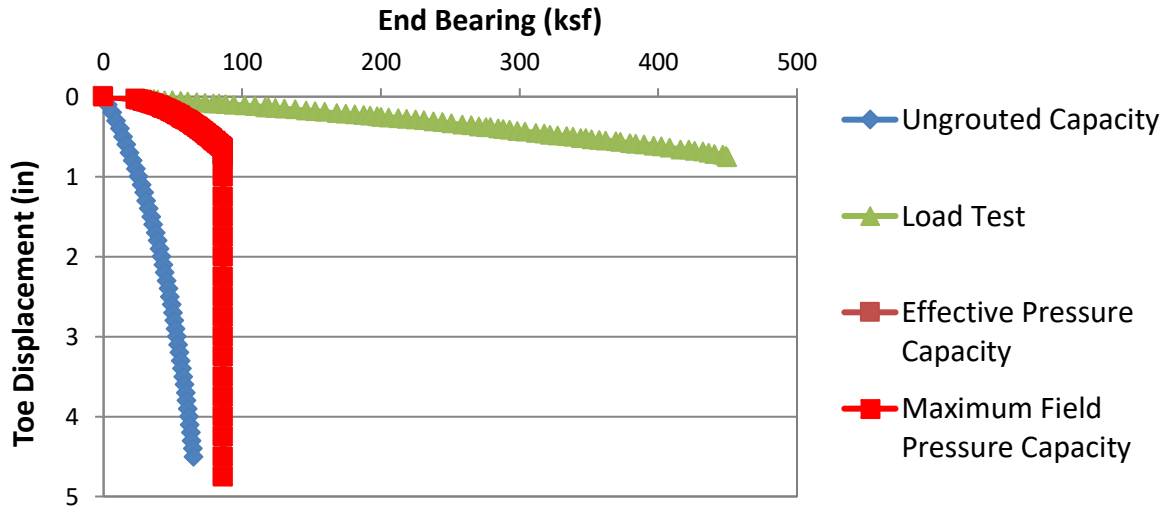


Figure C.22 Data set 22 Predicted/design and load test response (top); bias vs disp. (bottom)

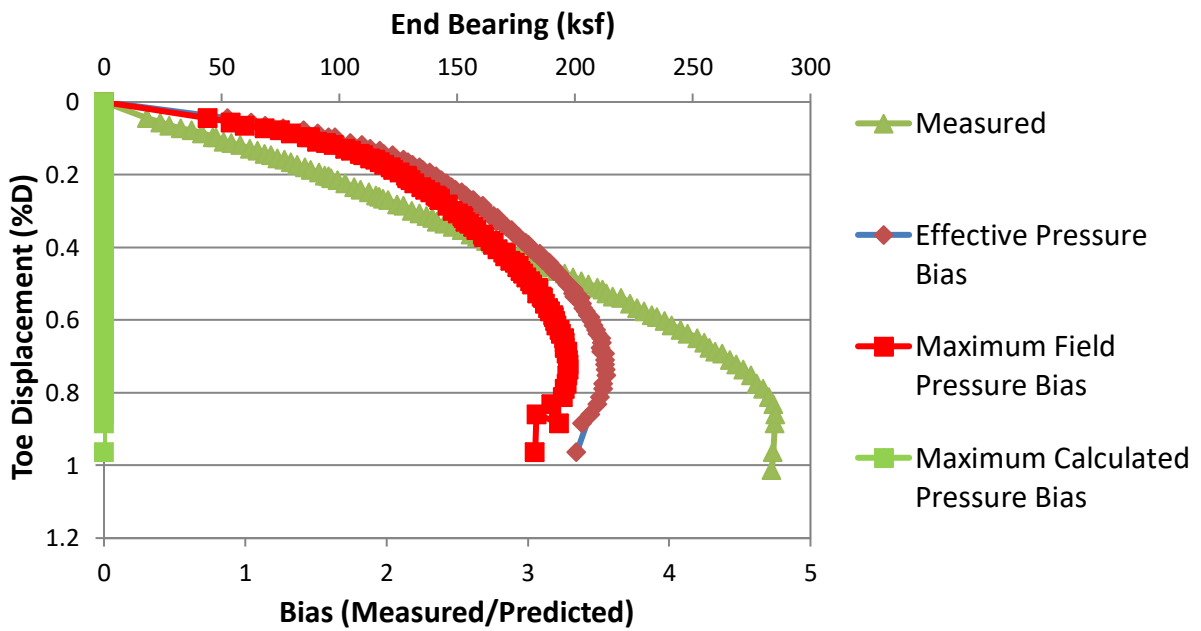
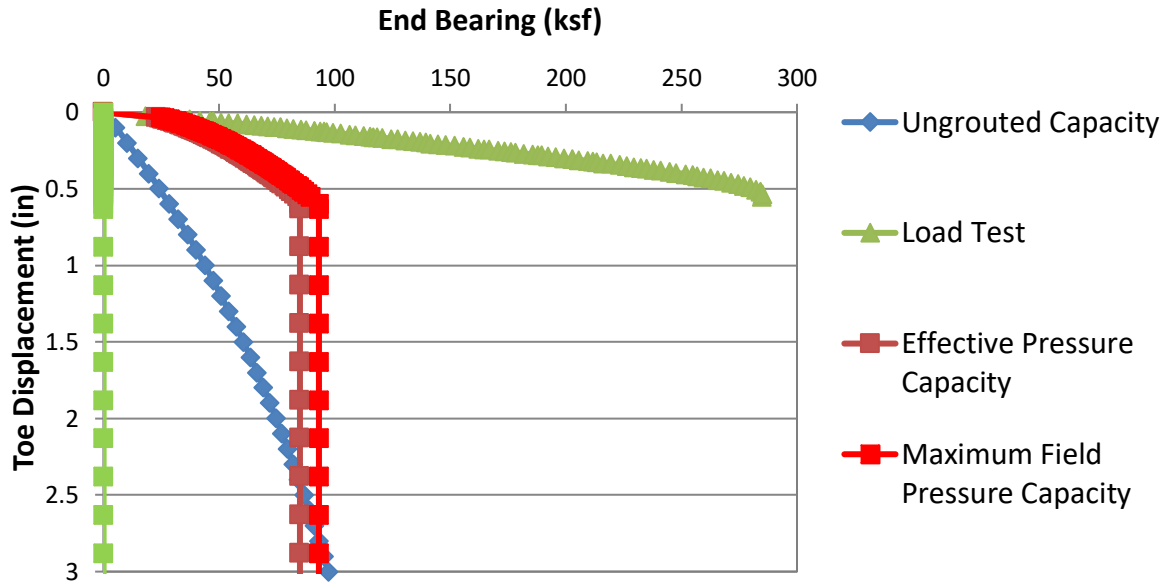


Figure C.23 Data set 23 predicted/design and load test response (top); bias vs disp. (bottom)

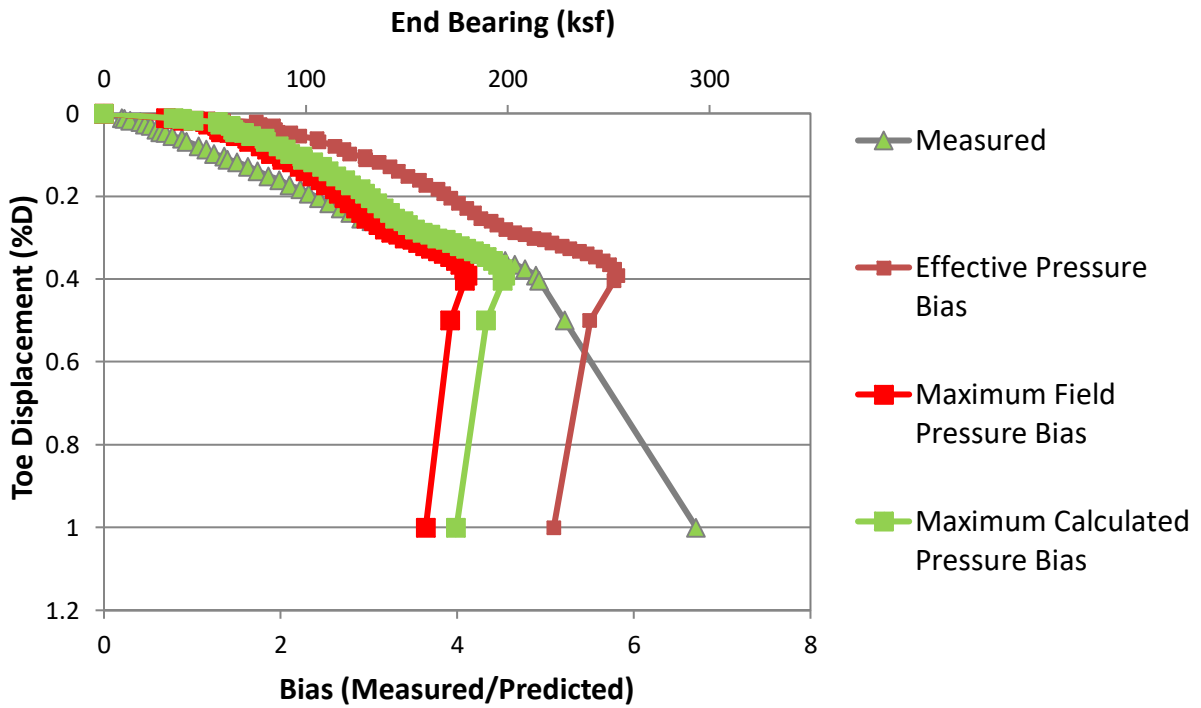
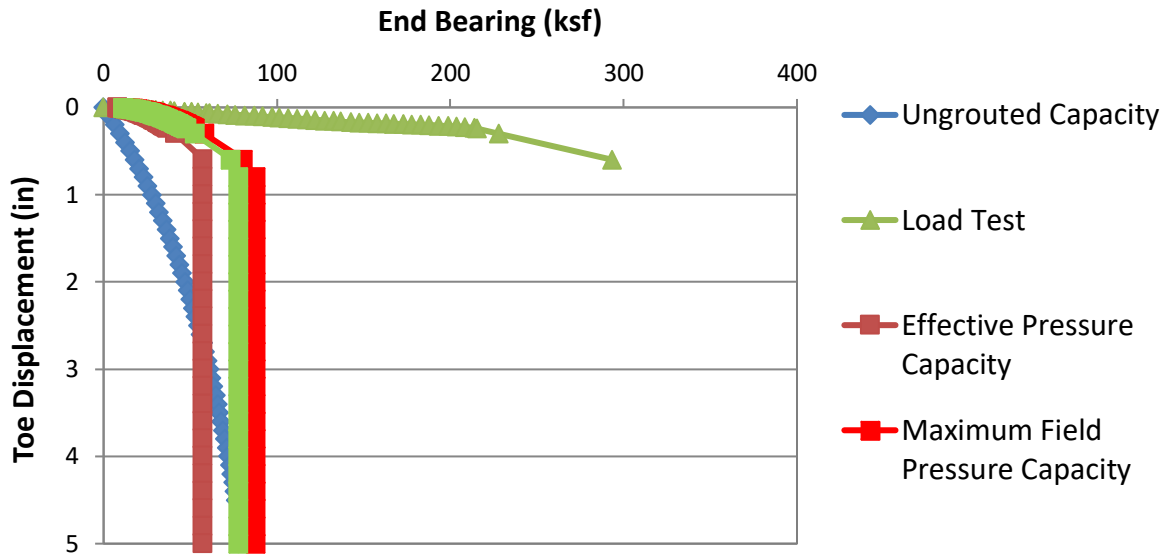


Figure C.24 Data set 24 predicted/design and load test response (top); bias vs disp. (bottom)

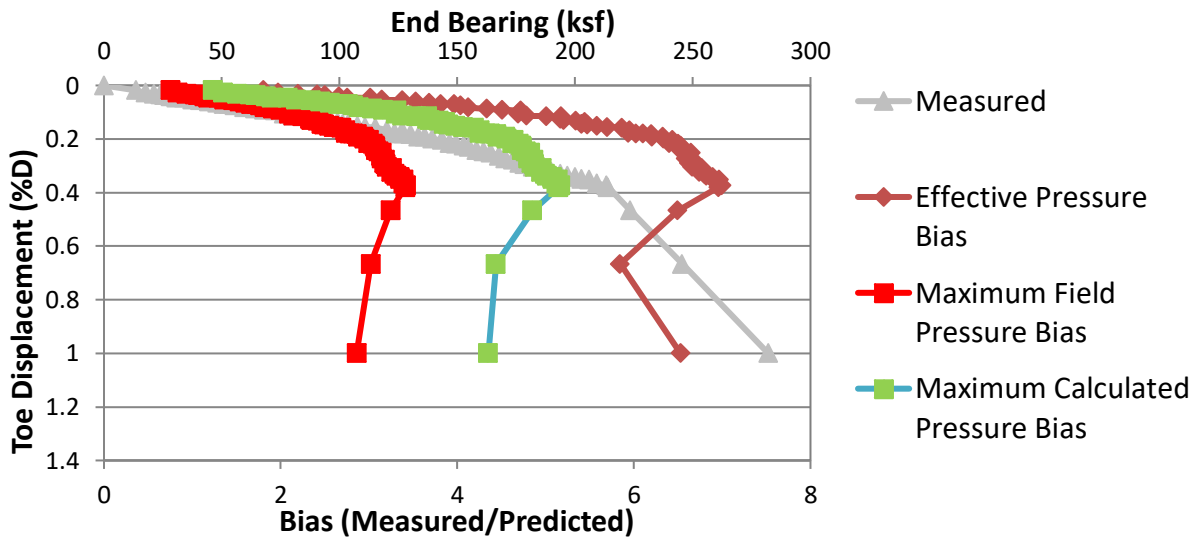
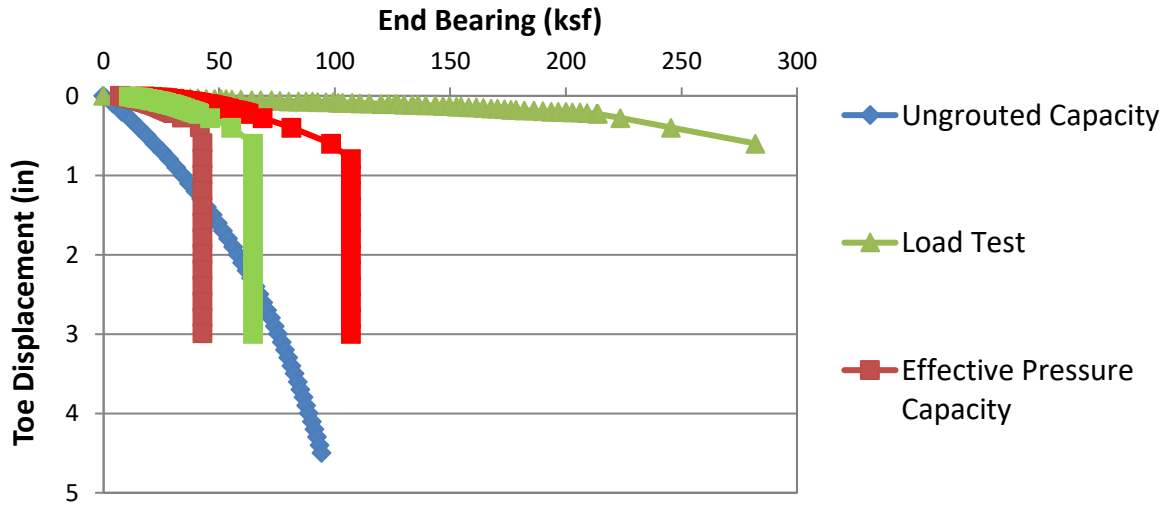


Figure C.25 Data set 25 predicted/design and load test response (top); bias vs disp. (bottom)

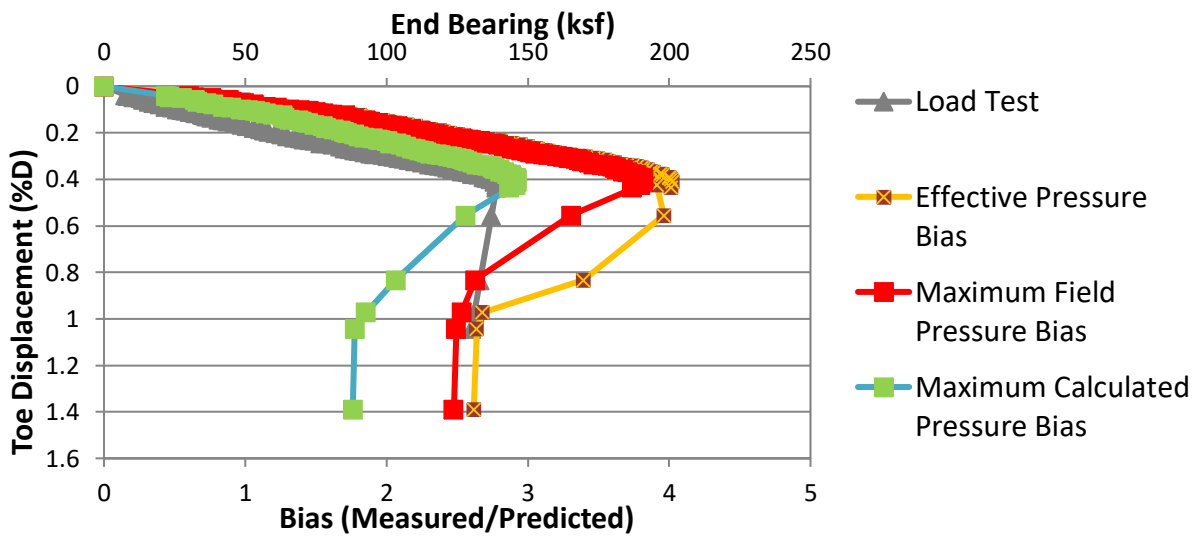
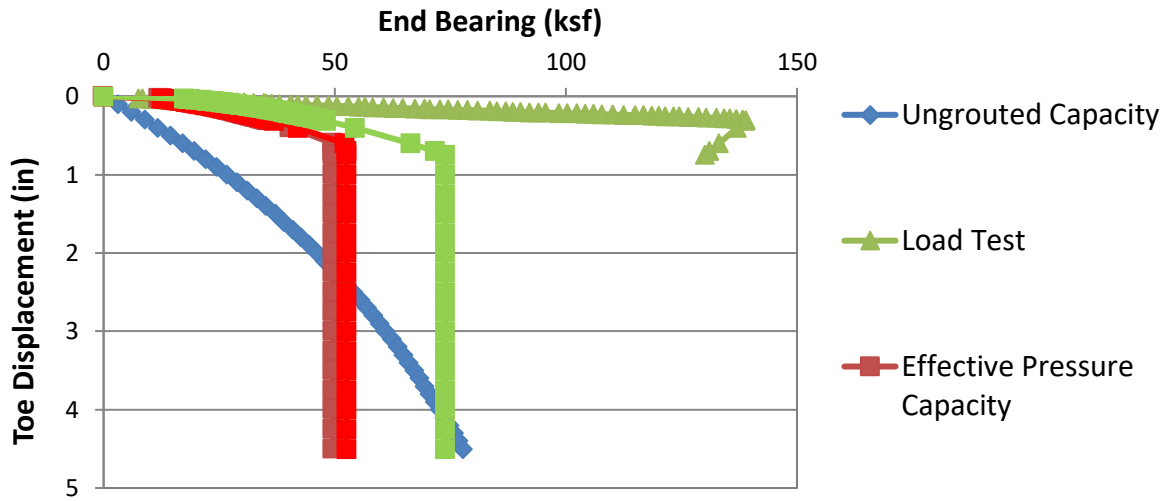


Figure C.26 Data set 26 predicted/design and load test response (top); bias vs disp. (bottom)

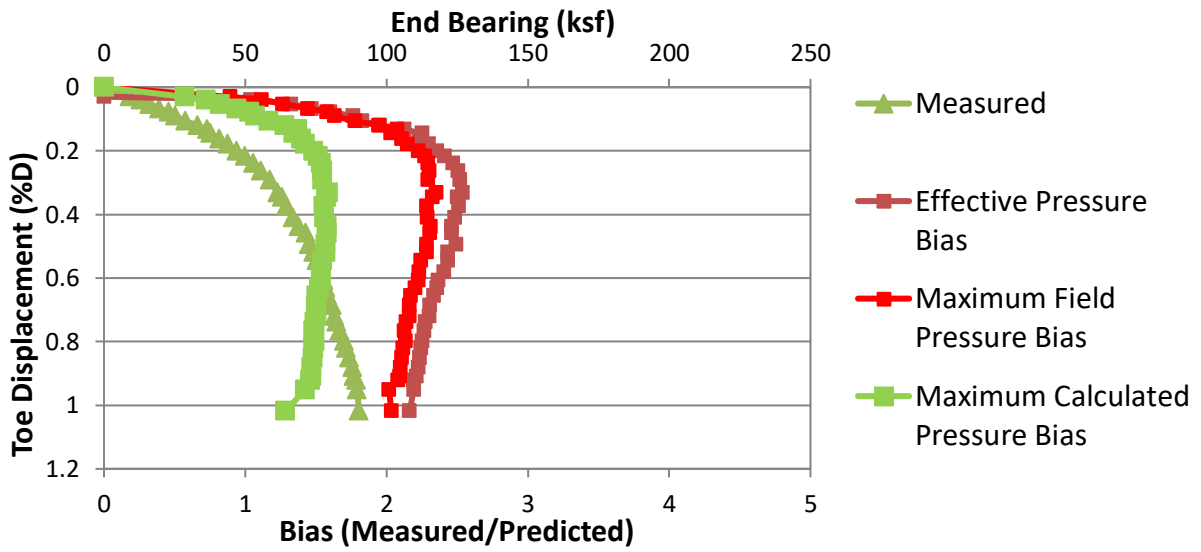
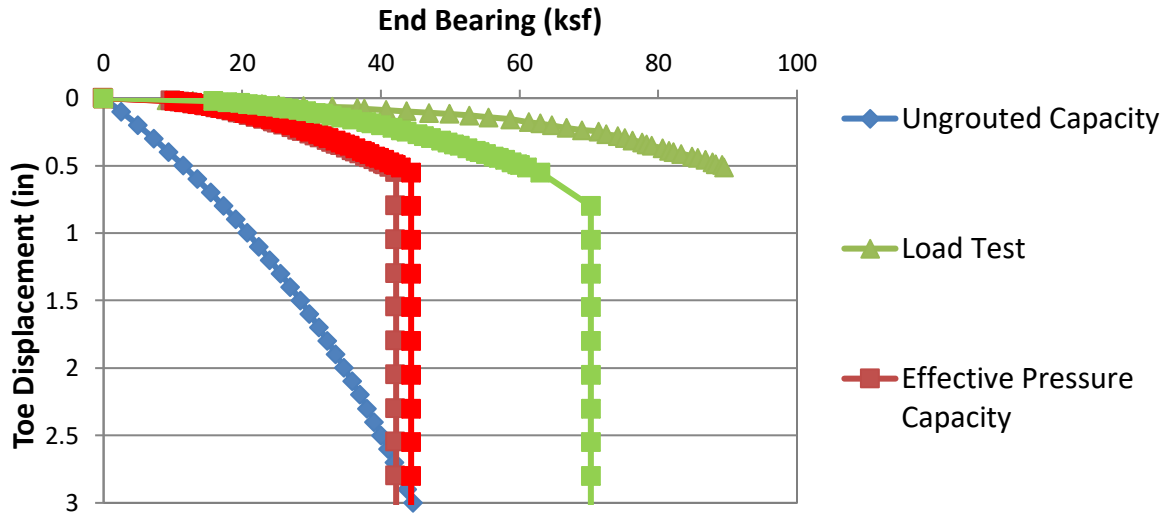


Figure C.27 Data set 27 Predicted/design and load test response (top); bias vs disp. (bottom)

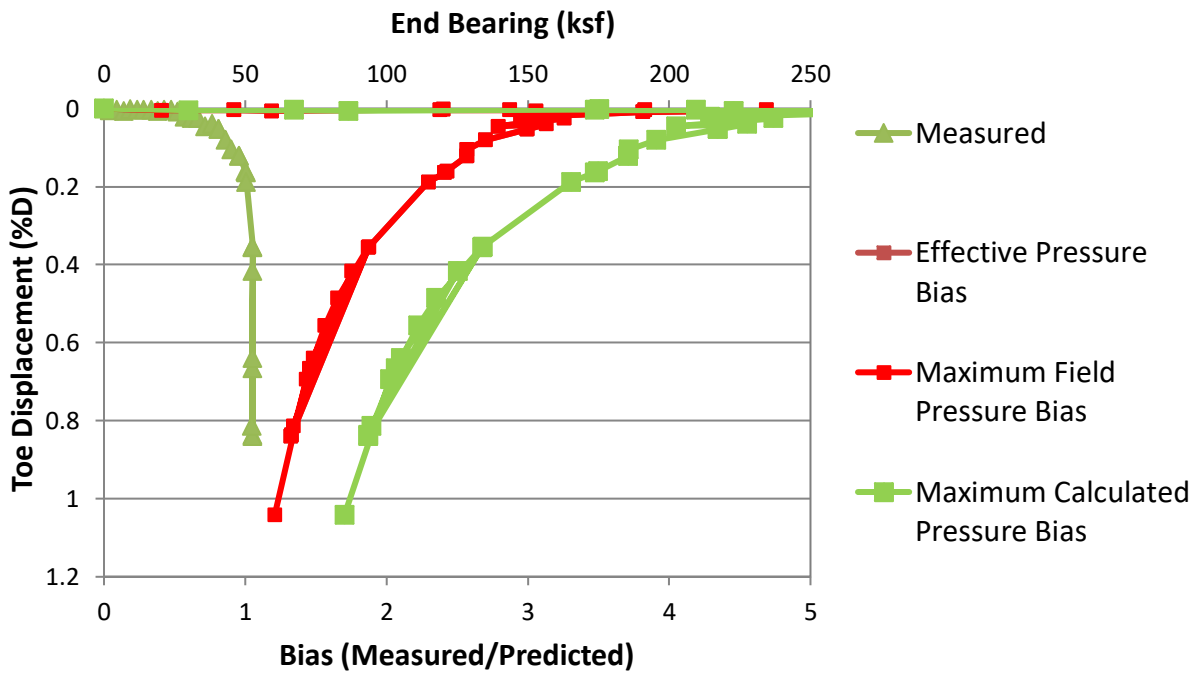
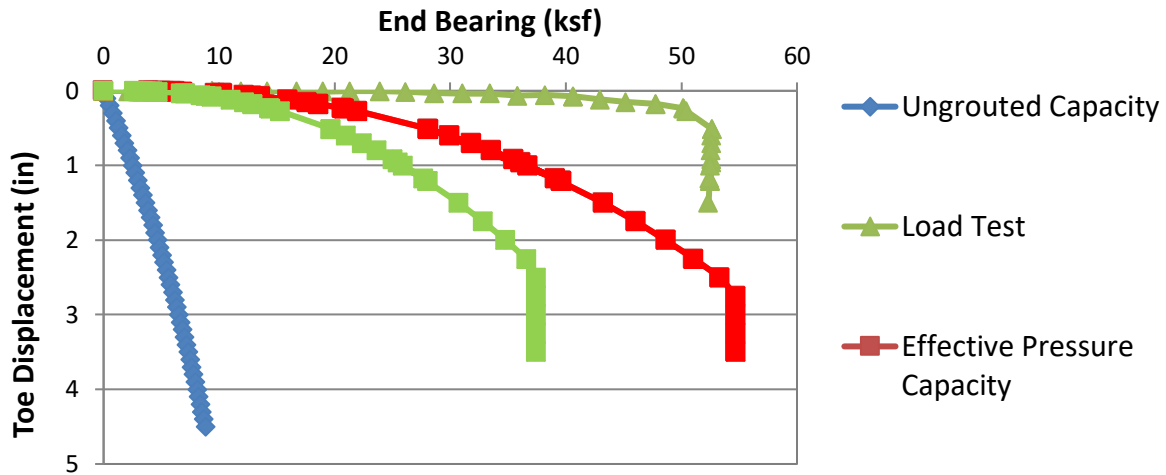


Figure C.28 Data set 28 predicted/design and load test response (top); bias vs disp. (bottom)

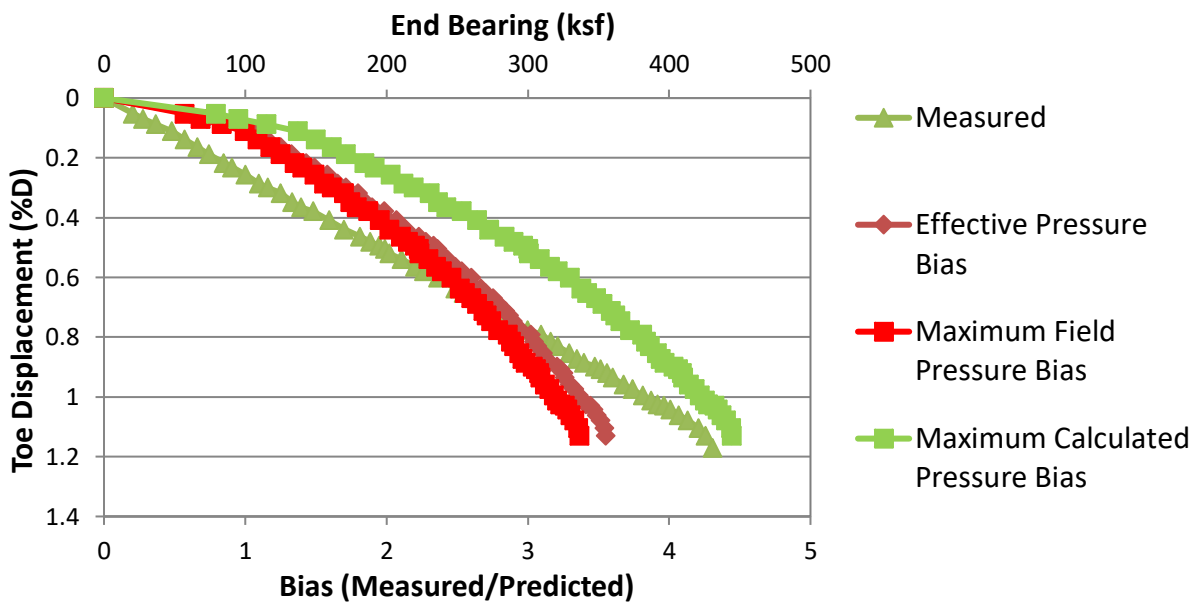
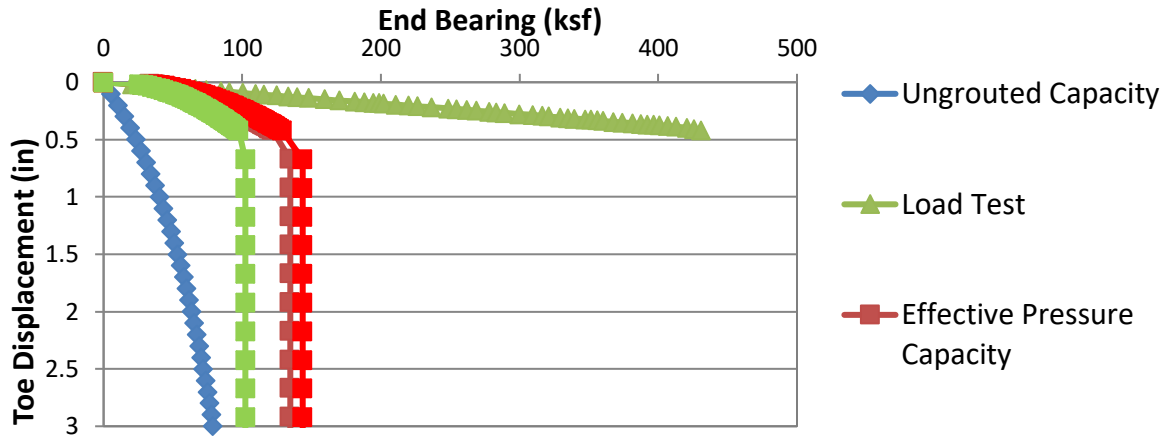


Figure C.29 Data set 29 predicted/design and load test response (top); bias vs disp. (bottom)

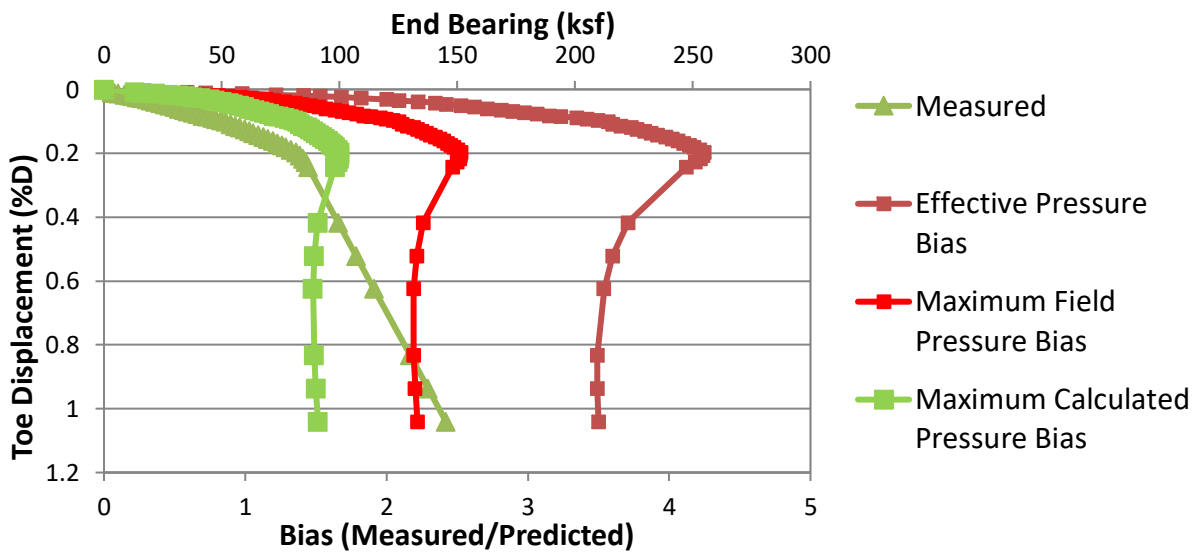
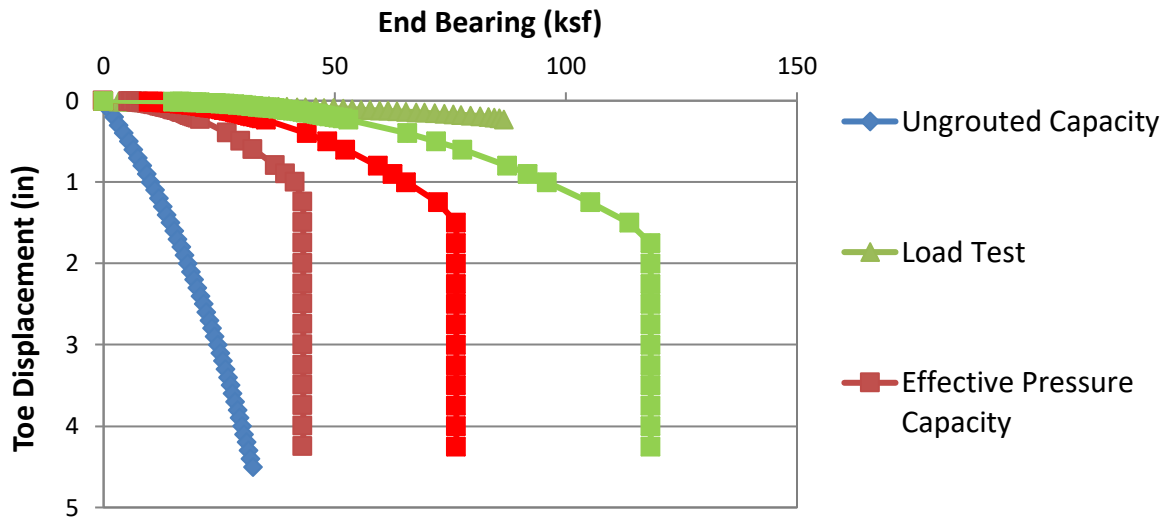


Figure C.30 Data set 30Predicted/design and load test response (top); bias vs disp. (bottom)

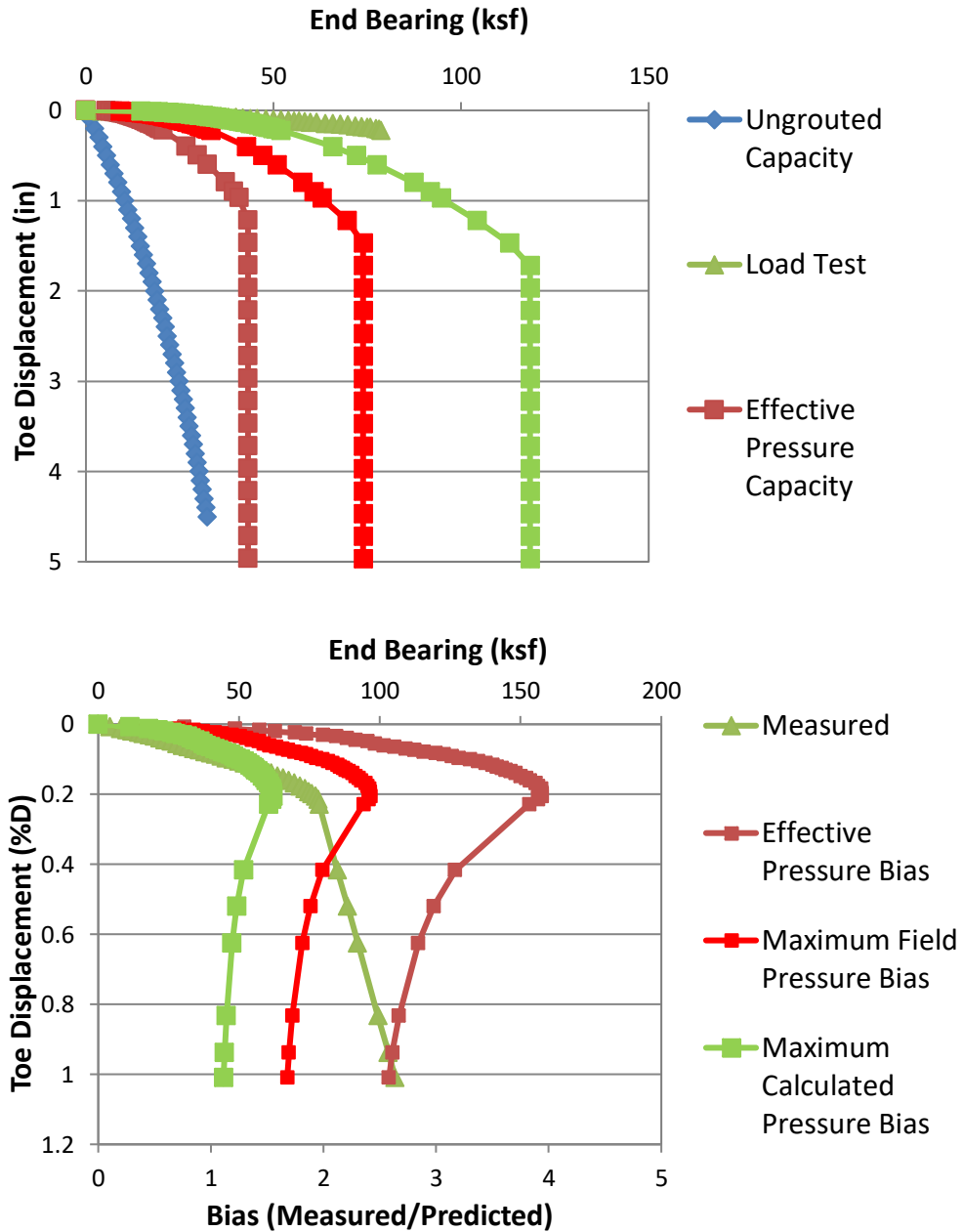


Figure C.31 Data set 31 Predicted/design and load test response (top); bias vs disp. (bottom)

APPENDIX D DESIGN EXAMPLE USING NEW FDOT DESIGN EQUATION

Design Method for Drilled Shaft with Pressure Grouted Tip

For a given shaft diameter and anticipated embedment length, the method for estimating the unit tip resistance of grouted shafts involves the following steps:

1. Calculate the *ungROUTED* nominal unit tip resistance of the shaft (q_{tip}^*) for 5% Diam. Tip settlement as per ASSHTO 10.8.2.2.2.
*The 5% settlement is also the default value used in the FB-Deep for drilled shafts founded in cohesionless soils, thus, one can use the FB-Deep to calculate $q_{tip} = 0.6 \times \text{SPT } N_{60}$, where SPT N_{60} is weighted average at shaft tip (Reese and O'Neill, 1988).
2. Calculate the nominal side shear resistance, F_s , for the given shaft diameter (D) and total embedded length of the shaft.
3. Determine the maximum anticipated grout pressure (GP_{max}) by dividing the nominal uplift side shear resistance, F_{SU} , by the cross-sectional area of the shaft, A .

$$GP_{max} = F_{SU} / A$$

4. Calculate the Grout Pressure Index, GPI, as the ratio of the maximum anticipated grout pressure (step 3) to the ungrouted unit tip resistance, q_{tip} (step 1).

$$GPI = GP_{max} / q_{tip}$$

5. Determine the TIP Capacity Multiplier using the following equation:

$$TCM = 0.713(GPI) + 0.3$$

6. Estimate the grouted unit tip resistance as the product of the tip capacity multiplier (Step 5) and the ultimate ungrouted end bearing capacity (Step 1)

$$q_{grouted} = (TCM)(q_{tip})$$

The design of the nominal resistance for post grouted shafts is simply the sum of the ultimate side shear resistance and the grouted tip resistance. Note that the side shear is assumed to develop with very little displacement, thus allowing for the use of this ultimate value. Care should be taken when specifying maximum allowable shaft uplift during grouting such that the side shear resistance (contributing to total resistance) is not displaced beyond possible peak strength and into a lower residual value. The Step 5 TCM value has been selected to coincide with maximum side shear at no more than 1%D tip settlement.

Design Example

Given: A 3 ft diameter drilled shaft tipped in sand (SPT $N_{60} = 30$ and $F_s = 300$ tons).

*Calculate the maximum anticipated grout pressure:

Grout Pressure = Side shear Force/ Tip Area

$$GP_{\max} = 300 \text{ tons} * 0.75 / ((3 \text{ ft})^2 \pi/4)$$

$$GP_{\max} = 31.8 \text{ tsf}$$

¹O'Neill cited uplift resistance of shafts to be 0.75 that of compression/downward loading. O'Neill, M. W. (2001). "Side Resistance in Piles and Drilled Shafts," *The Thirty-Fourth Karl Terzaghi Lecture, ASCE J. Geotech. Geoenviron. Eng.* 127:3-6.

*Calculate nominal end bearing @ 5%D settlement:

Nominal End Bearing = 0.6*SPT N₆₀ (Reese and O'Neill, 1988)

$$q_{\text{tip}} = 0.6 * 30$$

$$q_{\text{tip}} = 18 \text{ tsf}$$

*Calculate grout pressure index (GPI):

$$GPI = 31.8 \text{ tsf} / 18 \text{ tsf}$$

$$GPI = 1.77$$

*Calculate tip capacity multiplier (TCM)

$$TCM = 0.713 (1.77) + 0.3$$

$$TCM = 1.56$$

*Calculate grouted unit end bearing capacity

$$q_{\text{grouted}} = (TCM)(q_{\text{tip}}) = 1.56 * 18 = 28.1 \text{ tsf}$$

Nominal Side Shear and Tip Resistance after grouting:

$$R_{n \text{ Side Shear}} = 300 \text{ tons}$$

$$R_{n \text{ End Bearing}} = (q_{\text{grouted}})(A_{\text{tip}}^{**})$$

$$= (28.1 \text{ tsf})((3 \text{ ft})^2 * 3.1416/4)$$

$$= 199 \text{ tons}$$

$$\begin{aligned} \text{Factored Bearing Resistance} &= \phi_{\text{Side Shear}} * R_{n \text{ Side Shear}} + \phi_{\text{grouted end bearing}} * R_{n \text{ End Bearing}} \\ &= 0.6 * 300 \text{ tons} + 0.65 * 199 \text{ tons} \\ &= 309 \text{ tons} \end{aligned}$$

**The tip area of a grouted shaft has been shown to be larger than the shaft diameter due to cavity expansion of the soils beneath the tip. While values less than the constructed shaft diameter have been suggested to account for variability, the constructed diameter of the shaft was used to develop this design method and therefore statistically incorporates variations both larger and smaller than the nominal shaft diameter.